Identification and Quantification of Sperm Head Plasma Membrane Proteins Associated with Male Fertility

A Thesis Submitted to the

College of Graduate and Postdoctoral Studies

In Partial Fulfillment of the Requirements

For the Degree of Doctor of Philosophy

in the Department of Animal and Poultry Science

University of Saskatchewan

Saskatoon

By

MUHAMMAD IMRAN

PERMISSION TO USE

In presenting this thesis/dissertation in partial fulfillment of the requirements for a Postgraduate degree from the University of Saskatchewan, I agree that the Libraries of this University may make it freely available for inspection. I further agree that permission for copying of this thesis/dissertation in any manner, in whole or in part, for scholarly purposes may be granted by the professor or professors who supervised my thesis/dissertation work or, in their absence, by the Head of the Department or the Dean of the College in which my thesis work was done. It is understood that any copying or publication or use of this thesis/dissertation or parts thereof for financial gain shall not be allowed without my written permission. It is also understood that due recognition shall be given to me and to the University of Saskatchewan in any scholarly use which may be made of any material in my thesis/dissertation.

DISCLAIMER

Reference in this thesis/dissertation to any specific commercial products, process, or service by trade name, trademark, manufacturer, or otherwise, does not constitute or imply its endorsement, recommendation, or favoring by the University of Saskatchewan. The views and opinions of the author expressed herein do not state or reflect those of the University of Saskatchewan and shall not be used for advertising or product endorsement purposes.
Requests for permission to copy or to make other uses of materials in this thesis/dissertation in whole or part should be addressed to:

Head of the Department of Animal and Poultry Science
University of Saskatchewan,
6D34 Agriculture Building, 51 Campus Drive
Saskatoon, Saskatchewan, Canada S7N 5A8

OR

Dean
College of Graduate and Postdoctoral Studies
University of Saskatchewan
116 Thorvaldson Building, 110 Science Place
Saskatoon, Saskatchewan S7N 5C9 Canada

OVERALL ABSTRACT

The major objective was to characterize proteins in head plasma membrane (HPM) of sperm from animals of two species to identify species' and proteins' differences related to fertility. HPM's sodium/potassium-ATPase (Na^+/K^+-ATPase) acts as a receptor, inducing capacitation when bound by its hormone ouabain. Na^+/K^+-ATPase is an α/β dimer, each with several isoforms (α1, α2, α3, α4, β1, β2, β3) whose exact relationship to *in vivo* fertility and capacitation is unknown. In the first study, specific Na^+/K^+-ATPase isoforms in sperm HPM of boars with different Direct Boar Effects (DBEs) for farrowing rate (FR) and litter size, differed between low and high fertility boars (LF, HF, n=6/each; DBE-based). SDS-PAGE and immunoblotting detected more α3 ($P<0.05$) in HF HPM, correlating with FR; immunocytochemistry identified differing α3 and α2 localizations in HF vs LF whole sperm. In second study, tandem mass spectrometry (spectra aligned to UniProtKB 'mammals') revealed that non-ATPase HPM proteins differ between bulls of HF and LF Bull Fertility Index (BFI, BFI > or <100; Semex evaluated). Statistical analysis identified 67 differential abundance proteins (DAPs) between HF and LF (n=3/group; $P<0.05$), which associated by meta-analysis to BFI. Gene ontology assigned 48 up-regulated HF proteins to sperm fertilization, and 19 down-regulated to catalytic and transporter activity. 38-up-regulated DAPs (HF and LF, n=16) correlated positively (r^2=0.29 to 0.66; $P\leq0.05$) and 6 down-regulated negatively (r^2=0.26 to 0.44; $P\leq0.05$) to BFI. The third study characterized HPM Na^+/K^+-ATPase in 16 bulls with differing BFI but similar sperm motility kinetics. Normalized Spectral Abundance Factor (NSAF) of α1 was significantly greater in 8 higher- vs 8 lower-fertility bulls. Linear regression positively correlated BFI to NSAF of α1 and β2 (r^2=0.42 and 0.47, respectively; $P\leq0.05$), and negatively correlated BFI to α4 (r^2=0.37; $P\leq0.05$), confirmed by bioinformatics predictions. These results suggest involvement of α1 and β2 in fertilization as potential fertility

biomarkers. Overall, specific Na^+/K^+-ATPase isoforms identified in boar and bull sperm HPM significantly correlate with *in vivo* fertility, as do other specific bull HPM proteins. Elucidating potential fertility biomarkers in two species improves understanding of key proteins and their roles in various, complex mechanisms that enable successful sperm fertilization.

ACKNOWLEDGEMENTS

I would like to thank my supervisors and mentors, respected Dr. Mary M. Buhr and Dr. George Katselis for giving me the opportunity to gain experience under their guidance and for their immense support, and encouragement since commencement of my PhD program until its completion. I am incredibly grateful to my advisory committee members, respected Dr. Muhammad Anzar, Dr. Murray Pettitt, Dr. Natacha Hogan, and committee chair Dr. Ryan K. Brook for their insightful comments and constructive feedback throughout the development of the present work. I am also thankful to my external examiner Dr. Peter Sutovsky for reading the present thesis and providing helpful feedback. I would like to extent my thanks to Carla Protsko, Mrudhula Sajeevadathan and Dr. Paulos Chumala for their guidance.

I acknowledge the University of Saskatchewan, Mass Spectrometry laboratory, NSERC, Topigs Norsvin, Semex and Katie Hickey for facilities and material for this research.

Finally, my heartfelt thanks for my great mother who always has been dedicated, source of motivation and my ever first teacher. I am very indebted to her courage, spirit, and strong determination to enable my success in my life. My many prayers for my father, my amazing family: wife; Hira Imran, who supported me in my PhD research and in every matter, my lovely son Abdul-Rehman bin Imran, great thanks to my lovely brother Muhammad Irfan and my special thanks to my all sisters for their devoted prayers, without their support and continuous motivation, the dream of my PhD would not be possible.

DEDICATION

I wholeheartedly dedicate this work to my amazing and dear family: Loving Mother Ms. Hanif, Father Muhammad Hanif (late), Brother Muhammad Irfan Zaib, all devoted Sisters, my Wife, and my beloved Son Abdul-Rehman bin Imran, for their encouragement, patience, and immeasurable love.

TABLE OF CONTENTS

LIST OF TABLES

LIST OF FIGURES

LIST OF ABBREVIATIONS

ABC	Ammonium bicarbonate
ACRBP	Acrosin binding protein
ADP	Adenosine diphosphate
AI	Artificial insemination
ALH	Amplitude of lateral head displacement
AMP	Adenosine monophosphate
ANOVA	Analysis of variance
AE	Acrosomal Exocytosis
ART	Assisted reproductive techniques
ATA	United States index from farms on the west coast
ATH	Average to high
ATL	Average to low
ATP	Adenosine triphosphate
BCA	Bicinchoninic acid
BCF	Frequency of head displacement
BFI	Bull fertility index
BLAST	Basic local alignment search tool
BSA	Bovine serum albumin
CASA	Computer assisted semen analysis
CBM	Caveolin binding motifs
CDN	Canadian fertility numbers

DAG	1, 2 diacylglycerols
DAP	Distance of average path
DBE	Direct boar effect
DCL	Curvilinear distance
DDA	Data-dependent acquisition
DAP	Differentially abundant proteins
DSL	Straight line distance
DTT	Dithiothreitol
EDTA	Ethylenediaminetetraacetic acid
EGF	Epidermal growth factor
EGFR	Epidermal growth factor receptor
ELISA	Enzyme-linked immunosorbent assay
ERK	Extracellular signal regulated kinases
FC	Fold change
FDR	False discovery rate
FG	Fertility groups
FITC	Fluorescein isothiocyante conjugated
FR	Farrowing rate
GDP	Gross domestic product
GLM	Generalized linear model
GO	Gene ontology
GPI	Glycosyl phosphatidyl inositol
GRAVY	Grand average of hydropathicity

HCO^3	Bicarbonate
HDL	High-density lipoprotein
HEPES	N-(2-hydroxyethyl) piperazine-n′-(2-ethanesulfonic acid)
HF	High fertile
HMM	Hidden Markov models
HPLC	High-performance liquid chromatography
HPM	Head plasma membrane
HRP	Horse radish peroxidase
IAA	Iodoacetamide
IAM	Inner acrosomal membrane
IPPs	Interacting partner proteins
LC	Liquid chromatography
LF	Low fertile
LIN	Linearity coefficient
LS	Least square
MAPK	Mitogen activated protein kinases
MAPKAPK	Mitogen-activated protein kinase-activated protein kinase
MCODE	Molecular complex detection
MW	Molecular Weight
MPP	Mass profiler professional
MS	Mass spectrometry
NAD	Nicotinamide adenine dinucleotide
NADH	Nicotinamide adenine dinucleotide hydride

Na^+/K^+-ATPase	Sodium potassium ATPase
NRR	Non-return rate
NSAF	Normalized spectral abundance factor
PBS	Phosphate buffered saline
PCA	Principal component analysis
PE	Phosphatidylethanolamine
PEG	Polyethylene glycol
PKA	Protein kinase a
pI	Isoelectric point
PKC	Protein kinase c
PLC	Phospholipase c
PMSF	Phenylmethanesulfonyl fluoride
PPI	Protein-protein interaction
PPM	Parts per million
P4	Progesterone
PSS	Physiological saline solution
PTMs	Post-Translational Modifications
PVDF	Polyvinylidene fluoride
PWD	Position weight determination
RAF	Rapidly accelerated fibrosarcoma
RAB2A	Ras-related protein Rab-2A
RTK	Receptor tyrosine kinases
SARS	Severe acute respiratory syndrome

sAC	Soluble Adenyl Cyclase
SCR	Sire conception rate
SCX	Strong cation exchange chromatography
SDS-PAGE	Sodium dodecyl sulfate- polyacrylamide gel electrophoresis
SMO	Scoring matrix optimization
NaHCO3	Sodium bicarbonate
SRC	Sarcoma
TFE	Trifluoroethanol
TNB	Total number of born
Tyr	Tyrosine
Tyr-P	Tyrosine phosphorylation
VAP	Average path velocity
VCL	Curvilinear velocity
VSL	Linear velocity
WB	Western immunoblotting
WHO	World health organization
WOB	Wobble
ZP	Zona pellucida

CHAPTER 1: GENERAL INTRODUCTION

1. General Introduction

Low fertility originating from sires causes significant economic losses worldwide for animal producers, breeders, and related industries, whether females are bred by artificial insemination (AI) or naturally. To enhance the rate of genetic progress (Barquero et al., 2021), more than 70% of dairy cows are bred by AI with frozen semen from superior bulls with high genetic traits (Park et al., 2012; Kwon et al., 2015), while over 95% of sows are bred with AI (Zuidema et al., 2021), producing successful conception with rates of 50% in bovine (Park et al., 2012) and 80-92% of porcine inseminations (Ruiz-Sánchez et al., 2006; Zhao et al., 2021). Male infertility or subfertility is the major cause of reproductive failure in about half of the cases (Park et al., 2012), so boar and bull fertility contribute greatly to reproductive efficiency in both dairy (Pacheco et al., 2021) and swine industries (Zuidema et al., 2021).

Diagnosis of sire fertilizing ability is of prime importance to allow culling of low fertility sires at a younger stage, thereby reducing housing and feeding costs, and preventing reproductive losses. Moreover, accurate prediction of sperm fertility in semen used for AI will reduce inter-calving interval and will improve substantially overall reproductive and productive efficiency. A method that accurately predicts a sire's fertility will greatly benefit the dairy, beef, and porcine industries, and may find application in other species.

Proteomics is an emerging approach for studying human and animal andrology and to understand the biological mechanisms of sperm function and its interaction with the oocyte leading to fertilization (Wright et al., 2012). As compared to somatic cells, mammalian spermatozoa have unique functional and structural characteristics. Acquisition of fertilizing ability requires multiple processes commencing in the male gonad and continuing all the way through to the oviduct (Sutovsky, 2018).

The transmembrane protein sodium/potassium-ATPase (Na^+/K^+-ATPase) is ubiquitous in mammalian cells, maintaining the cell's resting membrane potential and regulating cellular volume through active transport of Na^+ and K^+ ions (Kaplan, 2002; Xie & Askari, 2002) and in sperm it supports motility (Jimenez et al., 2011). Also, in sperm as well as other cells, Na^+/K^+-ATPase activates a signaling cascade of downstream events to induce phosphorylation of proteins, a function independent of its pumping action (Xie & Askari, 2002; Thundathil et al., 2006; Pierre et al., 2008; Pierre & Blanco, 2021). In sperm, the phosphorylation leads to *in vivo* and *in vitro* sperm fertilization.

Na^+/K^+-ATPase is considered a member of a multiprotein complex with many partners forming protein-protein interactions with its α subunits (Reinhard et al., 2013). Na^+/K^+-ATPase has multiple roles. In addition to acting as an enzyme and maintaining electrochemical gradients across the cell membrane, it has been shown to acts as a receptor and signal transducer (Desfrere et al., 2009; Zuidema et al., 2021). Ligand bound Na^+/K^+-ATPase phosphorylates Src kinase but proof of high-affinity binding with Src kinase is inadequate (Reinhard et al., 2013). Alternatively, both Na^+/K^+-ATPase and Src kinase could be part of a signaling complex in the cell membrane, and ouabain binding to Na^+/K^+-ATPase could activate Src kinase via allosterism. The α subunit of Na^+/K^+-ATPase is appropriate to function as an allosteric modifier because during the reaction cycle, it undergoes conformational changes (Nyblom et al., 2013; Reinhard et al., 2013). Sodium and ATP both are known as allosteric modifiers of Na^+/K^+-ATPase (Jorgensen et al., 2003; Garcia et al., 2013) and the ATP/ADP ratio affects activation of Src kinase (Weigand et al., 2012).

Sperm membrane proteins have contributing roles in oocyte recognition, binding, and other protein interactions. As Na^+/K^+-ATPase engages in several functions in sperm (Thundathil et al., 2006; Hickey & Buhr, 2012; Sajeevadathan et al., 2019) and since reduction of its expression has

been associated to abnormal sperm (Thundathil et al., 2012) this molecule has potential to be a biomarker for sperm fertility. Na^+/K^+-ATPase interacts with many proteins which have important roles in aspects of fertilization. Therefore, careful study of the existence, expression, and possible roles of fertility-related proteins in the sperm head plasma membrane, including Na^+/K^+-ATPase isoforms, could elucidate details of capacitation and fertilization with possible future use to improve animal reproduction.

CHAPTER 2: REVIEW OF LITERATURE

2.0 Review of Literature

2.1 Animal Agriculture and Importance of Fertility

Agriculture and agri-food products have major role in the world's economy. Using Canada as an example, agriculture in 2020 generated $139.3 billion, equaling 7.4% of the national Gross domestic product (GDP) and employing 2.1 million people (Overview of Canada's Agriculture and Agri-Food Sector, 2021). The animal production sector contributed $5.4 billion to GDP and created 133,500 jobs, with the Canadian dairy ranking second after the red meat industry sector based on farm cash receipts of $7.13 billion. In 2020, total milk production from 1.405 million head was estimated to 93.51 million hectoliters, contributing $486.4 million for exported milk products, and $126.8 million from dairy genetics including bovine embryos, semen, and live dairy cattle (Overview of Canada's Agriculture and Agri-Food Sector, 2021).

Fertility, generally defined as ability to conceive offspring and to propagate next generations (Utt, 2016) is crucial for economically efficient animal production. In the dairy and beef industries, individual male fertility is more important than an individual female, because in natural service, semen from one bull may be used to breed up to 40 females while in AI, one ejaculate may breed hundreds to thousands of females (Kastelic, 2013). Commercial breeders and AI companies are developing different diagnostic methods to identify sires with superior genetic traits for production and high conception rates (Parisi et al., 2014), even though heritability of reproductive traits is low. Such sires will improve the financial success of producers (Walton, 2012) the sustainability, growth of animal agriculture, and the efficiency of production of high-quality animal protein.

2.2. Artificial Insemination in Farm Animals

By definition AI is a technique in which semen is manually deposited into female reproductive tract. This reproductive biotechnology technique is considered one of the oldest, as the first report of AI was over 200 years ago (Morotti et al., 2021). Since then, many studies have been conducted and this practice is widely used in livestock species. Even with the advancement of embryo transfer program *in-vivo* and *in-vitro*, AI is still considered an important assisted reproductive biotechnology in many herds due to its low cost and high potential for a herd's genetic improvement (Morotti et al., 2021). AI is still the key assisted-reproduction technology enhancing reproductive efficiency and genetic improvement among farm animals. Its benefits over natural breeding include more offspring from genetically superior males; control of infectious and reproductive diseases; greater safety for the female animal and producers; fewer males needed to impregnate females; ease of global distribution of male genetics; and, when semen can be stored long-term, maximized sperm production over a male's lifetime for use at the producer's convenience regardless of the male's lifespan. All these factors promote standardized management and focus on economic factors of the producer's operations and decisions (Morotti et al., 2021).

In dairy production, the reproductive performance of the sire is evaluated by non-return rate (NRR) and sire conception rate (SCR), meaning the percentage of cows that do not return to estrus within a specific time (e.g., 56 days) after being inseminated (Foote, 2003). Factors affecting fertility outcome of AI includes age of the bull, age and parity of the cow, farm management, inseminator, number, and quality of sperm in the insemination dose (de Oliveira et al., 2013; Muhammad Aslam et al., 2018; Narud et al., 2022). To predict dairy sire fertility, semen genetics companies pool these data from hundreds of bulls with thousands of inseminations per bull and through sophisticated statistical models, calculate a score for each bull (Zwald et al., 2004; de

Oliveira et al., 2013). Although the scores are given different commercial names, this BFI enables producers to include bull fertility when they are selecting sires for their dairy enterprise and provides AI companies with additional information for decisions on bulls to cull or whose male offspring might be considered for inclusion.

In addition to collecting these retrospective data on pregnancy success, semen production companies proactively assess each ejaculate that they collect prior to processing it for AI. They usually assess sperm motility parameters and morphology, discarding ejaculates that do not meet the company's standards. However, successful fertilization is impacted by less obvious sperm traits such as intactness of the acrosome and plasma membrane (Kumaresan et al., 2017) progressive motility (Farrell et al., 1998; Puglisi et al., 2012; Gliozzi et al., 2017; Narud et al., 2022), capacity for hyperactive motility and sperm metabolism for energy production (Garrett et al., 2008; Narud et al., 2022). No single *in vitro* lab analysis can accurately predict sire fertility from semen characteristics (Narud et al., 2022), but even multiplex tests cannot currently provide accurate sire fertility prediction.

Clearly bull fertility has many challenges. Despite the substantial annual economic losses due to poor fertility, the sperm physiological mechanisms responsible are still only partially understood and there are no reliable laboratory methods or cost-efficient bio-markers to predict male fertility (Parisi et al., 2014). Better understanding of sperm structure, physiology and molecular functions is needed to understand critical aspects of fertilization more fully. As multiple proteins participate in signaling pathways that control fertility, there is need to elucidate the proteins by proteomics of the plasma membrane especially in the sperm head, which is one of the first areas involved in capacitation and sperm-egg binding, while the tail and other cellular components drive hyperactivation, penetration and other critical processes .

2.3 Structure of the Mammalian Spermatozoa

An ejaculated mature mammalian spermatozoan is an elongated cell with a head containing the nucleus, connected at the head's base to a tail (Teves & Roldan, 2022) the whole of which is bounded by a continuous plasma membrane. The sperm morphology/ Bauplan is an important aspect of clinical examination (Mortimer, 1994; Coetzee, 1998; World Health Organization, 2010; Bjorndahl & Kvist, 2010). Generally, the ideal shape of a human spermatozoan is an oval head (4-5 μm long, 2-3 μm wide, 0.3-0.5μm thick; Maree et al., 2010), with smooth outline and prominent, clearly defined acrosome covering 40-60% of the anterior head (Bjorndahl & Kvist, 2010). The connecting piece (0.3-1.5 μm) connects the head to the tail (45 to 50 μm; Bjorndahl & Kvist, 2010) that contains the 9 + 2 microtubule structure of the axoneme (Linck et al., 2016) to provide motility (Saacke & Almquist, 1964; Garner & Hafez, 1993) and is symmetrically inserted with connecting piece cytoplasm in humans and cytoplasmic droplet in ungulates. The tail consists of the midpiece (10 μm long; Bjorndahl & Kvist, 2010), principal piece (45-50 μm) and terminal piece (2-4 μm; Garner & Hafez, 1993).

2.3 Detailed Structural Features of the Spermatozoon

2.3.1 Sperm Plasma Membrane

The sperm plasma membrane is the outermost part of the spermatozoa, with an important role in sperm motility, fertilizing ability and transport of ions across sperm membrane (Cornwall, 2008; Gadella & Boerke, 2016).The membrane bilayer contains phospholipids, cholesterol, and proteins (Gadella et al., 2008; Mortimer, 2018) organized non-randomly to accomplish necessary various functions (Rana et al., 1993; Flesch & Gadella, 2000). Lipids are asymmetrically distributed in the bilayer, with the majority of phosphatidylethanolamine (PE) and

phosphatidylserine (PS) in the inner leaflet of the bilayer and the majority of sphingomyelin (SM) and phosphatidylcholine (PC) in the outer leaflet. Transmembrane lipid transporter proteins such as flippases, floppases, and scramblases mediate lipid movement (also called a "flip-flop" transition) across the membrane (Contreras et al., 2010). All movement, both transmembrane (across the bilayer) and transverse (in the plane of a leaflet), of membrane molecules including lipids, proteins, and sterols, are impacted by membrane fluidity.

Like membranes from many cells, the sperm plasma membrane has specific regions known as domains and microdomains that have specialized composition (Kawano et al., 2011; Boerke et al., 2014; Gadella & Luna, 2014). Rafts are a particular type of microdomain that are highly dynamic in nature and house different lipids and signaling proteins with role(s) in sperm signaling pathways (Simons & Toomre, 2000; Simons & Sampaio, 2011; Rajamanickam et al., 2017; Sajeevadathan et al., 2021). During sperm capacitation, cholesterol efflux occurs from non-raft fraction of the plasma membrane with no or minimal depletion of cholesterol from rafts. The SNARE proteins in sperm go through lateral redistribution along as do complexes of ZP binding protein and raft marker proteins (Boerke et al., 2008).

The plasma membrane around the sperm is differentiated based on the specific regions like sperm head, acrosome cap, midpiece and tail, and the plasma membrane of each area has a different appearance, indicating that the membrane in each region performs unique/specific function(s) in sperm's life (Koehler, 1972; Stackpole & Devorkin, 1974; Peterson & Russell, 1985).

2.3.2 Acrosomal Membranes

The head of a mature spermatozoon has the plasma membrane as the outermost structure. Underlying the anterior portion of the head is the acrosome, which is a vesicle that lies like a cap over the nucleus (Garner & Hafez, 1993; Gadella & Evans, 2011). The acrosomal membrane

abutting the nucleus is the inner acrosomal membrane, while the outer acrosomal membrane lies closest to the plasma membrane. The acrosome originates from the Golgi complex in the spermatid during spermatid differentiation (Senge, 2012) and has two segments, the acrosomal cap (anterior acrosome) and the equatorial segment (posterior acrosome) (Senger, 2012; Chemes, 2017; Mortimer, 2018). The acrosome contains many hydrolytic enzymes including acrosin, hyaluronidase, zona lysine, esterases and acid hydrolases (Senger, 2012) that are involved in fertilization (Garner & Hafez, 1993; Teves & Roldan, 2022). In spermatozoa, the acrosomal membrane engages in gamete fusion due to the presence of some unique factors (Gadella & Evans, 2011). The nucleus underlying the acrosome contains the condensed chromatin material (Garner & Hafez, 1993; Teves & Roldan, 2022).

2.3.3 Sperm Tail

The sperm tail is composed of the middle piece, the principal piece, and the terminal piece (Senger, 2012; Mortimer, 2018). The capitulum which is one part of connecting piece fits into the implantation fossa, a depression in the posterior nucleus. Mitochondria are arranged in a helical pattern along the longitudinal fibers of the midpiece; this mitochondrial sheath provides energy for sperm metabolic activities. The sperm tail, similar to flagella or cilia, has nine pairs of microtubules that are arranged radially around two central filaments to provide motility (Saacke & Almquist, 1964; Senger, 2012; Linck et al., 2016; Mortimer, 2018).

2.4 Sperm Capacitation and the Acrosomal Exocytosis

The mammalian spermatozoa freshly produced by the testis pass through several maturation steps such as changes in membrane lipid composition, remodeling of raft membrane microdomains and other plasma membranes structures, modifications to surface glycoproteins, and surface antigen re-localization (Girouard et al., 2011) in the male reproductive tract, completing

in the female reproductive tract. These multistep changes in the female reproductive tract commencing from influx of bicarbonate and calcium ions, changes of pH, removal of decapacitating factors, and sperm proteasomal activities with increased tyrosine phosphorylation (Tyr-P) (Chang, 1951; Yanagimachi, 1994) are known as capacitation which leads to acrosomal exocytosis (AE; Austin, 1952; de Lamirande, 1997; Mostek et al., 2021). Sperm capacitation in the fluid of the female tract consists of a series of cellular, biochemical, functional, and physiological changes in sperm, including rearranging the protein and lipid molecules in the plasma membrane, loss of membrane cholesterol (thus changing the cholesterol/phospholipid molar ratio), as well as protein phosphorylation, ionic fluxes and increase in intracellular cyclic AMP levels (Fraser & Ahuja, 1988) enabling spermatozoa to bind and penetrate the zona pellucida (ZP) through a process known as the AE (Sutovsky, 2018). The AE involves a multiple fusion of the sperm's HPM with its outer acrosome membrane leading to vesiculation (Yanagimachi & Usui, 1974), that accompanies the altered motility kinetics known as hyperactivation (Senger, 2012).

Many events of capacitation, AE and hyperactivated motility are calcium dependent (Fraser & Ahuja, 1988). While these events naturally occur in the female reproductive tract *in vivo*, they can be induced *in vitro* facilitating scientific study.

Capacitation is known to be characterized by a cascade of cellular events that include cAMP production, activation of Ca^{2+} channels, generation of ROS species, efflux of cholesterol, increasing intracellular pH and stimulation of kinases proteins (de Lamirande & O'Flaherty, 2012), with *in vitro* induction of capacitation requiring species-specific agents like serum albumin, sodium bicarbonate ($NaHCO_3$) and Ca^{2+} (Harrison, 1996; Visconti et al., 1998). While early capacitation may be reversable, full capacitation primes sperm for AE.

As the spermatozoon contacts the oocyte, the AE releases the hydrolytic enzymes contained in the acrosome (Jin et al., 2011) in an irreversible exocytotic process that aids sperm penetration of the ZP. In mammalian sperm, the acrosome is a structure similar to a large secretory vesicle (Florman et al., 1998) and its exocytosis is comparable to a strictly regulated secretory event. Capacitation leads to the AE, and multiple fusions of the outer acrosomal membrane (OAM) with the overlying HPM. At the fusion points, OAM: HPM hybrid vesicles are formed, allowing acrosomal enzymes including the trypsin-like acrosin (Sutovsky, 2018) to be released into the milieu around the head of the sperm (Honda, 2002; Harper et al., 2006). Moreover, signal transduction events occurring during capacitation and AE alter the sperm actin cytoskeleton contributing to membrane structural changes (Breitbart, 1997; Breitbart et al., 2005). Loss of the OAM and acrosomal contents exposes the inner acrosomal membrane (IAM), and its components which are crucial for the next steps: sperm binding to the oolemma, followed by the steps of syngamy. These steps are known to be essential for fertilization

2.4.1 Membrane Changes during Capacitation

Capacitation occurs when decapacitating factors from the sperm's outer surface are removed. There are various decapacitating factors including GPI anchored proteins CD55, CD52, and seminal plasma proteins (Girouard et al., 2011), which are assimilated onto sperm during transit through male reproductive tract (Boerke et al., 2014). In the female reproductive tract, removal of these decapacitating factors exposes molecules which bind the spermatozoa to the oocyte (de Lamirande et al., 1997; Senger, 2012).

In conducive environments such as the female reproductive tract, the influx of HCO_3^- into sperm activates the cAMP-PKA pathway and loss of membrane asymmetry. Removal of cholesterol from the plasma membrane during capacitation also supports the activity of

scramblase. Scramblase is an enzyme on the sperm plasma membrane that destroys membrane architecture and symmetry. Scramblase is a phospholipid translocator protein that is responsible for the movement of phosphatidylcholine (PC) from the inner leaflet to the outer leaflet of the plasma membrane (Khalil et al., 2006).This process is called "flippase" and it is essential for the remodeling of the plasma membrane, which is important for various cellular processes such as cell signaling, cell division, and cell migration. Cholesterol efflux during capacitation largely removes cholesterol from non-raft regions of sperm plasma membrane (Khalil et al., 2006), while raft protein composition changes (Cross, 2004). Various proteins move in and out of the rafts, such as GM1 and CD59 leaving the raft regions of human sperm (Cross, 2004). The combined membrane changes of altered cholesterol: phospholipid ratio, change in ionic balance, lipid and protein remodeling alter plasma membrane fluidity and contribute to the activation of various pathways for signal transductions (Primakoff & Myles, 2002; Martínez-López et al., 2009).

Capacitation's influx of Ca^{2+} and $HCO3^-$ and the accompanying appearance of reactive oxygen species (Flesch & Gadella, 2000) accelerate sperm plasma membrane fluidization and depolarization (Flesch & Gadella, 2000), and the various activated pathways, result in Tyr-P of proteins. The appearance of Tyr-P proteins is considered diagnostic of sperm capacitation (Thundathil et al., 2006; Salicioni et al., 2007; Newton, et al., 2010).

2.4.1.1 Bicarbonate

Bicarbonate is of paramount importance in sperm capacitation (Battistone et al., 2013; Macías-García et al., 2015). The concentration of $HCO3^-$ is higher in the female reproductive tract than in the epididymis, and a $Na^+/HCO3^-$ cotransporter stimulates a rapid influx of $HCO3^-$ ions in the female tract, increasing sperm intracellular pH (Demarco et al., 2003). This activates soluble adenyl cyclase (sACs) producing cAMP, protein Kinase A (PKA) and the Tyr-P of sperm proteins

(Steckler et al., 2015). Increased HCO_3^- activates scamblase enzymes that move four phospholipid species (PC, SM, PE, and PS) inward and outward across the lipid bilayer destroying the asymmetric distribution of phospholipids (Contreras et al., 2010). This redistribution of phospholipids acts as a prerequisite for cholesterol efflux which renders the sperm membrane fusogenic and responsive to ZP glycoproteins (Gadella & Harrison, 2000; Harrison & Gadella, 2005).

2.4.1.2 Cholesterol Efflux

Addition of cholesterol during epididymal maturation in plasma membrane protects the sperm in initial transit through the reproductive tract (Saez et al., 2011). Under the influence of cholesterol acceptors such as high-density lipoproteins and albumin in the female tract, cholesterol is removed from the sperm plasma membrane (Visconti et al., 2002), increasing membrane fluidity and promoting membrane structural modifications. Hamster spermatozoa incubated in capacitation media lacking the cholesterol acceptor albumin fail to capacitate (Noguchi et al., 2008). Bicarbonate ions redistribute cholesterol on the sperm plasma membrane, because the scamblase's increased intracellular concentration modifies membrane architecture (Gadella & Harrison, 2000), making cholesterol more available to cholesterol acceptors in the reproductive tract (Salicioni et al., 2007; Visconti, 2009). Indeed, in the absence of $HCO3^-$ ions but with cholesterol acceptors present in capacitation medium, the cholesterol level in membrane is unchanged (Gadella & Leahy, 2015).

In addition to albumin, other cholesterol acceptors like High-density lipoprotein (HDL) and β-cyclodextrins effectively support capacitation (Jones et al., 2007). It is also interesting that the action of these β-cyclodextrins, serum albumin, and HDL is somehow coupled to the cAMP dependent pathway (Jones et al., 2007).

Cholesterol alters the bulk properties of biological membranes by increasing the orientation order of the membrane lipid hydrocarbon chains, restricting the ability of membrane proteins to undergo conformational changes in this less-fluid membrane. Hence high contents of cholesterol can inhibit capacitation indirectly by diminishing the conformational freedom and the biological activity of sperm surface proteins. Cholesterol might also directly interact with specific membrane proteins impacting their function. Therefore, either directly or indirectly, cholesterol could modulate ion transporters and effector enzymes like sAC (Martínez & Morros, 1996).

2.4.1.3 Calcium

Another key molecule involved in regulation of capacitation is calcium. During the process of capacitation concentration of intracellular Ca^{+2} is increased. pH associated structural changes and membrane hyperpolarization as well bicarbonate ion concentration causes the opening of various calcium-associated channels especially CatSper and voltage-gated channels which ultimately result in influx of Ca^{2+} in the sperm (Navarrete et al., 2015). Calcium plays a role in parallel to bicarbonate ions and induces capacitation by stimulating sAC. For activation of the sperm signaling pathways for hyperactivation and AE, the elevated amount of cytosolic Ca^{2+} is an essential process. Furthermore, Ca^{2+} is important for rafts aggregation towards the apical region of the plasma membrane (Gadella & Leahy, 2015) and low concentration of Ca^{2+} ions cause membrane proteins to randomly distribute in the head surface of boar sperm membrane (Aguas & Pinto da Silva, 1983).

2.4.1.4 Tyrosine Phosphorylation (Tyr-P)

Tyr-P is the most important molecular event in sperm capacitation and fertilization (Signorelli et al., 2012; Campbell, 2013). As sperm are transcriptionally inactive, the only way to alter their activity is through post-translational modifications (PTMs) controlled partially through

phosphorylation of sperm proteins. Indeed, an alternate role for $HCO3^-$ is the stimulation of a sperm-specific sAC that in turn increases production of cAMP that activates PKA causing Tyr-P of a myriad of target proteins. Increased Tyr-P leads to many of the important aspects of the process of capacitation, like the induction of hyperactivated motility. The PKA pathway can be further enhanced by cross-talk with an alternate pathway that is stimulated by removing decapacitating factors such as phosphatidylethanolamine binding protein 1(PEBP1), thereby removing its suppression of Raf-1, an important part of the extracellular signal regulated kinase family of protein kinases activated by mitogen (Visconti, 2009; Nixon et al., 2010). Tyr-P of serine/threonine residues of various kinases induced by cAMP/PKA and ERK1/2 pathways activate cytoskeletal, metabolic enzymes and ion channels proteins, stimulating hypermotility of sperm, subsequent AE, ZP binding and then fertilization (Sutovsky, 2018). A-kinase anchoring proteins (AKAPs) are a major target of Tyr-P in mammalian sperm, with AKAP4 being involved in Tyr-P pathways in sperm from human (Ficarro et al., 2003; Rahamim Ben-Navi et al., 2016) cattle (Jagan Mohanarao & Atreja, 2011; Byrne et al., 2012) mouse (Johnson et al., 1997; Moss et al., 1999; Jivan et al., 2009) and hamster (Jha & Shivaji, 2002; Kota et al., 2009). PKA is one of the important different domains in AKAPs, which when activated form complexes with other signaling molecules (Miki & Eddy, 1999; Skroblin et al., 2010; Welch et al., 2010) likely contributing to the loss of motility and sperm fertility when AKAP4 is deleted (Miki et al., 2002). Sperm proteomics through LC-MS/MS can provide in depth analysis for the tyrosine phosphorylated proteins in the capacitated sperm (Gur & Breitbart, 2008; Signorelli et al., 2012; Campbell, 2013).

2.5 Proteomics

The term “protein” was coined by Berzelius in 1838 (Cristea et al., 2004) from the Greek “proteios” meaning “the first rank”, and “proteome” denotes the proteins contained in an

organism's cell whether from human, (Schwenk et al., 2017); plants, (Mohanta et al., 2019); animals, (Chen et al., 2019) or bacteria (Aslam et al., 2017). 'Proteomics' assesses characteristics of proteins at a specific window in time including localization, structural analysis, expression, functions, protein-protein interaction, and PTMs (Domon & Aebersold, 2006). The proteome of eukaryotic cells is more dynamic over a cell's lifetime than that of prokaryotes (Krishna & Wold, 1993). Proteomics methodologies help identify the numerous functions of genes through the dynamic complexity of their products as cells respond to their changing environments (Lander et al., 2001).

2.5.1 Proteomics Technologies

Proteins have been purified and identified by chromatographic techniques (size exclusion, affinity, and ion exchange; (Jungbauer & Hahn, 2009; Voedisch & Thie, 2010; Hage et al., 2012); western blotting, and enzyme linked immunosorbent assays. Proteins in complex biological mixtures can be isolated by one (1D)- or two (2D)-dimensional sodium dodecyl sulfate (SDS)-polyacrylamide gel electrophoresis (PAGE) and 2D difference gel electrophoresis (Dunn, 1991; Marouga et al., 2005; Issaq & Veenstra, 2008). Mass spectrometry (MS) can analyze these biological proteins with higher sensitivity, high throughput (Yates, 2011), and accurately determine molecular weight, chemical structure, and quantity (Aicher et al., 1998; Loo et al., 1999).

2.5.2 Mass Spectrometry

MS is a powerful technique of analytical chemistry by which structural information of a wide range of molecules is determined by measuring their mass to charge ratio (m/z), and using that for molecular characterization (Ji, 2015). MS is a very sensitive and fast technique that needs very little sample for its analysis unlike other techniques that demand high sample purity and

relatively large amounts. MS's high accuracy, efficiency and sensitivity have led to its wide use as a reliable and indispensable technique in the field of proteomics (Yates et al., 2009) and today MS is playing a significant role in various fields such as analytical chemistry, molecular biology, environmental science, drug discovery, clinical diagnosis, and archeology (Ji, 2015).

2.5.2.1 Bottom-Up Proteomics

In bottom-up proteomics studies, proteins are proteolytically digested into peptides with the use of specific proteases. The peptides are separated either by 1D (reverse phase-high performance liquid chromatography; RP-HPLC) or 2D chromatographic separation (strong cation exchange chromatography; SCX and RP-HPLC) and then analyzed by LC-MS/MS to determine their fragmentation patterns, their precursor and product m/z ratios, and consequently their peptide sequence. All experimental methodologies starting from complete protein digestion to peptide analysis and protein characterization using a protein database are termed bottom-up proteomics (Dupree et al., 2020).

Peptides are used over proteins because they separate more easily in reversed-phase LC and their complete ionization fragmentation is more predictable (Rogers & Bomgarden, 2016), providing a more robust methodology for identification and quantification of thousands of different proteins in a complex mixture by high throughput analysis (Cristobal et al., 2017). Currently, bottom-up approaches which are based on data-dependent acquisition (DDA) workflows, also known as shotgun proteomics, are the key fundamental technologies in proteomics. This technique of DDA generates a large list of proteins that helps to solve the most complex and full proteomes including the human proteome (Kwon et al., 2014; Wilhelm et al., 2014).

Digestion in bottom-up proteomics is done by trypsin, the gold standard for about 96% of the deposited data sets generated through shotgun proteomics (Fenyö & Beavis, 2015). Trypsin is ideal for collision induced dissociation (CID) based MS/MS analysis because it efficiently cuts proteins at arginine and/or lysine residues at the C-terminus with specificity and high catalytic activity (Kiser et al., 2009). Also, about 56% of all the peptides produced have ≤ 6 amino acid residues, which are easily identified by MS (Tsiatsiani & Heck, 2015) .

2.5.3 Mass Analyzers

The central part of the mass spectrometer is mass analyzer which measures the m/z ratio of the generated ions. The key parameters that define the performance of the analyzer are mass resolution, mass accuracy and transmission efficiency (TE; Aebersold & Mann, 2003). Mass resolution power corresponds to the mass analyzer's differentiation of ions with closely separated m/z values. The mass accuracy describes the difference between theoretical and experimental m/z values and is usually shown as a ratio of mass measurement error to the theoretical mass in parts per million (PPM), with low mass measurement error (low PPM) indicating more reliable identification. The TE defines the percentage of ions that originate from the ions' source and successfully reach the detector. TE influences the sensitivity of the instrument and indicates the minimum amount of sample able to produce detectable signals. Therefore, for analyzing low abundant protein samples, high sensitivity of the instrument is especially important (Ji, 2015).

There are generally three basic components of the mass spectrometer including ion source, mass analyzer and detector (Fig 2.1). In the ionization chamber the intact molecular ions are produced and are transferred to the mass analyzer. The salient function of the mass analyzer is to sort and separate the ions according to their m/z ratio. The separated ions travel towards the detector system for the concentration measurement and are shown on a chart known as mass

spectrum. Due to high reactivity and short life of the ions in gas phase, their production and manipulation is performed under high vacuum (Ji, 2015).

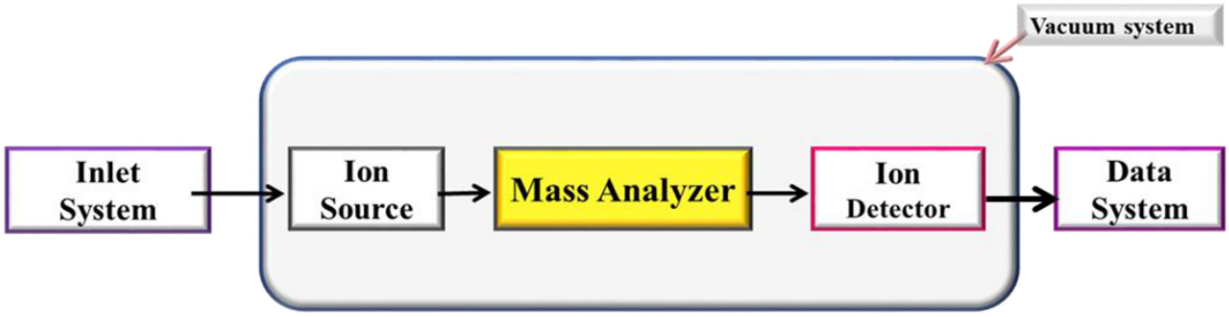

Figure 2.1. Overview of the components of a mass spectrometer (adapted from Sallam, 2017).

2.5.3.1 Ion Sources

In the past, due to unavailability of complete and reliable ionization methods, analysis of full proteins by MS was a hard goal to achieve with various challenges. Since proteins are large, thermally unstable, and nonvolatile molecules, they could not be volatized without thermal degradation (Ji, 2015), limiting MS for a long time to analysis of small molecules. With the discovery of soft ionization techniques, the application of MS spread to analysis of complex and larger biomolecules. This led to the emergence of modern proteomics and today the two most important ionization methods, electrospray ionization (ESI) and matrix-assisted laser desorption ionization (MALDI), are widely used (Ji, 2015).

2.5.3.1.1 Electrospray Ionization (ESI)

ESI was first introduced into the world of proteomics by Nobel Prize winner John Fenn (Fenn et al., 1989) and currently is the most popular ionization technique in modern MS (Wang et al., 2022). During ESI, the analytes are transferred under atmospheric pressure directly from solution to gas phase. The most widely accepted mechanism of the ESI is shown in Fig 2.2.

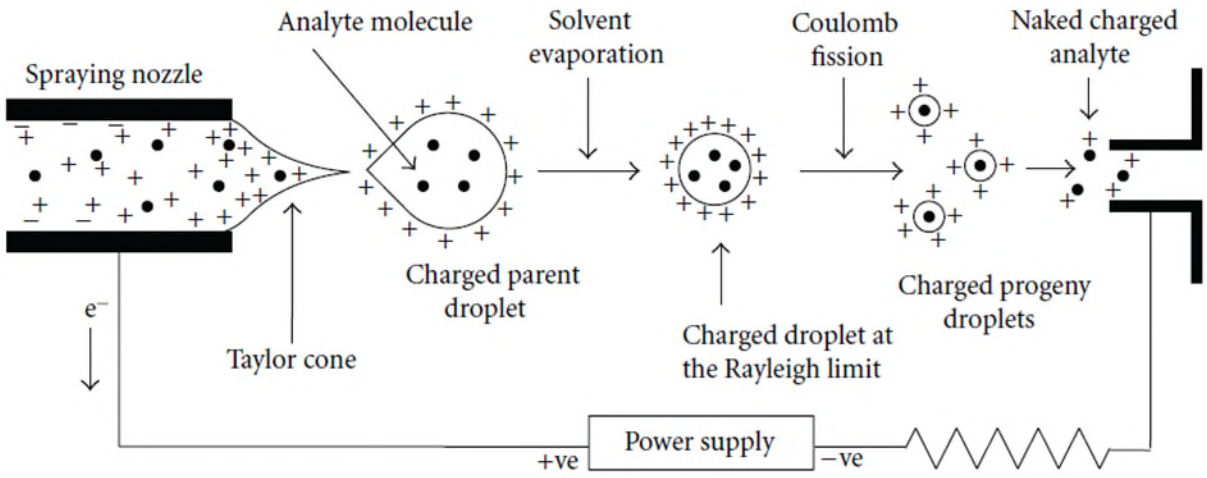

Figure 2.2. Schematic proposed representation of ESI technique, adapted from Banerjee & Mazumdar, (2012).

Briefly, the analyte is loaded into a capillary to which high voltage is applied. The strong electric field pushes the solution forward making a Taylor cone at the tip's end. When the electrostatic forces dominate the surface tension, the droplets carrying the charge bud off continuously from the Taylor cone. A fine mist of the charged droplets is formed with the help of nebulizer gas during this phase (Banerjee & Mazumdar, 2012).

Charged droplets evaporate while traveling towards the analyzer inlet, shrinking their size but increasing their surface charge density. Larger droplets are broken down to smaller droplets when charge repulsion rises, then surface tension shrinks droplets during the process known as Coulomb fission. This process of Coulomb fission and solvent evaporation repeats itself until each droplet consists of naked and charged analyte, produced by evaporation of the molecule (Banerjee & Mazumdar, 2012).

2.5.4 Tandem Mass Spectrometry

In modern MS technology, two spectrometers are used in conjunction, commonly known as tandem MS. In tandem MS, two mass analyzers or two different analyzers are combined in

tandem to enhance their efficiency. For example, a quadrupole (Q) and a time of flight (TOF) can be in tandem to form a Q-TOF mass analyzer (Emily, 2016).

In MS, the first precursor ion is separated then converted into fragment ions to determine the composition of the precursor ion. For the purpose of fragmentation, there is a fragmentation cell between two mass analyzers and different fragmentation techniques are employed depending on the mass analyzer's composition (Emily, 2016).

Collision-induced dissociation (CID) is a type of threshold dissociation in which weakest bonds are broken. In this technique, an electric field is applied to accelerate the precursor ions which collide with neutral gas molecules to induce bond cleavage in the precursor ions. In Electron-transfer dissociation (ETD) techniques, ions containing positive charge (≥2+) are transferred as an electron which causes destabilization of the precursor ions and fragmentation occurs. In CID fragmentation, b and y ions are produced as the fragmentation occurs between the R-COOH of one amino acid and the NH2 of the adjacent amino acid. In ETD, dissociation process fragments the proteins backbone from the C-terminus of NH2 group to produce C and z ions (Lingdong Quan, 2013).

2.6 Quantitative Proteomics

Increased sensitivity and accuracy of MS through improving sample preparation, protein/peptide fractionation and shotgun methods have made it possible to obtain complete lists of proteins in certain organisms with a reasonably analytical intricacies (de Godoy et al., 2008; Schrimpf et al., 2009). Moreover, MS has enabled characterization of more than 10,000 proteins in cultured cell lines (Beck et al., 2011; Nagaraj et al., 2011). Changes in biological functions may be detected through qualitative analysis of monitored changes in protein abundance or expression, potentially leading to relative quantification of the proteins present in a sample. Quantitative

proteomics use two approaches, label free and stable isotope labeling, to determine the relative amount of a peptide or protein present. Label free process assesses amounts of peptides or proteins either through MS ion intensity or number of acquired spectra matching proteins or peptides (Bantscheff et al., 2007; Zhang et al., 2013). In the isotope labeling approach, at various stages of the experiment, multiple samples are mixed, and absolute or relative protein abundance is attained with measurement of intensities of various isotopes coded-peaks (Washburn et al., 2001; Liu et al., 2004; Gilchrist et al., 2006). Isotope labeling has limitations including inefficient labelling, cost, additional steps in sample processing, limitation of sample number and limited ability to detect proteins of low abundance. Two label-free methods that minimize these drawbacks are spectral counting that quantifies spectra from a particular protein/peptide and ion intensity that quantifies the signal intensity of peptide peaks belonging to a particular protein (Bantscheff et al., 2007; Zhang et al., 2013).

2.6.1 Relative Quantification

2.6.1.1 Label Free Quantification

Label-free quantification can utilize either spectral counting or ion intensity. Spectral counting quantifies peptide spectral matches for a specific protein and associates the matches to the amount of the protein (Washburn et al., 2001; Liu et al., 2004; Gilchrist et al., 2006). This method is optimal when resolution is from low to moderate and employs simple normalization and statistical analysis. The normalized spectral abundance factor (NSAF) method (Florens et al., 2006; McIlwain et al., 2012; Langley & Mayr, 2015) is used for calculation of the abundance of proteins. In the ion intensity-based approach, all chromatographic peak areas of a target protein are integrated in the form of area under curve (AUC), which is directly associated with the concentration of peptides (Bondarenko et al., 2002; Chelius & Bondarenko, 2002) . This protein

quantification approach is based on AUC measuring the ion abundance of a given ionized peptide, called ion count, at a specific retention time. This quantification works best for the given detection limit of a particular MS instrument (Podwojski et al., 2010).

Various factors that need to be considered when one uses ion intensity-based approach include: coeluting peptides, when there is wider window of retention time for peptide signals; multiple signals from the same peptide due to retention time variation; sensitivity and speed of the MS instrument and background noise. These issues have been addressed by developing various computational tools that align retention times of peptides across various sets, to provide mass accuracy, optimize background noise and normalize peak abundance (Listgarten & Emili, 2005).

2.7 Bioinformatics Analysis

Bioinformatics databases and tools have been developed to deal with the huge quantity of proteomics data, enabling prediction of 3D protein structure, transmembrane domains, motifs, protein-protein interactions, and biological functions (Perez-Riverol et al., 2015). The alignment tools developed assist in identifying structure and sequences and deriving evolutionary relationships among proteins. Analysis of the proteome helps provide a complete picture of structure and function of the cell, including the cell signaling pathways that regulate the cell function in response to various endogenous and exogenous stimuli (Vihinen, 2001; Perez-Riverol et al., 2015; Aslam et al., 2017).

2.8 Proteomics of Mammalian Sperm

Identification of all the proteins present in the cell can help understand the dynamics of cell functions and the novel ‘omics of proteomics, genomics, transcriptomics, and metabolomics tools that may hold the key for accurate diagnosis of male infertility (Peddinti et al., 2008). Proteomics of sperm of various species have been investigated [human (Martínez-Heredia et al., 2006;

Schwenk et al., 2017); bull (Byrne et al., 2012; Park et al., 2012); boar (Kwon et al., 2015; Rahman et al., 2017); mouse (Baker et al., 2008); rat (Baker et al., 2008); ram (Pini et al., 2016); stallion (Swegen et al., 2015)], and increasingly proteomics is being applied specifically to the biological mechanisms of function and oocyte interaction (Wright et al., 2012). Proteomics have identified protein biomarkers in bull sperm associated with fertility (Peddinti et al., 2008; Somashekar et al., 2017; Muhammad Aslam et al., 2018) and sperm proteins from males of high and low fertility have been compared in buffalo (Muhammad Aslam et al., 2018; Singh et al., 2018) and Holstein bulls (D'Amours et al., 2018, 2019), in frozen bull semen (Singh et al., 2018), in Holstein Friesian × Sahiwal bull seminal plasma (Druart et al., 2013; Muhammad Aslam et al., 2014; Viana et al., 2018; Kasimanickam et al., 2019) and Brahman (Bos indicus) bulls' sperm surface proteome (Byrne et al., 2012).

Beyond simple lists of proteins, advanced proteomics have associated sperm functional states to abundances of sperm proteins from high and low fertility bulls (D'Amours et al., 2010; Kwon et al., 2014, 2015) from immature and mature sperm (Belleannee et al., 2011; Cui et al., 2016), epididymal and ejaculated sperm (Dacheux & Dacheux, 2014), frozen-thawed and fresh sperm (Chen et al., 2014) and capacitated (Kwon et al., 2015) and non-capacitated spermatozoa (Kwon et al., 2015; Rahman et al., 2017).

2.8.1 Fertility Associated Proteins in the Sperm

Fertility in mammalian sperm depends upon orchestrated complex reactions that commence from spermatogenesis in the male testes and terminate with sperm-oocyte penetration. In this multi-step process, any defect can lead to subfertility or infertility. One of the many approaches to predict sperm fertility is the identification of the important sperm proteins that differ among fertile, sub fertile, and diseased sperm at the proteome level (Ashrafzadeh et al., 2013;

Somashekar et al., 2017). The proteome of the bull sperm membrane consists of hundreds of different proteins, the majority of whose functions are unknown. In this proteome, there must be many proteins involved in different events of sperm fertilization. In this context, the presence, absence, over- or under-expression of specific proteins in the sperm membrane may change sperm functions, compromising or enhancing the sperm fertilizing ability. Such changes in expression can come from genes directly or indirectly encoding for "fertility" proteins.

2.8.2 Proteins involved in Signaling Pathways

Many signals are transduced by extracellular signals that bind to membrane proteins utilize pathways such as cAMP/PKA, MAPK, PI3K-Akt and PLC-PKC. Each of these involves activation of multiple kinase proteins and ultimately results in Tyr-P and stimulating the final response of the target cell.

In the cAMP/PKA pathway, on binding of the ligand, G-protein coupled receptors activate the G-protein which then activates sAC that cleaves ATP to produce cAMP (Larsson et al., 2016; Song et al., 2017); in sperm, $HCO3^-$ can stimulate a sperm specific sAC (Parrish, 2014). Regardless of how it is generated, the resultant elevated concentration of cAMP activates cytosolic PKA that phosphorylates serine/threonine residues that leads to Tyr-P of various sperm proteins (Bailey et al., 2010). Increase in concentration of Tyr-P induces many of the important aspects of the process of capacitation, as noted in section 2.4 above.

A separate, rapid response to extracellular signals utilizes a PLC/PKC pathway. Binding of a ligand to its membrane-bound receptor activates Phospholipase C (PLC), which is found in plasma membrane (Kadamur & Ross, 2013). PLC then cleaves the membrane phospholipid phosphatidylinositol 4, 5 bisphosphates (PIP2), producing 1, 2 diacylglycerol (DAG) and inositol 1, 4, 5 trisphosphates (IP3). IP3 and DAG both function as second messengers and act on different

target proteins. The IP3 binds to its receptor IP3R and causes an increase in intracellular Ca^{2+} ions (Rajamanickam et al., 2017), while DAG activates various enzymes and structural proteins while binding to conserved domain (Kadamur & Ross, 2013). Both $Ca^{2+}$and DAG act together to activate PKC (Yuan et al., 2005; Zhang et al., 2008; Reinhard et al., 2013; Aperia et al., 2016), which acts on target intracellular proteins to produce the cellular response (Kadamur & Ross, 2013; Rajamanickam et al., 2017).

2.9 Na^+/K^+-ATPase

Na^+/K^+-ATPase is transmembrane protein belonging to the P-type adenosine triphosphatase superfamily and is ubiquitous in mammalian cells (Kaplan, 2002; Morth et al., 2007). It has been found in various body cells with two distinct functions; first, it facilitates the transportation of the Na^+ and K^+ ions across the cell membrane against the concentration gradient (for this action it is named the Na^+/K^+ pump) (Kaplan, 2002) and secondly, it is involved in signal transduction (Thundathil et al., 2006). It is comprised of two major polypeptide subunits, the larger alpha (α) and the shorter beta (β).

2.9.1 Structure of Na^+/K^+-ATPase

The α subunit of Na^+/K^+-ATPase has a molecular weight of 110 kDa consisting of over 1000 amino acid residues that form ten transmembrane helices but is primarily located on the inner leaflet of the plasma membrane; there are four α isoforms (α1, α2, α3, α4; Kaplan, 2002; Morth et al., 2007; Geering, 2008). When it functions as an enzyme, conformational changes of the α subunit allow it to pump the Na^+ and K^+ ions in and out of the cell. The α isoforms also contain receptor site(s) for its specific hormone ouabain, and binding to ouabain stops the enzymatic function and stimulates the signaling function of Na^+/K^+-ATPase (Kaplan, 2002).

The β subunit consists of approximately 370 amino acids (Kaplan, 2002) and is heavily glycosylated (Hickey & Buhr, 2012), resulting in its molecular mass ranging from 35-60kDa. In mammalian tissues, β has three isoforms (β1, β2, β3). The β subunit has a significant portion external to the plasma membrane and is responsible for localizing and stabilizing the protein within the plasma membrane, aiding enzyme activity without catalytic involvement (Woo et al., 2000; Geering, 2008). The β subunit facilitates α's insertion in the plasma membrane, and its active transport of the ions across membrane aids maintenance of resting membrane potential (Geering, 2008). The β subunit also plays an important role during Na^+/K^+-ATPase signaling pathways in the cell; β1 is also involved in cell adhesion (Vagin et al., 2012).

2.9.2 Function of Na^+/K^+-ATPase as Sodium Pump

Na^+/K^+-ATPase aids cellular equilibrium by transporting Na^+ and K^+ ions across the membrane to maintain resting membrane potential and osmotic pressure, and support transportation of ions, amino acids, and glucose molecules across the membrane. The functioning of the sodium pump is based on energy that is derived from hydrolysis of ATP molecules, exchanging 3 Na^+ ions out of the cell and 2 K^+ ions into the cell (Kaplan, 2002). It is found in both raft and non-raft part of the cell membrane performing as a sodium pump (Liu et al., 2011).

2.9.3 Na^+/K^+-ATPase as a Signaling Molecule

The other important function of Na^+/K^+-ATPase is as a receptor stimulating signal transduction as reported in cardiac myocytes, neuronal cells, renal epithelial cells, vascular smooth muscle cells, and sperm (Xie & Askari, 2002; Xie, 2003; Liu & Askari, 2006; Thundathil et al., 2006; Tian et al., 2006; Tian & Xie, 2008; Zhang et al., 2008; Pierre et al., 2008; Quintas et al., 2010; de Juan-Sanz et al., 2013; Reinhard et al., 2013; Singh & Rizvi, 2015; Zhou et al., 2015;

Aperia et al., 2016; Peng et al., 2016; Cui & Xie, 2017; Rajamanickam et al., 2017; Sajeevadathan et al., 2019).

Na^+/K^+-ATPase binds specifically to the steroid ouabain, which inhibits the enzymatic function (Khalid et al., 2014) and acts as a hormone stimulating signal transduction (Sajeevadathan et al., 2019). The α subunit has two ouabain binding sites of differing affinity (Morrill et al., 2008; Sandtner et al., 2011; Alsaadi et al., 2014). The α subunit has two caveolin binding motifs (CBM), one towards N-terminus on helix 1 that functions mostly as receptor for ouabain (e.g., boar kidney cells, H. Wang et al., 2004) , and the other at the C-terminus on helix 10 (Xie, 2003). The binding of Na^+/K^+-ATPase to caveolin does not impact its pumping functions as the two CBM are located away from catalytic domain of Na^+/K^+-ATPase. Nevertheless, the other CBM is located on N-terminus which is sited close to the α subunit that has the ouabain binding domain. This structural proximity may support Na^+/K^+-ATPase's role as signal transducer, since Na^+/K^+-ATPase interacts with caveolins upon ouabain induction in porcine kidney cells (Wang et al., 2004). The αβ heterodimer of Na^+/K^+-ATPase is inserted into membrane caveolae where the α subunit can join to Src; this complex can then induce signaling pathways in boar kidney cells (Wang et al., 2004; Liu & Askari, 2006; Liu & Xie, 2010). During transduction of signals, the α and β subunits of Na^+/K^+-ATPase work together in the form of a dimer (Liu & Askari, 2006). In mammalian tissues, β has three isoforms (β1, β2, β3). In Sf-9 cell lines of *Spodoptera frugiperda* the β1 is found paired with α1 and α3 during ouabain-mediated signaling pathways (Guerrero et al., 2001; Pierre et al., 2008).

2.10 Na^+/K^+-ATPase in Bovine Sperm

Mammalian sperm are known to contain Na^+/K^+-ATPase (Zhao & Buhr, 1996) and the various isoforms have been identified in sperm HPM of bull (Hickey & Buhr, 2012; Sajeevadathan

et al., 2021) and in boar (Awda et al., 2022). A ouabain-dependent Na^+/K^+-ATPase signaling pathway inducing bull sperm capacitation was first identified in 2006 (Thundathil et al., 2006) that has since been confirmed (Newton et al., 2010). Interestingly, the variable ability of the steroid hormone progesterone (P4) to stimulate capacitation (Sajeevadathan et al., 2019) may be due to its less-effective, lower affinity binding to Na^+/K^+-ATPase's ouabain binding sites, as ouabain was the more effective inducer of bovine capacitation, implying that ouabain is the natural endogenous inducer of capacitation and P4 merely competes for ouabain's binding site (Sajeevadathan et al., 2019). In bull sperm, the signaling pathway induced by ouabain and Na^+/K^+-ATPase stimulates Tyr-P and capacitation (Thundathil et al., 2006) working through both receptor tyrosine kinases such as EGFR and non-receptor tyrosine kinases including Src, PKA, PKC, and ERK1/2 (Newton et al., 2010; Rajamanickam et al., 2017). Given that Na^+/K^+-ATPase induces sperm capacitation, identifying the specific subunits responsible is critical. While isoforms α1 and α4 are found in whole sperm homogenates and interact with signaling molecules Src, EGFR, ERK1/2 (Rajamanickam et al., 2017), the isoform(s) and their signaling partners that stimulate the initial signaling events of capacitation occurring in the head membrane of the sperm are unknown.

2.11 Prediction of Boar Fertility and Proteomics

The productivity and efficiency in a herd of pigs is significantly impacted by the fertility status of the boars. In the swine industry, sows are impregnated by extended liquid boar semen by means of AI, which significantly accelerates genetic improvement with reduced production cost, while substantially increasing the influence of boar on reproductive outcomes (Redgrove et al., 2011). Many researchers (Peddinti et al., 2008; Somashekar et al., 2017; Muhammad Aslam et al., 2018; Singh et al., 2018; D'Amours et al., 2018, 2019) have tried to associate sperm characteristics to field fertility, but results have been conflicting. The major problems were lack of repeatability

and objectivity and using subjective sperm evaluation techniques (Hoflack et al., 2007).With the development of computer assisted sperm analysis (CASA) technology, subjectivity is reduced, and objectivity and accuracy improved (Holt & Palomo, 1996). Current swine AI techniques provide a farrowing rate (FR) of 90%, with more than 12 live piglets per litter. This improvement in litter size (12-14 piglets) has improved the pig farm income by boosting reproduction efficiency and decreasing the number of culled sows from the herd (Andersson et al., 2015) .

Prediction and diagnosis of male fertility is a global multi-species challenge. Human male infertility/subfertility accounts for > 40% of infertility cases, with 40% female issues and 20% idiopathic infertility (Hirsh, 2003), and similar percentages were reported for breeding failure in animal industries (Peddinti et al., 2008; Park et al., 2012). Many research studies attempted development of diagnostic tools for sperm and semen analysis associated with fertility, including sperm morphology, sperm motility kinetics, penetration assays and swelling/eosin test (Kwon et al., 2015). These assessments provide initial sperm quality evaluations but, in most cases, their clinical value is debatable (Lewis, 2007). Therefore, innovative methods are needed to predict more reliably and accurately male, including boar, fertility (Kwon et al., 2014, 2015; Rahman et al., 2017).

Proteomics evaluation of fertility-associated proteins may be able to predict boar fertility in a more efficient way (Kwon et al., 2015). In past studies, researchers (Awda & Buhr, 2010) have employed different proteomics approaches to identify fertility related proteins/biomarkers in capacitated boar spermatozoa.

In non-capacitated ejaculated boar sperm, 11 differentially abundant proteins (DAPs; DAP>3fold change) were found in spermatozoa from boars producing higher litter size (12.3) than boars siring smaller litters (10.2; Kwon et al., 2014, 2015). The DAPs from high-litter-size sperm

were associated with five sperm functions: signal transduction, sperm egg interaction, metabolism, defense response, and vesicle association and the proteins were calmodulin, L-amino acid oxidase, malate dehydrogenase 2, NAD, cytosolic 5-nucleotidase 1B, and lysozyme-like protein 4. On the other hand, proteins highly abundant in low litter size sperm were related to functions of metabolism, sperm-egg interaction, and vesicle association, and included NADH dehydrogenase iron-sulfur protein 2 AWN, triosephosphate isomerase, Ras-related protein Rab-2A, Carbohydrate-binding protein AQN-3, and equatorin. The overall accuracy of determining male fertility with the identification of these protein biomarkers ranges from 60 to 85% (Kwon et al., 2014, 2015).

Fertility-associated proteins were also identified in capacitated boar spermatozoa, with 8 DAPs significantly more abundant in sperm from boars of high litter size (12.8) than sires of low litter size (10.19). DAPs belonged to sperm functions of respiration, structural proteins, sperm-egg interaction, and vesicle associated. Cytochrome bc1 complex subunit 2 was found significantly higher in capacitated sperm of boars of high litter size, whilst spermadhesin, equatorin, beta-tubulin, cytochrome b-c1 complex subunit 1, speriolin, seminal plasma sperm motility inhibitor and RAB2A, were abundant in low litter size animals (Kwon et al., 2015; Somashekar et al., 2017).

2.12 Hypotheses

The current research focuses on characterization of the proteins in sperm HPM of farm animals including boar and bull so that the potential differences across these species can be elucidated. These findings should assist in better understanding of the complex mechanisms that regulate fertility in both species and elucidate any existing differences in sperm fertility mechanism in high and low fertility boar and bull sires. Moreover, across species differences will assist to improve

farm productivity by identifying specific proteins involved in sperm capacitation and fertility. Based on the foundational knowledge presented, and the evident gaps in that knowledge, this research tested three hypotheses:

$H_0$1: The amount and localization of specific Na^+/K^+-ATPase isoforms in boar sperm HPM correlate with the *in vivo* boar fertility measures farrowing rate and total number born.

$H_0$2: Fertilizing ability of bull spermatozoa is closely associated with a limited number of sperm HPM proteins excluding Na^+/K^+-ATPase.

$H_0$3: Fertilizing ability of bull spermatozoa is closely associated with differences in amount or structure of specific isoforms of subunits of Na^+/K^+-ATPase in sperm HPM.

2.13 Objectives

1. Characterize the Na^+/K^+-ATPase isoforms in sperm HPM from boars of known *in vivo* fertility and identify any relationships (Hypothesis 1).
2. Identify, quantify, and evaluate proteins in HPM, other than Na^+/K^+-ATPase, contributing to bull *in vivo* fertility and determine functional pathways related to these proteins through Gene Ontology analysis (Hypothesis 2).
3. Identify, quantify, and evaluate the different isoforms of α and β subunits of Na^+/K^+-ATPase (α1,2,3,4; β1,2,3) in bull sperm HPM through MS (Hypothesis 3).
4. Identify the relationship of HPM Na^+/K^+-ATPase isoforms to field fertility, their unique peptide sequences, and potential interacting molecules (Hypothesis 3).

PREFACE TO CHAPTER 3

The amount and localization of the various isoforms of Na^+/K^+-ATPase in sperm HPM are specific and may correlate with *in vivo* boar fertility parameters [Direct Boar Effect (DBE) FR and DBE total number born]. In this chapter, we conducted a study to determine the amount (termed as volume, which was determined using the pixel volume of each individual protein band identified for each isoform measured by Image Quant analysis) of six isoforms of Na^+/K^+-ATPase (α1, α2, α3, β1, β2, β3) in fresh boar sperm HPM from low and high fertile boars by western immunoblotting, to test the association of the Na^+/K^+-ATPase isoforms to field fertility, and to locate the isoforms on intact and permeabilized whole sperm by immunocytochemistry. The total amount of α3 was highly significantly correlated with DBE farrowing rate. Immunofluorescence comparing sperm from high and low fertile boars found more intact sperm from high fertile boars had α3 equatorial fluorescence, while fewer permeabilized sperm from low fertility boars had detectable α2.

A version of this chapter is ready to submit to the journal Theriogenology under joint co-authorship with Mary M. Buhr and Murray Pettitt.

As first author, Muhammad Imran contributed to the experimental design, conducted the study, performed the data analysis, and wrote the first draft of the manuscript. Murray Pettitt contributed to experimental study and data analysis. Mary M. Buhr conceived the idea and contributed to the experimental design, revised the manuscript, and supervised the project.

CHAPTER 3: CHARACTERIZATION OF Na^+/K^+-ATPase ASSOCIATED WITH BOAR FERTILITY

3.1 Abstract

The ubiquitous transmembrane protein Na^+/K^+-ATPase affects sperm fertility and capacitation through ion transport and cell signaling. The objective of this study was to determine the association of isoforms of the α and β subunits of Na^+/K^+-ATPase to boar *in vivo* fertility. Boar fertility was determined by the DBE for both FR and litter size based on ≥ 20 inseminations per boar (n=12). Each ejaculate from high and low fertility boars (n=6 per fertility line) was analyzed for sperm motility by CASA, and for Na^+/K^+-ATPase in the sperm. Immunocytochemistry assessed whole sperm, and Western blotting assessed the isolated HPM from sperm of each ejaculate for six isoforms of Na^+/K^+-ATPase (α1, α2, α3, β1, β2, β3). The amount of each individual protein band identified for each isoform was determined using the pixel volume measured by Image Quant analysis and corrected for gel variation using an internal standard. Sperm motility parameters, and the immunocytochemistry patterns of each isoform (including total amount, and amount of each band) were compared between the high and low fertility groups using Randomized Complete Block Design with Proc Mixed model and the mean comparison was done by Tukey's test. Sperm function assessed by CASA did not differ between high and low fertility boars. Immunofluorescence of intact and methanol-permeabilized sperm found that more intact sperm from high fertility than low fertility boars had α3 equatorial fluorescence ($p<0.05$), while a lower percentage of permeabilized sperm from high fertility boars had detectable α2 compared to low fertility boars (10.3 ±13 versus 68 ± 13%, low versus high fertility, $p<0.05$). Western immunoblotting determined that the total amount of the isoform α3, and the amounts of 7 individual α3 bands, were significantly greater in the high fertility boars ($p<0.05$), and linear regression confirmed a highly significant relationship of total amount of α3 and α1 with FR ($r^2=0.90$; $P<0.0001$ and $r^2 =0.36$; $p<0.05$). In low fertility boars, several molecular weight (MW)

bands were missing from isoforms β1, β2 and β3. The total volume of β1 tended to be correlated to DBE for FR($r^2 = 0.2652$; $p = 0.0867$). These findings suggest that specific isoforms of Na^+/K^+-ATPase in the sperm head are correlated to boar *in vivo* fertility, probably through Na^+/K^+-ATPase's role in capacitation.

3.2 Introduction

The transmembrane protein Na^+/K^+-ATPase is ubiquitous in mammalian cells, maintaining resting membrane potential and regulating cellular volume through active transport of Na^+ and K^+ ions (Kaplan, 2002; Xie & Askari, 2002). Na^+/K^+-ATPase has long been known to exist in the membrane over the head of bovine spermatozoa (Zhao & Buhr, 1996) and is now known to induce *in vitro* capacitation through acting as a receptor for the steroid hormone ouabain (Sajeevadathan et al., 2019) and activating a cell signaling cascade causing Tyr-P (Thundathil et al., 2006).

Na^+/K^+-ATPase is an amphipathic protein having two subunits, alpha (α) and beta (β) (Blanco & Mercer, 1998). The generic α subunit is composed of 1000 amino acid residues with molecular mass of 110 kDa (Kaplan, 2002).It is the catalytic subunit, containing binding sites for cations, ATP and cardiac glycosides like ouabain, and is mostly located on the inner leaflet of the cell membrane (Blanco & Mercer, 1998; Daniel et al., 2010). The generic β subunit consists of 370 amino acids (Kaplan, 2002) and is heavily glycosylated (Hickey & Buhr, 2012) resulting in its molecular mass ranging from 35-60 kDa. The β subunit has a significant portion external to the plasma membrane and is responsible for localizing and stabilizing the protein within the plasma membrane, aiding enzyme activity without catalytic involvement (Geering, 1991; Woo et al., 2000).

In mammalian tissues the α subunit has four isoforms (α1, α2, α3, α4; Lingrel et al., 2003) and β has three isoforms (β1, β2, β3). The isoforms can differ in function and cell location

(Cereijido et al., 2004). Isoforms α1, β1 and β3 are omnipresent in all body tissues while α2 and β2 isoform are expressed in skeletal muscle, adipocytes, brain, and heart tissues (Juhaszova & Blaustein, 1997). The α3 isoform is present in nerves, brain, and heart tissues (Juhaszova & Blaustein, 1997). Our group had identified isoforms of Na^+/K^+-ATPase α1, α3 and β1, β2, β3 in bull sperm HPM (Hickey & Buhr, 2012) and in boar sperm HPM (Awda et al., 2022-submitted), while the α4 isoform had been found in the head region of bovine sperm (Newton et al., 2010) the testis and sperm midpiece (Blanco & Mercer, 1998; Crambert et al., 2000; Woo et al., 2000).

All isoforms exist in the HPM of bull and boar sperm (Hickey & Buhr, 2012; Rajamanickam et al., 2017) and Na^+/K^+-ATPase has been shown to be involved in bull sperm capacitation (Thundathil et al., 2006). In whole bull sperm, α4 increases as a result of mitochondrial ribosome-associated translation of mRNA during capacitation (Rajamanickam, et al., 2017) which, since mitochondria are confined to the midpiece, argues α4 could be involved in capacitation-associated hyperactivated motility, perhaps via signaling (Rajamanickam et al., 2017). The isoforms existing in the HPM could be involved in actual capacitation, with ouabain from the oviduct (Daniel et al., 2010) stimulating Tyr-P through SRC-dependent or independent pathways (Sajeevadathan et al., 2019).

Interestingly, rigorous semi-quantitative western immunoblotting of the isolated HPM from multiple ejaculates per male and multiple males proved that amount and localization of the various ATPase isoforms are specific and repeatable within an animal (Hickey & Buhr, 2012). Since male-to-male variability could possibly be aligned with differing fertilizing ability, the objective of this study was to characterize the Na^+/K^+-ATPase isoforms in sperm HPM from boars of known *in vivo* fertility and identify any relationships.

3.3. Materials and Methods

3.3.1 Semen

Semen was provided by TOPIGS Norsvin Inc (Winnipeg, MB, Canada) from six boars from a low fertility line and six from a high fertility line. Fertility categorization of each boar was based upon field fertility data from a minimum of 20 inseminations (range 20-144). Boar fertility was expressed as DBE for total number born (TNB) and FR by Topigs Norsvin Canada. Duroc boars with a DBE > 0.27 for TNB and > 1.0 for FR (range: TNB 0.27 to 1.25; FR 1.0 to 5.1; n=6) were considered high fertile and those with a DBE < -0.29 for TNB and < -1.3 for FR (range: TNB -0.29 to -1.44; FR -1.3 to -6.4; n=6) were considered low fertile boars. After semen collection by TOPIGs, each the ejaculate was diluted to 6 $x10^6$ sperm/mL with extender (proprietary composition, TOPIGS Norsvin), packed into 100 mL plastic tubes and shipped overnight at 16 ºC in a temperature-controlled container to the laboratory at the University of Saskatchewan. The temperature was checked on arrival and samples at 15-18 ºC were warmed to room temperature over 2 h by being placed on a fabric surface, covered, and held at room temperature with occasional rotation.

A 1.5 mL aliquot random sample for CASA, warmed in thermos in 37ºC incubator for an hour, and then was evaluated motility kinetics and concentration using CASA with a Hamilton-Thorne motility analyzer (Version 14 HTM-IVOS), using 4 µL semen and a 20 µm deep Leja standard count slide (Leja products B.V., Luzernestraat 10, 2153 GN Nieuw-Vennep, The Netherlands) kept at 37ºC. Ejaculates had to have > 60% total /55% progressive motility, and a temperature on arrival of 15-18 ºC to be included in the study. A 10 mL aliquot of the semen was used for immunolocalization of the different isoforms.

3.3.2. Reagents

Disodium phosphate, sodium dihydrogen phosphate monohydrate, dextrose, potassium chloride, sodium chloride, sucrose, dextran, polyethylene glycol, percoll and methanol were acquired from Thermo-Fisher Scientific (Unionville, ON, Canada). Milli-Q water was obtained from water purification system Serv A Pure (MIUS). Acrylamide: Bis 29.2:0.8mL, SDS, Ammonium Persulphate, Temed, protein assay dye concentrate reagent, precision plus protein standards (MW K Da: 37,50,75,100,150 for α isoforms and 25, 37,50,75,100,150 for β isoforms), hydrogen peroxide 30%, and streptactin were acquired from Bio-Rad Laboratories, Ltd. (Hercules, CA, USA). Hela cell lysate (Enzo Life Sciences, Inc, USA), Polyvinylidene fluoride (PVDF) Membrane (Merck Millipore Ltd, Darmstadt Germany), chromatography paper (Whatman, GE Health Care, Life Science, ON Canada), and goat anti-mouse HRP as the secondary antibody for α1, α3, β1 and β3 were obtained from EMD Millipore Corp, USA Enzo Life Sciences, Inc, USA and BD Biosciences Transduction Laboratories, Canada. Goat anti-rabbit HRP as the secondary antibody for α2 and β2 were obtained from EMD Millipore Corp, USA Abcam Inc, ON, Canada. A431 human endothelial Cell Lysate as positive control for β3 was purchased from BD Biosciences Transduction Laboratories, Canada. Primary antibodies of Na^+/K^+-ATPase α3 (mouse monoclonal IgG1; clone XVIF-G10) were purchased from Enzo Life Science (Farmingdale, NY, USA); β3 (mouse monoclonal; Clone 46), from BD Bio-sciences (Mississauga, ON, Canada); β2 (mouse monoclonal IgG2a; ab76509) from Abcam Inc. (Cambridge, USA); β1 (mouse monoclonal IgG2AK; clone C464.8), α1 (mouse monoclonal; IgG1K; clone C464.6), α2 (rabbit monoclonal IgG2AK; clone C464.8), goat anti-mouse IgG-HRP conjugate (polyclonal) and goat anti-rabbit IgG-HRP conjugate (polyclonal) were purchased from EMD Millipore Corporation (Single Oak Drive, Temecula, USA). Antifade was from Merck Millipore Ltd, (Darmstadt Germany). Glycerol,

tris-HCl, potassium chloride (KCl), bromophenol blue, magnesium chloride ($MgCl_2 \cdot 6H_20$), dithiothreitol (DTT), ethylenediaminetetraacetic acid (EDTA), glycerol, 4-(2-Hydroxyethyl) piperazine-1-ethanesulfonic acid, N-(2-Hydroxyethyl) piperazine-N′-(2-ethanesulfonic acid) (HEPES), luminol, N-α-p-tosyl-l-lysinechloromethyl ketone (TLCK), p-coumaric acid, pepstatin-A, phenylmethanesulfonyl fluoride (PMSF), sodium chloride (NaCl), tris-HCl, , trizma base, trizma hydrochloride, Carestream® Kodak® autoradiography GBX developer/replenisher, Carestream® Kodak® autoradiography GBX fixer and replenisher, Carestream® Kodak® X-Omat LS film were purchased from Sigma-Aldrich, Canada Ltd (Oakville, ON, Canada). For protein concentration determination, bovine serum albumin (BSA) was a standard and Bio-Rad Protein Assay kit was acquired from Bio-Rad Hercules, CA, USA. Staining kit for sperm morphology was purchased from BRED Life Science Technology Inc (Shajing, China).

3.3.3. Morphology Analysis

Sperm morphology was analyzed using the Hamilton Thorne Metrix Oval Head Morphology (Beverly, MA, USA) software, in the Hamilton-Thorne CEROS (version 12.1). Briefly, 10 mL of the warmed semen sample was washed (720 x g, 5 min, room temperature) with 5 mL of physiological saline solution (PSS; 0.9% NaCl in sterile H_2O; w:v) and the pellet was resuspended with PSS to a concentration of 50 $x10^6$ sperm mL^{-1}. Diluted semen was smeared on slides, air dried at room temperature and fixed by sequential passage (5min each) through fixative solution, Stain I, and Stain II using Diff-Quick staining method (Rijsselaere et al., 2004). Subsequently, slides were rinsed with distilled water and air dried. From each of three slides per animal, at least 100 sperm were examined (100x magnification, HTR 12.1 Metrix) and sperm were classified as normal, or as having abnormal head, proximal droplet, distal droplet, bent tail, coiled tail, absent tail, or double tail (Rijsselaere et al., 2004).

3.3.4. Immunofluorescence

All the isoforms of α and β subunits of Na^+/K^+-ATPase were localized by immunocytochemistry by modification of the established procedure (Thundathil et al., 2006; Hickey & Buhr, 2012). All steps were performed at room temperature. Briefly, each fresh ejaculate was diluted in PBS (125 mM NaCl, 8mM Na_2HPO_4, 2 mM $NaH_2PO_4 \cdot H_2O$, 5mM KCl, 5mM Dextrose), centrifuged (500g; 10 min; Jouan, Winchester, VA, USA) and pellets were gently resuspended in PBS. A 0.5 mL drop of diluted sperm was placed inside the ceramic ink-lined circle on poly-L-lysine coated slides, held for 30 min, and rinsed for 5 min in PBS. Sperm on half of the slides were permeabilized by immersion in 100% methanol for 30 sec; sperm on the remaining slides were left intact, by immersion in PBS for 30 sec. To block non-specific antibody binding sites, all slides were rinsed for 10 min in PBS, received 70 µL of 10% normal goat serum (NGS; 1:9 NGS: PBS, v: v) and incubated covered for 30 min to enable slow drying. Any remaining NGS was gently removed. Primary antibodies were prepared (antibody:10%NGS (v: v) α1 1:50: α2 1:100: α3 1:50: β1 1:20; β2 1:20; β3 1:10), 70 µL pipetted onto the appropriate slides and incubated (60 min). Controls received only 10% NGS and were kept completely separate from antibody-treated slides for the remaining processing. Slides were rinsed (3x 5 min in PBS + 10% NGS) to remove unbound primary antibody and inverted to place the slide's ceramic ink-lined circle onto a 70 µL droplet of secondary antibody [Fluorescein isothiocyanate (FITC)-conjugated Goat anti-mouse antibody] on parafilm and incubated 60 min in the dark. Slides were then rinsed for 10 min in NGS, antifade (0.1% P-phenylene di-amine and 90% glycerol in PBS) added and a coverslip placed. Slides were viewed immediately under fluorescent microscope (630x magnification) at FITC wavelengths (495 - 519 nm; Laborlux S; Leitz, Germany) and 3x100 sperm counted, noting any fluorescent pattern. A minimum of 3 representative fields per slide were photographed with

both phase contrast and fluorescent lighting. To help objectively characterize sperm fluorescence, 12 fluorescent patterns (Fig 3.1) were identified and used to count and categorize sperm for each antibody from each boar.

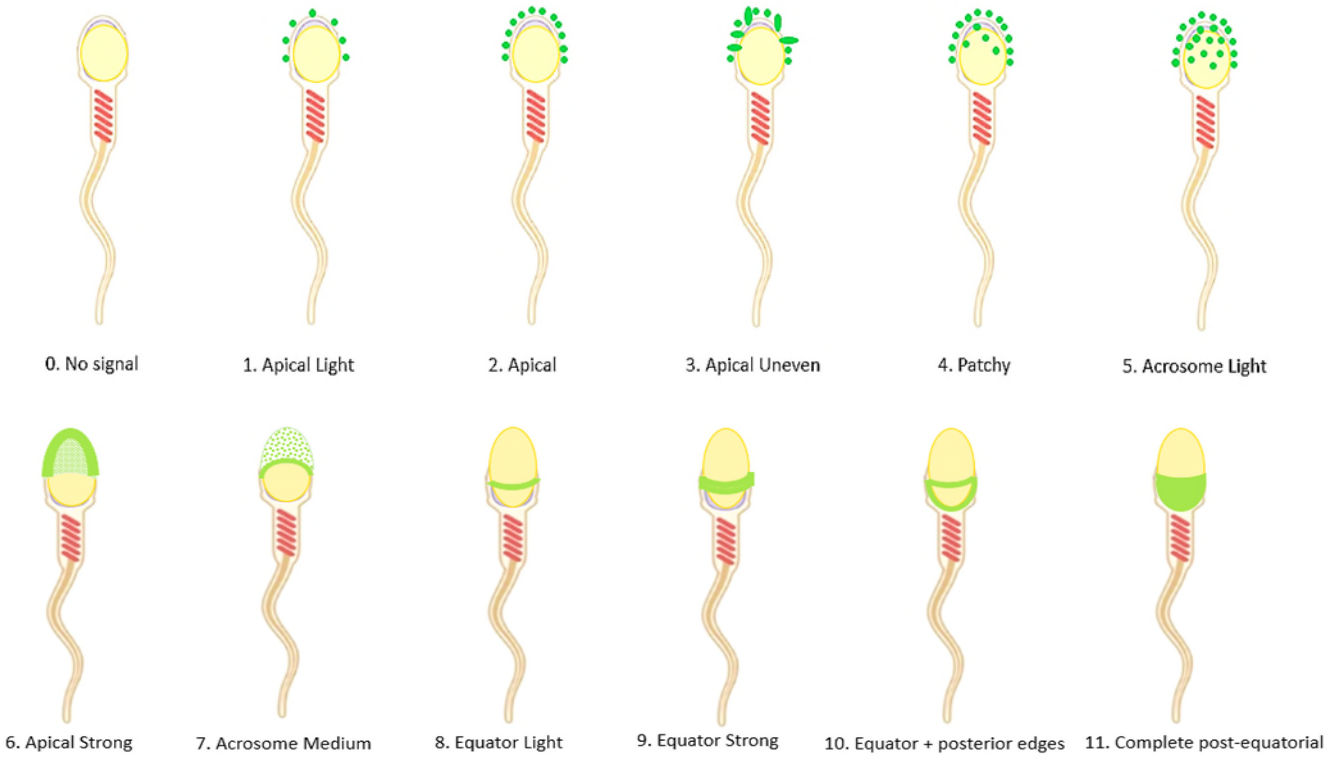

Figure 3.1. Fluorescence patterns used to categorize immunofluorescence detected on boar sperm after incubation with antibodies for the α1, α2, α3 and β1, β2, β3 subunits of Na^+/K^+-ATPase.

3.3.5. Isolation of HPM

The HPM was obtained by established procedure (Canvin & Buhr, 1989), conducted at room temperature unless specified otherwise. Briefly, semen was filtered through double layers of Miracloth (Mereck KGaA, Darmstadt Germany), centrifuged (500 x g, 10 min.), and pellets resuspended into dilution buffer (5 mM Tris-HCl, 250 mM Sucrose, pH 7.4). A mixture of 550 and 1107 silicon oils (Dow Corning, Mississauga, Ontario, Canada; 1:1 by volume) was centrifuged (1500 x g, 10 min), supernatant harvested, and the Tris-buffered sperm was layered

(1:2, v: v) over the silicon oil supernatant. Following centrifugation (2500 x g, 10 min), sperm pellets were harvested, resuspended in 40 mL of dilution buffer, and washed twice by centrifugation (2500 x g, 10 min.). The final pellet was resuspended in 25 mL of dilution buffer and subjected to nitrogen cavitation in a Parr Cell Disruption unit introducing nitrogen gas over 90 seconds to a final pressure of 650 psi, holding for 10 min and then releasing pressure over 90 seconds. The cavitate was centrifuged (1000 x g,10 min) with 30 mL of separation buffer (5 mM Tris-HCl, 250 mM Sucrose, pH 5.0) and the supernatant was saved. The process was repeated twice with the resuspended pellet. The combined supernatants were centrifuged (6684 x g, 10 min: Beckman Avanti J-E centrifuge, JA-14 fixed angle rotor). The resulting supernatant was removed and centrifuged (245,000 x g, 70 min, 4 ºC: Optima L-90K Ultracentrifuge, Fixed Angle 50.2 Ti rotor). The pellets were combined and resuspended in storage buffer (10 mM Tris, 154 mM NaCl pH 7.4) and centrifuged again (245000 x g, 40 min, 4 ºC) to get the final pellet (HPM) which was scraped free and placed into a hand-held homogenizer containing 1/3 tablet "complete mini EDTA-Free" protease inhibitor (Roche Diagnostic GmbH, Indianapolis, IN, USA), suspending with 200 µL PBS, homogenized, aliquoted into eppendorf tubes, covered with nitrogen gas, snap frozen in liquid nitrogen and then stored at -80 ºC.

3.3.6 Boar Kidney and Protein Concentration

Identical aliquots from one pooled porcine kidney membrane preparation were used as inter-assay controls (Hickey & Buhr, 2012) for electrophoresis. Each aliquot was thawed by holding on ice before using for western blotting proteomic analysis. Tissue protein concentration was determined (Hickey & Buhr, 2012) using the Bio-Rad Protein Assay using BSA as a standard, and Versa Max ELISA Microplate Reader (Molecular Devices, LLC.CA USA) and the SoftMax Pro Software.

3.3.7 Western Blotting

The extracted HPM from sperm of each boar was analyzed for α and β subunits of Na^+/K^+-ATPase (α1-3; β1-3) with SDS-PAGE western immunoblotting following established protocol (Thundathil et al., 2006; Hickey & Buhr, 2012). Briefly, 7% and 10% polyacrylamide gel were used for α and β subunits, respectively. Each gel included two controls, the manufacturer's positive controls (Hela or A431cell lysate) and the kidney membrane. The amount of protein loaded for per lane was optimized for each type of protein: kidney membrane 0.2 µg -10µg; Hela 2.3-13.8µg and A431 6µg. Isoforms were identified and characterized based on their molecular weight by electrophoresis (Mini-protean 3 electrophoresis cell; Bio-Rad Laboratories, Ltd.) at 75V for 15 min (stacking gel), then 100V for 80 min (running gel) and electro transferred (Mini transblot cell; Bio-Rad Laboratories, Ltd.) in 1x Tris/glycine Buffer (250 mM Tris, 1.92 M glycine, pH 8.3) and 20% methanol onto prepared PVDF membranes (7 x 9 cm: 100V; 60 min; 4 ºC) with filter paper (8 x 10 cm). Non-specific binding sites were blocked using 5% skim milk (w: v) powder in Tris-buffered saline (20mM Tris-buffered saline containing 0.1% Tween 20; v: v, TTBS) prepared and stored overnight at 4 C. Then membranes were incubated with shaking (2h) in the presence of one of the Na^+/K^+-ATPase (α1,2,3; β1,2,3) isoforms' primary antibodies in TTBS with 0.1% (w:v) sodium azide: α1 (1:2500), α2 (1:15000), α3 (1:3500), β1(1:1000), β2 (1:1000), or β3 (1:250). Each membrane was then washed in TTBS and membranes for α1, α3, β1, and β3 isoforms were incubated in anti-mouse HRP secondary antibody (1:2500 in TTBS) and α2 and β2 in anti-rabbit HRP secondary antibody (1:5000 in TTBS) for 1h (room temperature). The protein bands were detected using chemiluminescence (50 µL p-coumaric acid, 68 mM; 5 mL luminol, 1.25 mM; 15 µL 3% peroxide) with Kodak Scientific Imaging films. Both Western blotting (WB) and immunofluorescence binding were confirmed to be specific by the absence of response when the

primary was omitted, and, for WB, the positive response of the manufacturer's standard. Each band in each isoform was assessed for their volume (number of pixels), area and molecular mass (kDa) using Image Quant TL software (Ver 8.1; GE Healthcare Life Sciences, Mississauga, ON, Canada) and intensities of protein bands of each Na^+/K^+-ATPase isoform were calculated as volume/area.

3.3.8 Statistical Analysis

Using Image Quant analysis, the volume of each band in each isoform was assessed and corrected for the amount of HPM protein loaded and for gel to gel and day to day variation based on the volume of the kidney internal standard. Total amount of each isoform was calculated as the sum of the corrected volumes of all bands detected in the isoform. Data were checked for normality by Shapiro-Wilk method, and normalized as necessary; for α3, two high fertility and one low fertility boar were excluded as unreadable. Normalized results were tested for fertility-related differences using SAS statistical software (SAS; version 9.3; SAS Institute, Inc Cary, NC), Randomized Complete Block Design (RCBD) compared volumes and intensities, and sperm functional parameters (motility, sperm kinetics) between fertility groups, setting significance at $P < 0.05$. Proc Mixed Model assessed fixed and variable effects from animals of different fertility lines (n=6 high, n=6 low) evaluating fertility and immunofluorescence patterns (number of each pattern in each of the intact and permeabilized sperm within each isoform) using Tukey's test with significance at $P < 0.05$. The total amount of six isoforms of Na+/K+-ATPase (α1, α2, α3, β1, β2, β3) was compared within each fertility group with Proc GLM Model, using least square (LS) means with adjusted Tukey's test. Linear regression analysis tested correlations of the fertility measures of DBE FR and DBE total number of piglets born to the total volume of each measured isoform in each fertility group. A heatmap was created to illustrate differences in amounts of the

various isoforms and pairwise comparison in interactive mode was used (http://www.heatmapper.ca/; University of Alberta).

3.4 Results

3.4.1. Fertility and Ejaculate Quality

The DBE of high fertility (HF) boars was significantly higher than that of the low fertility (LF) boars for both (2.58 ± 0.68 vs -3.11 ± 0.77, mean ± SE, $p<0.05$) and for TNB (0.59±0.15 vs -0.566 ± 0.26, $p<0.05$).

The two fertility groups did not differ significantly in any major ejaculate, motility, or morphological parameters (Tables 3.1, 3.2) although there were tendencies ($0.10>p>0.05$) for LF boars to have a higher sperm concentration in the semen samples arriving from the AI center and more coiled tails. LF boars also tended to have fewer total sperm in their ejaculates (19743.8 vs 26519.5 ± 2009.9 $x10^6$, $p= 0.072$) which probably contributed to the tendency to get less total HPM from LF boars (1161.5 versus 872.8 ± 85.9 µg extracted HPM protein, $p=0.073$; HF versus LF respectively); there was no difference in amount of HPM acquired per million sperm (0.0443 versus 0.0438 ± 0.00027 µg HPM/10^6 sperm; HF vs LF $p= 0.26$).

Table 3.1. Concentration and Morphology of Whole Sperm.

Fertility Level	High	Low	SEM	p value
Parameter				
Concentration ($x10^6$/mL)	34.4	44.0	3.3	0.07
Normal Morphology	74.3	80.3	7.7	0.73
Abnormal Morphology	25.7	19.7	7.7	0.98
Abnormal Head*	19.7	16.5	6.0	0.71
Proximal Droplet*	31.3	41.8	9.4	0.45
Distal Droplet*	18.8	10.4	5.4	0.23
Bent Tail*	17.3	6.5	5.2	0.21
Coiled Tail*	10.3	24.4	5.2	0.09
Absent Tail*	1.8	0.4	1.1	0.46
Double Tail*	0.8	0	0.6	0.34

Assessment was done by CASA. All values are mean of 6 high fertility and 6 low fertility boars. All values are in percentage except concentration. SEM= Standard Error of Means; *: Parameters expressed as % of the abnormal sperm population.

Table 3.2. Motility Analysis of Sperm from High and Low Fertility Boars by CASA

Fertility Level	High	Low	SEM	p value
Parameter				
Motile Cells (% count)	86.2	86.3	4.3	0.98
Progressive Cells (% count)	77.7	72.7	3.9	0.39
Curvilinear Velocity (VCL)	148.7	134.9	6.3	0.17
Linear Velocity (VSL)	75.5	74.5	3.6	0.82
Average Path Velocity (VAP)	88.5	85.5	3.7	0.58
Linearity Coefficient (LIN)	51.8	55.7	2.2	0.23
Straightness Coefficient (STR)	84.1	85.3	1.3	0.53
Mean Amplitude of Lateral Head Displacement (ALH)	6.2	5.5	0.3	0.15
Frequency of Head Displacement (BCF)	36.0	36.2	0.9	0.90

Values are mean of 6 high fertility and 6 low fertility boars. SEM= Standard Error of Means.

3.4.2. Western Immunoblotting

All of the individual six Na^+/K^+-ATPase isoforms were detected in the boar HPM, positive controls and kidney inter-gel controls (Fig 3.3, 3.4). The α3 isoform was the most prevalent α isoform in the sperm HPM from all boars [total amount (volume) α3>α1=α2; $p<0.05$] regardless of fertility status (Fig 3.2A).

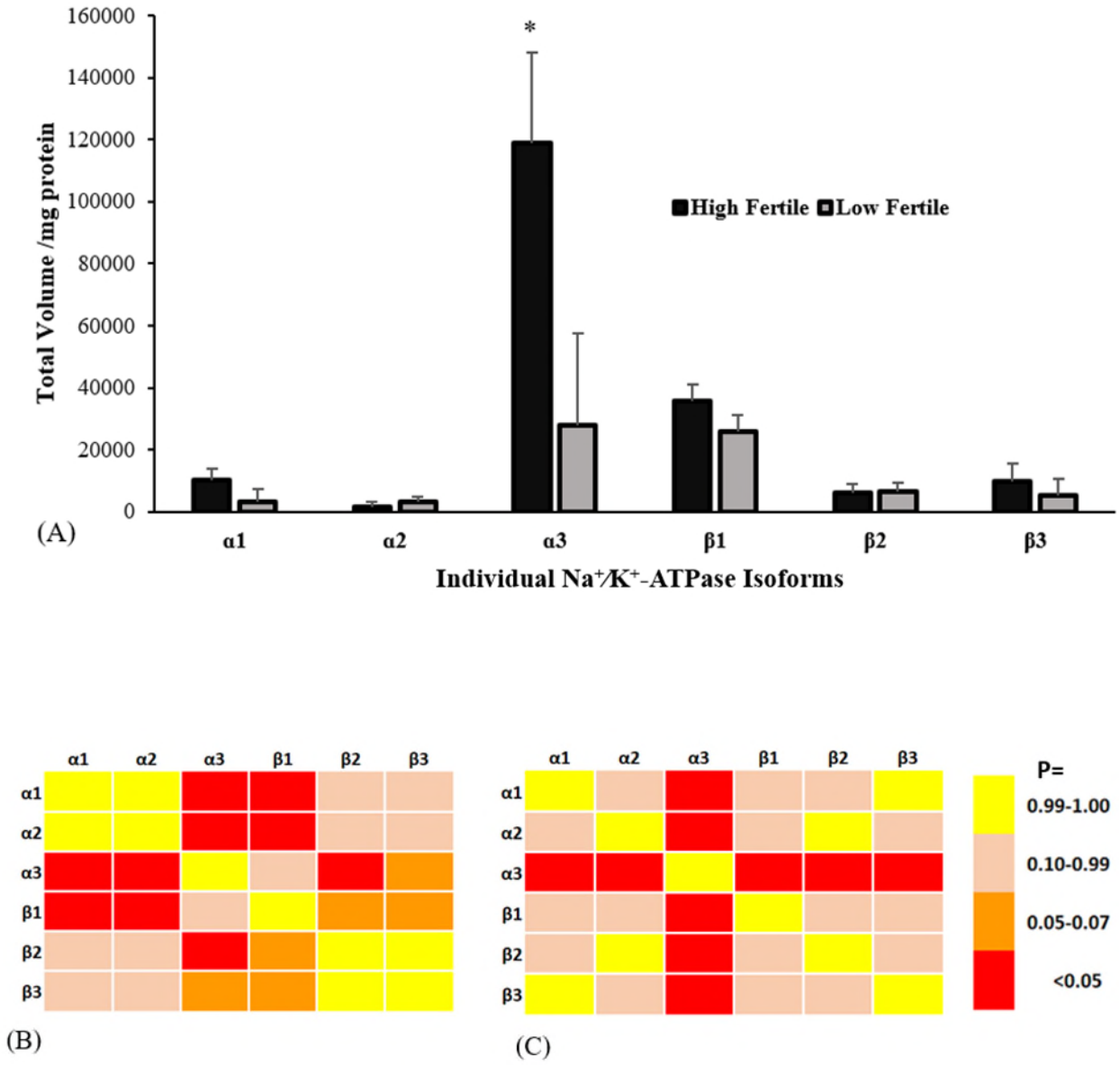

Figure 3.2. (A) Total amount of individual Na^+/K^+-ATPase isoforms in sperm HPM from boars of high and low fertility. Values are mean ± SEM of the total corrected volume (amount) of all bands in each isoform, expressed per mg of HPM protein (n=4-6 boars for each bar). * Amount of individual isoform differs between high and low fertility boars, $p<0.05$. (B, C) Heatmaps comparing total amounts of each isoform in low fertility (B) and high fertility (C) groups; the colors display the P-value of the difference in total amount of the two isoforms being compared; legend at the far right shows that p values of the different heatmap colours: red as significant ($p<0.05$), orange as $0.07>p<0.05$) and other colours indicate $p>0.10$.

All β isoforms were present in similar total amounts (Fig 3.2A, C) in sperm HPM of HF boars; in LF boars, the amount of β1 exceeded that of β3 ($p=0.05$) and β2 ($p=0.06$ Fig 3.2B). In

the HPM of HF boars, α3 was present in a significantly greater amount than the other isoforms; in LF boars, the amount of α3 exceeded that of α1, α2 and β2, and tended to exceed β3. In LF boars, β1 was present in the same amount as α3, and exceeded or tended to exceed that of the other isoforms (Fig 3.2B, C).

All isoforms had multiple positive western immunoblotting bands (Fig 3.3,3.4) some of whose amounts were correlated with fertility. Neither the α1 ($p=0.5$) nor α2 ($p=0.6$) isoforms showed any significant fertility-related differences in amounts of specific bands detected in both fertility groups (Fig 3.3 A, B), but two α2 bands (49 and 46 kDa) present in HPM of LF boars were missing in HF boars (Fig 3.3 B). For α3, however, seven individual bands were present in greater amounts in HPM from HF versus LF boars (Fig 3.3C; $p< 0.05$). Four β1 bands present in high HF were absent in LF boars, and LF boars had a 155±1.05 kDa band that was absent in HF boars (Fig 3.4 A; $p<0.05$). One band of 76 kDa of β2 isoform present in HPM of LF boars was missing in HF while four bands (61,52,50,44 kDa) of β2 isoform present in HPM of HF boars were not detected in LF boars. In β3, three bands (118,70,29 kDa) in HPM of LF boars were missing while no band was missing in HF boars.

(A) α1

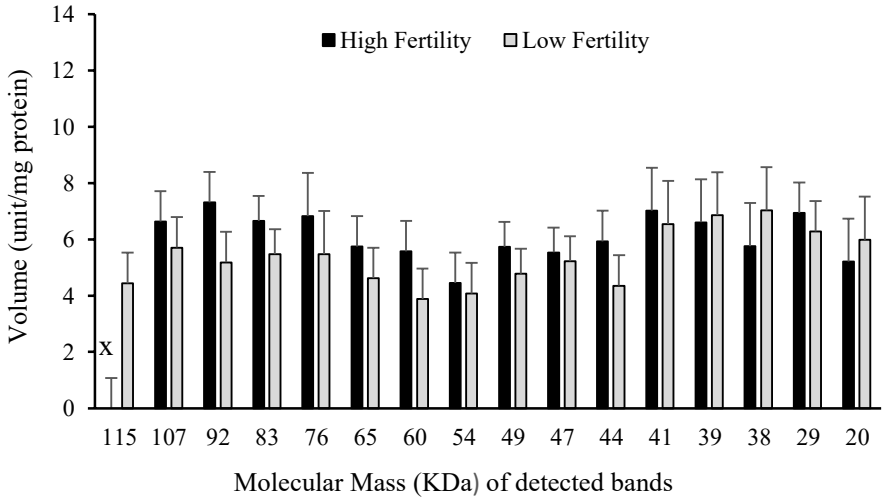
High Fertility
Low Fertility
Volume (unit/mg protein)
14
12
10
8
6
4
2
0
x
115 107 92 83 76 65 60 54 49 47 44 41 39 38 29 20
Molecular Mass (KDa) of detected bands

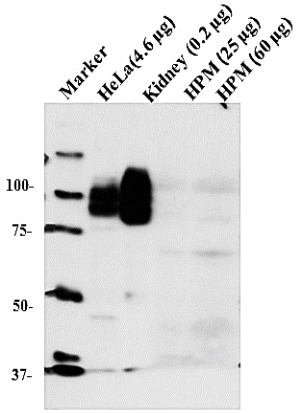
Marker
HeLa(4.6 µg)
Kidney (0.2 µg)
HPM (25 µg)
HPM (60 µg)
100-
75-
50-
37-

(B) α2

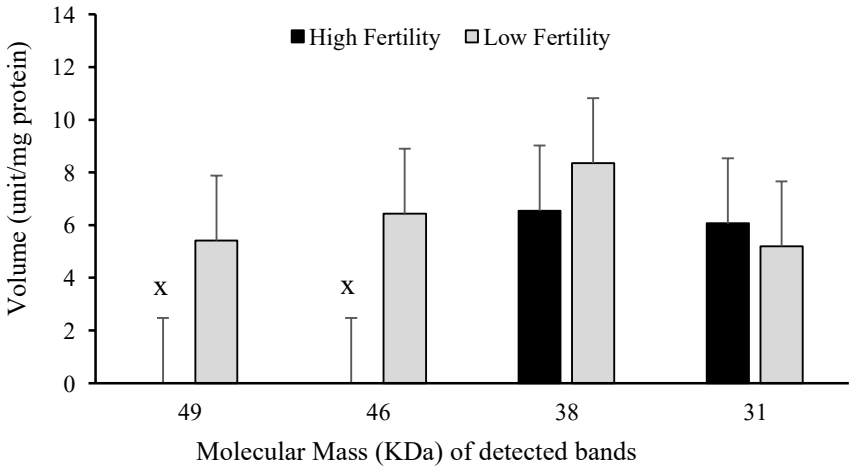
High Fertility
Low Fertility
Volume (unit/mg protein)
14
12
10
8
6
4
2
0
x
x
49
46
38
31
Molecular Mass (KDa) of detected bands

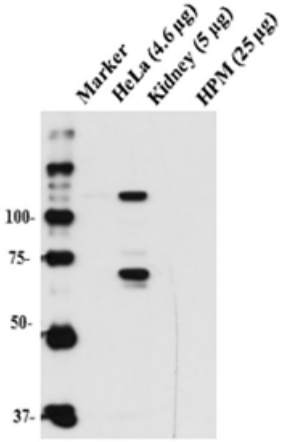
Marker
HeLa (4.6 µg)
Kidney (5 µg)
HPM (25 µg)
100-
75-
50-
37-

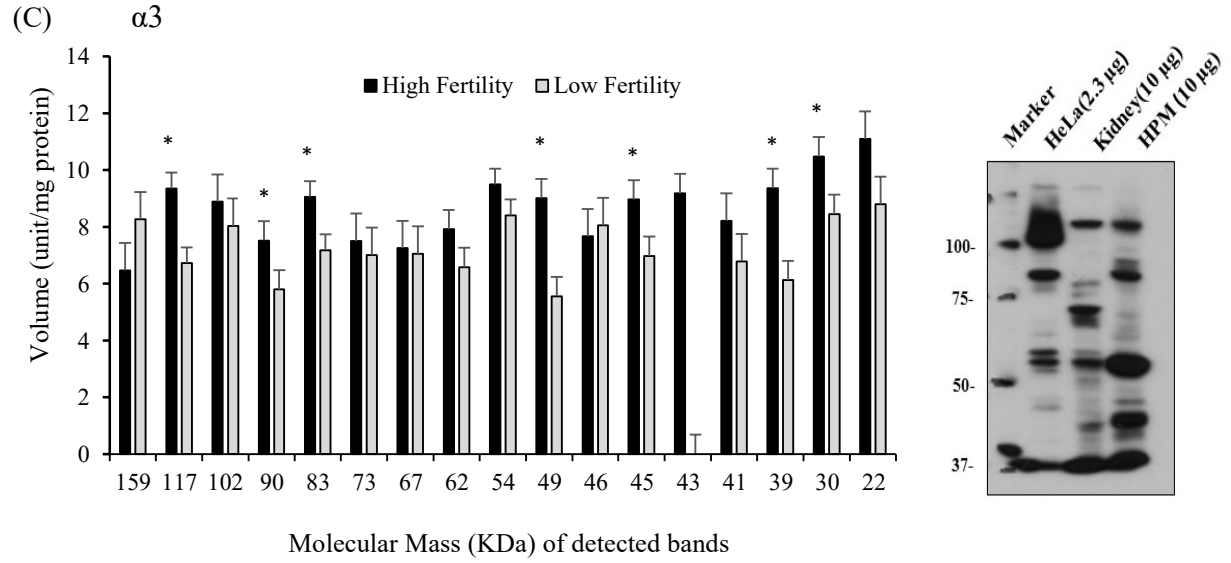

Figure 3.3. Protein bands in Western blots of Na^+/K^+-ATPase α isoforms in head plasma membranes (HPM) of sperm from boars of high and low fertility. A typical immunoblot for each isoform is provided with labelled lanes: Marker: Molecular weight standard; Hela: manufacturer's standard; Kidney: boar kidney pool as internal standard; µg= µg protein assessed on gel. Bar graph shows amounts of each band (actual mean volume from ImageQuant analysis ± SEM; log-transformed normalized data were analyzed) for 6 high and 6 low fertility boars, except α3 where gels from two high and one low fertility boar were excluded as bands were not clear enough for quantification. * Band volumes differ ($p<0.05$) between high and low fertility boars. "X" Band volume does not differ from zero.

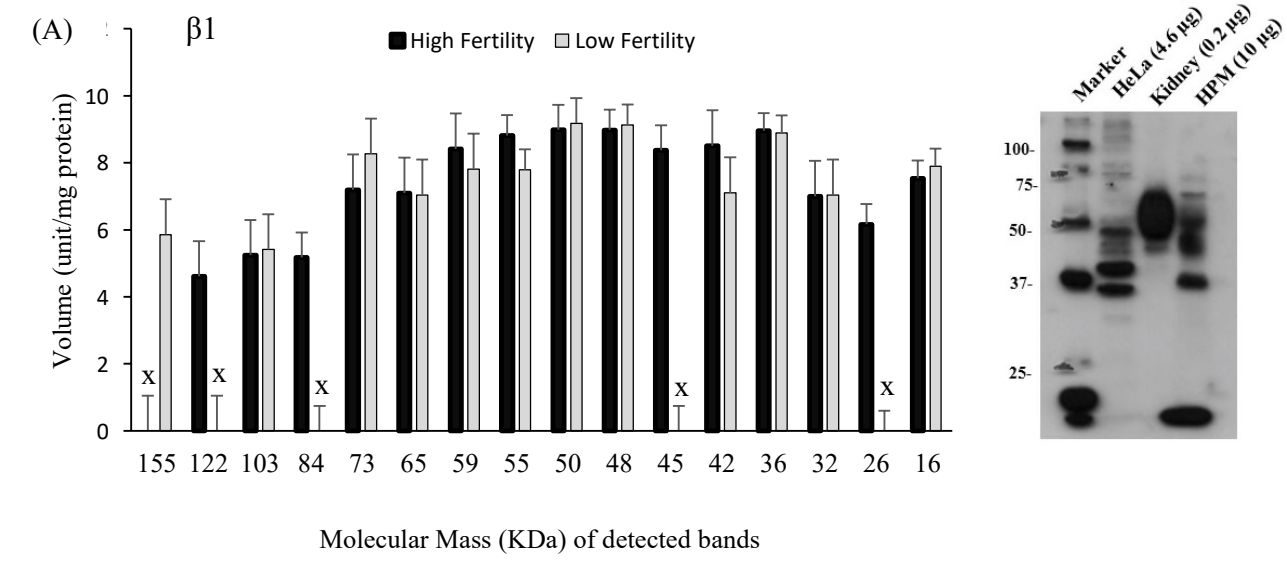

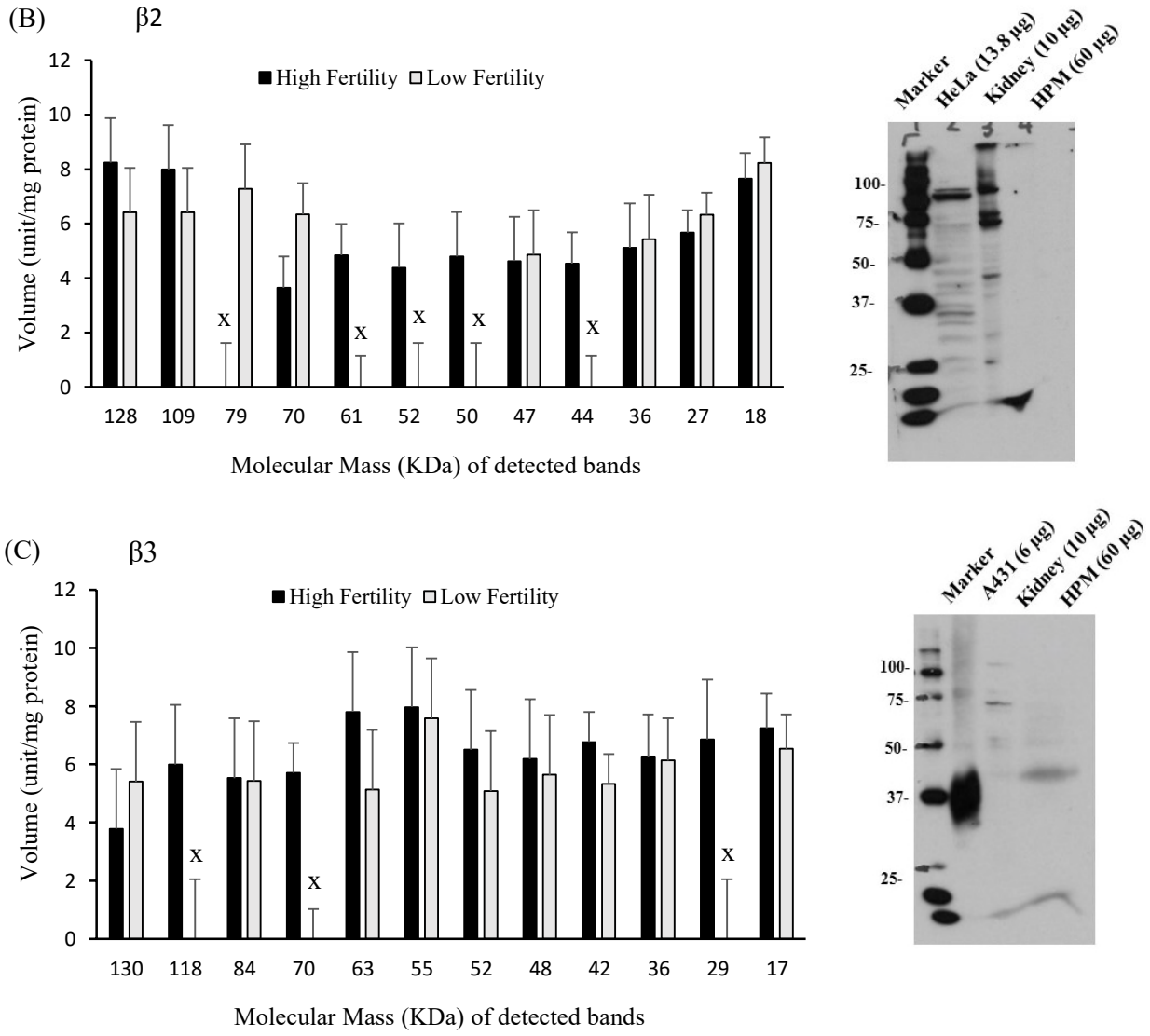

Figure 3.4. Protein bands in Western blots of Na^+/K^+-ATPase β isoforms in head plasma membranes (HPM) of sperm from boars of high and low fertility. A typical immunoblot for each isoform is provided with labelled lanes: Marker: Molecular weight standard; Hela: manufacturer's standard; Kidney: boar kidney pool as internal standard; µg= µg protein assessed on gel. Bar graph shows amounts of each band (actual mean volume from ImageQuant analysis ± SEM; log-transformed normalized data were analyzed) for 6 high and 6 low fertility boars, except in β3 where gel from one high fertility boar was excluded as bands were not clear enough for quantification. * Band volumes differ ($p<0.05$) between high and low fertility boars. "X" Band volume does not differ from zero.

3.4.3. Relationship of Na^+/K^+-ATPase Isoforms to Fertility Measures

Linear regression detected a highly significant positive relationship of volume of α3 (Fig 3.5) with DBE FR (r^2=0.90; p<0.0001). The total volume of α1 also positively correlated with DBE farrowing rate, with a lower r^2 (r^2 = 0.35; p < 0.04). The volume of α2 tended to be related to DBE for TNB (r^2 = 0.30; p = 0.06), as did β1 with DBE for FR (total volume; r^2 = 0.2652; p = 0.0867).

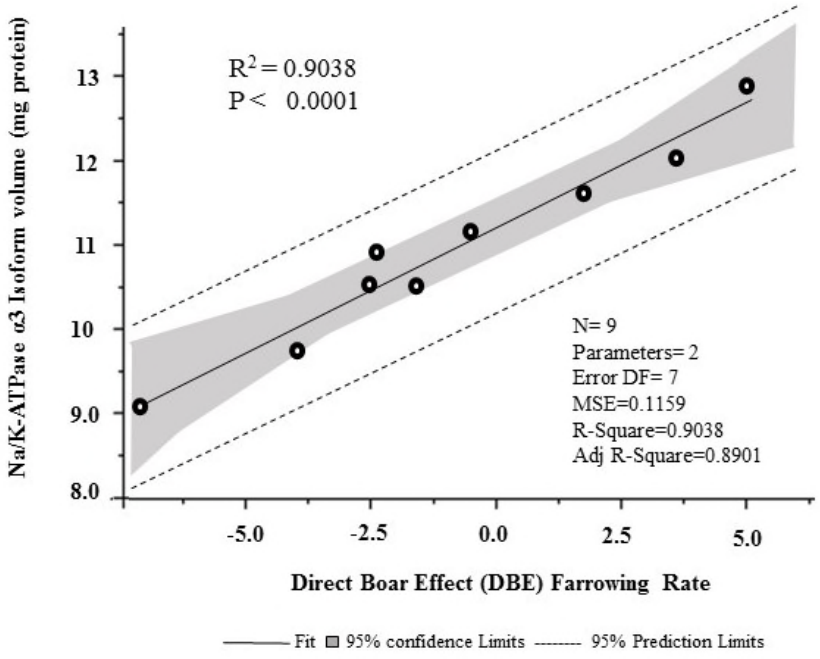

Figure 3.5. Linear regression of total amount of α3 with DBE for farrowing rate. The scatter diagram shows the Least Squares Regression Line best fit for all boars (n=9; equation y = 10.85203 x + 0.26302; r^2 =0.90, P<0.0001). Grey area along regression line shows 95% confidence limits and dotted lines shows 95% prediction limits.

3.4.4. Immunolocalization of the Isoforms

No intact sperm from either fertility group showed α1 fluorescence, but in methanol-permeabilized sperm; 16% from low fertility boars showed light apical fluorescence (pattern # 1) and all sperm from high fertility boars had no fluorescence (pattern #0). α2 was also rarely

Table 3.3. Immunofluorescence Pattern of Na^+/K^+-ATPase α Isoforms in Boar Sperm

Pattern	Intact sperm						Permeabilized sperm					
	α1		α2		α3		α1		α2		α3	
	High	Low	High	Low	High	Low	High	Low	High	Low	High	Low
0	99.8±.1	99.8±.1	83.1±13	82.1±13	69[a]±4.4	84.8[b]±4.4	100±8	83.3±8	67[a].6±13	10.3[b]±13	1.8±.3	1.6±.3
1	0	0	0.5±.25	0	0	0	0	16.3±8	0	17.5±7	0	0
3	0	0	0	10.8±5	0	0	0	0	0	0	0	0
4	0	0	15.8±10	7±10	0	0	0	0	0	0	0	0
5	0	0	.5±.25	0	0	0	0	0	32.3±18	23±18	0	0
6	0	0	0	0	0	0	0	0	0	16.3±8	0	0
7	0	0	0	0	0	0	0	0	0	32.8±10	0	0
8	0	0	0	0	0	2.5±2.2	0	0	0	0	0	0
9	0	0	0	0	23.1[a]±5	12.1[b]±5	0	0	0	0		0
10	0.1±.08	0	0	0	0	0.5±0.2	0	0.33±0.1	0	0	48.8±19	16.3±19
11	0	0.1±.08	0	0	1.6±0.8	0	0	0	0	0	49.3±19	82±19

Values are Mean ± SEM of sperm with that pattern, High fertility n=6, low fertility n=6, a-b, number of sperm with that pattern differ between high and low fertility boars ($p < 0.05$).

detected in intact sperm (Table 3.3), but permeabilized sperm showed distinct fertility-related differences: high fertility boars had detectable α2 fluorescence in one-third of permeabilized sperm, while sperm from low fertility boars had detectable α2 in 90% of permeabilized sperm ($p<0.05$). In the population of permeabilized sperm showing α2 one-third of high fertile displayed acrosomal light fluorescence (pattern 5), while from the 90% of permeabilized sperm from low-fertility boars that fluoresced, one-third showed acrosomal medium fluorescence (pattern 7),

while rest showed pattern 1(light apical; 17%), pattern 5 (acrosomal light, 23%) and pattern 6 (apical strong, 16%). More intact sperm from high than low fertility boars (Fig 3.6) had detectable α3 ($p<0.05$), virtually all as strong equator light over the post-equatorial segment (pattern 9, 23.1±5% vs 12.1±5% of sperm in high vs low fertility boars ($p<0.05$).

Virtually all permeabilized sperm had detectable α3 regardless of fertility, but while high fertility sperm were split equally between patterns 10 and 11 (48.8±19 and 49.3 ± 19%), low-fertility sperm were largely pattern 11 (16.3± 19 and 82 ± 19% for patterns 10 and 11, respectively).

Of β isoforms, β1 was detected (Table 3.4) in a few intact and permeabilized sperm from about half the boars, with no fertility-related differences; no sperm showed detectable fluorescence of β2 or β3. Overall, more intact sperm from HF boars while more permeabilized sperm from low fertile boars had immunocytochemically-detectable Na^+/K^+-ATPase.

Table 3.4. Immunofluorescence Pattern of Na^+/K^+-ATPase β Isoforms in Boar Sperm

Pattern	Intact sperm		Permeabilized sperm	
	β1		β1	
	High	Low	High	Low
0	88.3±11	80.8±11	84±15	85.3±15
2	0	16±8	0	14.6±7
3	3.1±2	2.3±2	0	0
4	0	0.66±.3	0	0
5	7.6±3.8	0	16±8	0
6	0	0.16±.08	0	0
7	0.8±.4	0	0	0

Values are Mean ± SEM of sperm with that pattern, High fertility n=6, low fertility n=6, 0= shows absence of any sperm under that pattern.

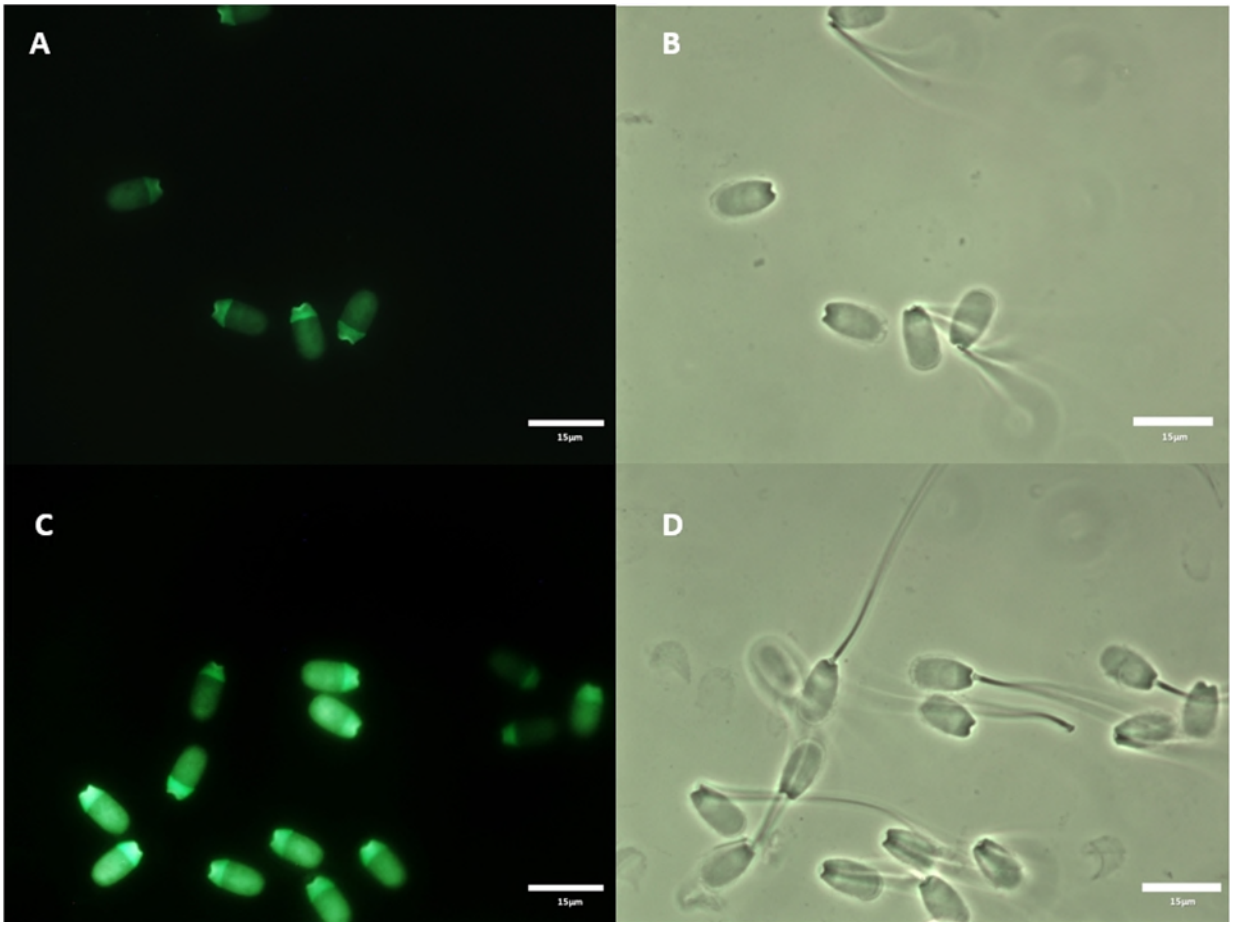

Figure 3.6. Immunofluorescence of isoform α3. Typical immunofluorescent images of fresh intact sperm from a (A) low fertility and (C) high fertility boar, after incubation with antibody specific to α3 isoform and exposure to FIT-Conjugated secondary antibody; imaged at 630 x magnification with fluorescence (495/519 nm). At right (B, D): same cells shown with phase-contrast imaging. Bar in 'A, B, C & D' indicates 15µm size.

3.5. Discussion

Boar *in vivo* fertility is strongly correlated here with the presence of various Na^+/K^+-ATPase isoforms, even though sperm motility are not correlated with fertility. The DBE for FR significantly correlated with semi-quantitative Western immunoblot analysis of the amount of α1 and α3 Na^+/K^+-ATPase isoforms, while β1 and α2 isoforms tended to positively correlate to DBE

for FR and total born, respectively. In immunofluorescence localization on fresh sperm, more intact sperm from high fertility boars had detectable α2 and α3 than in low fertile boars.

Boars have significant influence on FR and TNB, which may even exceed the sow's influence, particularly when females are bred by AI (Umesiobi, 2010). The DBE measures an individual boar's impact on FR and TNB against the average of the population being considered (Revay et al., 2015). Accuracy of DBEs for a particular boar depends upon the number of breedings considered and the number of boars in the comparator pool. The DBEs for each boar in this study were based on a minimum of 20 inseminations, and the DBEs for FR and TNB for high fertility boars were significantly above the population averages, while low fertility boars had DBEs for both FR and TNB that were significantly below those averages.

DBEs are quite accurate at predicting a boar's fertility, but they are retroactive assessments acquired after numerous breedings, and during the considerable time required, a poor DBE will be impacting the reproductive efficiency of the facilities where the breedings occur and resulting in the producer suffering economically for a low FR and/or TNB. Accurate early prediction of fertilizing capacity of a sire is highly desirable. Although commercial AI facilities widely use sperm motility measures in an attempt to assess fertility, and despite occasional studies that find a correlation of such a measure as progressive motility with FR (Broekhuijse et al., 2012), most research with boar sperm finds no evidence that CASA-assessed sperm motility is associated with fertility parameters once the extremely poor ejaculates are removed (Didion, 2008). This is particularly so in studies like the current one, where the boars' ejaculates have passed commercial quality standards; indeed, in this study, sperm from high and low fertility boars showed no differences in semen parameters, sperm morphology or CASA functional measures (Tables 3.1, 3.2) despite the boars' significant differences in *in vivo* FR and TNB. The tendency for LF boars

to have a higher sperm concentration in the semen samples received from breeding centre was unexplained; as the tendency was nonsignificant, it is difficult to speculate about any possible source or impact.

Fertilization is a complex process involving a large number of events (Jung et al., 2015). The reversible biochemical and physiological changes of capacitation (Yanagimachi, 1994) are part of that complexity, involving a series of membrane events including ion channel activations (Flesch & Gadella, 2000) and transmembrane signaling. Na^+/K^+-ATPase is an amphipathic HPM protein known in bull sperm (Zhao & Buhr, 1996; Hickey & Buhr, 2012; Rajamanickam et al., 2017) to be a hormone receptor, signaling Tyr-P and sperm capacitation (Thundathil et al., 2006; Sajeevadathan et al., 2019). Western immunoblotting and immunofluorescence here clearly demonstrate that boar sperm also contains Na^+/K^+-ATPase isoforms α1, α2, α3, β1, β2 and β3, confirming the findings of Awda et al. (2022, submitted). The two modes of detection provided generally similar results, with some unique findings that help interpret how this fascinating system is structured.

Immunofluorescent images were captured of both intact and methanol-permeabilised sperm exposed to fluorescently tagged Na^+/K^+-ATPase antibodies. The brief methanol-induced permeabilization allowed the fluorescent antibodies access to internal membranes and/or exposed more binding sites on the external membranes. Methanol preferentially dissolves lipid in the membrane bilayer, enabling antibodies to pass through sperm HPM and bind to isoforms exposed on intracellular membrane surfaces. Alternatively, lipid removal may expose more antigenic sites, enabling more of the larger heavier fluorescently tagged antibodies to bind. The α1 isoform was only evident in 16% of low fertility methanol-permeabilized sperm. This finding suggests that in LF, α1 isoform maybe localized in the inner leaflet of a very few sperm. It is also possible that,

the antigenic sites on α1 isoform of high fertility boars are more sensitive to damage induced by methanol. The minimal α1 immunofluorescence when WB detected the isoform suggests that the larger heavier fluorescently tagged antibody may interfere with the binding of paratopes to antigenic sites on α1 isoform.

The immunofluorescent images that we captured were similar to those obtained before. Immunofluorescently-detectable α2 differed with fertility, being more frequently detected ($p<0.05$) in permeabilized sperm from low fertility boars particularly in apical distributions, while significantly more sperm from fertile boars did not display α2 (Section 3.3.4). In Western immunoblotting of sperm HPM, α2 was present in extremely low amounts and total amounts of α2 was similar in high and low fertility groups (Fig 3.2). Given the immunohistochemical presence, the low presence in Western blotting could mean that α2's known lower structural stability (DiFranco et al., 2015) allowed it to be uniquely damaged during HPM isolation, so that it could not bind to the antibody. However, poorly-fertile boars did have two unique kDa α2 bands not detected in high-fertility boars (Fig 3.3B) and the presence of these bands, coupled with the greater visibility of immunofluorescing α2 in permeabilised sperm, may mean that in poorly fertile boars, α2 has some structural features that cause it to be more readily accessible in the membrane. Such accessibility could render it both more available to immunocytochemistry and also to being damaged in HPM purification.

The α3 isoform arguably had the most interesting characteristics, particularly as it relates to fertility. More intact sperm from high-fertility than low-fertility boars showed complete post-equatorial α3 presence, and there was more total α3 found in HPM from sperm of high fertility boars. The WB analysis was meticulously performed and each gel for each ejaculate included internal standards (per lane internal control were; kidney membrane 0.2 µg -10µg; Hela 2.3-

13.8µg; A431 6µg) and, as with previous work, protein loading was checked and verified (Sajeevadathan et al., 2019). This accurate measurement of the complete expression of the various immunosensitive protein bands for each isoform permitted rigorous statistical comparison among the isoforms and between the two different fertility groups (Fig 3.2-3.4). The greater total α3 ($p<0.05$) was largely centered around seven individual protein bands that were present in greater amounts (Fig 3.3C) in sperm HPM from high-fertility boars and a 43kDa band present that was undetectable in low fertility boars' HPM. Immunofluorescence also demonstrated a greater presence of detectable α3 in intact sperm, with unique patterns in the permeabilized sperm.

In cardiac cells, all α isoforms induce specific signaling after exposure to its hormone ouabain (Zhang et al., 2008; Peng et al., 2016). Ouabain is the steroid hormone that stimulates Tyr-P signaling cascades and capacitation in intact bull sperm (Thundathil et al., 2006) via cAMP/PKA, Src/ RTK/PLC/IP3/DAG/PKC and/or MAPK pathways (Newton et al., 2010; Rajamanickam et al., 2017). Interestingly, α3 is more sensitive to ouabain than α1 in rat brainstem axolemma (Blanco & Mercer, 1998). In a rat cell line, α3 Na^+/K^+-ATPase acts through Src-independent pathways involving PI3K and PKC (Madan et al., 2017). Coupling α3's role in ouabain-induced signaling in other studies with the significantly greater amount of α3 in high fertility boars and the strongly positive linear relationship of α3 with fertility (Fig 3.5), suggests that α3 has a critical role in fertilization by boar sperm. It is possible that α3 responds to ouabain binding by initiating a unique intracellular pathway not responsive to other α isoforms.

Part of this unique pathway may be the β unit binding to α3 to form the dimer to which the stimulating hormone ouabain binds. The total amount of β1 tended to be lower in low fertile boars (Fig 3.4b; $p=0.08$), there were non-significant 'missing' β1 bands in low-fertility boars, and β3 had significantly more of a 63 kDa band (Fig 3.4c; $p<0.05$) in high versus low-fertility boars.

Missing or different amounts of specific kDa bands could reflect the variability in structure of β subunits of Na^+/K^+-ATPase, and this structure could affect unique pairing of β subunits with α subunits. The specific composition of an αβ dimer could impact fertility by altering Na^+/K^+-ATPase 's signal transduction, which requires the pairing of the α and β subunits (Liu et al., 2000). Although β1 is the signaling partner with α1 or α3 in ouabain-mediated signaling in cardiac, renal, and neuronal cells (Guerrero et al., 2001; Pierre et al., 2008) and β1 plays a major role in cell adhesion and capacitation (Vagin et al., 2012), the actual αβ pair that optimizes Na^+/K^+-ATPase signaling in ouabain-mediated capacitation is unknown and of great physiological interest.

3.6. Conclusions

No sperm functional or gross morphological parameters were correlated to fertility in boars that had documented significant differences in farrowing rates and litter size. Immunofluorescence and/or Western immunoblotting detected all isoforms of Na^+/K^+-ATPase (α1, α2, α3, β1, β2, β3) in boar sperm, several of which were related to fertility. There was significantly more α3 Na^+/K^+-ATPase isoform presents in the sperm HPM from high than low-fertility boars, and there was a strong, significant linear relationship of the amount of the α3 isoform with DBE of farrowing rate. Understanding exactly which structural features of the individual isoform, or αβ paired isoforms, impact capacitation could improve the effectiveness of selecting boars for both AI and natural breeding, improving overall swine reproductive efficiency.

PREFACE TO CHAPTER 4

In the previous chapter, we identified and characterized the association of the various isoforms of Na^+/K^+-ATPase in sperm HPM to the *in vivo* fertility in boars. Fertility is a complex trait and involves interactions among multiple proteins in the sperm HPM, so to evaluate the fertility mechanisms difference in boar and bull and to elucidate the potential proteins playing key roles in regulating fertility in each species, bull sperm HPM was analyzed by MS. This chapter aims to identify and quantify all non-Na^+/K^+-ATPase proteins in sperm HPM which differ between Holstein bulls of differing *in vivo* fertility, measured by BFI. Tandem mass spectrometric analysis revealed 67 DAPs (differing by at least two-fold in spectral intensities) between bulls of high fertility (HF, n=3) and low fertility (LF, n=3); 48 proteins were up-regulated and 19 were down-regulated in HF vs LF. A variety of molecular and biological functions for these proteins were identified, including finding that up-regulated proteins have significantly more binding functions than do down-regulated proteins. When the 67 DAPs identified in HF and LF bulls were probed in 16 bulls of differing BFI (average to high fertile, ATH=8; average to low fertile; ATL=8), 38 of the up-regulated proteins positively correlated to BFI whilst 6 of the down-regulated negatively correlated to BFI.

A version of this chapter is ready to submit to Journal of Molecular Biology under joint co-authorship with George S. Katselis, Paulos Chumala and Mary M. Buhr.

As first author, Muhammad Imran contributed to the experimental design, conducted the study, performed the data analysis, and wrote the first draft of the manuscript. Paulos Chumala contributed to the data analysis. George S. Katselis and Mary M. Buhr conceived the idea and contributed to the experimental design, revised the manuscript, and supervised the project.

CHAPTER 4: COMPREHENSIVE PROTEOMICS ANALYSIS OF BOVINE SPERM HEAD PLASMA MEMBRANE ASSOCIATED WITH FERTILITY

4.1 Abstract

Bull fertility impacts herd fertility, but accurately predicting male fertility from sperm characteristics is difficult once extremes are removed. The objectives of this study are identification, relative quantification, and comparison of sperm HPM proteins in bulls of differing fertility (fertility characterized by Bull Fertility Index; BFI). HPM from one fresh ejaculate from 16 Holstein bulls (8 each high and low fertility) was assessed by liquid chromatography MS/MS. Proteins were extracted and digested. From each animal 9 fractions as, technical replicates were prepared and analyzed by liquid chromatography-tandem mass spectrometry (LC-MS/MS), their spectra were aligned to UniProtKB mammal's database using Spectrum Mill and HPM proteins were identified and characterized. Of the 22,117 total proteins identified [unique plus homologous, 1% false discovery rate (FDR)], Mass Profiler Professional (MPP) statistical analysis identified 67 DAPs in the HPM of 3 bulls each with highest and lowest BFI [BFI for high fertility (HF)105.66 ± 0.54; low fertility (LF) 91.33 ± 1.44; $p<0.01$]. DAPs differed in intensity by at least 2-fold (48 up-regulated, 19 down-regulated, HF vs LF) and meta-analysis confirmed their association to BFI. Gene ontology (GO) assigned the 48 up-regulated proteins to sperm fertilization mechanisms, and the 19 down-regulated to catalytic and transporter activity. Linear regression significantly positively correlated BFI of the 6 HF and LF bulls to all up-regulated DAPs (r^2=0.65 to 0.97, $p\leq0.05$), and negatively correlated BFI to all down-regulated DAPs (r^2=0.76 to 0.96, $p<0.05$). In the 16-bull population, linear regression positively correlated BFI to 38 of the up-regulated DAPs (r^2=0.29 to 0.66; $p\leq0.05$), and negatively correlated 6 of the down-regulated DAPs (r^2=0.26 to 0.44; $p\leq0.05$). Overall, this study identified and characterized proteins from highly purified bull HPM, which are correlated to bull fertility.

4.2 Introduction

Reproductive efficiency of the male includes the ability of sperm to fertilize oocytes (Amann et al., 2018). To fertilize the oocyte, spermatozoa must be motile with functional mitochondria, a nucleus capable of proper decondensation and reorganization inside the fertilized oocyte, and an active and intact sperm plasma membrane (Graham & Mocé, 2005), so they can reach, recognize, bind to and fuse with the oocyte (D'Amours et al., 2010). All these events are essential for successful fertilization and any defect can cause sub-fertility or infertility (Amann et al., 2018).

More than 70% of dairy cows are bred by AI using frozen semen from genetically superior bulls, but only 50% of inseminations successfully cause pregnancies. Dairy bull fertility is based on the failure of an inseminated cow to return to estrus (NRR; Doormaal, 1993; Watson, 2000) which is influenced by several factors including the cow's age and parity, herd management, inseminator, etc. The Canadian dairy industry defines a BFI based on all of these, and other, factors from thousands of inseminations from hundreds of bulls; a complex regression analysis derives the BFI having accounted for confounding factors and sets the population BFI at 100 (D'Amours et al., 2010; Butler et al., 2020).

Diagnosing and predicting bull fertility is essential in the breeding industry to optimize male fertility and reduce pregnancy failures (Tahmasbpour et al., 2014). To assess the bull fertility by natural mating or AI can be time consuming and expensive and limits the number of bulls to be assessed at a given time. Efficient economical laboratory diagnostic methods currently analyze sperm structural and functional parameters including sperm kinetic and motility parameters by CASA, sperm oocyte penetration assay (Hwang & Lamb., 2013), semen biochemical compounds, acrosome and plasma membrane integrity, mitochondrial membrane potential, and sperm DNA

fragmentation (Kasimanickam et al., 2019; Kim 2018). However, none of these is sufficiently accurate and repeatable in predicting *in vivo* bull fertility to be of use to the AI industry (Sudano et al., 2011; Kasimanickam et al., 2019).

Omics approaches including genomics, transcriptomics, proteomics, and metabolomics tools may hold the key for accurate diagnosis of male infertility (Peddinti et al., 2008). Proteomics is an emerging approach for studying andrological aspect in humans and animals and to understand the biological mechanisms of sperm function and its interaction with the oocyte leading to fertilization (Wright et al., 2012; Al-Amrani et al., 2021).

So far proteomics studies have been performed to identify protein biomarkers in bull sperm associated with fertility by comparing whole sperm from high versus low fertility bulls in buffalo (Singh et al., 2018; Muhammad Aslam et al., 2019) and cattle (D'Amours et al., 2018, 2019). Studies to characterize the semen proteome have also been done in frozen bull semen (Singh et al., 2018), in *Bos taurus* seminal plasma (Druart et al., 2013; Muhammad Aslam et al., 2014; Viana et al., 2018; Kasimanickam et al., 2019), fresh whole sperm (Kasimanickam et al., 2019), frozen whole sperm (Peddinti et al., 2008; Somashekar et al., 2017; Muhammad Aslam et al., 2018; Singh et al., 2018; D'Amours et al., 2018, 2019), and sperm surface proteins (Byrne, et al., 2012), as well as to *Bos indicus* whole sperm (Singh et al., 2018; Muhammad Aslam et al., 2019). These studies have, however, been limited by the smaller number of inseminations from bulls used in experiments, and lack in-depth analysis of sperm HPM and prediction of complex interactions among HPM proteins, which control sperm-oocyte binding and fertilization. Therefore, identification of a cohort of structural and functional sperm HPM proteins impacting the mechanism of fertilization makes our work unique, important, and necessary.

A spermatozoon is a highly specialized and differentiated cell composed of different compartments (head, midpiece, tail) whose specialized proteins confer unique compositional, morphological, and functional properties (Martínez-Heredia et al., 2006). Whole sperm proteomics analysis does not localize identified proteins to specific compartments (Baker et al., 2013). Proteomics analysis of sperm specific compartments isolated by subcellular fractionation not only identifies these unique proteins but enables enrichment of less concentrated proteins in the subcellular sample. It also gives more probability for identification of low abundance proteins in the sperm (de Mateo et al., 2011; Amaral et al., 2013; Baker et al., 2013). The proteomics analysis of the isolated heads and tails from the same sperm samples supports the idea of the compartmentalized expression of proteins in the sperm (Baker et al., 2013).

Subcellular components of sperm have specialized proteins. Human sperm nuclei contain chromatin-related proteins, histone variants, transcription factors and zinc fingers, and modified proteins involved in regulatory roles (Castillo et al., 2014; de Mateo et al., 2011).Tail proteomics identified proteins involved in energy production (Amaral et al., 2013; Baker et al., 2013), metabolic pathways, and peroxisomal proteins (Amaral et al., 2013; Codina et al., 2015) .The ADP/ATP carrier protein in the midpiece of human sperm may indicate that the fibrous sheath is capable of generating and regulating ATP independently from mitochondrial oxidation (Kim et al., 2007).

Sperm membrane proteins are involved in recognition, binding to, and interaction with the oocyte. Heat shock proteins, calcium binding proteins (Naaby-Hansen & Herr, 2010) and proteins having binding affinity for ZP of oocyte were identified in human sperm plasma membrane (Nixon et al., 2011; Redgrove et al., 2011).

The plasma membrane of bull sperm has significant roles in progressive motility, fertilization, and transport of various ions across the membrane (Cornwall, 2008; Gadella & Boerke, 2016). Capacitation of sperm in the female tract involves remodeling of the plasma membrane, predominantly the HPM, that primes sperm for AE and binding to oocyte (Gadella & Boerke, 2016) and various important physiological functions during fertilization (Caballero et al., 2012).

The importance of the HPM in capacitation, AE and sperm-oocyte interactions are well established, but its unique protein composition is unknown. The objectives of this proteomics analysis were the identification and relative quantification of proteins in sperm HPM from bulls of differing fertility, the elucidation of protein-protein interactions, and the cellular functions as well as biological pathways that are associated with bull fertility.

4.3. Materials and Methods

4.3.1. Semen

One fresh double ejaculate (two ejaculates collected from same animal within 20-30 minutes and then pooled together) from each of 16 Holstein Friesian bulls of known field fertility (average-to-high fertility, ATH n=8; average-to-low fertility ATL n=8) was provided by SEMEX (Guelph, ON, Canada). Bull fertility was assessed as the international multi-factor BFI which is a Semex internal calculation composed of NRR (56 days post service: Canadian Index), sire conception rate (SCR) (USA index) and Agri-Tech analyses (ATA, USA index). Average BFI is100 based on >1000 inseminations per bull, and bulls were identified as having BFI > or < 100 (ATH, ATL; n=8 each). As before (Sajeevadathan et al., 2021), two ejaculates were collected from each bull on one day by artificial vagina, combined, and the ejaculates with ≥80% motile sperm were diluted to 60×10^6 spermatozoa per mL with clear egg yolk-free extender (Semex proprietary

composition) and shipped overnight at 16 ºC to the laboratory at the University of Saskatchewan (Sajeevadathan et al., 2021). The temperature was checked on arrival and samples between 15-20 ºC were warmed to room temperature over 2h by being placed in a partially opened container, covered, and occasionally rotated until they reached room temperature 24 ± 1 ºC (≈ 90 min). On arrival, a 500 µL aliquot was transferred into an Eppendorf tube and incubated at 37 ºC for slow warming (70 min). Following that it was evaluated for motility kinetics using CASA, Hamilton Thorne IVOS II (MA, USA) utilizing a 4 µL semen on a 20 µm deep Leja standard count slide (Leja products B.V., Nieuw-Vennep, The Netherlands) while kept at 37 ºC (Anzar et al., 2009, 2011; Sajeevadathan et al, 2021). Ejaculates whose temperature on arrival was 15-20 ºC, and whose CASA parameters included ≥ 60% total/ 55% progressive motility, were processed to obtain the HPM once the ejaculate reached room temperature (Hickey & Buhr, 2012).

4.3.2 Reagents and Equipments

Disodium phosphate, sodium dihydrogen phosphate monohydrate, dextrose, 1.5 M sucrose, polyethylene glycol (40%), methanol HPLC grade, and trypsin were purchased from Thermo-Fisher Scientific (Unionville, ON, Canada) and percoll from GE Healthcare (Mississauga, ON, Canada). Potassium chloride, 20% dextran, sodium chloride were acquired from Sigma-Aldrich, (Oakville, ON, Canada). Milli-Q water obtained from water purification system Serv A Pure (MIUS) and MS-SAFE protease and phosphatase inhibitor cocktail from Merck KGaA (Darmstadt, Germany). Bicinchoninic acid protein assay kit including BSA were purchased from Thermo Fisher Scientific (Waltham, MA, USA). LC/MS grade water, and LC/MS grade acetonitrile, were purchased from Fisher Scientific, (Fair Lawn, NJ, USA), as were ABC buffer, trifluoroethanol (TFE) and iodoacetamide (IAA). DTT was purchased from MP Biomedicals (Solon, OH, USA). SCX Spin Tips sample preparation kit was from Protea Biosciences

(Morgantown, WV, USA), ammonium formate from Sigma (St. Louis, MO, USA) and trypsin from Pierce (Rockford, IL, USA). MS vials and Polaris-HR-Chip 3C18 were purchased from Agilent (Agilent Technologies Canada Ltd., Mississauga, ON, CA).

4.3.3 Isolation of Sperm HPM

The HPM was obtained according to an established procedure (Buhr et al., 1993; Zhao & Buhr, 1996; Hickey & Buhr, 2012), performing all steps at room temperature unless specified otherwise. Briefly, the sample was centrifuged (Jouan CT 4.22; Jouan S.A., Saint-Herblain, France; 800 x g; 10 min), and pellets resuspended into phosphate buffered saline (PBS; 125 mM NaCl, 8 mM Na_2HPO_4, 2 mM NaH_2PO_4.H2O, 5 mM KCl, 5 mM dextrose) with repeated gentle aspiration, pooled to ~40 mL and centrifuged (800 x g; 10 min). The resulting pellets were resuspended in PBS to 40 mL, layered onto 35% percoll (1:2 v: v; percoll: PBS) centrifuged (800 x g; 10 min), the supernatant discarded, and the pellet washed twice with PBS (800 x g, 10 min). The final pellet was subjected to nitrogen cavitation in a cell disruption Parr cavitation unit (Parr instrument company, IL, USA; 650 psi, 10 min) introducing nitrogen gas over 90 sec to a final pressure of 650 psi, holding for 10 min and then releasing pressure over 90 sec. Finally, the cavitate was centrifuged at 800 x g for 10 min. Phase partition tubes were prepared by mixing 3.94 g 20% dextran (1:5 g: g; dextran: water), 1.97 g 40 % PEG (1:2.5 g: g; PEG: water), 0.19 g PBS (in 1000 mL water), 2.42 g 1.5 M sucrose (in 100 mL water), covering and keeping in fridge overnight. The resulting supernatant was layered onto four phase partition tubes. Tubes were mixed by inversion 20 times, centrifuged (800 x g; 10 min), and the top portion harvested. This portion was layered onto four fresh phase partition tubes, mixed, and centrifuged as before. The final top layers were centrifuged (206,000 x g; 30 min; 5 ºC), the pellets resuspended in PBS, pooled, and centrifuged (206,000 x g; 20 min; 5 ºC). The final pellet (HPM) was scraped out into a hand-held homogenizer

by stepwise adding 200 µL PBS, and homogenized. To inactivate endogenous proteolytic and phospholytic enzymes that degrade the HPM proteins, and its activation states, MS-SAFE Protease and Phosphatase Inhibitor cocktail was added (1.33 mL per mg of HPM). The samples were homogenized, aliquoted into eppendorf tubes, covered with nitrogen gas, snap frozen in liquid nitrogen, and stored at -80 ºC.

4.3.3.1 Protein Digestion

For measuring HPM protein concentration, an aliquot was thawed at room temperature and the concentration of the HPM protein was determined by bicinchoninic acid analysis using the BioTek ELx808 (BioTek- Instruments Inc., VT, USA) multi detection plate reader (wavelength 562 nm) and BSA as the standard protein (Nair et al., 2021).

Triplicates made from each HPM sample were digested into peptides using in-solution trypsin digestion protocol developed in our laboratory (Nair et al., 2021; Koziy et al., 2022). Briefly, HPM samples with concentration > 5.0 µg protein/µL were diluted with water to make it 5.0 µg/µL and samples with concentration <5.0 µg/µL were mixed (without dilution) with 1 M ABC (45 µL sample in 5 µL ABC), and proteins in HPM were denatured with addition of 50 µL TFE (total sample volume 100 µL). Disulfide bonds in HPM proteins were reduced by adding 1 µL of DTT solution (1 M DTT in 100 mM ABC: final concentration of 10 mM DTT) upon incubating for 1 h at 6ºC while shaking on Eppendorf Thermomixer (Eppendorf, ON, Canada) at 500 rpm. To prevent disulfide bonds from reforming, proteins in HPM samples were alkylated with 55 Mm IAA (100 µL of 100 mM IAA) and incubated in the dark at 37ºC for 30 min while shaking at 300 rpm. Samples were then evaporated (25 min, 37ºC) in a speed-vac (Labconco, Kansas City, MO, USA) to a final volume of 100 µL. Later, to remove salts, polymers and lipid contaminations, sample proteins were precipitated with excess acetone (-80ºC, 1h), centrifuged

(30 min, 4ºC, 13,000 x g) in Eppendorf centrifuge 5430 R (Eppendorf AG, Hamburg, Germany), the supernatant discarded, and acetone precipitation repeated. The samples were then completely dried (25 min, 37ºC) in speed-vac (Koziy et al., 2022) and resuspended in 300 µL of 100 mM ABC. Finally, HPM proteins were digested by adding trypsin digestion buffer (20 µg /µL trypsin in 1 mM HCl and 200 mM ABC solution; protein: trypsin, 40:1, v: v) and incubating overnight with shaking (37 ºC, 300 rpm). For complete sample protein digestion, the same amount of trypsin buffer was added the next morning, and samples incubated (2 h, 37ºC, shaker 300 rpm), dried (speed vac), and stored at -80ºC until SCX fractionation (Koziy et al., 2022).

4.3.3.2 Strong Cation Exchange (SCX) Peptide Fractionation

Peptide fractionation, using SCX Spin Tips was incorporated as an orthogonal approach coupled to reverse phase LC to minimize sample complexity and increase resolution prior to MS/MS analysis (Mirzaei & Regnier, 2006; Creese et al., 2013). From each animal's HPM, 9 fractions were acquired and considered as technical replicates for further in-depth MS study. Briefly, the manufacturer's protocol was followed, in which the SCX Spin Tip column was conditioned by adding 50 µL SCX reconstitution solution and centrifuging in Eppendorf centrifuge 5430 R (Eppendorf AG, Hamburg, Germany) at 4000 x g for 6 min. The liquid was discarded, and the process was repeated. To achieve charge-based peptide separation, trypsin-digested sperm HPM peptides were reconstituted in 100-200 µL of SCX reconstitution solution (pH < 3, adjusted with formic acid), loaded on the SCX Spin Tip column, and centrifuged at 4000 x g for 6 min. The Spin Tip column was then eluted by centrifugation (4000 x g, 6 min) using a solution of ammonium formate in 10% acetonitrile in stepwise increasing strength (20, 40, 60, 80, 100, 150, 250 and 500 mM, respectively; 150 µL each; pH ~ 3). A total of 9 fractions, including the flow through fraction,

were acquired, and stored at -80 ºC until MS analysis. The increasing ionic strength of the solution displaces cations, thereby displacing and separating peptides (Henry et al., 2017; Nair et al., 2021).

4.3.4 Label Free Mass Spectrometry Analysis

The dried SCX 9 fractions containing tryptic peptides were reconstituted (MS grade water: acetonitrile: formic acid; 97:3:0.1; v:v, total vol 20 mL), vortexed (1-2 min), centrifuged (18000 g, 10 minutes, 4ºC) and 3µL aliquots of each sample were transferred to a MS vial for LC-MS/MS analysis (Brandt et al., 2019; Nair et al., 2021; Koziy et al., 2022). The MS analysis was performed using an Agilent 6550 iFunnel quadrupole time of flight (Q-TOF) mass spectrometer (Agilent Technologies, Mississauga, ON, CA) coupled with liquid chromatography (Willems et al., 2016) using an Agilent 1260 series and an Agilent Chip Cube LC/MS interface respectively (Agilent Technologies, Mississauga, ON, CA) (Nair et al., 2021; Koziy et al., 2022).

Reversed phase chromatographic separation of peptides was achieved by employing a high-capacity Agilent HPLC-Chip; G4240-62030 chip cube, Polaris-HR-Chip 3C18 containing of a 360 nL enrichment column and a 75 µm × 150 mm analytical column (Agilent Technologies, Mississauga, ON, CA); both columns were packed with Polaris C18, 180Å, 3 µm stationary phase for improved peptide resolutions and peak capacity. Peptide fractions were suspended in 50% solvent A (0.1% formic acid in MS water) and 50% solvent B (0.1% acetonitrile: formic acid) then loaded onto the enrichment column (flow rate 2.0 µL/min; Brandt et al., 2019).

After loading, fractionated peptides were separated on the analytical column with linear gradient solvent system. On analytical column, the linear gradient program was used for peptide separation in presence of Solvent A and B. The linear gradient for solvent B was set at (3–25%, for 50 min) then at (25–90 %, for10 min) using flow rate of 0.3 µL/ minute. Mass spectra, from electron spray positive ions were obtained under conditions of: capillary voltage (1900 v), ion

fragmentor voltage (360 V), temperature (225ºC) and flow of nitrogen gas (12.0 L/min) (Brandt et al., 2019). For spectral results the parameters were: MS data mass range of 250–1700 (mass/charge; m/z) at a scan rate of 8 spectra/s, MS/MS data range (100–1700 m/z), isolation width of 1.3 atomic mass units. For auto MS/MS, a maximum of 20 precursor ions were selected at an absolute threshold (3000 counts) and a relative threshold (0.01% with a 0.25 min active exclusion) (Brandt et al., 2019; Nair et al., 2021; Koziy et al., 2022).

4.3.5 Database Search and Analysis

The acquired raw MS/MS spectra were searched against proteins from *Mammals* species using the Swiss Prot database (UniProt release 2020_06), by the Agilent Spectrum Mill search engine (Agilent Technologies, ON Canada). The database search parameters were trypsin as enzyme for protein digestion; trypsin cleavages specificity; fragment mass error 50 PPM, a parent mass error of 20 PPM and carbamidomethylation as fixed modification of cysteine. Additionally, four stages of database search in variable modification mode were conducted with different sets of variable modifications. During the first stage, the phosphorylated serine, tyrosine, and threonine, carbamylated lysine, oxidized methionine, acetyl lysine, pyroglutamic acid and deaminated asparagine were set as variable modifications. The second stage included validated hits from the first stage were searched using the following variable modifications: phosphorylated serine, tyrosine, and threonine, oxidized methionine, acetyl lysine, pyroglutamic acid and deaminated asparagine. In the third stage, the validated hits from the second stage were searched using semi-trypsin non-specific C-terminus, generating validated hits at the third stage, which were subsequently searched in fourth stage using semi trypsin non-specific N-terminus without specific variable modifications. During each stage, Spectrum Mill validation was performed both peptide level as well protein level. At peptide level, validation was performed with criteria of ; 1% FDR,

precursor charge range 2 to 7, and minimum peptide sequence length was 6, while at protein level, with 1% FDR the identified proteins were validated. Additionally, each DAP was manually validated through a rigorous validation process using Mass Hunter software (Agilent Technologies, ON Canada) and employing a mass difference cutoff of $\Delta m < 10$ PPM between observed and theoretical mass (Nair et al., 2021; Koziy et al., 2022). From identified total proteins in each animal, a comparison of proteins was made across ATH (n=8) and ATL (n=8) bulls. The proteins which were present in both groups were designated as common proteins, while proteins found only in one group were termed as unique proteins to that fertility group.

4.3.6 Statistical Analysis and Protein Network Analysis

The three bulls with the highest BFI were designated as high fertility (HF; BFI of 105,105,107) and the three with the lowest BFI were designated as low fertility (LF; BFI of 88,92,94*)*. For statistical analysis, t-test was used (Katselis et al., 2007; Koziy et al., 2022) and the two groups were compared by MPP (version 15.0, Agilent, Santa Clara, CA, USA) software. The multiple testing correction, Benjamini and Hochberg at FDR < 1% and cut-off value $p < 0.05$ was set and classification of proteins as up- or down-regulated was designated by using a fold change (FC) of ≥ 2 in spectral intensities between the comparing groups. The identified 67 significantly expressed proteins (DAPs) were manually validated by Mass Hunter software.

During the database search process (4.3.5), the raw spectra were searched against proteins in species of mammals, and a considerable number of proteins from some mammal's species are not well annotated. Therefore, the accession numbers of significant ($p < 0.05$) DAPs (up- and down-regulated) from multiple species were converted into homologous proteins of *Homo sapiens* in order to determine further protein-protein interaction (PPI) and networking. Subnetworks of up- and down-regulated DAPs with all identified non-differentially abundant (non-DAPs) proteins in

HPM were constructed with Cytoscape version 3.8.2 (Shannon et al., 2003). Cytoscape is an online bioinformatics tool that works for visualizing complex networks, loading molecular and genetic interaction data sets, establishing powerful visual mapping, analyzing, and visualizing human curated pathway data sets, and performing advanced modeling analysis. For determining PPI for each DAP, the first protein neighborhood forming interactions with each DAP was clustered together to make a sub-network of each target protein/DAP. The interacting partner proteins (IPPs, neighboring proteins in the interactome) in a cluster developed using Cytoscape v3.8.2, identified different PPI in each cluster/sub-network.

PPI network among DAPs were performed by the STRING (PPI Networks Functional Enrichment Analysis; https://string-db.org/) analysis. STRING is an online bioinformatics analytical tool that provides known (physical) and predicted protein-protein interactions among the input proteins. This database acquires the information from seven different channels in order to construct the PPI network clusters. STRING database evaluated the PPI clusters of these DAPs with known and predicted protein-protein interactions in each fertility group and their functional (molecular, and biological) networks in each of the fertility group (Szklarczyk et al., 2019). A Cytoscape analysis was performed to construct a complete interactome of HPM. To identify the most significant clusters in the DAPs' STRING PPI networks, the plugin molecular complex detection (MCODE) tool was used. A linear regression was performed stepwise with SAS statistical software (SAS; version 9.3; SAS Institute, Inc Cary, NC) on intensities of the DAPs to BFI, first with HF and LF (n=3 per group) and then for the whole population (n=16) of the bulls. The deterministic model used in equation (4.1) was;

$$y = a + bx \quad \text{(4.1)}$$

where a= intercept, b is = slope of the regression line.

4.4. Results

4.4.1 Protein Identification and Complete Interactome of HPM

The combined unique and common sperm HPM proteins from 16 bulls totalled 22,117. The 3 LF bulls had 4,040 total identified proteins (1,199 unique) and HF had 4,074 (1,156 unique).

Figure 4.1. Complete interactome of sperm HPM developed by Cytoscape v3.8.2 of annotated proteins (n=4,273) out of total proteins (2,2117) in population of 16 Holstein Friesian bulls. This demonstrates the clustering and complexity of the identified proteins. Elliptical dots in red and green represent proteins differing in intensity by at least 2-fold between the three bulls with the highest fertility index and the three bulls with the lowest fertility index (red=up-regulated; green=down-regulated).

Of the 22,117 bovine sperm HPM proteins, 4,273 could be annotated (statement of connection between a gene and its designated term in an ontology) and Cytoscape software constructed a complete interactome (Fig 4.1) that had 4,273 nodes and 27,473 edges. Fig 4.1 conveys the complexity and connectivity of the interactome, with each node representing an identified HPM protein (annotated to mammals) and each edge indicating interaction.

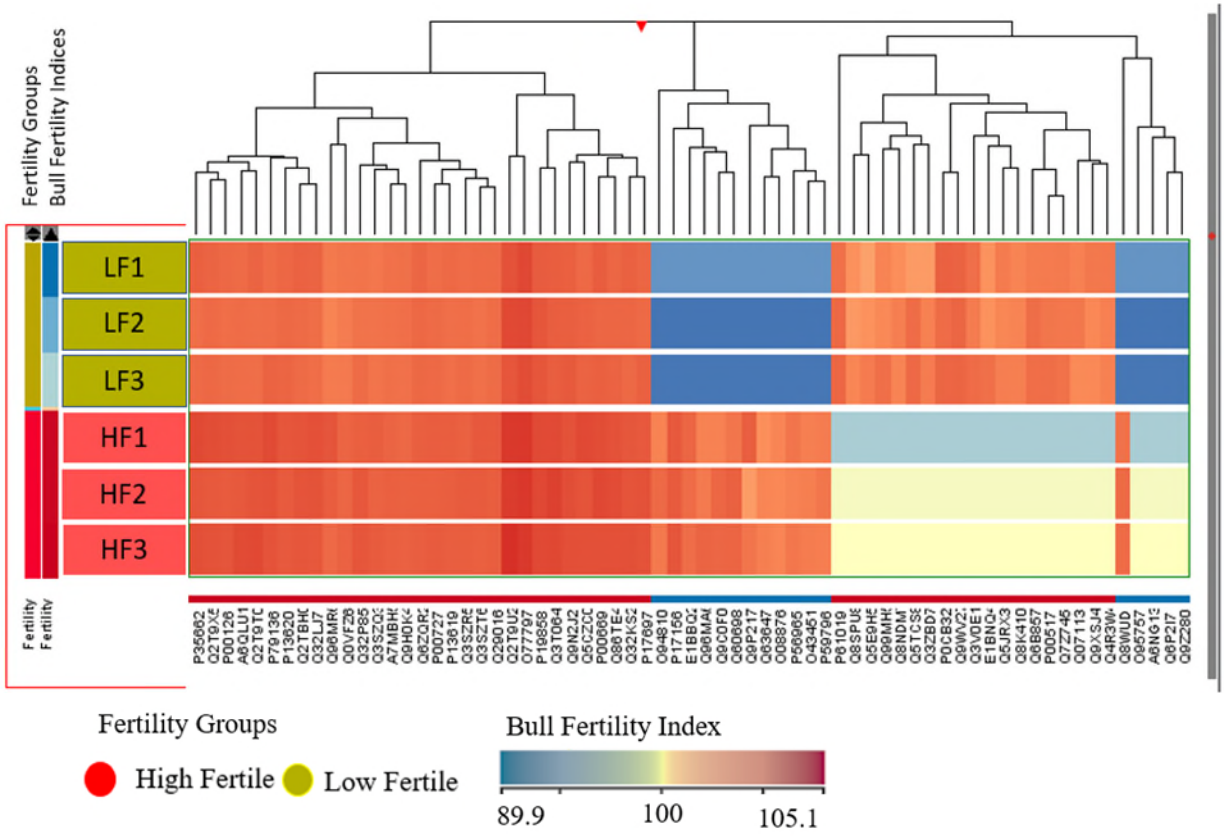

Figure 4.2. Heat map showing meta-analysis of the HPM DAPs differing by ≥ 2-fold in spectral count between high- versus low-fertility groups (HF, LF; n=3 per group) and their Bull Fertility Indices. The two vertical bars at the extreme left show Fertility Group (high, low), and Bull Fertility Indices (a scale of BFI is provided at bottom right below the heat map). Boxes between the vertical fertility bars and the heat map identify the individual bull (LF 1,2,3; HF 1,2,3) color-matched to Fertility Group (green LF, red HF). Heat map rows show individual bulls and heat map columns indicate protein accession numbers.

MPP compared the intensities of the annotated proteins in LF and HF, finding 67 proteins whose spectral intensities differed by at least 2-fold [DAPs; $p<0.05$; FDR at < 1%). Interestingly,

of the two major clusters in the interactome (Fig 4.1), all down-regulated DAPs occur in one of the clusters. The relationship of the 67 DAPs to BFI of the animals was confirmed by meta-analysis, as indicated in the heat map (Fig 4.2), where the 67 DAPs demonstrate a well-defined association with the fertility group/BFI.

4.4.2 Multivariate Analysis of Identified Proteins

Multivariate analysis of the DAPs identified clear fixed clustering (red and yellow circles) separating the two fertility groups. Principal component analysis (PCA) showed the 3-dimensional spread of the 67 DAPs differing between LF and HF bulls (Fig 4.3a) as did the spread of the average DAPs (Fig 4.3b). Protein abundance, as shown by the dot size, also differed in both analyses.

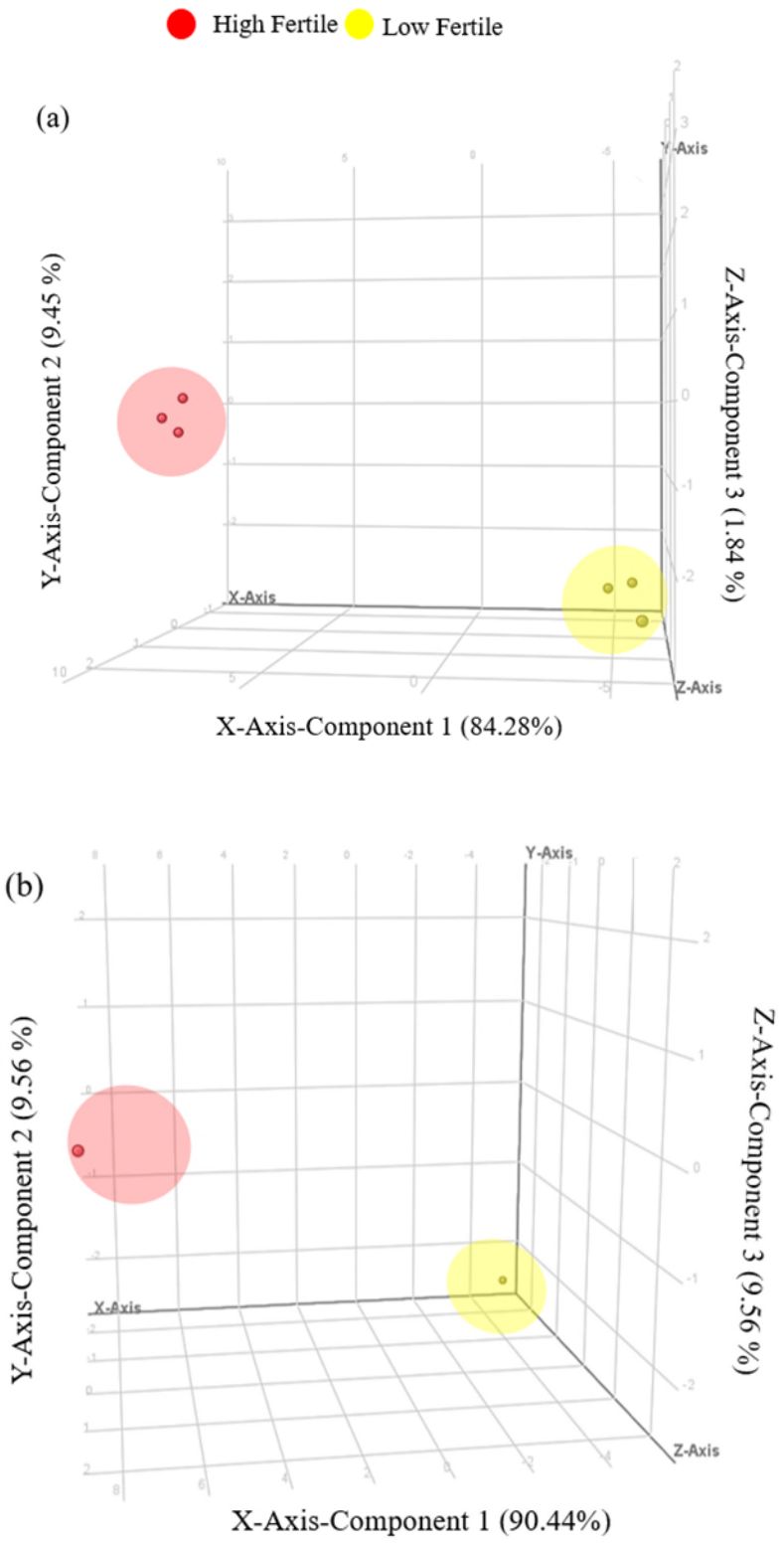

Figure 4.3. PCA plots of 67 DAPs in HPM of bull sperm of low and high fertility (n=3 per group). (a) Three-dimensional hard cluster of 67 proteins ($p < 0.05$; FC ≥ 2) (b) average of DAPs. Red

dots: High Fertile; yellow dots: Low Fertile; dot size: DAPs intensity. Red circle= High fertile cluster, yellow circle= Low fertile cluster.

Heat maps were drawn for the 67 DAPs, separately representing the 48 DAPs that were up-regulated in HF vs LF (Fig 4.4a) and the 19 that were down-regulated in HF vs LF (Fig 4.4b).

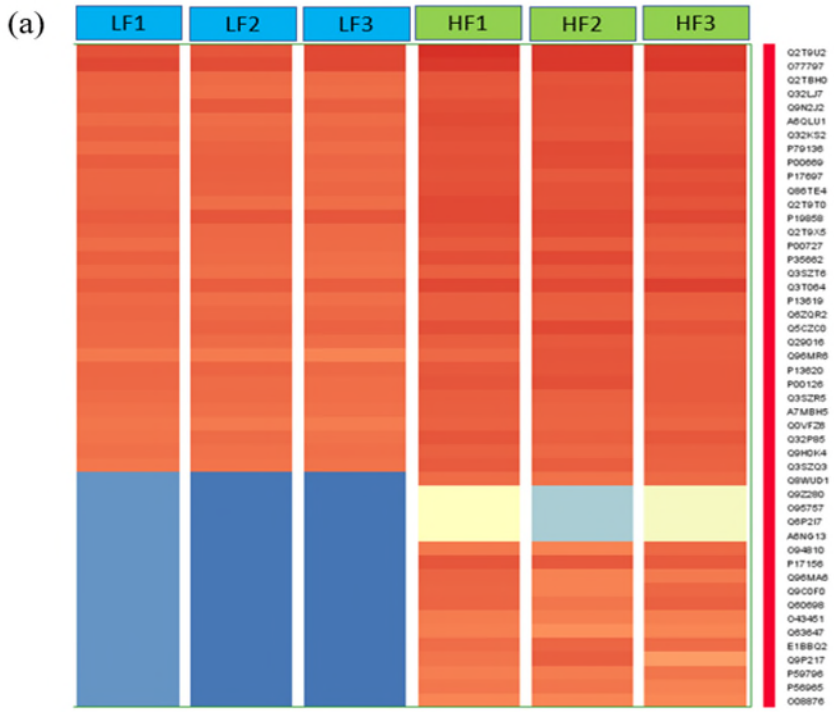

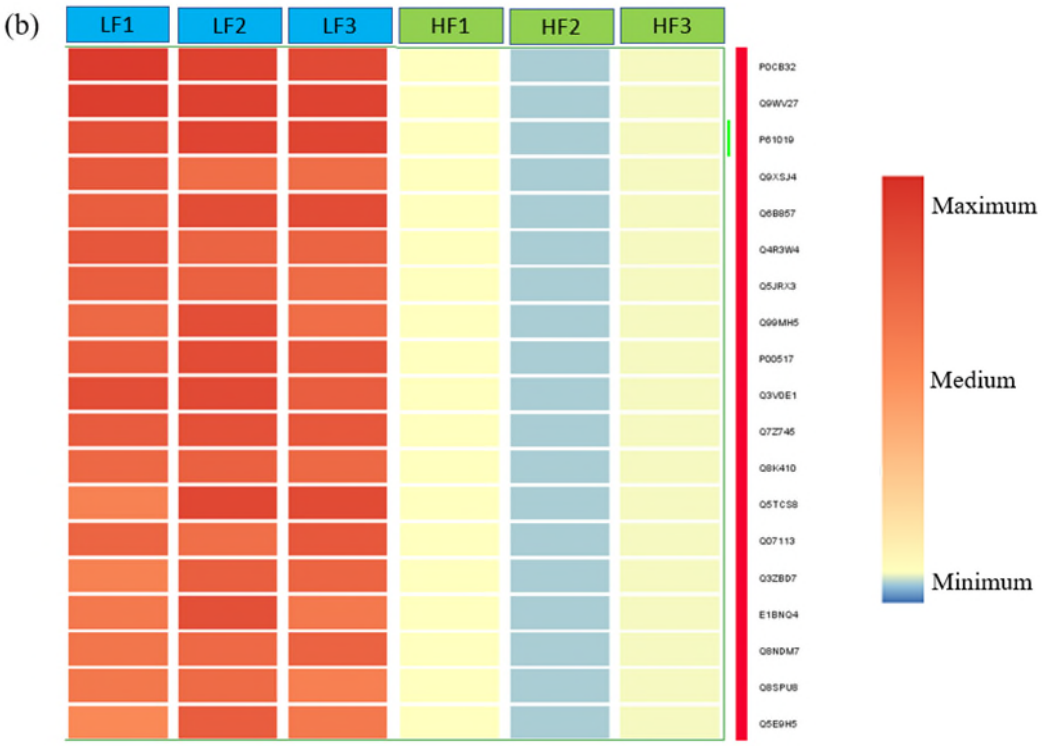

Figure 4.4. Heat map of DAPs ($p < 0.05$; FC ≥ 2) in sperm HPM of Holstein Friesian bulls of LF, and HF (n=3 per group). (a) up-regulated DAPs in sperm HPM of HF bulls. (b) down-regulated FC proteins in sperm HPM of HF bulls. Each row indicates accession numbers of every DAPs while every column shows individual bull. LF= low fertile and HF= high fertile bulls, respectively. A legend for color scale based on DAPs intensity is shown to the right of heat map.

4.4.3 Identification of Sub-Networks with FC Proteins

Cytoscape software visualized integrated sperm regulatory sub-networks for each of the sperm HPM DAPs with non-DAPs. Representative networks selected from these illustrate sperm function networks identified (Fig 4.5 a-n, upregulated DAPs: Fig 4.6 a-b, down-regulated DAPs).

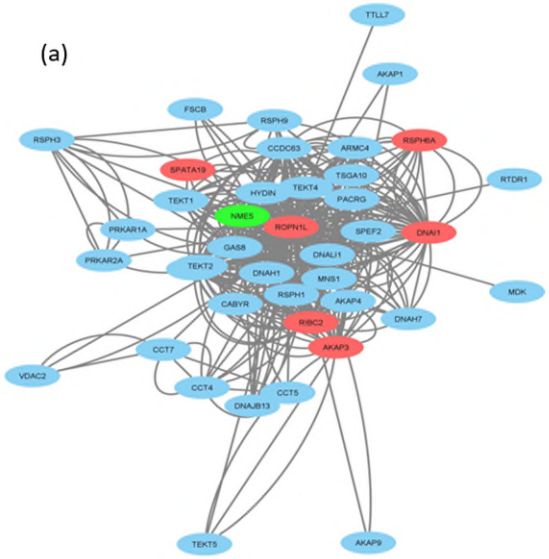

Ropporin-1-like protein

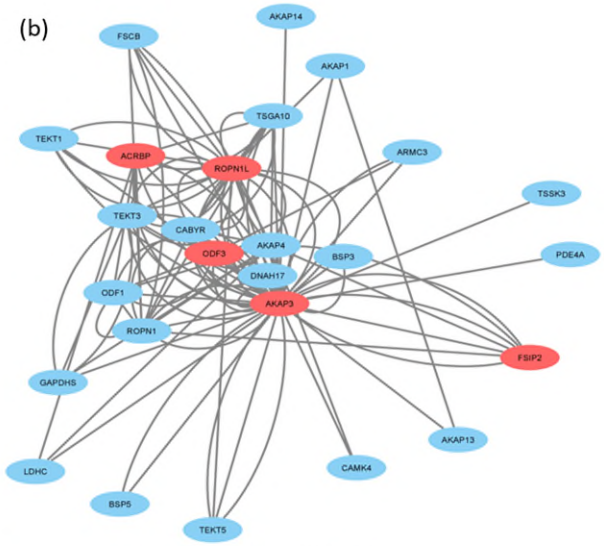

A-kinase anchor protein 3

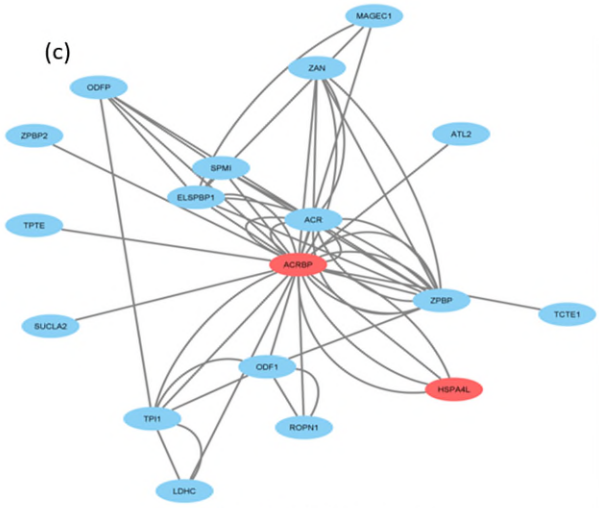

Acrosin-binding protein

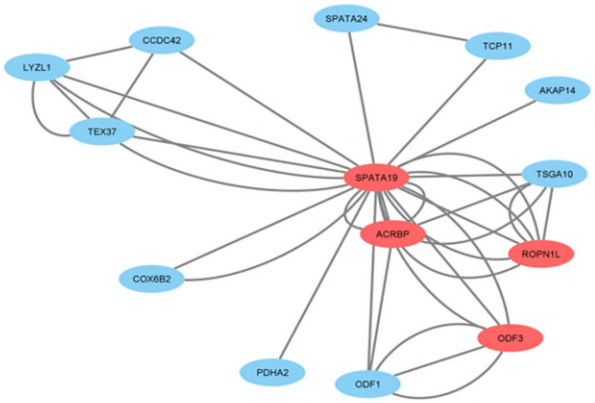

Spermatogenesis-associated protein 19

(e)

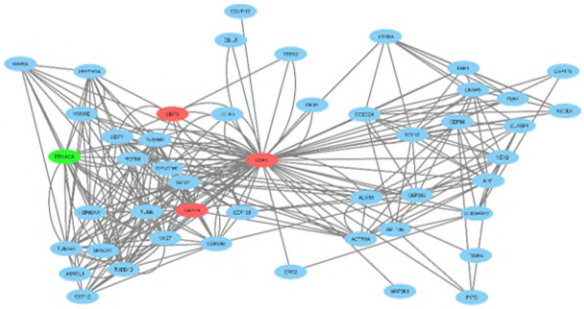

Outer dense fiber protein 2

(f)

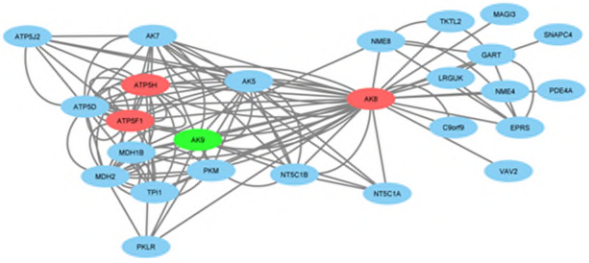

Adenylate kinase 8

(g)

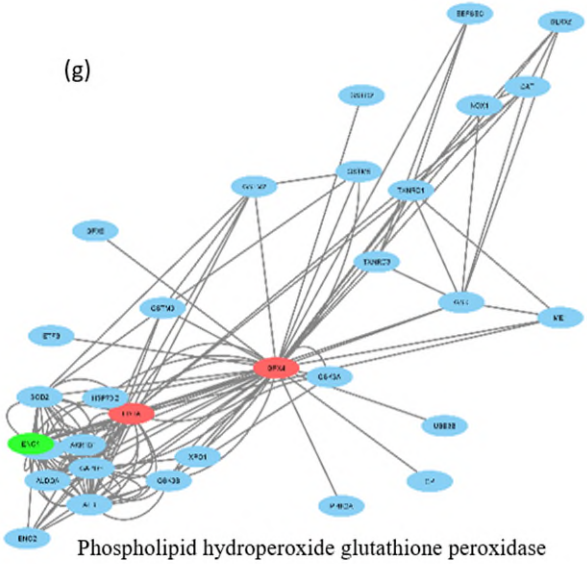

Phospholipid hydroperoxide glutathione peroxidase

(h)

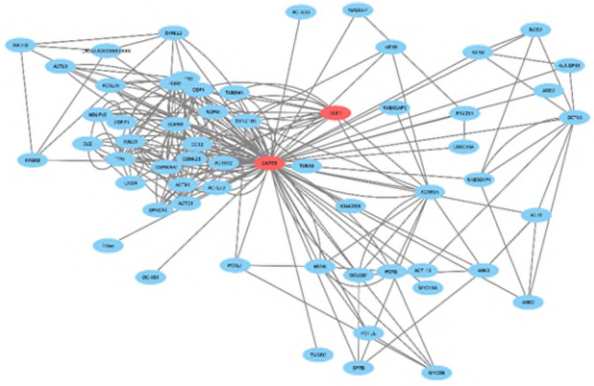

F-actin-capping protein subunit beta

(i)

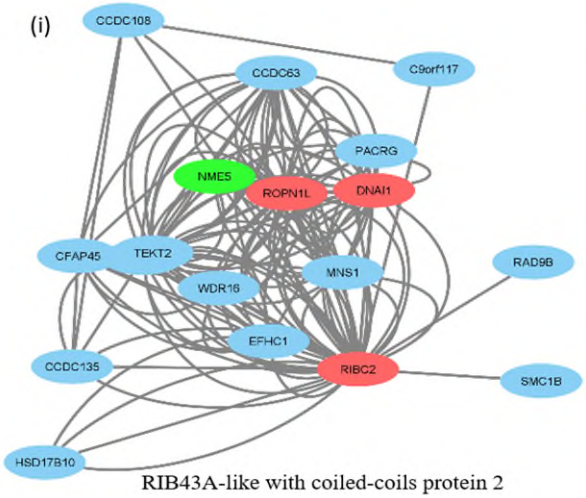

RIB43A-like with coiled-coils protein 2

(j)

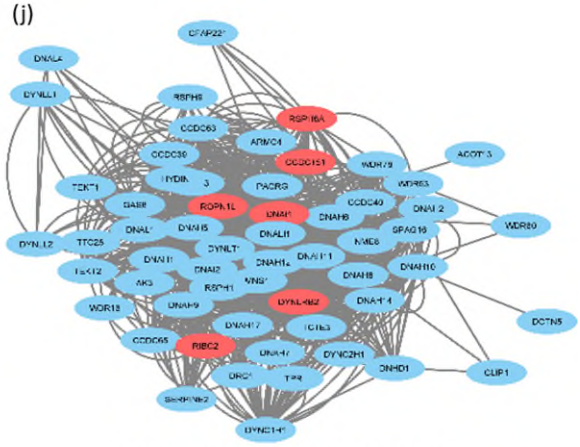

Dynein intermediate chain 1, axonemal

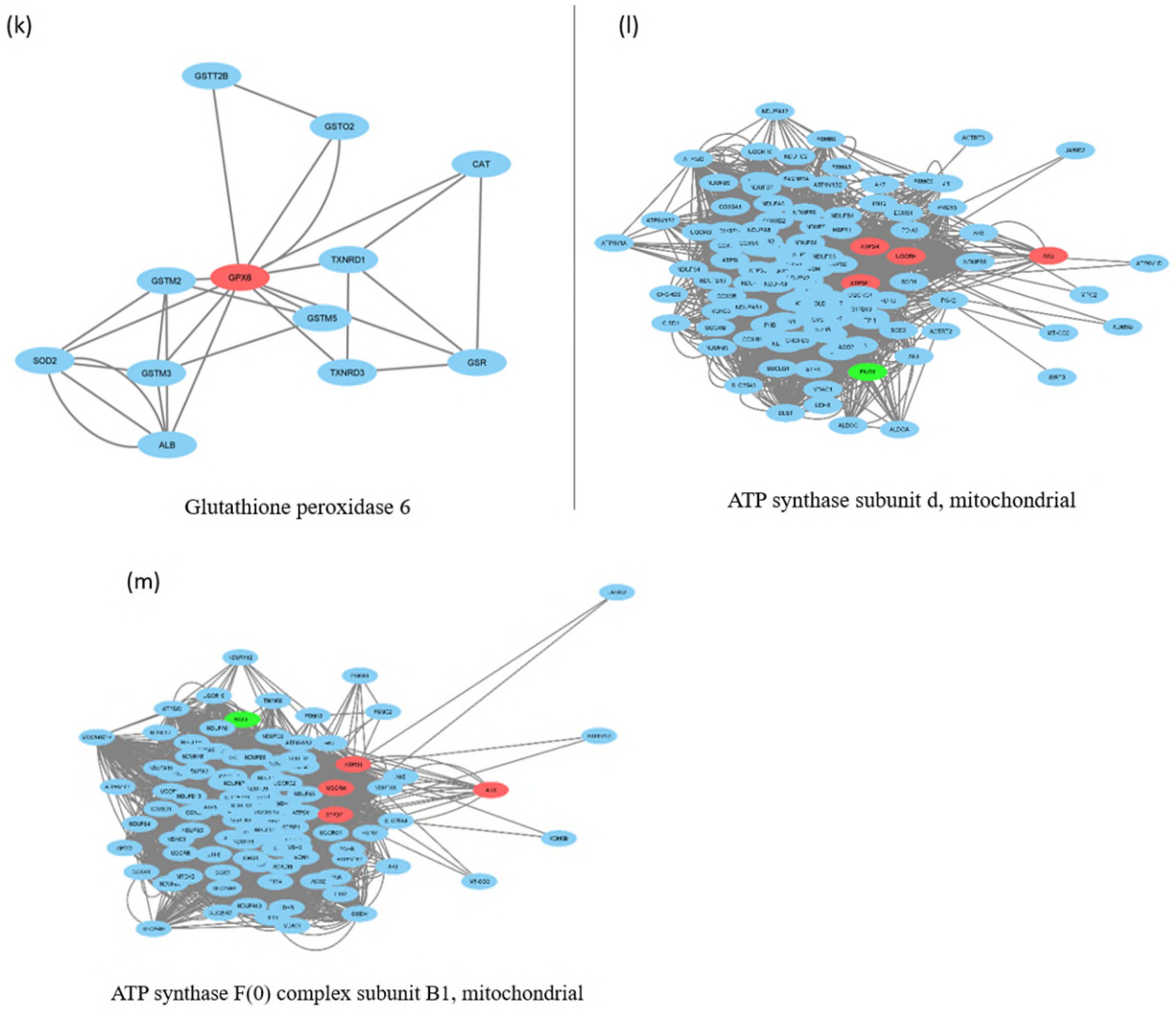

Figure 4.5. Sub-networks of selected up-regulated DAPs ($p < 0.05$; FC ≥ 2) proteins along with their IPPs (neighbor proteins in the interactome) showing different protein-protein interactions in each cluster. Ovals in red and green represent proteins differing in intensity by at least 2-fold between the three bulls with the highest fertility index and the three bulls with the lowest fertility index (red=up-regulated; green=down-regulated; blue=non-DAPs). DAPs in (a) were: Spermatogenesis-associated protein 19, Ropporin-1-like protein, RIB43A domain with coiled-coils 2, A-kinase anchor protein 3, Dynein intermediate chain 1, axonemal, Radial spoke head 6 homolog A in up-regulated and Nucleoside diphosphate kinase homolog 5 in down-regulated DAPs; (b) Acrosin-binding protein, Outer dense fiber protein 3, A-kinase anchor protein 3, Ropporin-1-like protein, Fibrous sheath interacting protein 2; (c) up-regulated DAPs: Acrosin-binding protein, Heat shock 70 kDa protein 4L; (d) up-regulated DAPs: Spermatogenesis-associated protein 19, Acrosin-binding protein, Ropporin-1-like protein, Outer dense fiber protein 3; (e) up-regulated DAPs: Outer dense fiber protein 3, Outer dense fiber protein 2, F-actin-capping protein subunit beta, down-regulated DAPs: cAMP-dependent protein kinase catalytic subunit alpha; (f) up-regulated DAPs: Adenylate kinase 8; ATP synthase F(0) complex subunit B1, mitochondrial, ATP synthase subunit d, mitochondrial; down-regulated DAPs: Adenylate kinase

9; (g) up-regulated DAPs: Phospholipid hydroperoxide glutathione peroxidase, mitochondrial; Lactate dehydrogenase A, down-regulated DAPs: Alpha-enolase; (h) up-regulated DAPs: F-actin-capping protein subunit beta; Outer dense fiber protein 2; (i) up-regulated DAPs: RIB43A domain with coiled-coils 2, Ropporin-1-like protein, Dynein intermediate chain 1, axonemal, down-regulated DAPs; Nucleoside diphosphate kinase homolog 5; (j) up-regulated DAPs: Dynein intermediate chain 1, axonemal, Ropporin-1-like protein, RIB43A domain with coiled-coils 2, Dynein light chain roadblock-type 2, Coiled-coil domain-containing protein 151, Radial spoke head 6 homolog A; (k) up-regulated DAPs: Glutathione peroxidase 6; (l) up-regulated DAPs: ATP synthase subunit d, mitochondrial, ATP synthase F(0) complex subunit B1, mitochondrial, Cytochrome b-c1 complex subunit 6, mitochondrial, Adenylate kinase 8; (m) Cytochrome b-c1 complex subunit 6, Adenylate kinase 8, ATP synthase F(0) complex subunit B1, mitochondrial, ATP synthase subunit d, mitochondrial and down-regulated DAPs: Mitochondrial chaperone BCS1.

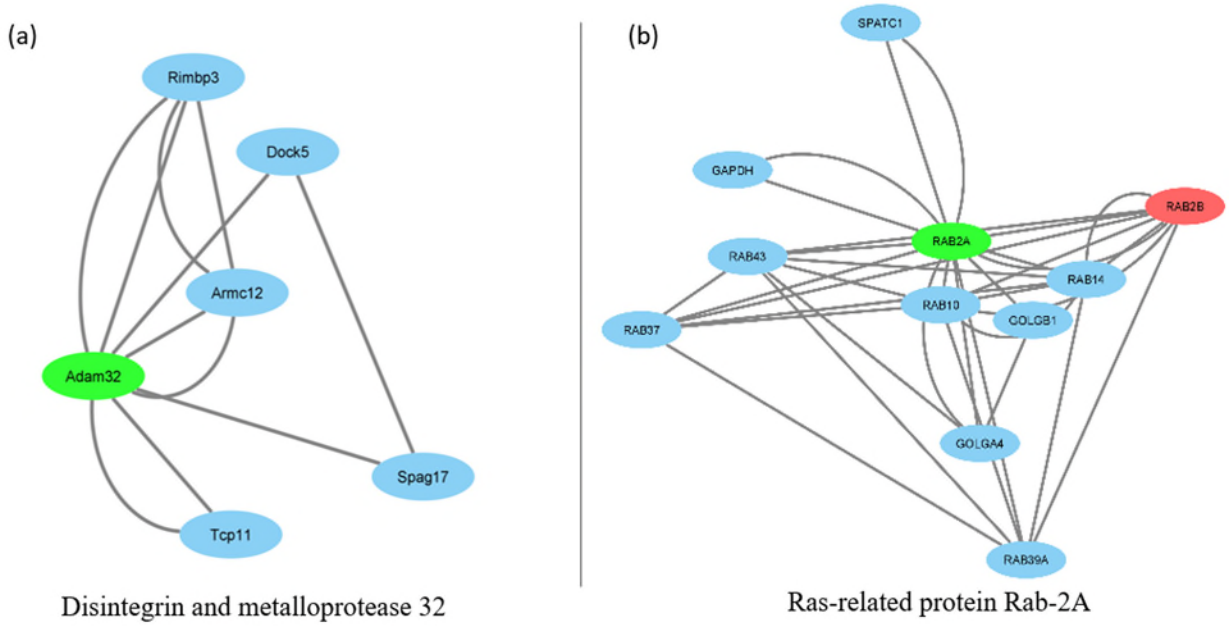

Figure 4.6. Sub-networks of selected down-regulated DAPs along with their IPPs (neighbor proteins in the interactome) showing different PPI in each cluster. Ovals in red and green represent proteins differing in intensity by at least 2-fold between the three bulls with the highest fertility index and the three bulls with the lowest fertility index (red=up-regulated; green=down-regulated; blue=non-DAPs). (a) down-regulated DAP: Disintegrin and metalloproteinase domain-containing protein 32; (b) up-regulated DAP: Ras-related protein Rab-2B, down-regulated DAP: Ras-related protein Rab-2A.

4.4.4 DAPs Protein-Protein Interaction and STRING Network

The STRING PPI network constructed on the setting ‘evidence based’ and mapping 7

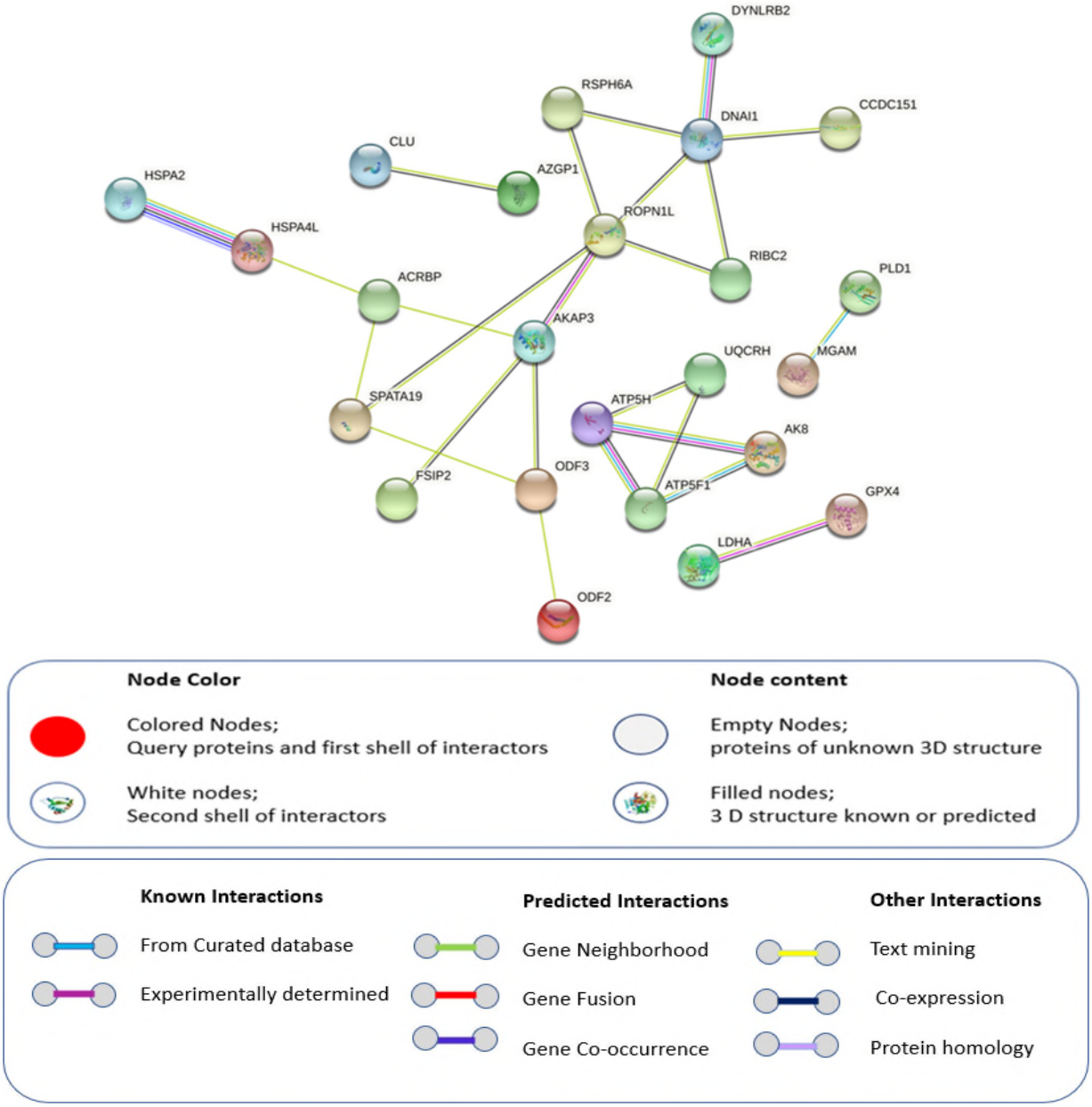

Figure 4.7. Visual mapping of up-regulated DAPs in HF sperm HPM, visualized onto a composite network based on predicted PPI network created using STRING v11.0 software together with a ‘Homo sapiens’ database. Each protein is symbolized as a node and associations as edges in different interactions between proteins (see legend for detail), based on the actions view of STRING v11.0. Thickness of the edges is based on confidence score.

database channels, found 24 connected nodes in the 48 up-regulated DAPs with 28 edges with significant PPI enrichment ($p<0.05$; $9.21x10^{-12}$; Fig 4.7), representing both functional and physical protein associations. The network of the 19 down-regulated DAPs was non-significant (PPI enrichment 0.177; $p>0.05$), indicating no significant interaction among DAP nodes.

4.4.5 Identification of Key Proteins

The MCODE analysis of the up-regulated DAPs PPI networks shown in Fig 4.7 detected densely connected regions based on highest k-core of the vertex neighborhood, whereas a k-core is core-clustering coefficient, and the highest k-core of a graph shows central most densely connected area of subgraph. MCODE mapped three different clusters (Fig 4.8, Table 4.1) with 12 key proteins in the up-regulated DAPs; no clusters were detected by MCODE in the down-regulated DAPs.

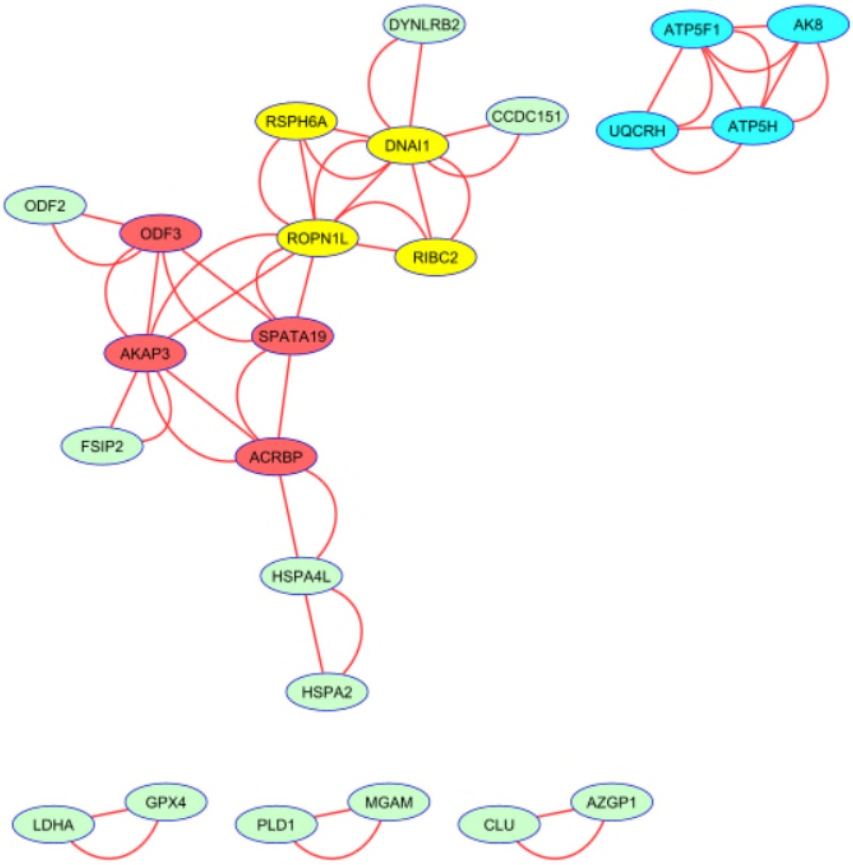

Figure 4.8. The hub protein network developed by MCODE (tool in Cytoscape v3.8.2). Three clusters exist, based on densely connected regions in the STRING network of the up-regulated DAPs. Blue ovals show hub proteins in cluster 1 having 4 nodes and 10 edges; yellow ovals show hub proteins in cluster 2 with red ovals (hub proteins in cluster 3) having 4 nodes and 8 edges; green ovals are IPPs connected to the hub proteins. The three small clusters of green ovals at the bottom are up-regulated DAPs not interacting with hub proteins.

Table 4.1. MCODE Analysis of the Up-Regulated DAPs.

Clusters	Protein Name	Accession Number	MCODE score
Cluster 1	UQCRH	P00126	3.33
	ATP5H	P13620	
	ATP5F1	P13619	
	AK8	Q96MA6	
Cluster 2	ROPN1L	Q3T064	3.33
	RIBC2	Q32LJ7	
	RSPH6A	Q9H0K4	
	DNAI1	Q32KS2	
Cluster 3	AKAP3	O77797	2.67
	ACRBP	Q29016	
	SPATA19	Q3SZQ3	
	ODF3	Q2TBH0	

MCODE (Molecular Complex Detection) analysis. MCODE Scored: the cluster's computed score which is defined as the product of the number of proteins (vertices) and the density in the complex subgraph (|V| x DC). The default threshold score is 0.2; values above threshold indicate that clusters are more densely connected.

4.4.6 Gene Ontology Functional Analysis of DAPs (Molecular, and Biological Functions)

GO analysis by PATHER databases detected functional enrichment of molecular functions of both the up- and down-regulated DAPs (Fig 4.9). Significantly more up-regulated than down-regulated DAPs have binding functions (50.0 vs 30.80%, $p < 0.05$, Fig 4.9 a, b), while more down-regulated proteins have catalytic activity than do up-regulated proteins (61.5 vs 40.0%, $p \leq 0.05$).

Down-regulated DAPs uniquely included transporter activity, while up-regulated proteins uniquely included molecular function regulation.

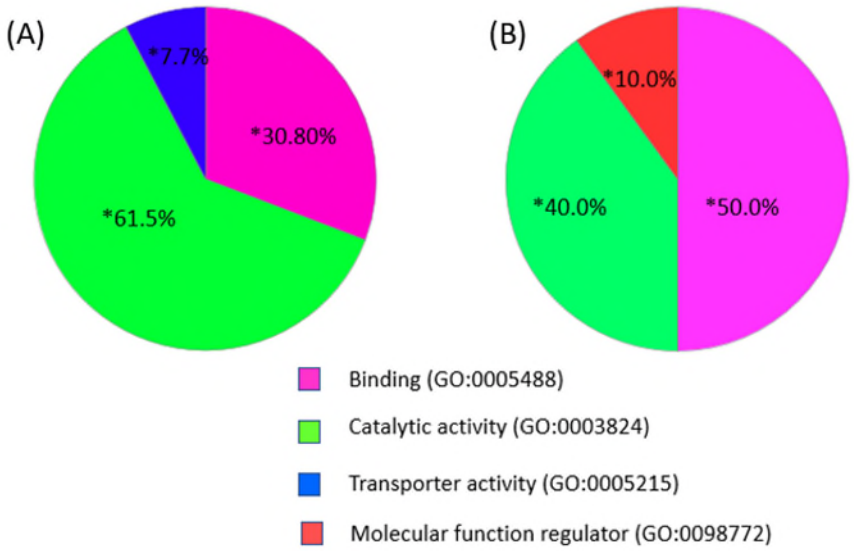

Figure 4.9. Classified sperm HPM proteins that differ by ≥ 2-fold (DAPs) between bulls with high and low fertility (HF vs LF; n= 3 bulls per group), analyzed for Molecular Functions with PANTHER database. (A) DAPs down-regulated in HF vs LF; (B) DAPs up-regulated in HF vs LF. *Molecular functions significantly different between groups.

STRING databases identified GO biological processes (Table 4.2) which included eight biological processes in the up-regulated proteins that are highly relevant and essential for sperm development and function, and eight biological processes in the down-regulated proteins that are relevant to catalytic enzymes and metabolic processes. The nucleoside triphosphate biosynthetic process was the one common process identified in both up- and down-regulated proteins.

Table 4.2. Functional Enrichment Analysis from GO of DAPs Up- or Down-regulated (Up/Down) in HPM of High vs Low Fertility Bulls - Biological Process.

Term ID	Up/Down	Term Description	OGC[a]	BGC[b]	Strength	FDR[c]
GO:0007283	Up	spermatogenesis	9	490	0.8	0.003
GO:0019953	Up	sexual reproduction	10	764	0.7	0.005
GO:0009142	Up	nucleoside triphosphate biosynthetic process	4	103	1.2	0.018
GO:0003341	Up	cilium movement	3	61	1.3	0.043
GO:0007286	Up	spermatid development	4	137	1.0	0.043
GO:0009123	Up	nucleoside monophosphate metabolic process	5	262	0.9	0.043
GO:0009141	Up	nucleoside triphosphate metabolic process	5	246	0.9	0.043
GO:0022414	Up	reproductive process	11	1350	0.5	0.043
GO:0006165	Down	nucleoside diphosphate phosphorylation	5	56	1.9	2.36E-06
GO:0009142	Down	nucleoside triphosphate biosynthetic process	5	103	1.7	1.07E-05
GO:0009165	Down	nucleotide biosynthetic process	6	291	1.3	4.50E-05
GO:0009206	Down	purine ribonucleoside triphosphate biosynthetic process	4	86	1.7	0.001
GO:0006757	Down	ATP generation from ADP	3	39	1.9	0.006
GO:0009435	Down	NAD biosynthetic process	3	51	1.8	0.009
GO:0009152	Down	purine ribonucleotide biosynthetic process	4	189	1.3	0.001
GO:0019674	Down	NAD metabolic process	3	66	1.7	0.001

a = Observed gene count; b = Background gene count; c = False Discovery Rate

4.4.7 Relationship of DAPs to Fertility Measures

Linear regression first compared DAPs intensities identified with HF and LF bulls and their respective BFIs (n=3 each), and secondly compared these same proteins taking the intensities and BFIs from the entire population of all 16 bulls. Not surprisingly, regressions of the 48 up-regulated DAPs intensities to their BFIs in the HF and LF bulls were significantly positive (Table 4.3;

r^2=0.65 to 0.97, $p \leq 0.05$), and the regressions of the HF's and LF's 19 down-regulated DAPs intensities to their BFIs were all significantly negative (Table 4.4; r^2= 0.76 to 0.96, $p \leq 0.02$).

Table 4.3. Regression Analysis of Up-regulated DAPs Intensities on BFI (HF: n=3; LF: n=3)

		Linear Regression of FC Protein intensities to BFI	
Accession #	Protein Name	r^2	p-Value
Q2T9U2	Outer dense fiber protein 2	0.904	0.003
O77797	A-kinase anchor protein 3	0.882	0.005
Q2TBH0	Outer dense fiber protein 3	0.704	0.036
Q32LJ7	RIB43A-like with coiled-coils protein 2	0.700	0.037
Q9N2J2	Phospholipid hydroperoxide glutathione peroxidase	0.882	0.005
A6QLU1	Glycerol-3-phosphate dehydrogenase, mitochondrial	0.885	0.005
Q32KS2	Dynein intermediate chain 1, axonemal	0.794	0.017
P79136	F-actin-capping protein subunit beta	0.836	0.010
P00669	Seminal ribonuclease	0.717	0.033
P17697	Clusterin	0.793	0.017
Q86TE4	Leucine zipper protein 2	0.896	0.004
Q2T9T0	Protein phosphatase 1 regulatory subunit 32	0.773	0.021
P19858	L-lactate dehydrogenase A chain	0.977	0.002
Q2T9X5	Uncharacterized protein C7orf61 homolog	0.759	0.023
P00727	Cytosol aminopeptidase	0.954	0.008
P35662	Cylicin-1	0.651	0.052
Q3SZT6	Protein Flattop	0.712	0.034
Q3T064	Ropporin-1	0.885	0.005
P13619	ATP synthase F (0) complex subunit B1, mitochondrial	0.792	0.017
Q6ZQR2	Cilia- and flagella-associated protein 77	0.881	0.005
Q5CZC0	Fibrous sheath-interacting protein 2	0.906	0.003

Q29016	Acrosin-binding protein (Fragment)	0.828	0.011
Q96MR6	Cilia- and flagella-associated protein 57	0.654	0.051
P13620	ATP synthase subunit d, mitochondrial	0.877	0.005
P00126	Cytochrome b-c1 complex subunit 6, mitochondrial	0.775	0.020
Q3SZR5	Protein FAM166C	0.860	0.007
A7MBH5	Coiled-coil domain-containing protein 151	0.921	0.002
Q0VFZ6	Coiled-coil domain-containing protein 173	0.837	0.010
Q32P85	Dynein light chain roadblock-type 2	0.889	0.004
Q9H0K4	Radial spoke head protein 6 homolog A	0.842	0.009
Q3SZQ3	Spermatogenesis-associated protein 19, mitochondrial	0.959	0.006
Q8WUD1	Ras-related protein Rab-2B	0.930	0.001
Q9Z280	Phospholipase D1	0.788	0.018
O95757	Heat shock 70 kDa protein 4L	0.793	0.017
Q6P2I7	Endogenous Bornavirus-like nucleoprotein 2	0.788	0.018
A6NG13	Alpha-1,3-mannosyl-glycoprotein 4-beta-N-acetylglucosaminyltransferase-like protein MGAT4D	0.781	0.019
O94810	Regulator of G-protein signaling 11	0.914	0.002
P17156	Heat shock-related 70 kDa protein 2	0.933	0.001
Q96MA6	Adenylate kinase 8	0.934	0.001
Q9C0F0	Putative Polycomb group protein ASXL3	0.9244	0.002
Q60698	Ski oncogene	0.927	0.002
O43451	Maltase-glucoamylase, intestinal	0.931	0.001
Q63647	Proline-rich nuclear receptor coactivator 1	0.933	0.001
E1BBQ2	Probable G-protein coupled receptor 158	0.925	0.002
Q9P217	Zinc finger SWIM domain-containing protein 5	0.871	0.006
P59796	Glutathione peroxidase 6	0.922	0.002
P56965	N(G),N(G)-dimethylarginine dimethylaminohydrolase 1	0.929	0.002
O08876	Krueppel-like factor 10	0.929	0.001

r^2= r-rquare, BFI=Bull Fertility Indexes, Accession # = Accession number of DAPs derived from UniProt database.

Table 4.4. Regression Analysis of Down-regulated DAPs Intensities on BFI (HF: n=3; LF: n=3)

Accession #	Protein Name	Linear Regression of DAPs intensities to BFI	
		r^2	p-Value
P0CB32	Heat shock 70 kDa protein 1-like	0.952	0.009
Q9WV27	Sodium/potassium-transporting ATPase subunit alpha-4	0.939	0.001
P61019	Ras-related protein Rab-2A	0.912	0.003
Q9XSJ4	Alpha-enolase	0.967	0.004
Q6B857	Cilia- and flagella-associated protein 20	0.895	0.004
Q4R3W4	Adenylate kinase 8	0.955	0.008
Q5JRX3	Presequence protease, mitochondrial	0.954	0.008
Q99MH5	Nucleoside diphosphate kinase homolog 5	0.912	0.003
P00517	cAMP-dependent protein kinase catalytic subunit alpha	0.913	0.003
Q3V0E1	Uncharacterized protein C9orf131 homolog	0.949	0.001
Q7Z745	Maestro heat-like repeat-containing protein family member 2B	0.920	0.002
Q8K410	Disintegrin and metalloproteinase domain-containing protein 32	0.930	0.002
Q5TCS8	Adenylate kinase 9	0.769	0.022
Q07113	Cation-independent mannose-6-phosphate receptor	0.905	0.003
Q3ZBD7	Glucose-6-phosphate isomerase	0.840	0.010
E1BNQ4	ATP-dependent (S)-NAD(P)H-hydrate dehydratase	0.870	0.006
Q8NDM7	Cilia- and flagella-associated protein 43	0.887	0.004
Q8SPU8	Dehydrogenase/reductase SDR family member 4	0.931	0.001
Q5E9H5	Mitochondrial chaperone BCS1	0.842	0.009

r^2 = r-square and has negative values, BFI=Bull Fertility Indexes, Accession # = Accession number of DAPs derived from UniProt database.

Of greater interest are the outcomes of regressions of the BFIs of the entire bull population against the intensities in the entire 16-bull population of the pre-determined DAPs (identified from the HF and LF bulls). Of the 48 up-regulated DAPs, 10 were missing in 5-7 bulls with a range of BFI. The intensities of 38 of the 48 up-regulated proteins had a significantly positive relationship to BFI (Table 4.5, $p \leq 0.034$), and of those, 10 had an $R^2 > 0.50$ ($p \leq 0.026$). The three DAPs with the highest r^2 were: Ras-related protein Rab-2B ($r^2=0.780$, $p=0.0003$); phospholipid hydroperoxide glutathione peroxidase ($R^2=0.661$, $p=0.0007$); and fibrous sheath interacting protein ($r^2=0.58$, $p=0.0006$).

Table 4.5. Regression Analysis of Intensity of Up-Regulated DAPs with BFI of 16 Bulls.

		Linear Regression of DAPs intensities to BFI	
Accession #	Protein Name	r^2	p-Value
Q2T9U2	Outer dense fiber protein 2	0.493	0.002
O77797	A-kinase anchor protein 3	0.424	0.006
Q2TBH0	Outer dense fiber protein 3	0.429	0.005
Q32LJ7	RIB43A-like with coiled-coils protein 2	0.451	0.004
Q9N2J2	Phospholipid hydroperoxide glutathione peroxidase	0.661	0.007
A6QLU1	Glycerol-3-phosphate dehydrogenase, mitochondrial	0.554	0.009
Q32KS2	Dynein intermediate chain 1, axonemal	0.367	0.012
P79136	F-actin-capping protein subunit beta	0.468	0.003
P00669	Seminal ribonuclease	0.341	0.017
P17697	Clusterin	0.346	0.016
Q86TE4	Leucine zipper protein 2	0.387	0.010
Q2T9T0	Protein phosphatase 1 regulatory subunit 32	0.338	0.018
P19858	L-lactate dehydrogenase A chain	0.560	0.009
Q2T9X5	Uncharacterized protein C7orf61 homolog	0.230	0.060
P00727	Cytosol aminopeptidase	0.432	0.005

P35662	Cylicin-1	0.294	0.030
Q3SZT6	Protein Flattop	0.490	0.002
Q3T064	Ropporin-1	0.563	0.008
P13619	ATP synthase F (0) complex subunit B1, mitochondrial	0.432	0.005
Q6ZQR2	Cilia- and flagella-associated protein 77	0.437	0.005
Q5CZC0	Fibrous sheath-interacting protein 2	0.581	0.006
Q29016	Acrosin-binding protein (Fragment)	0.370	0.012
Q96MR6	Cilia- and flagella-associated protein 57	0.537	0.001
P13620	ATP synthase subunit d, mitochondrial	0.319	0.022
P00126	Cytochrome b-c1 complex subunit 6, mitochondrial	0.282	0.034
Q3SZR5	Protein FAM166C	0.302	0.027
A7MBH5	Coiled-coil domain-containing protein 151	0.016	0.637
Q0VFZ6	Coiled-coil domain-containing protein 173	0.149	0.139
Q32P85	Dynein light chain roadblock-type 2	0.287	0.032
Q9H0K4	Radial spoke head protein 6 homolog A	0.189	0.091
Q3SZQ3	Spermatogenesis-associated protein 19, mitochondrial	0.479	0.003
Q8WUD1	Ras-related protein Rab-2B	0.780	0.003
Q9Z280	Phospholipase D1	0.057	0.536
O95757	Heat shock 70 kDa protein 4L	0.004	0.817
Q6P2I7	Endogenous Bornavirus-like nucleoprotein 2	0.023	0.575
A6NG13	Alpha-1,3-mannosyl-glycoprotein 4-beta-N-acetylglucosaminyltransferase-like protein MGAT4D	0.029	0.527
O94810	Regulator of G-protein signaling 11	0.323	0.021
P17156	Heat shock-related 70 kDa protein 2	0.338	0.077
Q96MA6	Adenylate kinase 8	0.325	0.021
Q9C0F0	Putative Polycomb group protein ASXL3	0.555	0.021
Q60698	Ski oncogene	0.489	0.003
O43451	Maltase-glucoamylase, intestinal	0.255	0.054
Q63647	Proline-rich nuclear receptor coactivator 1	0.343	0.017
E1BBQ2	Probable G-protein coupled receptor 158	0.552	0.021

Q9P217	Zinc finger SWIM domain-containing protein 5		0.530	0.026
P59796	Glutathione peroxidase 6		0.221	0.066
P56965	N(G), dimethylaminohydrolase 1	N(G)-dimethylarginine	0.556	0.021
O08876	Krueppel-like factor 10		0.352	0.019

r^2 =r-square, BFI=Bull Fertility Index, Accession # = Accession number of DAPs derived from UniProt database.

All 19 down-regulated DAPs were detected in all 16 bulls (Table 4.6). Four had significant negative regressions to BFI (r^2= 0.27 to 0.44; $p \leq 0.05$) relationships. The three with the most negative r^2 values were: uncharacterized protein C9orf131 homolog (r^2= 0.440; p = 0.0071); sodium/potassium-transporting ATPase subunit alpha-4 (r^2= 0.272, p = 0.0385); and mitochondrial chaperone BCSI (r^2= 0.266; p = 0.0491).

Table 4.6. Regression Analysis of Intensities of Down-Regulated DAPs with BFI of 16 Bulls

Accession #	Protein Name	Linear Regression of DAPs intensities to BFI	
		r^2	p-Value
P0CB32	Heat shock 70 kDa protein 1-like	0.235	0.057
Q9WV27	Sodium/potassium-transporting ATPase subunit alpha-4	0.271	0.038
P61019	Ras-related protein Rab-2A	0.187	0.094
Q9XSJ4	Alpha-enolase	0.192	0.089
Q6B857	Cilia- and flagella-associated protein 20	0.231	0.059
Q4R3W4	Adenylate kinase 8	0.197	0.085
Q5JRX3	Presequence protease, mitochondrial	0.241	0.063
Q99MH5	Nucleoside diphosphate kinase homolog 5	0.185	0.095
P00517	cAMP-dependent protein kinase catalytic subunit alpha	0.246	0.050
Q3V0E1	Uncharacterized protein C9orf131 homolog	0.439	0.007
Q7Z745	Maestro heat-like repeat-containing protein family member 2B	0.253	0.047
Q8K410	Disintegrin and metalloproteinase domain-containing protein 32	0.245	0.051
Q5TCS8	Adenylate kinase 9	0.188	0.093
Q07113	Cation-independent mannose-6-phosphate receptor	0.223	0.064
Q3ZBD7	Glucose-6-phosphate isomerase	0.172	0.109
E1BNQ4	ATP-dependent (S)-NAD(P)H-hydrate dehydratase	0.133	0.181
Q8NDM7	Cilia- and flagella-associated protein 43	0.221	0.076
Q8SPU8	Dehydrogenase/reductase SDR family member 4	0.067	0.351
Q5E9H5	Mitochondrial chaperone BCS1	0.266	0.049

r^2 = r-square and has negative values, BFI=Bull Fertility Index, Accession # = Accession number of DAPs derived from UniProt database.

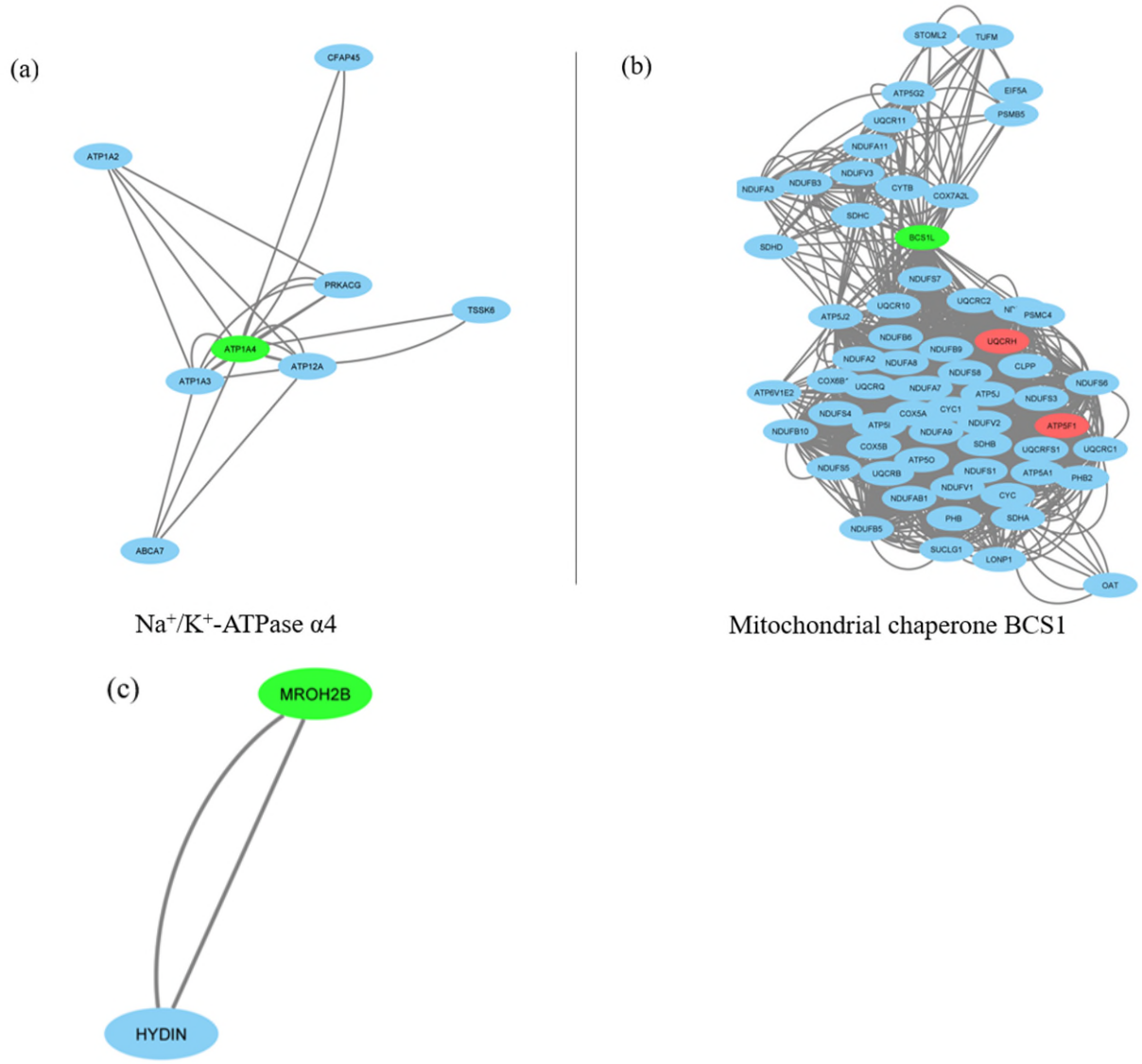

Figure 4.10. Sub-networks of selected down-regulated DAPs along with their IPPs (neighbor proteins in the interactome) showing different PPI in each cluster (n = 16). Ovals in red and green represent proteins differing in intensity by at least 2-fold between ATH (n = 8) and ATL (n = 8) bulls (red = up-regulated; green = down-regulated; blue = non-DAPs).

The sub-networks of three significant ($p < 0.05$) but with negative r^2 values down-regulated DAPs along with their IPPs detected in all 16 bulls are shown in Fig 4.10 a-c. The down-regulated DAP, sodium/potassium-transporting ATPase subunit alpha-4 (Fig 4.10 a) is connected to non-

DAPs interacting partners: sodium/potassium-transporting ATPase subunit alpha-3, sodium/potassium-transporting ATPase subunit alpha-2, potassium-transporting ATPase alpha chain 2, cilia- and flagella-associated protein 45, cAMP-dependent protein kinase catalytic subunit gamma, testis-specific serine/threonine-protein kinase 6, and phospholipid-transporting ATPase ABCA7. The cluster depicted in Fig 4.10 b is largely comprised of the mitochondrial proteins: mitochondrial chaperone BCS1 down-regulated DAP connected to up-regulated DAPs; cytochrome b-c1 complex subunit 6, mitochondrial; and ATP synthase F (0) complex subunit B1, mitochondrial. In non-DAPs, majority of the proteins are multiple isoforms of cytochrome b-c1 complex and NADH dehydrogenase. In Fig 4.10 c, the down-regulated DAP, maestro heat-like repeat-containing protein family member 2B only interacts with non-DAP Hydrocephalus-inducing protein homolog.

4.5 Discussion

This first comprehensive analysis to compare sperm HPM proteomics between high and low fertility Holstein bulls advances our understanding of sperm fertilization and its relationship to regulatory mechanisms that control fertility. Results show that bull *in vivo* fertility is strongly correlated with the presence of a cohort of structural and functional DAPs that are differentially expressed between bulls of differing fertility, including membrane proteins associated with sperm motility, sperm capacitation, AE, sperm oocyte recognition, metabolism, signaling pathways, and cytoskeletal structure. The rigorously measured BFI was significantly correlated with the relative amount of spectral intensities of 67 DAPs identified by semi-quantitative MS analysis. These proteins differed in amount by at least two-fold in bulls with high or low BFIs, with 48 being more-highly expressed (up-regulated) in HPM from high fertility (HF bulls) and 19 being at least two-

fold depleted (down-regulated) in HF bulls. Analysis of their roles and molecular interactions cast light on the involvement of proteins in regulating bovine sperm fertility.

Fresh ejaculates were analyzed in this research, although commercial AI is conducted with frozen-thawed semen. One salient reason for using fresh semen was to analyze sperm HPM unaffected by cryopreservation components and processes which could compromise the plasma membrane integrity and molecular structure. The cryoprotectant medium used in frozen semen can denature sperm proteins and induce plasma membrane fragility (Khan et al., 2021). One pooled ejaculate was assessed from each of 16 mature Holstein Friesian bulls with a range of BFI, a multi-factor measure of *in vivo* fertility based on >1000 inseminations per bull; average BFI is 100. Bulls were divided into two cohorts of eight bulls each having BFI > 101 ATH) or BFI < 101 (ATL); all HPM preparation and MS was done blind to BFI, including extraction of HPM, digestion, fractionations, LC-MS/MS analysis, and data searching, which confers a unique feature of completely unbiased investigation on this study. The HPM is highly enriched in the plasma membrane from over the anterior sperm head, with minor amounts of membrane from mitochondrial and acrosomal membranes and tail components (Zhao & Buhr, 1996; Byrne et al., 2012; Hickey & Buhr, 2012). Sperm HPM is of key importance because its major remodeling in capacitation is critical for normal interactions with the oocyte and inducing the preliminary physiological changes during fertilization (Caballero et al., 2012). While other proteomics studies have identified fertility-related protein biomarkers in whole sperm from *Bos taurus* (Peddinti et al., 2008; Somashekar et al., 2017; Muhammad Aslam et al., 2018; D'Amours et al., 2018, 2019) including frozen bull semen (Singh et al., 2018) and bull seminal plasma (Druart et al., 2013; Muhammad Aslam et al., 2014; Viana et al., 2018; Kasimanickam et al., 2019) and in buffalo bull (Singh et al., 2018; Muhammad Aslam et al., 2019) and even in buffalo bull sperm surface

proteome (Byrne et al., 2012), this is the first in-depth proteomic analysis of *Bos taurus* sperm HPM across fertility lines.

LC-MS/MS identified 22,117 unique and homologous proteins, when aligned to the UniProt mammals database, which were rigorously validated (Koziy et al., 2022) by Spectrum Mill at both peptide level as well protein level. At peptide level, validation was performed with criteria of 1% FDR, precursor charge range 2 to 7, and minimum peptide sequence length was 6, while at protein level, the identified proteins were validated with 1% FDR. These identified HPM proteins displayed significant interactions, forming different clusters in an interactome (Fig 4.1). This is the first report of big data analytics, including interactions and networks, of all the proteins present in HPM of bull sperm.

To determine if fertility was affected by different amounts of specific proteins, we sought HPM proteins that differed by at least two-fold in amount as measured by spectral intensities (DAPs), between the three bulls with the highest fertility (HF, with BFIs of 105, 105, 107) and the three with the lowest fertility (LF, BFI =88, 92, 94, respectively). Of the 67 DAPs identified, HF bulls had significantly more of 48 and less of 19 DAPs than did LF bulls. Heat maps and PCA plots (Fig 4.2 – 4.4) show the DAPs clearly delineate and align with field fertility. Sub-networks created by STRING and densely connected regions identified by MCODE analysis (Table 4.1) showed that proteins in cluster 1 play important roles in energy production of sperm by converting ADP to ATP; cluster 2 proteins are sperm flagellar proteins with roles in sperm motility and cluster 3 proteins participate in sperm motility, capacitation, AE, and sperm fertility. Furthermore, almost all of these 67 DAPs form sub-networks with the proteins that are non-DAPs which sometimes include one or more other DAPs (examples shown in Fig 4.5). Many of the DAPs have previously been associated with sperm quality, and these DAPs and their sub-networks and interactions can

be roughly categorized into groups that affect either sperm structure/motility, capacitation/AR, or sperm-oocyte binding (Byrne et al., 2012; D'Amours et al., 2010, 2018, 2019).

DAPs associated with general cell functions and structure include LDHC, a sperm metabolic enzyme associated with local energy production (Fig 4.5; Muratori et al., 2009; Souza et al., 2020); TPI (Fig 4.5c), a glycolytic enzyme (Gracy, 1982) essential for sperm glucose metabolism; spermatogenesis-associated protein 19 mitochondrial (SPATA19); and disintegrin and metalloprotease 32 (ADAM 32), one of the ADAM family of membrane-anchored proteins. ADAM32 has not previously been clearly associated with fertility (Lee et al., 2020), although ADAM32's being one of the down-regulated DAPs in high fertility bull HPM suggests it, possibly through its wide network of IPPs (Fig 4.6 a) and does impact some crucial aspect(s) of fertility.

4.5.1 Sperm Structure/Motility

Proteins associated with sperm structure and motility mostly reside in the midpiece and tail, which are present as minor contaminants in the HPM, although cytoskeletal elements underlie and bind to the plasma membrane surrounding the whole sperm. The up-regulated DAP RIMBP3 is a component of the manchette involved in sperm head morphogenesis (Zhou et al., 2009) and is most likely active during spermatogenesis, while SPAG17 is important for motile cilia function in mature sperm (Teves et al., 2013). CAPZB, also up-regulated in HF bulls, increases depolymerization, assembly and capping of actin filaments to enhance sperm motility (Carlier & Pantaloni, 1997; Shimada et al., 2005; Vignjevic & Montagnac, 2008), and other actin-affected actions. The up-regulated DAPs ROPN1L, a sperm-specific binding protein of the outer fibrous sheath that regulates motility in human spermatozoa (Chen et al., 2011), works together with outer dense fiber proteins 2 and 3 to induce sperm hyperactivation during capacitation, protects the integrity of the axoneme and promotes sperm motility at a molecular level (Zhao et al., 2018). Our

findings of the high expression and clustering of the DAP's ROPN1L, ODF2 and ODF3 in high fertility bulls are consistent with these actions, and with the association of decreased ROPN1L expression with reduced sperm motility (Chen et al., 2011). Motility, flagellar/microtubule structure, and assembly are linked to the DAPs DNAI1, RSPH6A, RIBC2, and SPATA19 that are up-regulated in HF bulls (Fig 4.5 j; (Norrander et al., 2000; Zuccarello et al., 2008; Abbasi et al., 2018; Whitfield et al., 2019) and mutation or absence of one or more of their genes may cause asthenozoospermia or multiple morphological abnormalities in sperm flagella (Baccetti et al., 1993; Whitfield et al., 2019). ROPN1L also clusters with AKAP3 (Fig 4.5 a, b) possibly reflecting its collaboration with other membrane proteins for sperm motility and fertility (Xu et al., 2020), although the impact on fertility could also be due to AKAP's involvement in signaling complexes (Li et al., 2011). The positive correlations of these motility proteins to the BFI were paralleled with a strong negative regression (table 4.4) of the DAP nucleoside diphosphate kinase homolog 5 (NME5) to BFI. This could be directly attributable to the NME5's gene regulation of primary ciliary dyskinesia (defects in the function or structure of motile cilia) in humans (Cho et al., 2020), but, like AKAP3, NME5 has an action other than on motility which could impact fertility. NME5 modifies the function of several antioxidant enzymes that protect peroxide damage in sperm membrane lipids including epididymal secretory glutathione peroxidase. The membrane actions of AKAP3 and NME5 suggest their respective positive and negative impacts on fertility could be related to their impact on the HPM control of capacitation and sperm-oocyte binding.

4.5.2 Capacitation

Sperm capacitation involves cellular, biochemical, functional, and physiological changes (Austin, 1952; de Lamirande, 1997; Mostek et al., 2021) triggered by various known and unknown signals from tubal fluids and other sources, ultimately rearranging the protein and lipid molecules

in the sperm HPM that induce and regulate various signaling pathways. Capacitation's signaling leads to internal physiological/biochemical responses and fusion of the HPM and outer acrosomal membrane, culminating in the AE. The DAPs triosephosphate isomerase (TPI1), putative tyrosine-protein phosphatase (TPTE), heat shock 70 kDa protein 4L (HSPA4L), L-lactate dehydrogenase C chain (LDHC), atlastin-2 (ATL2), succinate CoA ligase (ADP-forming) subunit beta have mostly been previously located in the head region of sperm (Petit et al., 2013) and are more likely candidates for involvement in capacitation. TCP11 in mouse sperm has a key role stimulating capacitation and inhibiting spontaneous AE (Fraser, 1998). TPTE engages in function of a signal transduction pathway (Chen et al., 1999), as are a number of modifiers of ATP/ADP/AMP, which could either be involved in cAMP-dependent signaling or ion transport, impacting sperm membrane depolarization during capacitation. Such modifiers include the up-regulated HPM DAP proteins phosphotransferase enzyme, which reversibly interconverts ATP and AMP into two ADP molecules (Tükenmez et al., 2016), adenylate kinase 8 (AK8), ATP5H and ATP5F1 proton-transporting ATP synthase, the latter identified in Drosophila testes during spermatogenesis (Yu et al., 2019). This cluster of AK8, ATP5H and ATP5F1 up-regulated DAP membrane proteins is strongly correlated with BFI (Table 4.3) and form networks (Fig 4.5) with other similar proteins that are not DAPS such as AK5, AK7, ATP5D, ATP5J2, NT5C1A, NT5C1B, NME4 and NME8. This network also interacts with the down-regulated DAP AK9 that is negatively correlated with BFI in HF/LF (table 4.4)) but not with the BFI in the whole population of bulls (Table 4.6). AK9's unique features are not fully elucidated in sperm (Ionescu, 2019). It is tempting to speculate that predominance of AK8 supports or shapes a signaling pathway critical for fertilization, that is impeded when AK9 expression is high, thereby interfering with critical capacitation signals. Only four of the DAPs had significantly negative linear regressions with BFI of the whole 16-bull

population: sodium/potassium-transporting ATPase subunit alpha-4 (Na^+/K^+-ATPase α4), protein C9orf131 homolog, maestro heat-like repeat-containing protein family member 2B and mitochondrial chaperone BCS1. Na^+/K^+-ATPase α4's subnetwork (Fig 4.10 a) shows it interacting with its isoforms Na^+/K^+-ATPase α2 and Na^+/K^+-ATPase α3 that may complement or inhibit its effects; kinases that may impact signaling (testis-specific serine/threonine-protein kinase 6, cAMP-dependent protein kinase catalytic subunit gamma), transporters (potassium-transporting ATPase alpha chain 2, Phospholipid-transporting ATPase) and most tellingly since Na^+/K^+-ATPase α4 is most abundant in sperm tail (Rajamanickam et al., 2017), cilia- and flagella-associated protein 45. Since Na^+/K^+-ATPase α4 is strongly negatively correlated with fertility, meaning more α4 aligns with poorer fertility, it will be intriguing to untangle which of its potential partner pathways and roles in energy, transporting, and/or signaling are the critical one(s) for fertilization. The other down-regulated DAP in bull population is maestro heat-like repeat-containing protein family member 2B (MRO2B; Fig 4.10 c), which plays a key role in process of sperm capacitation (Martin-Hidalgo et al., 2020), interacts with hydrocephalus-inducing protein homolog to influence ciliary motility. It is hypothesized that decreasing the amount of MRO2B result in the reduced ciliary motion along with reduced amount of mitochondrial chaperone BCS1 protein (Fig 4.10 b), the function of mitochondrial respiratory chain was reduced, causing effect on mitochondrial tubular networks, reduced cilia motion and altogether leads to low/incomplete sperm capacitation (Talbot et al., 2018; Martin-Hidalgo et al., 2020).

The up-regulation found in the HPM of HF bulls of the antioxidant enzyme phospholipid hydroperoxide glutathione peroxidase (GPX4; Fig 4.5k) correlates positively with the population fertility (Table 4.5) and is known to prevent peroxidative damage of membrane lipids (Cho et al., 2020), and prevent reactive oxygen species (ROS) from interfering with capacitation through

changing a cAMP-driven Tyr-P pathway (Awda et al., 2009; Awda & Buhr, 2010) needed for capacitation. Others have also found GPX4 in sperm from high fertility bulls (Park et al., 2012; Özbek et al., 2021), in Malnad Gidda bulls (Ramesha et al., 2020) and in human sperm anterior membranes and post-acrosomal membranes (O'Flaherty & Rico de Souza, 2011), and have suggested GPX4 maintains cytoskeletal integrity (Maiorino et al., 2005) and is involved in fertilization (Rahman et al., 2013). It is interesting that MCODE linked GPX4 to lactate dehydrogenase A (LDHA; Fig 4.8), which has been identified as an attractive target for development of male contraception (Goldberg, 2021); it would be interesting to explore a potential relationship among membrane-bound dehydrogenase and peroxidase and sperm fertility.

Two RAB DAPs identified in HF HPM, the down-regulated RAB2A (Fig 4.6b) and the up-regulated RAB2B also have a potentially very interesting inter-relationship for capacitation. RAB2A regulates vesicular transport to the developing acrosome during spermiogenesis (Mountjoy et al., 2008), while RAB2B is depleted in patients with unexplained fertilization failure (Torra-Massana et al., 2021). RABs are small GTP-binding proteins of approximately 20–40 kDa with key roles in sperm fusion events, membrane transport (Stenmark, 2009) and membrane-bound signaling (reviewed by Nassari et al., 2020). RABs are GTPases, acting like "molecular switches" by shuttling between being inactive when bound to GDP and active when bound to GTP (Lin et al., 2017). Of note are the many other members of the RAB family identified as non-DAPS in this same cluster (Fig 4.6 b: RAB10, 14, 37, 39A, 43). Various RABs in various cell types regulate physiological changes known to be important in capacitation, including calcium ($Ca^{++)}$ release from cellular organelles, EGFR stabilization or degradation (depending on whether SRC phosphorylates a RAB tyr, or PTEN phosphorylates both ser and tyr RAB residues), and regulation of phosphatidyl-inositol3P levels (Nassari et al., 2020). The up-regulation and positive regression

of RAB2B, coupled with the down-regulation with trending-towards-significant negative regression of RAB2A (p=0.09, Table 4.6) suggest these two RABs may have inverse roles or antagonistic actions on one or more critical steps in capacitation.

4.5.3 Sperm-Oocyte Recognition and Binding

Sperm-oocyte binding also is a multi-step function of the HPM, and a number of DAPs implicated in these processes were identified (Fig 4.5). Zona pellucida-binding protein 1 (ZPBP1) was seen to have close interconnection with its IPPs, ZPBP2, zonadhesin (ZAN Sutovsky, 2018), acrosin-binding protein (ACRBP), acrosin (ACR), epididymal sperm-binding protein 1(ELSPBP1), mitochondrial (SUCLA2), ODF1, and ROPN1. ZPBP2 is the paralog of acrosomal matrix protein ZPBP1 and involved in interactions between sperm and the ZP of oocyte (Yu et al., 2006; Lin et al., 2007; Sutovsky, 2009, 2018; Souza et al., 2020). ZPBP1 is found more broadly over the acrosome cap, and its presence is required for normal compaction of the murine acrosome during spermatogenesis (Lin et al., 2007). ZPBP2 is confined to the apical ridge of the acrosome and its absence results in male subfertility largely correlated with defects in sperm ZP interaction (Lin et al., 2007; Ferrer et al., 2013). In boars, ZAN is an inner-acrosomal membrane protein, involved in sperm-oolemma interaction (Shur, 2008; Ashrafzadeh et al., 2013; Souza et al., 2020). ACRBP is elevated in capacitated boar spermatozoa, stimulating release of acrosin from the acrosome and subsequent sperm-egg binding; indeed, it has been suggested as a potential biomarker of fertility (Fraser & Quinn, 1981; Kwon et al., 2014). The glycolytic enzyme TPI has been implicated in ZP interaction and fertilization (Auer et al., 2004). The HSP proteins are molecular chaperones, with the up-regulated HSPA4L (previously identified in Malnad Gidda bull spermatozoa; Ramesha et al., 2020) known to play a vital role in sperm-zona interactions (Naaby-Hansen & Herr, 2010; Radons, 2016; Sutovsky, 2018) and the down-regulated HSP701L is

involved in steroid hormone: ligand chaperoning. As with other up-and-down-regulated protein pairs, the possibility exists of these two similar forms competing for involvement in vital steps in sperm: zona recognition and binding.

4.6 Conclusions

This first rigorous in-depth proteomics analysis of sperm HPM in Holstein Friesian bulls found their rigorously measured field fertility significantly correlated to the amount of DAPs identified by semi-quantitative MS analysis. Of the over 20,000 proteins identified, only 67 differed in amount by at least two-fold between high and low fertility bulls, with over 40 of these proteins significantly correlated to the wide range of *in vivo* fertility of 16 bulls. This unique identified orchestra of significantly abundant proteins participate in various key roles in sperm motility, capacitation, oocyte recognition, metabolism, signaling pathways, and cytoskeletal structure, and overall cast light on the proteins that regulate bovine sperm fertility.

PREFACE TO CHAPTER 5

Previous chapters identified that in HPM of boar sperm, specific isoforms of Na^+/K^+-ATPase correlate to *in vivo* fertility, and 67 non-ATPase bovine proteins differed by at least two-fold in sperm HPM from bulls of differing *in vivo* fertility in a manner that correlated with bull fertility measured by BFI. The current study evaluates, quantifies, and characterizes the different α and β isoforms of Na^+/K^+-ATPase (α1,2,3,4; β1,2,3) in the sperm HPM from bulls of differing *in vivo* fertility. Interestingly, although sperm motility and kinetics parameters by CASA did not differ among bulls of differing fertility, the average to high fertility bulls (ATH, n=8) had significantly more α1 than average to low fertility bulls (ATL, n=8). Linear regression found the BFI was positively correlated to α1 and β2, and negatively related to α4. Bioinformatics analysis predicted more, discontinuous B-cell epitopes and Tyr-P sites in Na^+/K^+-ATPase isoform residues found in HPM of high versus low fertility bulls.

A version of this chapter is ready to submit to Journal of Biology of Reproduction under joint co-authorship with George S. Katselis, and Mary M. Buhr.

As first author, Muhammad Imran contributed to the experimental design, conducted the study, performed the data analysis, and wrote the first draft of the manuscript. George S. Katselis and Mary M. Buhr conceived the idea and contributed to the experimental design, revised the manuscript, and supervised the project.

CHAPTER 5: CHARACTERISTICS OF Na^+/K^+-ATPase IN HEAD PLASMA MEMBRANE OF BOVINE SPERMATOZOA

5.1 Abstract

Male fertility is a complex trait involving many molecules, proteins, and signal transduction pathways in spermatozoan. Proteomics here identifies, relatively quantifies, and compares Na^+/K^+-ATPase isoforms (α1, α2, α3, α4, β1, β2 and β3) in the sperm HPM of Holstein Friesian bulls of known fertility and associates these isoforms with cellular functions and fertility. Sperm kinetics of one ejaculate from each of 16 bulls did not differ between those whose *in vivo* fertility was either average to low (BFI 88-101; n=8, ATL) or average to high (BFI 102-107; n=8; ATH). HPM was individually isolated, and proteins digested, fractionated, and spectra aligned to *Bos taurus* Na^+/K^+-ATPase isoforms from NCBI database. Relative quantification of Na^+/K^+-ATPase, assessed by NSAF, found more α1 in ATH than ATL ($P<0.05$). Linear regression confirmed a positive relationship of α1 ($r^2=0.42$; $p<0.006$) and β2 ($r^2=0.47$; $p<0.003$) with BFI while α4 was negatively correlated ($r^2=0.37$; $p<0.01$). Representative tryptic signature peptides in each isoform in both groups were identified. Spectral residues from the three bulls with the highest and lowest BFIs (HF, LF) were pooled group-wise, duplicates removed, pooled sequences aligned for each isoform, and bioinformatics found the predicted location, physical and chemical properties, discontinuous B-cell epitopes, and Tyr-P of most of the isoforms differed between HF and LF. Therefore, specific isoforms of Na^+/K^+-ATPase in the sperm HPM are correlated to bull *in vivo* fertility, probably through Na^+/K^+-ATPase's role as receptor for signaling pathways in bovine sperm capacitation.

5.2 Introduction

Fertility is generally defined as the ability to conceive offspring and to propagate next generations (Utt, 2016). In bovine reproduction, individual bull fertility is more important than that of an individual cow, because in natural service, one bull may be used to breed up to 40 females and in artificial insemination, one ejaculate may be divided to breed hundreds to thousands of females (Kastelic, 2013). Fertility *in vivo* is a complex process that involves sperm transport in the female reproductive tract and a series of biochemical and physiological changes known as capacitation that enable a sperm to fertilize the oocyte (Chang, 1951; Austin, 1952; Yanagimachi, 1994). During capacitation, molecular rearrangement in the plasma membrane including loss of decapacitation factors and cholesterol, enables the subsequent AE to occur.

Capacitation in bovine sperm involves a series of cell signaling events mediated by proteins in the HPM including Na^+/K^+-ATPase (Thundathil et al., 2006; Sajeevadathan et al., 2019). Na^+/K^+-ATPase acts as a receptor to its hormone ouabain that induces *in vitro* capacitation by activating a cell signaling cascade that leads to Tyr-P (Thundathil et al., 2006).

Na^+/K^+-ATPase is a transmembrane protein ubiquitous in mammalian cells that is a heterodimer of α and β subunits. The α subunit is the larger molecule of approximately 1000 amino acid residues and molecular weight of 110kDa, and has four isoforms α1, α2, α3 and α4 (Kaplan, 2002). The β subunit is a comparatively smaller molecule with 370 amino acid residues with a molecular weight of 35-60 kDa, and has three isoforms known as β1, β2 and β3 (Blanco & Mercer, 1998; Daniel et al., 2010). In somatic cells, the α isoforms are mostly located on the inner leaflet of the plasma membrane while β isoforms locate towards the outer surface (Woo et al., 2000; Geering, 2008).

Previously, our group noted Na^+/K^+-ATPase in bull sperm (Zhao & Buhr, 1996) and identified all isoforms in the HPM of bull (Hickey & Buhr, 2012; Sajeevadathan et al., 2021) and boar spermatozoa including α4 isoform (Awda et al., 2022-submitted). In boar sperm the intensity/band density of the α3 Na^+/K^+-ATPase bands in Western blots were strongly associated with boar *in vivo* fertility and FR (Chapter 3, Imran et al., 2023). However, all these studies used methodologies other than MS that had limitations in sensitivity and accuracy. So, for the first time, a comprehensive analysis of the sperm HPM from Holstein Friesian bulls for the determination and quantification of the seven isoforms of Na^+/K^+-ATPase was performed.

Male fertility is a complex trait. Other studies have examined the proteomic profile of entire sperm (including head, tail, mitochondria etc), for association with fertility (de Mateo et al., 2011; Byrne et al., 2012; Amaral et al., 2013; Baker et al., 2013; Druart et al., 2013; Castillo et al., 2014; Muhammad Aslam et al., 2018; Singh et al., 2018; Viana et al., 2018; D'Amours et al., 2018, 2019; Kasimanickam et al., 2019).

Since the sperm HPM is a critical component of many fertilization events (sperm-egg interactions including membrane fusion, capacitation, AE, sperm-zona penetration, etc), we recently examined the total sperm proteomics of the HPM from sperm of bulls of known fertility (Chapter 4, Imran et al., 2023). The current study focuses on the critically important HPM signaling proteins, the Na^+/K^+-ATPase isoforms (α1, α2, α3, α4, β1, β2 and β3).

The specific objective of this high throughput proteomic analysis is to identify and reveal previously unknown sperm characteristics of HPM Na^+/K^+-ATPase isoforms that might be associated with *in vivo* bull fertility, including relative quantification (based on spectral counts), peptide sequence, cellular and biological functions, prediction of transmembrane helices, physical and chemical properties, discontinuous B-cell epitopes, phosphorylation sites and signal

transduction pathways specific to fertility. Identifying exactly which features of specific ATPase isoforms impact fertility will aid understanding both how this novel signaling molecule works, and how to improve sperm fertilizing ability.

5.3 Materials and Methods

5.3.1 Reagents and Equipment

Similar reagents and equipment were used as before (section 4.3.2). Disodium phosphate, sodium dihydrogen phosphate monohydrate, dextrose, 1.5 M sucrose, polyethylene glycol (40%), methanol HPLC grade, and trypsin were purchased from Thermo-Fisher Scientific (Unionville, ON, Canada) and percoll from GE Healthcare (Mississauga, ON, Canada). Potassium chloride, 20% dextran, and sodium chloride were acquired from Sigma-Aldrich, (Oakville, ON, Canada). Milli-Q water obtained from water purification system Serv A Pure (MIUS) and MS-SAFE protease and phosphatase inhibitor cocktail from Merck KGaA (Darmstadt, Germany). Bicinchoninic acid protein assay kit including BSA were purchased from Thermo Fisher Scientific (Waltham, MA, USA). LC/MS grade water, and LC/MS grade acetonitrile, were purchased from Fisher Scientific, (Fair Lawn, NJ, USA), as were ABC buffer, TFE and IAA. DTT was purchased from MP Biomedicals (Solon, OH, USA). SCX Spin Tips sample preparation kit was from Protea Biosciences (Morgantown, WV, USA), ammonium formate from Sigma (St. Louis, MO, USA) and trypsin from Pierce (Rockford, IL, USA). MS vials and Polaris-HR-Chip 3C18 were purchased from Agilent (Agilent Technologies Canada Ltd., Mississauga, ON, CA).

5.3.2 Semen Collection and Processing

Similar approaches were used as before (section 4.3.1). One fresh double ejaculate (two ejaculates collected from the same animal within 20 minutes and then pooled together) from each of 16 Holstein Friesian bulls of known field fertility (average-to-high fertility ATH n=8, average-

to-low fertility ATL n=8) was provided by SEMEX (Guelph, ON, Canada). Bull fertility was assessed as the international multi-factor BFI which is a Semex internal calculation composed of NRR (56 days post service: Canadian Index), SCR (USA index) and Agri-Tech analyses (ATA, USA index). Average BFI is100 based on >1000 inseminations per bull, and bulls were identified as having BFI > or < 100 (ATH, ATL; n=8 each). As before (Sajeevadathan et al., 2021), two ejaculates were collected from each bull on one day by artificial vagina, combined, and the ejaculates with ≥80% motile sperm were diluted to 60×10^6 spermatozoa per mL with clear egg yolk-free extender (Semex proprietary composition) and shipped overnight at 16 ºC to the laboratory at the University of Saskatchewan (Sajeevadathan et al., 2021). The temperature was checked on arrival and samples between 15-20 ºC were warmed to room temperature over 2h by being placed in a partially opened container, covered, and occasionally rotated until they reached room temperature 24 ± 1 ºC (≈ 90 min). On arrival, a 500 µL aliquot was transferred into an Eppendorf tube and incubated at 37 ºC for slow warming (70 min). Following that it was evaluated for motility kinetics CASA, Hamilton Thorne IVOS II (MA, USA) utilizing a 4 µL semen on a 20 µm deep Leja standard count slide (Leja products B.V., Nieuw-Vennep, The Netherlands) while kept at 37 ºC (Anzar et al., 2009, 2011; Sajeevadathan et al, 2021). Ejaculates whose temperature on arrival was 15-20 ºC, and whose CASA parameters included ≥ 60% total/ 55% progressive motility, were processed to obtain the HPM once the ejaculate reached room temperature (Hickey & Buhr, 2012). Fresh semen motility kinetics, ejaculate volume (mL), weight (g), concentration ($x10^6$/mL) and total sperm count from each of the 16 bulls were determined (Table 5.1).

5.3.3 Materials and Extraction of Sperm HPM

Similar methods were used as before (section 4.3.3). The HPM was obtained according to an established procedure (Buhr et al., 1993; Zhao & Buhr, 1996; Hickey & Buhr, 2012),

performing all steps at room temperature unless specified otherwise. Briefly, the sample was centrifuged (Jouan CT 4.22; Jouan S.A., Saint-Herblain, France; 800 x g; 10 min), and pellets resuspended into phosphate buffered saline (PBS; 125 mM NaCl, 8 mM Na_2HPO_4, 2 mM NaH_2PO_4.H2O, 5 mM KCl, 5 mM dextrose) with repeated gentle aspiration, pooled to ~40 mL and centrifuged (800 x g; 10 min). The resulting pellets were resuspended in PBS to 40 mL, layered onto 35% percoll (1:2 v: v; percoll: PBS) centrifuged (800 x g; 10 min), the supernatant discarded, and the pellet washed twice with PBS (800 x g, 10 min). The final pellet was subjected to nitrogen cavitation in a cell disruption Parr cavitation unit (Parr instrument company, IL, USA; 650 psi, 10 min) introducing nitrogen gas over 90 sec to a final pressure of 650 psi, holding for 10 min and then releasing pressure over 90 sec. Finally, the cavitate was centrifuged at 800 x g for 10 min. Phase partition tubes were prepared by mixing 3.94 g 20% dextran (1:5 g: g; dextran:water), 1.97 g 40 % PEG (1:2.5 g: g; PEG:water), 0.19 g PBS (in 1000 mL water), 2.42 g 1.5 M sucrose (in 100 mL water), covering and keeping in fridge overnight. The resulting supernatant was layered onto four phase partition tubes. Tubes were mixed by inversion 20 times, centrifuged (800 x g; 10 min), and the top portion harvested. This portion was layered onto four fresh phase partition tubes, mixed, and centrifuged as before. The final top layers were centrifuged (206,000 x g; 30 min; 5 ºC), the pellets resuspended in PBS, pooled, and centrifuged (206,000 x g; 20 min; 5 ºC). The final pellet (HPM) was scraped out into a hand-held homogenizer by stepwise adding 200 µL PBS, and homogenized. To inactivate endogenous proteolytic and phospholytic enzymes that degrade the HPM proteins, and its activation states, MS-SAFE Protease and Phosphatase Inhibitor cocktail was added (1.33 mL per mg of HPM). The samples were homogenized, aliquoted into eppendorf tubes, covered with nitrogen gas, snap frozen in liquid nitrogen, and stored at -80 ºC.

5.3.4 Digestion of HPM

Similar approaches were used as before (section 4.3.3.1). For measuring HPM protein concentration, an aliquot was thawed at room temperature and the concentration of the HPM protein was determined by bicinchoninic acid analysis using the BioTek ELx808 (BioTek-Instruments Inc., VT, USA) multi detection plate reader (wavelength 562 nm) and BSA as the standard protein (Nair et al., 2021).

Triplicates made from each HPM sample were digested into peptides using in-solution trypsin digestion protocol developed in our laboratory (Nair et al., 2021; Koziy et al., 2022). Briefly, HPM samples with concentration > 5.0 µg protein/µL were diluted with water to make it 5.0 µg/µL and samples with concentration <5.0 µg/µL were mixed (without dilution) with 1 M ABC (45 µL sample in 5 µL ABC), and proteins in HPM were denatured with addition of 50 µL TFE (total sample volume 100 µL). Disulfide bonds in HPM proteins were reduced by adding 1 µL of DTT solution (1 M DTT in 100 mM ABC: final concentration of 10 mM DTT) upon incubating for 1 h at 6ºC while shaking on Eppendorf Thermomixer (Eppendorf, ON, Canada) at 500 rpm. To prevent disulfide bonds from reforming, proteins in HPM samples were alkylated with 55 mM IAA (100 µL of 100 mM IAA) and incubated in the dark at 37ºC for 30 min while shaking at 300 rpm. Samples were then evaporated (25 min, 37ºC) in a speed-vac (Labconco, Kansas City, MO, USA) to a final volume of 100 µL. Later, to remove salts, polymers and lipid contaminations, sample proteins were precipitated with excess acetone (-80ºC, 1h), centrifuged (30 min, 4ºC, 13,000 x g) in Eppendorf centrifuge 5430 R (Eppendorf AG, Hamburg, Germany), the supernatant discarded, and acetone precipitation repeated. The samples were then completely dried (25 min, 37ºC) in speed-vac (Koziy et al., 2022) and resuspended in 300 µL of 100 mM ABC. Finally, HPM proteins were digested by adding trypsin digestion buffer (20 µg /µL trypsin

in 1 mM HCl and 200 mM ABC solution; protein: trypsin, 40:1, v: v) and incubating overnight with shaking (37 ºC, 300 rpm). For complete sample protein digestion, the same amount of trypsin buffer was added the next morning, and samples incubated (2 h, 37ºC, shaker 300 rpm), dried (speed vac), and stored at -80ºC until SCX fractionation (Koziy et al., 2022).

5.3.5 SCX Peptide Fractionation

Similar methods were used as before (section 4.3.3.2). Peptide fractionation, using SCX Spin Tips incorporated as an orthogonal approach coupled to reverse phase LC to minimize sample complexity and increase resolution prior to MS/MS analysis (Mirzaei & Regnier, 2006; Creese et al., 2013). From each animal's HPM, 9 fractions were acquired and considered as technical replicates for further in-depth MS study. Briefly, the manufacturer's protocol was followed, in which the SCX Spin Tip column was conditioned by adding 50 µL SCX reconstitution solution and centrifuging in Eppendorf centrifuge 5430 R (Eppendorf AG, Hamburg, Germany) at 4000 x g for 6 minutes. The liquid was discarded, and the process was repeated. To achieve charge-based peptide separation, trypsin-digested sperm HPM peptides were reconstituted in 100-200 µL of SCX reconstitution solution (pH < 3, adjusted with formic acid), loaded on the SCX Spin Tip column, and centrifuged at 4000 x g for 6 min. The Spin Tip column was then eluted by centrifugation (4000 x g, 6 min) using a solution of ammonium formate in 10% acetonitrile in stepwise increasing strength (20, 40, 60, 80, 100, 150, 250 and 500 mM, respectively; 150 µL each; pH ~ 3). A total of 9 fractions, including the flow through fraction, were acquired, and stored at -80 ºC until MS analysis. The increasing ionic strength of the solution displaces cations, thereby displacing and separating peptides (Henry et al., 2017; Nair et al., 2021).

5.3.6 Tandem Mass Spectrometric Analysis

Similar approaches were used as before (section 4.3.4). The dried SCX 9 fractions containing tryptic peptides were reconstituted (MS grade water: acetonitrile: formic acid; 97:3:0.1; v:v, total vol 20 mL), vortexed (1-2 min), centrifuged (18000 g, 10 minutes, 4ºC) and 3µl aliquots of each sample were transferred to a MS vial for LC-MS/MS analysis (Brandt et al., 2019; Nair et al., 2021; Koziy et al., 2022). The MS analysis was performed using an Agilent 6550 iFunnel Q-TOF mass spectrometer (Agilent Technologies, Mississauga, ON, CA) coupled with liquid chromatography (Willems et al., 2016) using an Agilent 1260 series and an Agilent Chip Cube LC/MS interface respectively (Agilent Technologies, Mississauga, ON, CA) (Nair et al., 2021; Koziy et al., 2022).

Reversed phase chromatographic separation of peptides was achieved by employing a high-capacity Agilent HPLC-Chip; G4240-62030 chip cube, Polaris-HR-Chip 3C18 containing of a 360 nL enrichment column and a 75 µm × 150 mm analytical column (Agilent Technologies, Mississauga, ON, CA); both columns were packed with Polaris C18, 180Å, 3 µm stationary phase for improved peptide resolutions and peak capacity. Peptide fractions were suspended in 50% solvent A (0.1% formic acid in MS water) and 50% solvent B (0.1% acetonitrile: formic acid) then loaded onto the enrichment column (flow rate 2.0 µl/min; Brandt et al., 2019).

After loading, fractionated peptides were separated on the analytical column with linear gradient solvent system. On analytical column, the linear gradient program was used for peptide separation in presence of Solvent A and B. The linear gradient for solvent B was set at (3–25%, for 50 min) then at (25–90%, for10 min) using flow rate of 0.3 µL/ minute. Mass spectra, from electron spray positive ions were obtained under conditions of: capillary voltage (1900 v), ion fragmentor voltage (360 V), temperature (225ºC) and flow of nitrogen gas (12.0 L/min) (Brandt

et al., 2019). For spectral results the parameters were: MS data mass range of 250–1700 (mass/charge; m/z) at a scan rate of 8 spectra/s, MS/MS data range (100–1700 m/z), isolation width of 1.3 atomic mass units. For auto MS/MS, a maximum of 20 precursor ions were selected at an absolute threshold (3000 counts) and a relative threshold (0.01% with a 0.25 min active exclusion) (Brandt et al., 2019; Nair et al., 2021; Koziy et al., 2022).

5.3.7 Database Search and Analysis

Similar methods were used as before (section 4.3.5). The acquired MS/MS spectra from raw data were searched against isoforms α1, α2, α3, α4, β1, β2 and β3 of Na^+/K^+-ATPase with species *Bos Taurus* from NCBI (National Center for Biotechnology Information) Database by Agilent Spectrum Mill (Agilent Technologies, ON Canada) search engine. The database search parameters were trypsin as enzyme for protein digestion; two missed cleavage per peptide; fragment mass error 50 PPM; carbamidomethylation as fixed modification; Precursor mass shift range was -18 to 177 Da, and data were validated at a) peptide level (1% FDR) with precursor charge range 2 to 7 and a minimum peptide sequence length of 6 and b) protein level at 1% FDR. Additionally, each isoform of Na^+/K^+-ATPase was manually validated through a rigorous validation process using Mass Hunter software (Agilent Technologies, ON Canada) and employing a mass difference cutoff of $\Delta m < 10$ PPM between observed and theoretical mass (Nair et al., 2021; Koziy et al., 2022).

5.3.8 *In-silico* Digestion

The *in-silico* digestion of all 7 Na^+/K^+-ATPase isoforms was achieved by ExPASy-Peptide Cutter (https://web.expasy.org/peptide_cutter/) using trypsin enzymes (Wilkins et al., 1999). The unique peptide sequences in each isoform were identified separate from the homologous parts of the α and β isoforms. Predicted peptides from in-silico digestion assisted in identifying unique

peptides in each of the Na^+/K^+-ATPase isoform. From these tryptic peptides of unique sequences per isoform from the *in-silico* digestion, peptides from the experimental raw data with unique sequence for each isoform, were manually extracted and identified in all the isoforms (α1,2,3,4; β1,2,3) and in all 16 bulls.

5.3.9 Relative Quantification of Na^+/K^+-ATPase

Relative quantification of each Na^+/K^+-ATPase isoform was done using the NSAF, based on spectral counting with slight modifications (Florens et al., 2006; McIlwain et al., 2012; Langley & Mayr, 2015). Total spectral count from each of the Na^+/K^+-ATPase isoform was determined. From the known molecular weight of each of the isoform, the spectral counts were normalized and converted into NSAF for each individual isoform in each animal by using the following equation (5.1):

$$(NSAF)k = \left(\frac{SpC}{MW}\right) k / \sum_{i=1}^{N} \left(\frac{SpC}{MW}\right) i \quad \text{..... (5.1)}$$

where, SpC = total number of MS/MS spectra matching peptides from protein k,

MW = molecular weight of protein k, N = total number of proteins.

5.3.10 Protein-Protein Interaction Network

All proteins in ATH and ATL identified by Spectrum mill were converted into their respective gene codes and two interactomes one from ATH and other from ATL were drawn using Cytoscape v3.8.2. For each Na^+/K^+-ATPase isoform's protein-protein interaction, the first neighborhood proteins forming interaction with each of the Na^+/K^+-ATPase isoform was clustered together to make a sub-network of each isoform. The IPPs (neighbor proteins in the interactome) in a cluster developed using Cytoscape v3.8.2, identified different PPI in each cluster/sub-network.

5.3.11 Statistical Analysis

Shapiro-Wilks tests checked the normality ($p>0.05$) of all appropriate data. The sperm functional parameters (ejaculate characteristics, sperm kinetics) and the NSAF were compared between ATH and ATL fertility groups using SAS statistical software (SAS; version 9.3; SAS Institute, Inc Cary, NC, USA), with student t-test, while setting significance at $p< 0.05$. A linear regression was performed with SAS statistical software on NSAF of all isoforms (α1, 2,3,4: β1,2,3) of Na^+/K^+-ATPase to BFI of all 16 bulls. The deterministic model used in equation (5.1) was:

$y = a + bx$……. (5.2)

where a= intercept, b = slope of the regression line.

For all in-depth bioinformatics analysis (sequence alignment of the residues, physical and chemical properties, isoform's localization, and structural features), the three bulls with the highest BFI values (range 105-107, mean BFI±SEM 105±0.66) were categorized as high fertile (HF) whilst the three bulls with lowest BFI (range 88-94, mean BFI ± SEM 91±1.7) were classified as low fertile (LF).

5.3.12 Bioinformatics Analysis

5.3.12.1 Sequence Alignment of the Residues from Na^+/K^+-ATPase Isoforms

For each individual isoform, their residues were pooled within the HF and LF groups. The replicate/ duplicate peptides with similar sequences were removed leaving a pool of peptides for each group. The residue's sequence of each isoform was aligned to the known peptide sequence of that Na^+/K^+-ATPase isoform in from *Bos taurus* species in the NCBI database. The local similarity of the regions between sequences (experimental and known) was aligned with LALIGN, a basic local alignment search tool (https://embnet.vital-it.ch/software/LALIGN_form.html) and this sequence alignment was used to build the primary structure for each isoform.

5.3.12.2 Physical and Chemical Properties

From the primary structure of each Na^+/K^+-ATPase isoform residue, the physical and chemical properties/parameters were determined with ProtParam (https://web.expasy.org/protparam/; accessed 24 September 2021), a component of the ExPASy server (Gasteiger et al., 2005).

5.3.12.3 Prediction of Na^+/K^+-ATPase Isoforms' Subcellular Localization and Structural Features

The HSLPred server (https://webs.iiitd.edu.in/raghava/hslpred/submit.html; accessed 24 September 2021) predicted the subcellular localization of Na^+/K^+-ATPase isoforms from primary structure of each isoform which was created with the pooled data from HF and LF (n=3 each). The HSLPred is a support vector machine-based online bioinformatics technique for prediction of four major subcellular localization sites, including plasma membrane, nuclear membrane, cytoplasm, and mitochondrial membranes with an overall prediction accuracy is from 73 to 78%. This tool was used with the default method of hybrid-based approach (Garg et al., 2005), to increase the prediction accuracy up to 85%. The discontinuous B-cell epitopes for each Na^+/K^+-ATPase isoforms were predicted by immune epitope database (http://www.iedb.org/, accessed 24 September 2021) analysis server (Jespersen et al., 2017) based on hidden Markov models (HMM), and using the Bepipred Linear Epitope Prediction 2.0 with a threshold 0.600. Phosphorylation sites with their cognate PKs in residues for each isoform were predicted with Group Based Prediction System (GPS) 5.0 analytical software (The CUCKOO Work group, Wuhan, Hubei, China). The prediction of phosphorylation sites is based on two novel methods of position weight determination (PWD) and scoring matrix optimization (SMO) in GPS (Wang et al., 2020).

5.4 Results

5.4.1. Fertility and Sperm Motility Analysis

CASA motility kinetics did not differ significantly ($p>0.05$) between ATH and ATL, nor did any major ejaculate parameter (Table 5.1).

Table. 5.1. Ejaculate and Motility Characteristics of the Bulls (n=16). Each ejaculate (one per bull) from all bulls (n=16) was analyzed immediately after collection at the bull unit (Fresh) and after extension in liquid protein-free extender and overnight shipping to the laboratory (CASA). ATL: eight bulls with BFI 88-101; ATH: eight bulls with BFI 102-107. All values are mean ± SEM; significance for SAS t-test comparing ATL to ATH set at p≤0.05.

Parameter	ATL	ATH	p-value
Fresh Semen			
Concentration ($x10^6$/mL)	1407.63 ± 148.65	1380.44± 82.80	0.44
Ejaculate Volume (mL)	12.51 ±1.60	10.70 ± 1.39	0.18
Ejaculate weight (g)	23.72 ±1.21	21.82 ±1.45	0.18
Motility %	79.37± 0.73	79.37± 0.96	0.50
Sperm Count	17616.42 ±1997.44	14772.40 ±1952.12	0.21
CASA Extended Semen			
Static %	63.82 ± 3.77	69.86±4.80	0.34
Motile %	34.94±3.90	32.28±4.75	0.67
Progressive %	21.13±4.34	21.54±5.35	0.95
Slow %	1.07±0.29	1.04±0.24	0.94
Motile			
DAP µm	40.37 ± 4.07	36.33 ± 3.63	0.47
DSL µm	34.14 ± 3.14	29.64 ± 2.73	0.30

DCL µm	64.13 ± 4.47	62.15 ± 3.30	0.73
VAP µm/sec	69.56 ± 6.98	61.67 ± 6.92	0.44
VSL µm/sec	61.82 ± 5.86	56.19 ± 5.80	0.51
VCL µm/sec	110.59 ± 8.03	103.17 ± 7.86	0.52
STR %	85.53 ± 1.01	85.53 ± 0.88	1.00
LIN %	53.17 ± 1.82	51.25 ± 2.01	0.49
ALH µm	4.40 ± 0.14	4.50 ± 0.19	0.67
BCF Hz	33.42 ± 1.50	32.28 ± 1.35	0.58
WOB %	60.71 ± 2.27	57.78 ± 2.35	0.39
	Progressive		
DAP µm	40.58± 5.25	45.93 ± 3.54	0.41
DSL µm	39.07± 5.26	39.03 ± 1.02	0.99
DCL µm	64.22± 6.25	65.94 ± 2.28	0.80
VAP µm/sec	82.35± 9.61	84.53 ± 2.22	0.83
VSL µm/sec	73.73± 10.07	75.09 ± 2.14	0.90
VCL µm/sec	123.66± 10.22	121.76 ± 3.25	0.86
STR %	86.45± 4.61	89.83 ± 0.77	0.48
LIN %	58.24± 4.74	61.58± 1.27	0.51
ALH µm	4.82± 0.13	4.81± 0.26	0.99
BCF Hz	31.73± 1.87	31.52± 1.71	0.93
WOB %	65.46± 2.86	67.97± 1.29	0.44

DAP=Distance of Average Path, DSL= Straight Line Distance, DCL=Curvilinear Distance, VAP=Average Path Velocity, VSL=Linear Velocity, VCL=Curvilinear Velocity, STR=Straightness Coefficient, LIN=Linearity Coefficient, ALH=Mean Amplitude of Lateral Head Displacement, BCF=Frequency of Head Displacement, WOB=wobble.

5.4.2 Relative Quantification of Na^+/K^+-ATPase Isoforms

NSAF calculation found that the relative abundance of isoform α1 was greater in ATH than ATL ($p<0.05$). All other isoforms were present in similar abundance, although isoform α4 tended to exhibit greater abundance in ATL ($p=0.06$; Table 5.2).

Table 5.2. Relative Quantification of all Isoforms of Na^+/K^+-ATPase. Isoforms of Na^+/K^+-ATPase were identified by LC-MS/MS from the sperm HPM from each ejaculate of 8 bulls with mean BFI of 91.33 ± 1.44 (ATL) and from 8 bulls with mean BFI of 105.66 ± 0.54 (ATH) and quantified by NSAF. All values are mean NSAF ± SEM; significance for SAS t-test comparing ATL to ATH set at p≤0.05.

Na^+/K^+-ATPase Isoforms	ATL	ATH	p-Value
α1	0.85±0.02	0.95±0.03	0.04
α2	0.85±0.02	0.88±0.09	0.77
α3	0.74±0.01	0.81±0.05	0.27
α4	1.55±0.04	1.39±0.06	0.06
β1	0.92±0.08	0.82±0.15	0.60
β2	0.61±0.06	0.69±0.04	0.35
β3	1.42±0.07	1.27±0.10	0.29

ATL=Average to Low fertile group; ATH=Average to High fertile group; NSASF=Normalized Spectral Abundance Factor, which is a dimensionless factor that is unitless.

5.4.3 Protein-Protein Interaction Network of Isoforms of Na^+/K^+-ATPase

The IPPs that made clusters with each isoform of Na^+/K^+-ATPase were identified by Cytoscape v3.8.2 (Fig 5.1). The ATH α1 clustered solely to plasma membrane calcium-transporting ATPase 1 while there was no IPPs for ATL α1 identified (Fig 5.1 a). Isoforms α2 in both ATH and ATL (Fig 5.1 b, c) clustered with 7 common IPPs (cAMP-dependent protein kinase catalytic subunit α; Plasma membrane calcium-transporting ATPase subunit-4; Na^+/K^+-ATPase β3, Trifunctional enzyme subunit beta, Voltage-dependent anion-selective channel protein 2, AFG3-like protein 2, and ATP synthase gamma chain 1, chloroplastic ; Fig 5.1 b,c). In addition to

these seven common IPPs, ATH α2 also had 6 other proteins that uniquely clustered with it [K-transporting ATPase α chain 2; Na^+/K^+-ATPase subunits α3 and α4; cAMP-dependent protein kinase catalytic subunits (β and γ); plasma membrane calcium-transporting ATPase (subunit-2)], while α2 in ATL had only one IP that uniquely clustered with (V-type proton ATPase catalytic subunit A).

(a) Na^+/K^+-ATPase α1- ATH-BFI

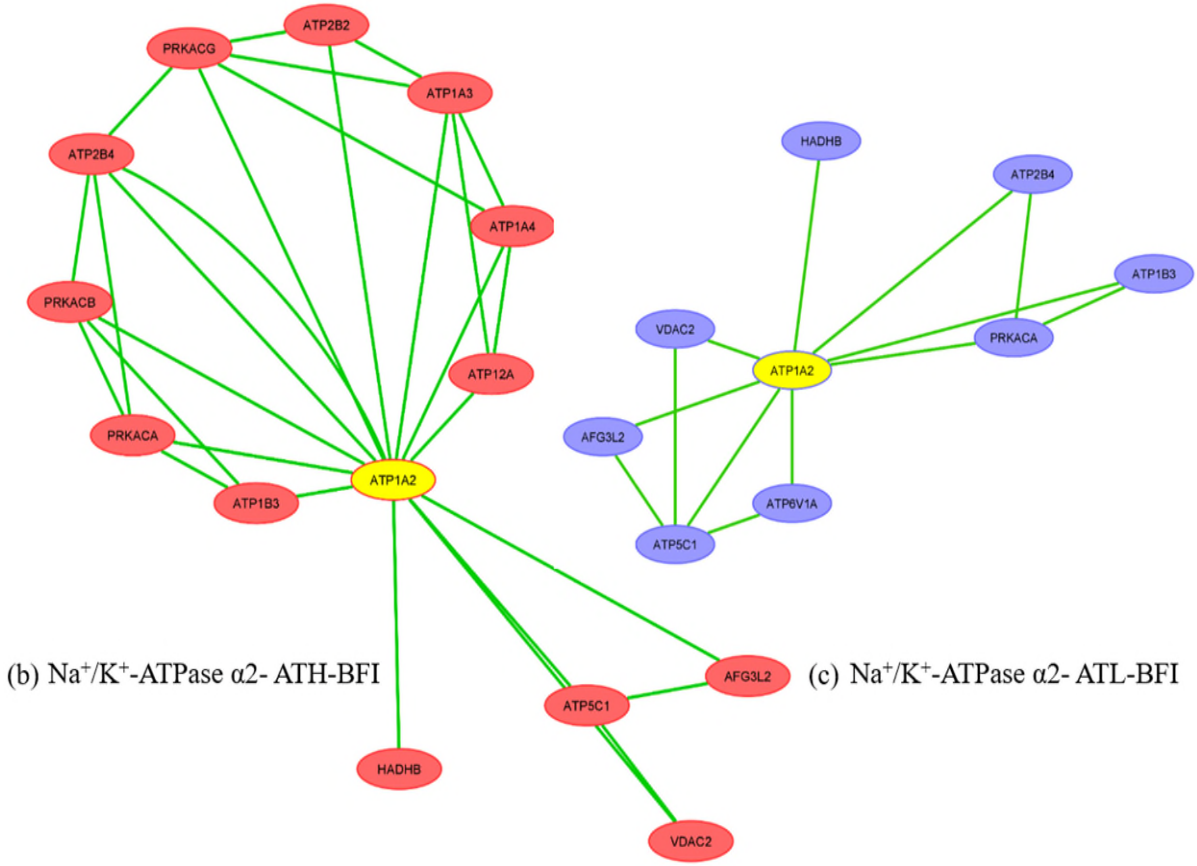

(b) Na^+/K^+-ATPase α2- ATH-BFI (c) Na^+/K^+-ATPase α2- ATL-BFI

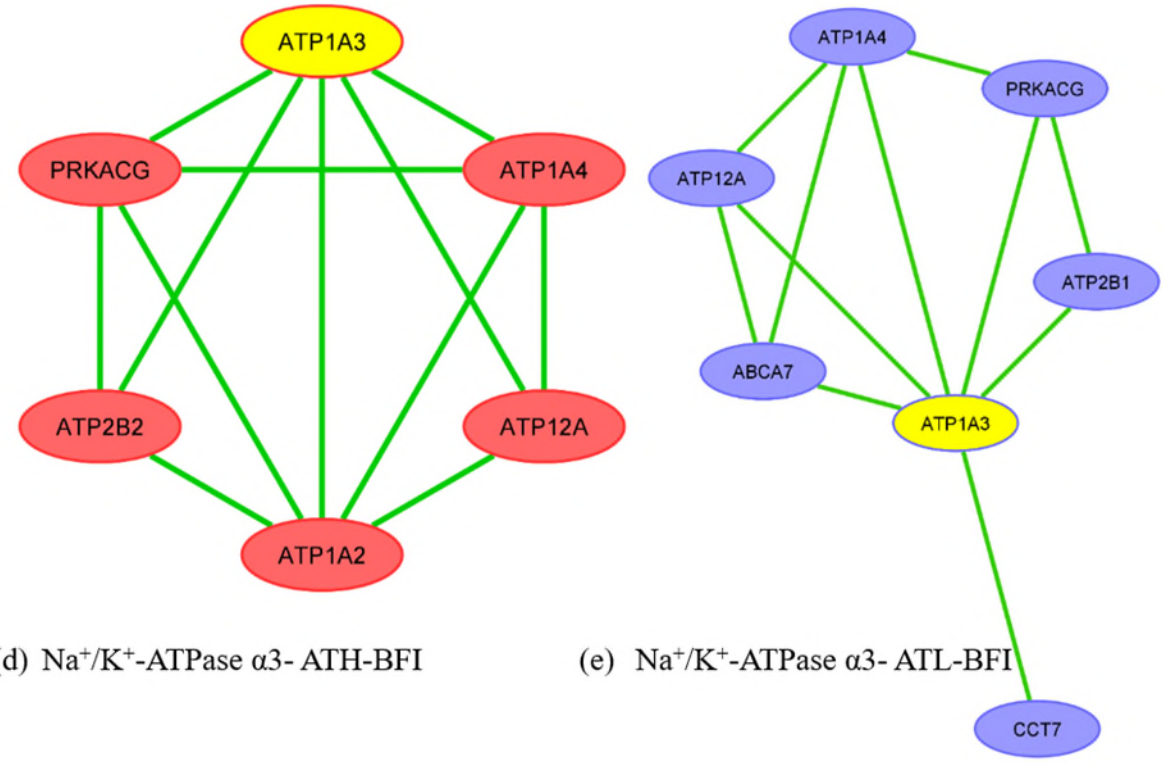

(d) Na^+/K^+-ATPase α3- ATH-BFI (e) Na^+/K^+-ATPase α3- ATL-BFI

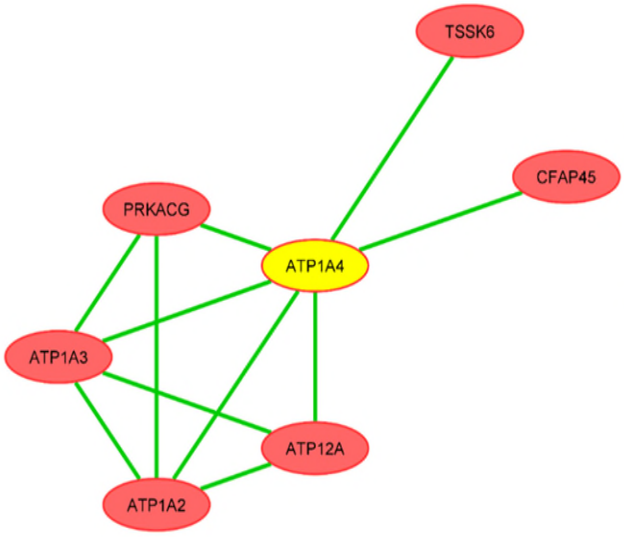

(f) Na^+/K^+-ATPase α4- ATH-BFI

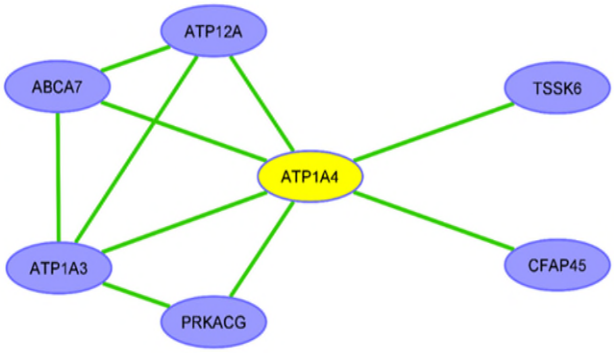

(g) Na^+/K^+-ATPase α4- ATL-BFI

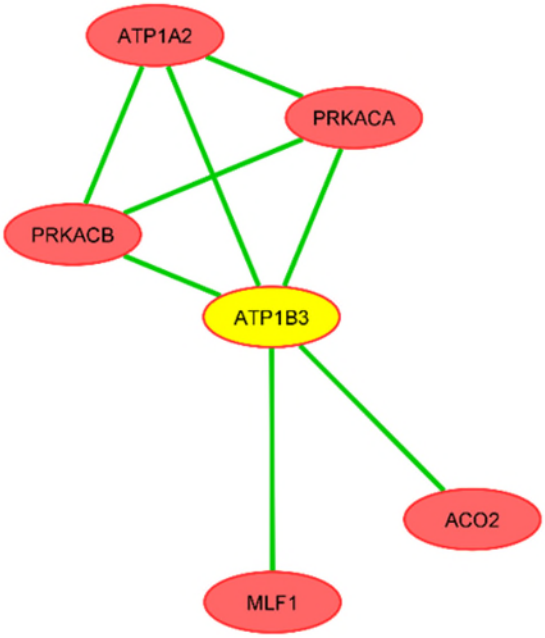

(h) Na^+/K^+-ATPase β3- ATH-BFI

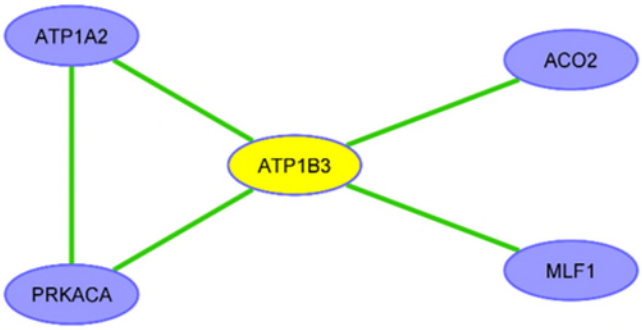

(i) Na^+/K^+-ATPase β3- ATL-BFI

Figure 5.1. Sub-Networks of Na^+/K^+-ATPase isoforms α1, α2, α3, α4, and β3 in HPM proteins from bull sperm, showing their IPPs (neighbor proteins in the interactome) developed by Cytoscape (v3.8.2). Yellow hub proteins are the indicated isoforms; red nodes are Interacting Proteins (IP) in ATH fertility group (n=8); purple nodes are IPPs from ATL group. a: α1; b, c: α2; d, e: α3; f, g: α4; h, i: β3. No IP clusters were detected for β1 or β2.

Isoform α3 (Fig 5.1 d, e) had 3 IPPs common to ATH and ATL: cAMP-dependent protein kinase catalytic subunit γ; Na^+/K^+-ATPase α4; K-transporting ATPase alpha chain. ATH α3 additionally had two unique IPPs: plasma membrane calcium-transporting ATPase 2; Na^+/K^+-ATPase subunit alpha-2 while ATL α3 had 3 unique additional IPPs: plasma membrane calcium-transporting ATPase 1, phospholipid-transporting ATPase ABCA7; T-complex protein 1 subunit eta were found in its sub-network.

Isoform α4 (Fig 5.1 f, g) had 5 IPPs common to ATH and ATL: Testis-specific serine/threonine-protein kinase 6, cAMP-dependent protein kinase catalytic subunits- γ, Na^+/K^+-ATPase α3, K-transporting ATPase α chain 2 and Cilia- and flagella-associated protein 45. ATH α4 additionally had one unique IP: Na^+/K^+-ATPase α2 while ATL α4 had 1 unique additional IP: Phospholipid-transporting ATPase ABCA7.

Isoform β3 (Fig 5.1 h, i) had 4 IPPs common to ATH and ATL: cAMP-dependent protein kinase catalytic subunits-α, Na^+/K^+-ATPase α2, Aconitate hydratase, mitochondrial and Myeloid leukemia factor 1. ATH β3 additionally had one unique IP: cAMP-dependent protein kinase catalytic subunits-β while in ATL β3 no unique additional IP was found. No IPPs were found for β1 or β2 in either ATH or ATL.

5.4.4 Identification and Relative Quantification of Common Signature Peptides

Since isoforms by definition have highly similar peptide sequences, isoform identity was confirmed by seeking 'signature' peptide sequences: sequences that were unique to a particular isoform and occurred in a minimum of at least 2 of the 8 bulls in each fertility group. Table 5.3 provides the total number of peptides, plus the signature peptides (tryptic peptides with unique

sequences existing in ≥2 animals) for the seven isoforms of Na^+/K^+-ATPase. All the representative tryptic signature peptides shown in the table have scores ≥5. The average total number of peptides identified for each isoform did not differ significantly between ATH and ATL. More peptides were identified for the α than β isoforms, as would be expected given the established size of the proteins. Signature peptides were found for all isoforms, with more than one signature peptide found for all isoforms except α2 and α3. Signature peptides were present in more than 50% of the bulls for all isoforms except for α3, whose single signature peptide was found in the HPM of two ATH and two ATL bulls.

Table 5.3. Peptide Sequences of representative Unique Peptides across all Isoforms of Na^+/K^+-ATPase in the Sperm HPM from Bulls of differing Fertility

Isoform	Accession number	MW (kDa)	Bull Fertility	Number peptides identified Mean ±SEM	Representative unique peptide	Number of bulls with representative peptide	Peptide's Score Mean ±SEM
Na^+/K^+-transporting ATPase subunit alpha-1	>NP_001070266.1	114.0	ATH	60±6	(K) IVEIPFNSTNK (Y)	8	6.3±0.5
					(R) ILDRCSSILIHGK (E)	6	6.2±0.7
					(R) IPADLRIISANGCK (V)	5	5.4±0.3
			ATL	59±6	(K) IVEIPFNSTNK (Y)	8	5.8±0.5
					(R) ILDRCSSILIHGK (E)	7	7 ±0.7
					(R) IPADLRIISANGCK (V)	4	6.4±0.6
Na^+/K^+-transporting ATPase subunit alpha-2 precursor	>NP_001074993.1	113.5	ATH	68±5	(R) ILDRCSSILVQGK (E)	4	6.4±0.5
			ATL	63±6	(R) ILDRCSSILVQGK (E)	7	7.2±0.5
Na^+/K^+-transporting ATPase subunit alpha-3 polypeptide	>DAA19667.1	113.2	ATH	52±5	(R) IATLASGLEVGK (T)	3	5.7±0.1

			ATL	46±5	(R) IATLASGLEVGK (T)	3	5.7± 0
Na^+/K^+-transporting ATPase subunit alpha-4	>NP_001137575.2	114.7	ATH	81±5	(R) LKIPVSK (V)	8	11.7±0.8
					(K) YSVDLTR (G)	8	9.4±0.6
					(K)EVVMDDHKLTLDELSAK (Y)	5	13±0.5
			ATL	84±4	(R) LKIPVSK (V)	8	12.4±0.4
					(K) YSVDLTR (G)	8	10.3±0.5
					(K)EVVMDDHKLTLDELSAK(Y)	2	17±0.2
Na^+/K^+-transporting ATPase subunit beta-1	>NP_001030411.1	35.5	ATH	7±1	(K) FIWNSEK (K)	5	6±0.6
			ATL	9±0.8	(K) FIWNSEK (K)	3	7.5±0.8
Na^+/K^+-transporting ATPase subunit beta-2	>NP_777102.1	33.8	ATH	12±1	(R) VISFYAGANQSMNVTCVGKR(D)	8	8.7±0.3
			ATL	11±1	(R) VISFYAGANQSMNVTCVGKR(D)	8	9.3±0.5

Na^+/K^+-transporting ATPase subunit beta-3	>NP_001030470.1	32.1	ATH	20±3	(K)YFPYYGKK (L)	5	8.5±0.4
			ATL	23±1	(K)YFPYYGK(K)	7	10.6±0.7

ATL: average to low BFI; ATH average-to-high BFI; MW: Molecular weight in kDa of each isoform; Amino acids in parentheses are cleavage residues with C terminus on the right side and N-terminus on the left side.

5.4.5 Relationship of Isoforms of Na^+/K^+-ATPase to Fertility Measures

Linear regression of the spectral counts (NSAF) for each isoform in all 16 bulls (Fig 5.2) positively correlated α1 and β2 to BFI (r^2 +0.42, p= 0.006; r^2 +0.47, p= 0.003, respectively), and negatively correlated α4 (r^2 0.37; p=0.01). The spectral counts of β3 showed a slight tendency to be negatively correlated with BFI (r^2 0.18; p=0.09); no other isoforms showed any correlation to BFI.

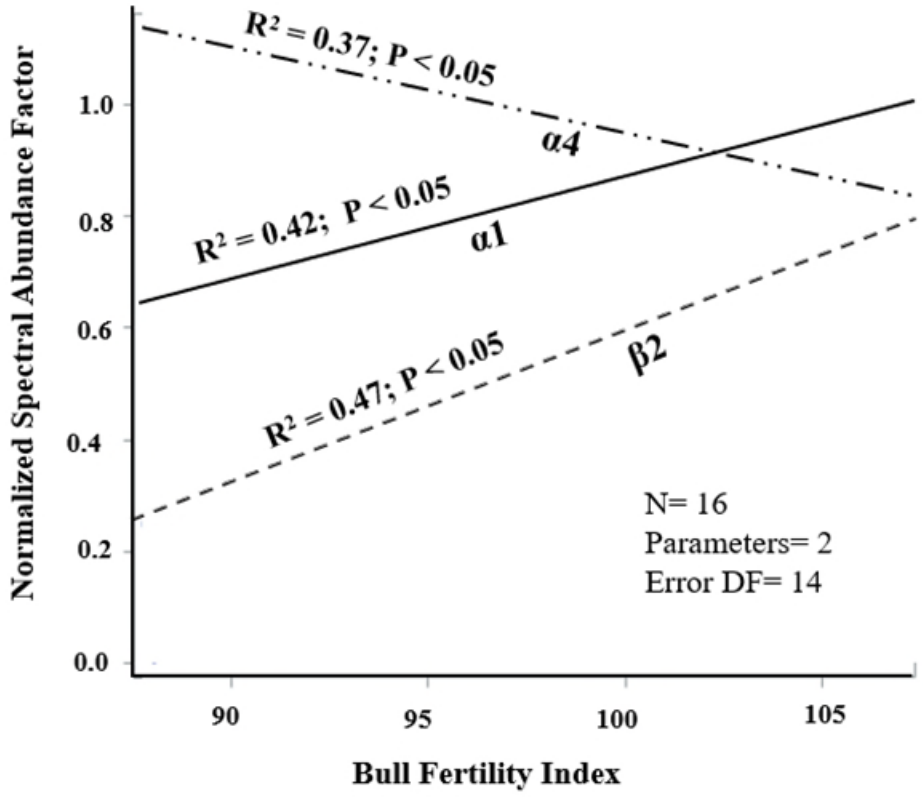

Figure 5.2. Regression analysis of spectral counts (NSAF) of Na^+/K^+-ATPase Isoforms α1, α4 and β2 in sperm HPM to BFI (N=16)

5.4.6 Bioinformatics Analysis

5.4.6.1 Localization of the Residues of Na^+/K^+-ATPase Isoforms

All the subsequent bioinformatics analyses were performed on the primary structure of each isoform of Na^+/K^+-ATPase. Predicted subcellular localization of the residues of Na^+/K^+-ATPase isoforms confirmed their origin in the plasma membrane of the sperm, with prediction accuracies (%) for α1,2,3,4, and β1,2,3 of HF/LF 79.6/79.6; 67.8/79.6; 79.6/67.8; 95.0/58.4; 58.4/51.0; 58.4/58.4; 67.8/58.4, respectively.

5.4.6.2 Physical and Chemical Properties of Na^+/K^+-ATPase Isoforms

ProtParam identified differences between some of the physical and chemical properties of the Na^+/K^+-ATPase isoforms from the HF and LF fertility groups (Table 5.4-5.5). The isoelectric point (pI) of all HF α isoforms was <8 except for α2, with a pI of ≥8; LF pI for α2 and α4 was ≥8 and α1 and α3 was < 8. The pI of HF β1 isoform was >8 and pI of β2 and β3 ≤ 8; for LF both β1 and β3 had pIs >8 while β2's was <8. The estimated half-life in all α and β isoforms except α1 and β1 was higher in HF than LF residues. α1's positive grand average of hydropathicity (GRAVY) in LF and HF indicate it is hydrophobic; while α4's negative GRAVY indicates it is hydrophilic in both fertility groups. LF's α2 and α3 had positive GRAVY values, but negative GRAVY in HF. β1 and β2 GRAVY values were negative in HF and LF, while β3 was negative in LF but positive in HF. Instability index of all isoforms in both groups were found stable.

Table 5.4. Physicochemical Properties of Residues from Na+⁄K+-ATPase α1, α2, α3, and α4 Isoforms (based on Primary Structures)

Properties	BFI	α1	α2	α3	α4
pI	HF	6.09	8.77	6.25	6.48
	LF	5.07	8.66	6.44	8.50
Est half life	HF	$1.4h^{-M}$ $3m^{-Y}$ $>10h^{-E}$	$30h^{-M}$ $20h^{-Y}$ 10^{h-E}	$30h^{-M}$ $20h^{-Y}$ $10h^{-E}$	$1.4h^{-M}$ $3m^{-Y}$ $>10h^{-E}$
	LF	$7.2h^{-M}$, $20h^{-Y}$ $10h^{-E}$	$4.4\ h^{-M}$ $20h^{-Y}$ $10h^{-E}$	$1.4h^{-M}$ $3m^{-Y}$ $>10h^{-E}$	$1.2h^{-M}$ $20h^{-Y}$ $10h^{-E}$
Instability index	HF	21.85, stable	33.36, stable	32.99, stable	24.50, stable
	LF	26.32, stable	23.53, stable	18.59, stable	33.15, stable
GRAVY	HF	0.16	-0.03	-0.13	-0.01
	LF	.085	0.13	0.12	-0.28

BFI= Bull fertility index, HF high fertility (n=3), LF low fertility (n=3); pI= Isoelectric point ; $^{-M}$=mammals, $^{-Y}$=Yeast, $^{-E}$=E.coli; h=hour, m=minutes.

Table 5.5. Physicochemical Properties of Residues from Na^+⁄K^+-ATPase β1, β2, and β3 Isoforms (based on Primary Structures)

Properties	BFI	β1	β2	β3
pI	HF	9.33	7.68	7.86
	LF	9.50	6.33	9.26
Est half life	HF	$1.3h^{-M}$ $3m^{-Y}$ $3m^{-E}$	$1.3h^{-M}$ $3m^{-Y}$ $3m^{-E}$	$3.5h^{-M}$ $10m^{-Y}$ $>10^{h-E}$
	LF	$1.3h^{-M}$ $3m^{-Y}$ $3m^{-E}$	$1h^{-M}$ $2m^{-Y}$ $2m^{-E}$	$1h^{-M}$ $30m^{-Y}$ $>10^{h-E}$
Instability index	HF	37.90, stable	30.65, stable	31.19, Stable
	LF	30.64, stable	28.91, stable	29.61, Stable
GRAVY	HF	-0.21	-0.44	0.06
	LF	-0.49	-0.44	-0.49

BFI= Bull fertility index, HF high fertility (n=3), LF low fertility (n=3); pI= Isoelectric point ; $^{-M}$=mammals, $^{-Y}$=Yeast, $^{-E}$=E.coli; h=hour, m=minutes.

5.4.6.3 Prediction of Na+⁄K+-ATPase Antigenic Epitope Analysis

The discontinuous B-cell epitopes for each of the isoforms of Na^{+}/K^{+}-ATPase were predicted by immune epitope database (http://www.iedb.org/, assessed 24 September 2021) analysis server (Fig 5.3).

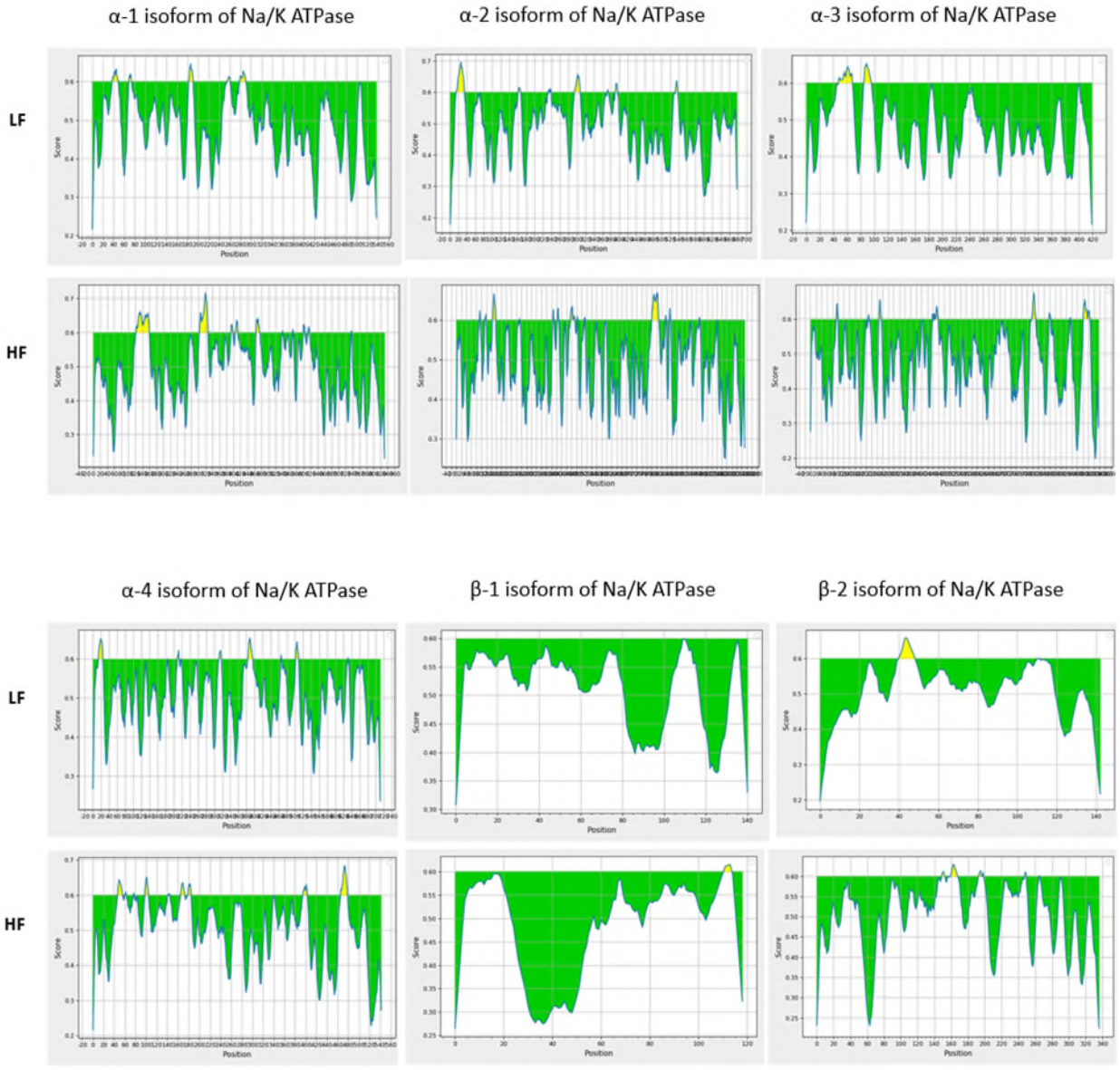

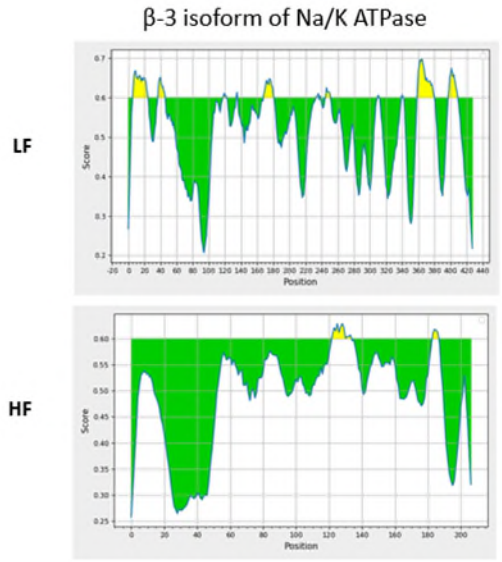

Figure 5.3. Predicted discontinuous B-cell epitopes for each of the isoform of Na^+/K^+-ATPase. X-axis indicates position of the epitopes and Y-axis shows score of the epitopes. Yellow peaks are above, and green peaks are below, a score of 0.6; peaks with scores >0.6 are regarded as discontinuous B-cell epitopes.

Comparatively, there were more discontinuous B-cell epitopes isoforms α1, 2,3,4 and β1 and β2 in HF than LF ($p<0.05$), while β3 had more epitopes in LF than HF ($p<0.05$). In LF, β1 detected no discontinuous epitope while one epitope was observed in HF group. The number of predicted discontinuous epitopes appeared to differ among alpha isoforms in HF [α2(12) > α1(10) > α3(9) = α4 (9)], as did their range of minimum to maximum Receiver Operating Characteristic-AUC scores (0.178 to 0.692; analysis not shown) but statistical testing for significance was not possible because there were too few replicates for statistical analysis between groups. In LF, the number of discontinuous epitopes did differ in alpha isoforms but in almost the reverse order to HF [(α4 (7) = α2 (7) > α1(5) >α3 (2)], their range of min to max AUC scores (0.199 to 0.716) was similar to HF. In HF β isoforms, the number of epitopes differed (β2> β3> β1) with a range of min to max AUC scores of 0.224 to 0.629; again, statistical testing for significance was not possible. The number of epitopes in LF β isoforms differed in a similar but more pronounced pattern than

that of HF (β3> β2> β1), and their range of min to max AUC scores was somewhat greater (0.196 to 0.697).

5.4.6.4 Prediction of Phosphorylation Sites in Na^+/K^+-ATPase Isoforms

The GPS 5.0-predicted phosphorylation sites in Na^+/K^+-ATPase isoforms differed between α and β isoforms and, for each isoform, between HF and LF (Fig 5.4A, B; Table 5.6).

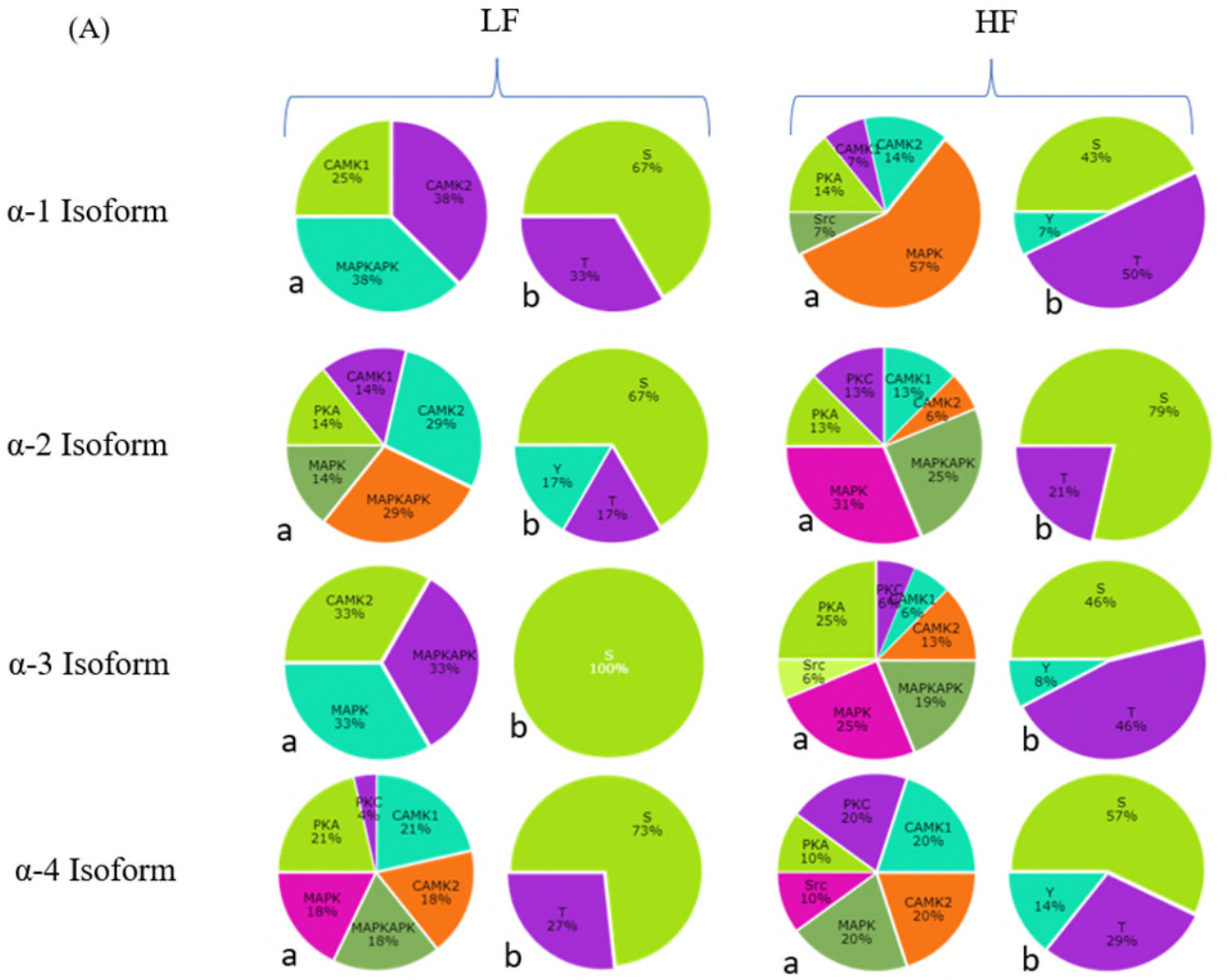

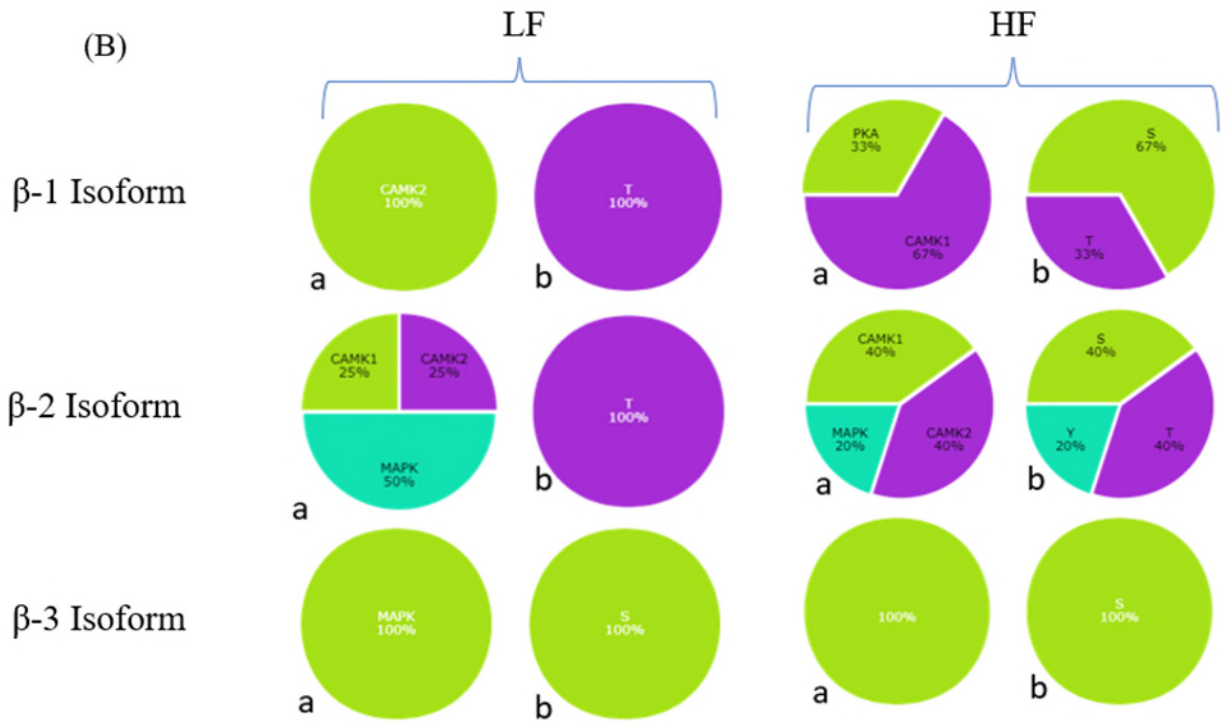

Figure 5.4. Phosphorylation sites predicted indicated Na^+/K^+-ATPase isoforms in HPM from bulls of differing fertility [(HF (n=3) vs LF (n=3)]. a: distribution of S/T/Y sites in kinase families of MAPK, MAPKAPK, RAF, PKA, PKC, Src, EGFR; b: distribution of S/T/Y P-sites (Ser/thr, Tyr, Ser, Thr).

Table 5.6. Predicted locations of Phosphorylation Sites in HPM Proteins from Bulls of High and Low Fertility (HF, LF, n=3 per group)

Isoform	Fert	MAPK	MAPKAPK	RAF	PKA	PKC	Src	EGFR	Ser/thr	Tyr	Ser	Thr
α1	HF	+	+	+	+		+	+	+	+		
	LF		+	+					+			
α2	HF	+	+	+	+	+			+			
	LF	+	+	+	+				+	+		
α3	HF	+	+	+	+	+	+	+	+	+		
	LF	+	+								+	
α4	HF	+		+	+	+	+	+	+	+		
	LF	+	+	+	+	+			+			
β1	HF				+				+			
	LF	+										+
β2	HF	+							+	+		
	LF	+										+
β3	HF			+					+			
	LF	+									+	

+: predicted presence of phosphorylation site.

5.5 Discussion

Sperm membrane Na^+/K^+-ATPase from Holstein bulls is shown here to have proteomic structure and extrapolated functions that correlate with bull fertility, when no differences were detected by the whole-sperm quality measures traditionally used in semen labs. The obvious structural changes of Na^+/K^+-ATPase composition and molecular signaling networks strongly correlate with bull fertility, clearly supporting Na^+/K^+-ATPase's direct role in important fertility pathways, and also indicate which specific isoforms are responsible.

Sperm from bulls with a wide range of highly reliable field fertility did not differ in the traditional commercial and research measures of sperm CASA motility (Table 5.1). This is not unexpected, as commercial semen laboratories eliminate ejaculates with poor physical

characteristics, and once those extremes are removed, sperm motility kinetics often do not reflect male fertility (human: Wang & Swerdloff, 2014; bovine: Somashekar et al., 2017).

The use here of highly-purified sperm HPM facilitates precise understanding of the molecules and events in capacitation, because the minor contributions from the acrosome and midpiece/tail in HPM (Zhao & Buhr, 1996; Hickey & Buhr, 2012) mean the results can be reliably attributed to the Na^+/K^+-ATPase and its isoforms (α1,2,3,4; β1,2,3) that occur in this critical membrane which controls the very initiation of capacitation and sperm:oocyte binding (Gadella & Boerke, 2016; Sajeevadathan et al., 2021). When stimulated by its steroid hormone ouabain, Na^+/K^+-ATPase acts as a receptor stimulating Tyr-P and capacitation in bovine sperm (Thundathil et al., 2006; Sajeevadathan et al., 2019), while its well-known enzymatic actions transport ions across membranes in different types of cells (Kaplan, 2002; Geering, 2008). Therefore, it seems reasonable to anticipate that specific α:β isoform pair combinations have predilections for signaling or ion transport functions as predicted in studies of different body organs of zebrafish during embryogenesis (Canfield et al., 2002).

The α1 isoform is ubiquitous in most mammalian cells and in whole bull spermatozoa and has been closely associated with Src kinase-mediated cell signaling involving Src/EGFR/Ras/Raf/ERK1/2 and PLC/PKC pathways which lead to Tyr-P (Xie et al., 2015) by a pathway potentially similar to that in sperm capacitation. The α1 isoform has been implicated in downstream signaling in whole sperm raft and non-raft fractions (Rajamanickam et al., 2017). Bovine HPM contains rafts, but no one isoform was restricted to this purported signaling platform, although the western blot profiles of specific isoforms differed in rafts, suggesting some unique structural features (Sajeevadathan et al., 2021). Among unique features, one important role of Na^+/K^+-ATPase as receptor for cardiotonic steroids such as ouabain has already been identified

(Pivovarov et al., 2019; Kinoshita et al., 2022). This unique feature contributes to signal transduction during *in vitro* sperm capacitation (Rajamanickam et al., 2017; Sajeevadathan et al., 2021). The proteomic approach used here on HPM from bulls of known fertility clearly identified specific molecular aspects of specific Na^+/K^+-ATPase isoforms that indicate their role in fertilization.

The PPI Networks (Fig 5.1) provided interesting information about the preferred αβ isoform partners and showed some interesting fertility-related differences and similarities in particularly the α isoforms. Only α1 in HPM from high fertility bulls had calcium-transporting ATPase as an IPP, α1 from low fertility bulls did not. The α2 isoform in HPM from high fertility bulls had the other α isoforms as IPPs suggesting they may exist and/or work within a cluster, while the α2 from low fertility lacked this connectivity. Interestingly, no IPP was found in β1 and β2 from either fertility group. The β3 forms the same four IPPs in both fertility groups, but high fertility HPM uniquely contained cAMP-dependent protein kinase catalytic subunit beta which could trigger signals through binding of G-protein-coupled receptors and activation of PKA (Rajamanickam et al., 2017). The networks also provide possible insight into interactions among the isoforms. Isoform α2 is always associated with β3, suggesting a possible preferred partnership. Also, α2 in high-fertility, but not low-fertility bulls, clusters with α3 and α4 while in low fertility α4 uniquely cluster with Phospholipid-transporting ATPase ABCA7 which is suggesting that some interaction of these α isoforms impacts pathways affecting fertility.

Signature peptides are peptides with unique sequences that can be used as surrogates for the protein of interest for purpose of quantification, measurement, and screening of biomarkers. In MS-based proteomics methods, signature peptides provide more selectivity and greater ease of quantification of multiple proteins in a complex mixture of proteins (Geng et al., 2000; Halquist

& Thomas Karnes, 2011). The signature peptides in this study were selected based on critical factors such as uniqueness of their peptide sequence across all Na^+/K^+-ATPase isoform (α1, α2, α3, α4; β1, β2, β3), and their reproducibility in HPM samples from bulls (minimum n ≥2 of the 8 bulls in each fertility group). Although the analytical algorithm positively identified all isoforms, it is possible that the great similarity among the α isoforms, and the βs, caused the algorithm to mis-assign some sequences to an inappropriate isoform. Therefore, to provide additional surety and rigor of identification, signature peptides were sought that were unique to a particular isoform, to differentiate among, and positively identify, the various α isoforms and the β isoforms. Signature peptides have previously been used for authentication (Wang et al., 2022) in samples from bovine (Zhang et al., 2013), human (Browne et al., 2019; Rashid et al., 2021), and influenza (Schwahn et al., 2010). This approach has here confirmed the presence of Na^+/K^+-ATPase isoforms in HPM previously identified with Western immunoblotting (Thundathil et al., 2006; Hickey & Buhr, 2012; Sajeevadathan et al., 2019; Awda et al., 2022), but more importantly the rigorous and unique combination of MS analytical techniques provides insight into molecular connections and pathways that affect fertilization.

ATH had a higher average total number of peptides in α1,2,3 isoforms than did ATL. There was minor or no differences between fertility groups in peptide sequence, frequency, length, and cleavage sites of the representative tryptic signature peptides (Table 5.3). Interestingly, a greater number of unique peptides were found in α1, α4 and β3 as compared to rest of the isoforms (α2, α3, β1, and β2) in both fertility groups. Although absence of a unique peptide could simply be due to its not being detected, and certainly the greater amount of α1 in ATH (Table 5.2) would likely affect amount and detectability of the unique peptides, the greater number of unique sequences noted in α1, α4 and β3 compared to α2, α3, β1, and β2 could indicate either larger amount of these

isoforms or longer polypeptide chains of these isoforms in all animals, either of which could affect the amount of other isoforms or on signaling pathway including capacitation. Alternatively, the vicinity to the free N terminal amino group may also reduce the rate of cleavage or even total resistance to trypsin cleavage (Manea et al., 2007). It is also possible that the differences in the membrane structure surrounding the isoforms (e.g., annular lipids; Hickey & Buhr, 2011) affects peptide ease of extraction. Mutation of these peptides also could affect fertility, just as transforming a proline into an arginine residue at site P681R in Alpha SARS-CoV-2 spike protein (Callaway, 2021; Liu et al., 2021) made the Delta variant of the virus more highly transmissible and enhanced its replication and pathogenicity (Liu et al., 2021; Peacock et al., 2021).

Isoforms α1 and β2 were highly positively correlated to the BFIs of the 16-bull population (r^2 = 0.42 and 0.47, respectively; $p \leq 0.006$); α4 was negatively correlated (r^2 0.37, p= 0.01,) with β3 trending similarly (r^2 0.18, p = 0.09; Fig 5.3). Similarly, the amount of α1 isoform in the HPM was significantly correlated with DBE FR in boar sperm (Chapter 3). It is tempting to speculate that an α1/β2 dimer promotes successful capacitation, and more α4 and other isoform(s) in the membrane interfere with this successful pairing. The IPPs networks found that α2 only combines with α3 and α4 in high fertility bulls, suggesting perhaps that interaction of α 2, 3 and 4 allows α1 more ready access to its preferred partner, β1. Certainly, α1 has been shown to be involved in downstream signaling leading to capacitation in homogenized whole bull sperm (Rajamanickam et al., 2017). Interestingly, the same authors found a positive association of α4 to *in vivo* bull fertility, which probably reflects α4 high concentration in the sperm tail, prevalent in a whole sperm homogenate, and aligns with α4's positive support of successful propulsion/hyperactivation. Capacitation is an event of the head plasma membrane occurring with tail hyperactivation, so the isoforms in the current results from highly purified HPM are much more likely reflective of actual

capacitation. The western blotting analysis of porcine sperm HPM (Chapter 3) also found both α3 and α1 were positively associated with *in vivo* fertility, although it was with α3 not α1. The current results clearly identified the isoforms and interactions that should be the focus of future work on sperm capacitation events mediated through Na^+/K^+-ATPase.

In-depth bioinformatics analysis of the bulls with extremely high and low BFI (HF, LF; n=3 each) helped predict the primary structure of each of the seven isoforms. Results from bioinformatics analysis of HPM isoforms could of course be impacted by the potentially random assignment of homologous peptides from one isoform to another isoform by the algorithm of the MS database search engine used to align spectra with NCBI database of Na^+/K^+-ATPase isoforms (a small database and specific to *Bos taurus*). The absence of complete protein sequencing due to the low concentration of Na^+/K^+-ATPase isoforms in the HPM of a single ejaculate hampers interpretation. These limitations, however, apply equally to all the samples and so bioinformatic predictions between high and low fertility samples provide valuable insights into the future analysis.

The unique physicochemical properties of the HPM Na^+/K^+-ATPase's isoforms differed in low and high BFI bulls.

Hydropathicity of a transmembrane protein is a fingerprint of the 3D-structure, interacting between the peptide sequence and the three-dimensional structure of the protein (Lolkema, 1998). Isoform α1 was hydrophobic (positive GRAVY) while α4 was hydrophilic. Both α2 and α3 were hydrophobic in LF, but hydrophilic in HF. All β isoforms in both groups were hydrophilic except for β3 which was hydrophobic in HF. These hydropathicity influences the orientation (inside/outside) of the isoform in lipid bilayer of the plasma membrane and affects its ability to

interact with hydrophilic lipid head groups or hydrophobic fatty acyl tails (Choudhary et al., 2016; Qian et al., 2021).

The Na^+/K^+-ATPase dimer is an amphipathic protein, and as such is believed to have transmembrane helices (Sarvazyan et al., 1997; Morrill et al., 2016). Such TM helices were sought with TMPred which uses an algorithm based on statistical analysis of its database (TMbase) of naturally occurring TM proteins to predict TM protein regions and directions. Although this state-of-the-art bioinformatic technique can be highly accurate in ideal circumstances (Cabelli et al., 1991; Chen et al., 1996, 1998; Ramamurthy & Oliver, 1997; Bertaccini & Trudell, 2002; Zhang et al., 2020), it can produce false positives and negatives. Although the HPM analyses did suggest differences in TM helices in HPM from HF and LF bulls, the number of predicted helices differed substantially from those in the NCBI database, most likely due to the failure to detect many peptide sequences due to the rarity of the protein in the HPM. Consequently, TM helices' predictions were not included, and further detailed research is needed to validate the TM helical structure of the sperm HPM Na^+/K^+-ATPase.

Epitopes are antigenic determinants that can be recognized by the antibodies of the immune system (Mahmoudi Gomari et al., 2020) or specific ligands. B-cell epitope identification plays an important role in the structure and function of the isoforms of Na^+/K^+-ATPase (Sanchez-Trincado et al., 2017). Prediction of B cell epitopes of proteins by BepiPred uses physicochemical properties of the protein like surface accessibility, hydrophilicity, flexibility, beta-turns, and machine learning (Fleri et al., 2017; Jespersen et al., 2017) and BepiPred by Immune Epitope Database (IEDB) uses more than 120,000 curated epitopes largely from scientific data (Backert & Kohlbacher, 2015) to produce prediction accuracy moderate to high (AUC score 0.6 to 0.7; Fleri et al., 2017). Epitope predictions have been made for acrosome membrane associated protein 1 of human sperm (Zhang

et al., 2020), hemagglutinin H7 subtype influenza virus (Wang et al., 2016), aquaporin-3 from *Schistosoma japonicum* (Song & He, 2012), and bacterial peptides causing bacteriospermia (Parida & Samanta, 2017). In the current study, the α1,2,3,4 and β1, β2 isoforms from high fertility bulls had more epitopes than those from low fertility bulls; and β3 in contrast had fewer (Fig 5.3). The maximum AUC scores predicted in HF/LF were in α1,2,3,4; 0.72/0.65, 0.67/0.69, 0.68/0.65, 068/0.65 and in β1,2,3; 0.62/0.59, 0.63/0.65, 0.63/0.69 respectively. The number of epitopes observed with moderate to high confidence in HF/LF in α1,2,3,4 were; 10/5, 12/7, 9/2, 9/7 and in β1,2,3 1/0, 7/1, 3/12 respectively. In HF α1,2,3,4 and β2 have significantly ($p<0.05$) a greater number of discontinuous epitopes than the corresponding isoforms in LF, while in LF β3 has significantly more epitopes than HF. Isoform β1 in LF has no epitope while one epitope was predicted in HF. These findings suggest that all isoforms in HF except β3 provide more anchoring sites for various ligands that could alter the protein's interactions with intra- and extra-cellular components of functional pathways including signaling. Binding of more ligands to more epitopes could create more protein-ligand complexes supporting conformational changes that transduce substantial signals and subsequently initiate a sequence of events leading to sperm capacitation. Furthermore, formation of protein-ligand complexes in Na^+/K^+-ATPase isoforms also support their functioning as receptors in sperm cell (Zhu & Lu, 2022). Epitopes have also been identified on α1β1 heterodimer of Na^+/K^+-ATPase in plasma membrane and endoplasmic reticulum (Laughery et al., 2004), and may provide the isoforms from the HF sperm more binding sites for fertility-related external stimuli/ligands.

Tyr-P is a well-known activator of biological signaling and activities (Naz & Rajesh, 2004; Salicioni et al., 2007; Newton et al., 2010; Jagan Mohanarao & Atreja, 2011; Kamacioglu et al., 2021) and protein phosphorylation of serine, threonine, and tyrosine residues can change activity

and structure (Wang et al., 2020). Bioinformatics tools have been used to predict protein kinase specific phosphorylation sites from protein sequences (Wang et al., 2017), with GPS 2.1 and 2.2 predicting phosphorylation from peptide sequence with 83% fidelity (Obenauer, 2003; Blom et al., 2004; Xue et al., 2011; Vlachakis et al., 2015) and the new version GPS 5.0 used here has further improved accuracy (Wang et al., 2020; Kamacioglu et al., 2021). GPS has been widely used to predict protein physical behavior and phosphorylation (virus: Alomair et al., 2021; receptors, Guzmán-Silva et al., 2022; vegetables; Xie et al., 2021; mammals; Kamacioglu et al., 2021; Kliche & Ivarsson, 2022). In the current study, the α1,3,4 isoforms in HPM from high-fertility bulls all were predicted to have Tyr-Psites (Fig 5.4), while only α2 did in low fertility bulls. The presence of Tyr-P sites on α isoforms, and appearance of α Tyr-P sites on isoforms primarily in high fertility animals, suggests that the higher amount/expression of α1 isoform in sperm HPM, with its higher number of discontinuous epitopes binding and Tyr-P sites is probably correlated with greater fertility.

Notably, Src and EGRFR phosphorylation was exclusively associated with α1,3 and 4 in high-fertility bulls, which supports previous findings in kidney cells (Tian et al., 2006; Liu & Xie, 2010) where α1 was found in close association with Src kinase. Binding of ouabain to α isoform induces signaling pathways including Src/EGFR/ ERK1/2, and PLC/PKC pathways in renal tissues (Xie et al., 2015). The α2 isoform found in porcine renal epithelia cells does not regulate Src, and in the absence of α1, can maintain ion pumping action but does not activate Src kinase nor downstream signaling involving ERK and Akt pathways when bound to ouabain (Xie et al., 2015). The similarity of α1, α3 and α4 Tyr, SRC and EGFR phosphorylation suggest involvement of these isoforms in capacitation. However, as α4 is located predominately in sperm tail region and is known to be engaged in sperm motility (McDermott et al.,2015), it may primarily connect

with hyperactivation. The other isoforms, α1 and α3 are found in sperm HPM and have recently been associated with boar fertility (Chapter 3), suggesting that there may be species-specific uses of α1 and α3. Careful and thorough development of the complete peptide sequences and three-dimensional structure of these isoforms could unravel the final details of Na^+/K^+-ATPase signaling in capacitation.

The results detailed here demonstrate relationship of field fertility to amounts of certain Na^+/K^+-ATPase isoforms and their predicted structural and functional characteristics. In particular, α1 and β2 in bull sperm HPM may function as an α1β2 dimer stimulating signaling pathways leading to capacitation and fertilization, and interaction(s) with other isoforms impact optimal αβ dimer formation and signal transduction.

5.6 Conclusions

The higher amount (based on NSAF calculations) of α1 isoform of Na^+/K^+-ATPase is associated with bull *in vivo* fertility. The α1 and β2 showed significant positive correlation while α4 negatively correlated to *in vivo* bull fertility. In both fertility groups, positive GRAVY of α1 indicated its hydrophobic nature while negative hydropathicity of α4 demonstrated it as hydrophilic. Relatively, a higher number of discontinuous B-cell epitopes noted in α1,2,3,4 and β1, β2, and predicted phosphorylation sites in high fertile bulls may indicate how these isoforms are involved and their unique role in signaling pathways important for sperm capacitation and fertilization.

CHAPTER 6: GENERAL DISCUSSION AND CONCLUSION

6.1 General Discussion

This research has identified the specific Na^+/K^+-ATPase isoforms in boar and bull sperm that are significantly associated with *in vivo* fertility. In boar sperm, the amount of α3 isoform highly correlated to DBE FR with α1 isoform showing medium correlation. In bull sperm α1 and β2 were positively correlated, and α4 was negatively correlated to *in vivo* bull fertility. In addition to Na^+/K^+-ATPase isoforms, 67 other proteins (48 up- and 19 down-regulated) were identified that correlate significantly with fertility. This novel elucidation of proteins involved in fertility contributes to expanded understanding of the signaling and other interactions involved in the early sperm-driven steps of fertilization. The potential fertility biomarkers in boar and bull sperm improve our understanding of key proteins and their roles in various, complex, mechanisms that enable successful sperm fertilization. These fertility biomarkers may have future use in selecting sires with high fertility in agriculturally important species for the best use of farmers, breeders, and AI industries to enhance the efficient sustainable production of animal-based proteins supporting food security.

6.2 Overview and Objectives

Animal fertility is a complex trait and encompasses numerous molecular mechanisms. There are significant challenges stemming from the currently limited accuracy of predicting fertility and result in reproductive failure which financially burdens AI industries, breeders, farmers and ultimately consumers on an annual basis. Sperm physiological, cellular, and molecular mechanisms that are responsible for male fertility are largely unknown, and there are no simple completely reliable laboratory methods to predict male fertility. Many proteins are involved in sperm signaling pathways that control fertility and are often found in the sperm HPM which controls sperm: oocyte recognition and binding. One of these HPM signaling proteins is Na^+/K^+-

ATPase, which, when stimulated by binding with the hormone ouabain, is well known to initiate downstream signaling and Tyr-P of the proteins that induce sperm capacitation (Rajamanickam et al., 2017; Sajeevadathan et al., 2019). Elucidating the HPM proteome, including in-depth characterization of Na^+/K^+-ATPase, should aid in our understanding of the process of fertilization. These studies conducted in two varied species, boar, and bull, also demonstrated the similarities and differences of the amount and involvement of specific Na^+/K^+-ATPase isoforms responsible for fertility mechanisms.

The overall objective of this research was to characterize Na^+/K^+-ATPase and other proteins in sperm HPM from males of known *in vivo* fertility and identify any relationships with fertility. To address this aim, three studies were undertaken; one study, which evaluated fresh individual ejaculates from 12 boars of low and high fertility lines, using semi-quantitative Western immunoblotting, which found that the amounts of α3 and α1 isoform in HPM correlate significantly with farrowing rate. The second study analyzed a different mammalian species (bovine, n=16 Holstein bulls) through MS-based proteomics for the contribution of non-ATPase sperm HPM proteins to fertility. Sixty-seven proteins differed by at least two-fold in amount (based on mass spectra intensities) between the high and low fertility bulls (48 up-regulated, 19 down-regulated in high versus low fertility bulls). Linear regression confirmed the relationship of these proteins to fertility. The third study characterized isoforms of Na^+/K^+-ATPase in sperm HPM in the same 16 Holstein bulls through MS-based proteomics. Results of this study identified significantly more α1 isoform, in comparison to the other Na^+/K^+-ATPase isoforms, in high fertility bulls and in addition, isoforms α1 and β2 were positively correlated to fertility while isoform α4 was negatively correlated.

The overarching goal of my research was to elucidate the fertility mechanism by characterizing the protein Na^+/K^+-ATPase and by better understanding other non-ATPase proteins found in the sperm HPM that are involved in sperm fertility, to support the long-term aim of improving reproductive efficiency of important agricultural species, thereby enabling more efficient food production from limited resources.

6.3 Specific Isoforms of Na^+/K^+-ATPase in the Sperm HPM are Correlated to Boar *In Vivo* Fertility

Over 80% of all swine are bred by AI in major pork producing countries (Zuidema et al., 2021). Boars in AI studs are selected for their superior genetic qualities (feed efficiency, muscling, growth rate, etc) that are important for the production of high-quality meat protein. In an AI stud, each boar's ejaculate is tested and those ejaculates with adequate sperm concentration and motility are diluted in a liquid buffer (extender) and used, usually within three days of production, to inseminate up to 30 females. Actual *in vivo* boar fertility is ascertained long after breeding many females, measured as the DBE on FR (number of females bred compared to those farrowing) and the DBE on TNB. The sperm from boars of differing DBEs for FR and TNB had similar overall motility and morphological parameters (Tables 3.1, 3.2) and HPM (acquired per million sperm), and WB revealed that sperm HPM from all boars contained all six isoforms of Na^+/K^+-ATPase (α1,2,3; β1,2,3). Although most isoforms were present in similar amounts (WB volume/band density), there was significantly more α3 isoform in the HPM of high fertility boars. Linear regression confirmed a highly significant positive relationship of the amount of α3 with DBE Farrowing Rate, and also detected a medium positive correlation for α1 with DBE Farrowing Rate. Immunocytochemistry studies revealed more α isoforms visible on intact sperm from high fertility boars, while there was more α2 visible in permeabilized sperm from low fertility boars. In bulls,

the hormone ouabain interacts with its receptor Na^+/K^+-ATPase in the sperm plasma membrane and is well known to initiate downstream signaling from plasma membrane that leads to Tyr-P of the proteins that induce sperm capacitation (Rajamanickam et al., 2017; Sajeevadathan et al., 2019). Interestingly, α3 is more sensitive to ouabain than α1 in rat brainstem axolemma (Blanco & Mercer, 1998) and in a rat cell line, α3 Na^+/K^+-ATPase acts through Src-independent pathways involving PI3K and PKC (Madan et al., 2017). The increased amount of α3 in boar sperm HPM, and its possible greater accessibility on the exterior sperm HPM seen in immunocytochemistry, may increase α3 binding to ouabain to stimulate capacitation in high fertility boars. Another likely possibility is that the greater amount of α3 as compared to other isoforms may increase its probability for binding to its partner β isoform, thereby inducing a signaling pathway required for sperm capacitation. Understanding exactly which structural features of the individual isoform, or αβ paired isoforms, or other proteins critical to the complex pathways governing capacitation, could help select more fertile boars for both AI and natural breeding, improving overall swine reproductive efficiency.

6.4 Sperm HPM Proteins associated with *In Vivo* Fertility

To determine what HPM proteins other than Na^+/K^+-ATPase might be associated with fertility, high throughput mass spectrometric analysis examined all the proteins in sperm HPM from 16 Holstein bulls of differing fertility. Holstein fertility is assessed by BFI which is an international multi-factor BFI (Semex; average BFI=100 based on >1000 inseminations per bull) that was used here to separate Holstein bulls with BFI > or < 101 (ATH; ATL; n=8 each). BFI is a Semex internal calculation composed of NRR (56 days post service, Canadian Index), SCR (US index) and Agri-Tech analyses (ATA, US index from farms on the west coast).

The HPM proteins from three bulls with the lowest BFIs and three with highest BFI (91.33 ± 1.44 versus 105.66 ± 0.54 BFI, $p < 0.01$; low fertility, LF and high fertility, HF, respectively) were first examined, by MS-based proteomics, for proteins that differed in intensity by at least two-fold (DAPs). Fold change assesses how much an entity changes from one state to another, and here compared the abundance ratio of one protein between two fertility groups, using a specified cut off value of two-fold (twice as much) between the conditions. There were 67 DAPs that differed significantly between the HF and LF fertility groups, 48 that were up-regulated (present in greater amounts based on MS signal intensity) and 19 that were down-regulated (Fig 4.5 a, b) in HF versus LF. Each DAP was manually validated through a rigorous validation process by Mass Hunter MS software using as a criterion, a mass difference (Δm) of < 10 PPM between observed and theoretical masses, as was seen in peptide fragments of major histocompatibility complex I in human and mouse cells (Escobar et al., 2011). Multivariate analysis of DAPs identified fixed clusters that differed between the fertility groups, and a quantitative statistical meta-analysis which tested the pooled data from different ways, confirmed the association of DAPs to BFI. The DAPs identified here as being up-regulated in HF bulls include proteins that have been associated with sperm capacitation (Fujita et al., 2000; Mostek et al., 2017), regulation of motility (Chen et al., 2011; Xu et al., 2020), signaling complexes (Li et al., 2011), sperm egg binding functions (Fraser & Quinn, 1981; Kwon et al., 2014), spermatid differentiation (Nourashrafeddin et al., 2014; Mi et al., 2015), cytoskeletal structural formation, acceleration of motility to achieve fertilization (Norrander et al., 2000; Muhammad Aslam et al., 2018; Özbek et al., 2021), protection from oxidative damage (Norrander et al., 2000) and sperm fertilization (Rahman et al., 2013). Several of them have previously been reported in high fertility bulls (Park et al., 2012; Özbek et al., 2021). As expected, linear regression revealed that the relative quantification of the 48 up-regulated DAPs

was highly positively correlated to BFI of HF and LF, while the amount of the 19 down-regulated proteins was negatively correlated (Table 4.4, 4.5, $r^2 = 0.97$ and 0.95, respectively, $p < 0.05$). Of greater importance was that the linear regressions examining the relationships of the relative amount of these 48 and 19 proteins present in all 16 bulls, covering the full range of BFI, found the identical relationships of the up- and down-regulated DAPs to fertility, albeit with lowered but still significant correlations ($r^2= 0.78$ and 0.43; $p<0.05$; Table 4.6, 4.7). This strongly supports the importance of these specific HPM proteins to events critical for fertilization and warrants deeper understanding of their characteristics and roles.

The PPI networks found significant interactions (PPI enrichment p-value $9.21x10^{-12}$) among various groupings of up-regulated DAPs (Fig 4.7) whilst down-regulated DAPs showed no significant interactions. MCODE analysis in the Cytoscape analyzed the densely connected regions based on highest k-score in clusters of up-regulated DAPs and identified 3 clusters in the up-regulated DAPs that interacted with each other and neighboring proteins in the networks (Fig 4.8). Each cluster had a hub protein that influenced their IPPs. These hub proteins would support their involvement in regulation of motility (Zhao et al., 2018), bull sperm capacitation (Fraser & Quinn, 1981; Kwon et al., 2014), sperm-egg binding (Ramesha et al., 2020) and in signal transduction (Li et al., 2011). Key hub proteins such as spermatogenesis associated up-regulated DAP SPATA19 interact with up-regulated DAPs; ACRBP, ODF3, and ROPN1L (Fig 4.8). SPATA19 functions in mice sperm for spermatid differentiation, sperm motility and fertility (Nourashrafeddin et al., 2014; Mi et al., 2015) and has been found in Malnad Gidda bull spermatozoa (Ramesha et al., 2020). ACRBP is elevated in capacitated boar spermatozoa and is involved in sperm egg binding through the release of acrosin from the acrosome. It is considered as a potential biomarker of fertility (Kwon et al., 2014). ODF3 is involved in induction of sperm

hypermotility during capacitation (Zhao et al., 2018), and may reflect the known minor content of mitochondrial and tail membranes in HPM. These capacitation-associated proteins are highly correlated to BFI (table 4.3) and their abundance in high fertile bulls' sperm suggests the regulatory function for sperm motility, capacitation, and sperm-oocyte binding.

It is generally held that a spermatozoon is transcriptionally silent (Miller & Ostermeier, 2006a). Mature sperm have no or little cytoplasm or intracellular machinery for translation, and any transcripts correspond to remnants of stored mRNAs from post-meiotic spermatogenesis (Miller & Ostermeier, 2006b). Indeed, RNA has been found in sperm after continuous density gradient washing, and under certain circumstances, sperm appear to translate their mRNAs *de novo* (Miller & Ostermeier, 2006a; Miller & Ostermeier, 2006b; García-Herrero et al., 2010) – different sets of mRNAs were found in fertile and infertile men (Garrido et al., 2009). Therefore, genes that transcribed proteins for sperm membrane during spermatogenesis were associated to their Gene Ontology terms by GO analysis to identify their specific functions (García-Herrero et al., 2010). Since mature sperm as investigated here are almost always transcriptionally silent, GO databases was employed here simply to assign and extrapolate information on the function of the proteins identified in the sperm HPM and the results do not imply active transcription. GO analysis suggested DAPs up-regulated in the sperm HPM of high BFI bulls were involved in spermatogenesis, development of spermatid cilium movement, metabolic processes of nucleoside mono- and tri-phosphates and, more generally in sexual reproduction and reproductive processes that were not found in low fertile bulls. Fertile human sperm gave remarkably similar GO results, in particular with regards to functions relating to energy (García-Herrero et al., 2010; Liu et al., 2018). The discovery of GO functions associated with gaining energy in sperm from HF bulls is consistent with the spermatozoal requirement of a large amount of energy for motility. The

nucleoside mono- and tri-phosphate metabolic processes GO analysis identified in this study are known to act as a source of energy for cellular processes such as motility. The nucleosides also act as precursors for RNA, and spermatozoal RNA has been associated with fertility in cattle (Feugang et al., 2010; Chen et al., 2015), pigs (Gòdia et al., 2018), horses (Kadivar et al., 2020) and humans (Jodar et al., 2013).

GO suggested that binding molecules are functionally enriched (up-regulated) in HPM of high fertility bulls, while catalytic functions are more prevalent in low fertility bulls. Similar findings were reported for asthenozoospermic versus normal human spermatozoa (Liu et al., 2018). Elevated binding functions in HF sperm HPM may improve efficacy of sperm: zona binding, whilst the enhanced catalytic activity in LF sperm HPM may deplete sperm energy for metabolic functions associated with capacitation and reduced fertility in LF bulls.

Clearly this research has identified significant differences in the types and amounts of specific proteins existing in the HPM of sperm from bulls of high and low *in* vivo fertility. Different bioinformatics tools identified these proteins to be involved in networks and functions related to sperm motility, capacitation, and sperm: egg binding. Furthermore, both the types of HPM proteins and their relative amounts are correlated with bull fertility.

6.5 Specific Isoforms of Na^+/K^+-ATPase in HPM are Correlated to Bull *In Vivo* Fertility and are associated with Signaling Pathways contributing to Bovine Sperm Capacitation

Na^+/K^+-ATPase signaling pathway(s) involved in capacitation and fertility were more thoroughly evaluated in the same semen and HPM samples from the 16 bulls of varying *in vivo* fertility (Chapter 5). Sperm motility kinetics and concentration were assessed by the semen production lab on the fresh ejaculates and again on arrival of the liquid-extended semen within 24-

36 hours at the research lab, at which time HPM was isolated for in-depth characterization of the seven isoforms of Na^+/K^+-ATPase (α1,2,3,4; β1,2,3) by MS-based proteomics.

The features of the fresh ejaculates obtained by the semen lab (ejaculate volume and weight, sperm concentration, sperm count, motility) did not differ between ATH (n=8) and ATL (n=8) bulls (Tables 5.1). Similar results for sperm motility and kinetics parameters were obtained for the extended semen on arrival at the lab (Tables 5.1), and similar amounts of HPM per million sperm were obtained.

However, α1 in the ATH HPM had significantly more spectral counts/NSAF (Table 5.2 $p<0.05$), and overall α1 and α4 tended to have more tryptic peptides (Tables 5.3). Tryptic peptides found in the other isoforms were similar between the two fertility groups. This may suggest structural differences, with some of the isoforms having longer polypeptide chains; different sequences of Na^+/K^+-ATPase α1 isoform were found in different regions of *Etroplus suratensis* (Sebastian et al., 2018). Shorter peptides may be due to weak amide or peptide bonds in the chains themselves making the chain more fragile (Goettig, 2016). Alternatively, the presence of acidic residues in positions next to the cleavage site, or the presence of a positive charge, specifically adjacent to Lys and Arg residues or the vicinity to the free N terminal amino group may also reduce the rate of cleavage or even total resistance to trypsin cleavage (Manea et al., 2007). It is also possible that the differences in the membrane structure surrounding the isoforms affects peptide ease of extraction (e.g., annular lipids; Hickey & Buhr, 2011).

There were significant correlations of the amount of three isoforms with *in vivo* fertility. Calculations based on NASF found relatively more α1 ($p<0.05$) in the HPM from the ATH than the ATL (Table 5.2), which was confirmed by the significant positive relationship that linear regression identified for α1's NASF to the BFI (Fig 5.3). Interestingly, linear regression also

identified a positive relationship of β2, and a negative relation of α4, to BFI. This may suggest that specific αβ dimers support Na^+/K^+-ATPase's signal transduction and thereby, potentially, fertility. In high fertility bulls, the greater numbers of α1 and β2 may support their dimerization, so they can respond to ouabain with induction of signaling, Tyr-P and capacitation as our group has identified (Sajeevadathan et al., 2019). Presence of α4 in whole sperm (Jimenez et al., 2011; Jimenez et al., 2012; Rajamanickam et al., 2017) and tail (Wagoner et al., 2005; Jimenez et al., 2011) would support proper motility and possibly hyperactivation, but increased numbers of α4 isoforms in the head membrane could presumably compete with α1, preventing the α1β2 capacitation signaling and reducing fertility.

To identify differences more precisely in membrane protein that are critical to fertility, two sub-populations of bulls were selected, the three bulls with the highest BFI (105,105,107) and the three with lowest BFI (88,92,94). Bioinformatics analyses of the structures of Na^+/K^+-ATPase's isoforms from high fertility bulls predicted more discontinuous B-cell epitopes in isoforms α1, 2,3,4, β1 and β2 of Na^+/K^+-ATPase in HF than LF bulls, potentially impacting their involvement in signaling pathways for sperm capacitation.

Tyr-P sites in residues of HF bulls were predicted in isoforms of α1, α3, α4 and β2, but only in α2 of LF bulls (Fig 5.4a in chapter 5). This higher number of isoforms that could be tyrosine phosphorylated in HF bulls than LF supports the importance of Tyr-P of Na^+/K^+-ATPase in signaling pathways supporting fertilization The predicted phosphorylation sites (Fig 5.4 a) could imply that α1, α3 and/or α4 isoform are involved in Tyr-P that leads to sperm capacitation. Among β subunits, Tyr-P was predicted in the β2 isoform of high fertile animals. Since Na^+/K^+-ATPase works as a αβ dimer in cell membrane (Linnertz et al., 1998; Santos et al., 2002; de Lima Santos

& Ciancaglini, 2003; Bagrov et al., 2009) both subunits may function in various signaling pathways.

The α and β subunits of Na^+/K^+-ATPase function as a dimer (αβ) or double dimer $(\alpha\beta)_2$ in the cell membrane (Linnertz et al., 1998; Santos et al., 2002; de Lima Santos & Ciancaglini, 2003; Bagrov et al., 2009). Across all the 16 bulls, relative amounts of α1 and β2 are positively related to fertility (Fig 5.2), and the presence of several signaling residues aligns with fertility (Table 5.6). Interestingly, the protein–protein interacting networks (Fig 5.1) show α2, α3, and α4 cluster in high but not in low-fertility bulls. A possible interpretation is that clustering of isoforms α2, 3 and 4 could interfere with any of them binding effectively with their preferred β, allowing α1 more ready access to β2 to promote capacitation and fertilization. Of the α isoforms, only α1 is not associated with PKC phosphorylation, and α1 only shows MAPK, PKA, SRC, EGFR and Tyr-Pin high fertility bulls (Table 5.6), corresponding to its maintenance of Src kinas in the active state in other cell types (Liang et al., 2007; Li et al., 2011; Xie et al., 2015).

Na^+/K^+-ATPase isoform α1 interacts with other proteins c-Src and caveolin-1 in the cell membrane and form a receptor complex. This crosslinking among proteins induces important signaling pathways (Nie et al., 2020). The interaction between Na^+/K^+-ATPase isoform α1 and Src regulate the metabolic capacity in pig kidney epithelial cells and muscles, so this interaction between isoform α1 and Src may be a novel molecular target for pharmacological approaches in treatment of disorders associated with metabolism (Kutz et al., 2021). The enhanced metabolic capacity due to Na^+/K^+-ATPase isoform α1/Src interaction could support a signaling pathway in sperm metabolism in addition to, or as a part of, capacitation. Na^+/K^+-ATPase, Src and caveolin-1 regulate cholesterol in cell membranes, and reduction of cholesterol decreased the expression of α1 and α3 isoforms but not α2 isoform of Na^+/K^+-ATPase in pig kidney epithelial cell line (Zhang

et al., 2020). Previously, it was hypothesized that isoform α1 interacts with Caveolin 1 and induces downstream signals for bovine sperm capacitation (Rajamanickam et al., 2017). Therefore the interplay of Na^+/K^+-ATPase α with β isoforms with other membrane signaling proteins preferentially stimulate the signaling pathways and appear critically important for good fertility. This corresponds with the correlations found here of isoform α1 to fertility measures in sires of boar and bull species.

In porcine renal proximal tubule LLC-PK1 cultured cells, Na^+/K^+-ATPase isoform α1 interacts with Src to form a receptor complex inducing important signaling pathways (Nie et al., 2020; Kutz et al., 2021), including capacitation-related downstream signaling (Rajimanickam et al., 2017). This same complex regulates cell membrane cholesterol, with reduction of cholesterol decreasing the expression of α1 and α3 but not α2 isoforms in in pig kidney epithelial cell line (Zhang et al., 2020), and we have found that sperm HPM lipids influence the transmembrane orientation of Na^+/K^+-ATPase in artificial liposomes (Hickey & Buhr, 2011). Therefore, the interplay of Na^+/K^+-ATPase α with other membrane proteins and lipids appear critically important for good fertility, and current findings importantly extend the fertility relationship to more than one species.

6.6 Challenges, Limitations, and Future Prospects

The research in chapters 3 and 5 studied males in two farm species, swine and cattle, whose field fertility, determined by two rigorous and species-specific methods, differed significantly despite having acceptable, statistically-similar results for the common laboratory-based whole sperm and ejaculate characteristics. This confirmed that traditional methods of computer-assisted sperm analyses of sperm kinetics and motility parameters cannot accurately predict *in vivo* male fertility once extremes in the fertility levels among sires are removed. This persistent failure causes

inefficiencies at farm and commercial enterprises and emphasizes the need for other methods that may easily identify sperm traits linked to fertility, such as sperm proteomics in HPM. Since sperm proteins in HPM play key roles in sperm motility, sperm-egg binding, capacitation, ion transport, and other processes occurring in sperm, identifying the HPM proteins as done in Chapter 4, has the additional potential to tease out the mechanism of action for and metabolic pathways associated with fertility.

Chapters 3 and 5 focused on Na^+/K^+-ATPase, a novel sperm signaling protein. Two different proteomic methodologies evaluated and characterized the α and β isoforms of Na^+/K^+-ATPase in sperm HPM from two different species, boar, and bull. Western immunoblotting provided semi-quantitative assessment of the amount of six Na^+/K^+-ATPase isoforms from high and low fertility boars. Both α1 and α3 isoforms were present in significantly greater amounts in high fertility than low fertility boars. Comparison of amounts of the isoforms by immunoblotting is challenged by the potential difference in the affinity and specificity of the antibodies to any of the six isoforms of Na^+/K^+-ATPase. Non-specific binding of the antibodies to any other non-ATPase proteins should be minimal or nil, as the antibodies were all monoclonal. Another limitation with western blot studies is its inability to determine any PTMs like as phosphorylation of any of the six isoforms of Na^+/K^+-ATPase because of the need to use specific antibodies against the phosphorylated residues of isoforms. As our group had previously characterized bull sperm HPM by Western blotting, and to overcome these issues in the western blotting, the more sensitive and rigorous technique of MS was used to analyze bull HPM Na^+/K^+-ATPase. LC-MS/MS and bottom-up proteomics characterized the seven isoforms of Na^+/K^+-ATPase and other non-ATPase proteins existed in HPM of bull sperm. Using rigorous analytical techniques for protein extraction, stepwise sample preparation and mapping fingerprints of each isoform's peptide/protein residues,

done via Q-TOF, found that the amounts of α1 and β1 were positively correlated to bull fertility, and α4 was negatively correlated. However, MS techniques also have limitations, the most important perhaps being the algorithm of the MS database search engine that aligned spectra with the NCBI database of Na^+/K^+-ATPase isoforms (a small database and specific to *Bos taurus*). The great similarity of peptide sequences among the α isoforms, and the β isoforms, means that the algorithm possibly randomly assigned the homologous peptides to one isoform or another, which could lead to errors in estimating amounts of each isoform. In addition, the NCBI reference sequence originated from cells of various body tissues, so any sperm-specific sequences would be missed; however, Na^+/K^+-ATPase is highly conserved, so this is a more minor concern. It is important to note that bottom-up proteomics cannot completely characterize Na^+/K^+-ATPase's long polypeptide chains, especially in α isoforms.

Regardless of the limitations of immunoblotting and MS, these two studies with different methodologies in different species both concluded that Na^+/K^+-ATPase in sperm HPM is involved in *in vivo* male fertility, and both found a significant relationship of one isoform, α1, to fertility. This is highly supportive of the hypothesis that specific isoforms of Na^+/K^+-ATPase are involved in fertilization.

The mechanism by which Na^+/K^+-ATPase works could potentially be implied by the results from Chapter 4, which looked at the other HPM proteins related to bull fertility and might identify other sperm membrane proteins with which Na^+/K^+-ATPase collaborates. The PPI analysis in chapter 4 established that some signaling proteins which play a central role in sperm motility, cytoskeletal structure, capacitation, oocyte recognition, metabolism, and signaling pathways strongly interact with the various isoforms of Na^+/K^+-ATPase, creating larger clusters with hub protein of Na^+/K^+-ATPase in HPM of bulls with high than low fertility. There were 67 DAPs in

HPM that were significantly aligned to fertility differences. In sperm from highly fertile bulls, 48 DAPs were present in 2-fold greater quantity, indicating that they might be actively involved in cellular machinery contributing to fertilization, including perhaps conducting signals from Na^+/K^+-ATPase receptor complex (Nie et al., 2020), since it is logical that a greater amount of Na^+/K^+-ATPase would require more cellular machinery to achieve improved sperm capacitation. The existence of 19 DAPs found in 2-fold lower quantity in highly-fertile sperm HPM suggests there is an orchestra of proteins, at least some of which may interact with Na^+/K^+-ATPase, and ultimately either stimulate or debilitate the fertility in animals.

Future research should more fully characterize the full polypeptide chains of HPM Na^+/K^+-ATPase isoforms by top-down proteomics, mapping complete amino acid composition and determining 3D structure for each isoform. The fully-elucidated structures would enable *in vitro* studies of the Na^+/K^+-ATPase signaling pathway. In addition, assessing the structural differences related to fertility could then lead to mapping of potential antigenic epitopes and development of antibodies for fertility diagnosis kits to assess sires in the AI industry and by producers.

6.7 General Conclusions

This research has clearly identified some important fertility biomarkers in the HPM of sperm from two mammalian species, providing novel insights into capacitation signaling and possible applications for improving sire fertility and the efficiency of high-quality animal protein. The salient findings from these studies are;

1. When extremes are removed, the traditional method of CASA cannot completely predict fertility of boar or bull sires.

2. There exists a positive correlation with two of the α isoforms (in boar) and one α and one of the β isoform (in bull) to field fertility measures, with some species-specific similarities and differences among the identified isoforms.

3. From 67 non-ATPase DAPs identified in sperm HPM, 48 DAPs were two-fold high in highly fertile bulls and significantly correlated to the wide range of *in vivo* fertility of 16 bulls. Non-ATPase proteins interact with Na^+/K^+-ATPase isoforms and/or are predicted to be involved in sperm motility, capacitation, oocyte recognition, metabolism, signaling pathways, and cytoskeletal structure, casting light on the membrane proteins that regulate bovine sperm fertility.

REFERENCES

Abbasi, F., Miyata, H., Shimada, K., Morohoshi, A., Nozawa, K., Matsumura, T., Xu, Z., Pratiwi, P., & Ikawa, M. (2018). RSPH6A is required for sperm flagellum formation and male fertility in mice. *Journal of Cell Science*, *131*(19). https://doi.org/10.1242/jcs.221648

Aebersold, R., & Mann, M. (2003). Mass spectrometry-based proteomics. *Nature*, *422*(6928), 198–207. https://doi.org/10.1038/nature01511

Aguas, A. P., & Pinto da Silva, P. (1983). Regionalization of transmembrane glycoproteins in the plasma membrane of boar sperm head is revealed by fracture-label. *Journal of Cell Biology*, *97*(5), 1356–1364. https://doi.org/10.1083/jcb.97.5.1356

Abbasi, F., Miyata, H., Shimada, K., Morohoshi, A., Nozawa, K., Matsumura, T., Xu, Z., Pratiwi, P., & Ikawa, M. (2018). RSPH6A is needed for sperm flagellum formation and male fertility in mice. *Journal of Cell Science*, *131*(19). https://doi.org/10.1242/jcs.221648

Aebersold, R., & Mann, M. (2003). Mass spectrometry-based proteomics. *Nature*, *422*(6928), 198–207. https://doi.org/10.1038/nature01511

Aguas, A. P., & Pinto da Silva, P. (1983). Regionalization of transmembrane glycoproteins in the plasma membrane of boar sperm head is revealed by fracture-label. *Journal of Cell Biology*, *97*(5), 1356–1364. https://doi.org/10.1083/jcb.97.5.1356

Aicher, L., Wahl, D., Arce, A., Grenet, O., & Steiner, S. (1998). New insights into cyclosporine A nephrotoxicity by proteome analysis. *Electrophoresis*, *19*(11), 1998–2003. https://doi.org/10.1002/elps.1150191118

Al-Amrani, S., Al-Jabri, Z., Al-Zaabi, A., Alshekaili, J., Al-Khabori, M. (2021). Proteomics: Concepts and applications in human medicine. *World Journal of Biological Chemistry*. 12(5):57-69. doi: 10.4331/wjbc.v12.i5.57.

Alomair, L., Almsned, F., Ullah, A., & Jafri, M. S. (2021). In Silico Prediction of the Phosphorylation of NS3 as an Essential Mechanism for Dengue Virus Replication and the Antiviral Activity of Quercetin. *Biology*, *10*(10), 1067. https://doi.org/10.3390/biology10101067

Alsaadi, M. M., Erzurumluoglu, A. M., Rodriguez, S., Guthrie, P. A. I., Gaunt, T. R., Omar, H. Z., Mubarak, M., Alharbi, K. K., Al-Rikabi, A. C., & Day, I. N. M. (2014). Nonsense mutation in coiled-coil domain containing 151 gene (CCDC151) causes primary ciliary dyskinesia. *Human Mutation*, *35*(12), 1446–1448. https://doi.org/10.1002/humu.22698

Amann, R. P., Saacke, R. G., Barbato, G. F., & Waberski, D. (2018). Measuring Male-to-Male Differences in Fertility or Effects of Semen Treatments. *Annual Review of Animal Biosciences*, *6*(1), 255–286. https://doi.org/10.1146/annurev-animal-030117-014829

Amaral, A., Castillo, J., Estanyol, J. M., Ballescà, J. L., Ramalho-Santos, J., & Oliva, R. (2013). Human Sperm Tail Proteome Suggests New Endogenous Metabolic Pathways. *Molecular & Cellular Proteomics*, *12*(2), 330–342. https://doi.org/10.1074/mcp.M112.020552

Andersson, E., Frössling, J., Engblom, L., Algers, B., & Gunnarsson, S. (2015). Impact of litter size on sow stayability in Swedish commercial piglet producing herds. *Acta Veterinaria Scandinavica*, *58*(1), 31. https://doi.org/10.1186/s13028-016-0213-8

Anzar M, Kroetsch T, Buhr M.M. (2009). Comparison of different methods for assessment of sperm concentration and membrane integrity with bull semen. *Journal of Andrology* ,30(6):661-8. doi: 10.2164/jandrol.108.007500. Epub 2009 May 28. PMID: 19478330.

Anzar M, Kroetsch T, Boswall L. (2011). Cryopreservation of bull semen shipped overnight and its effect on post-thaw sperm motility, plasma membrane integrity, mitochondrial membrane

potential and normal acrosomes. *Animal Reproduction Science*, 126(1-2):23-31. doi: 10.1016/j.anireprosci.2011.04.018. Epub 2011 May 4. PMID: 21621352.

Aperia, A., Akkuratov, E. E., Fontana, J. M., & Brismar, H. (2016). Na + -K + -ATPase, a new class of plasma membrane receptors. *American Journal of Physiology-Cell Physiology*, *310*(7), C491–C495. https://doi.org/10.1152/ajpcell.00359.2015

Ashrafzadeh, A., Karsani, S. A., & Nathan, S. (2013). Mammalian Sperm Fertility Related Proteins. *International Journal of Medical Sciences*, *10*(12), 1649–1657. https://doi.org/10.7150/ijms.6395

Aslam, B., Basit, M., Nisar, M. A., Khurshid, M., & Rasool, M. H. (2017). Proteomics: Technologies and Their Applications. *Journal of Chromatographic Science*, *55*(2), 182–196. https://doi.org/10.1093/chromsci/bmw167

Auer, J., Camoin, L., Courtot, A.-M., Hotellier, F., & de Almeida, M. (2004). Evidence that P36, a human sperm acrosomal antigen involved in the fertilization process is triosephosphate isomerase. *Molecular Reproduction and Development*, *68*(4), 515–523. https://doi.org/10.1002/mrd.20107

Austin, C. R. (1952). The 'Capacitation' of the Mammalian Sperm. *Nature*, *170*(4321), 326–326. https://doi.org/10.1038/170326a0

Awda, B. J., & Buhr, M. M. (2010). Extracellular Signal-Regulated Kinases (ERKs) Pathway and Reactive Oxygen Species Regulate Tyrosine Phosphorylation in Capacitating Boar Spermatozoa1. *Biology of Reproduction*, *83*(5), 750–758. https://doi.org/10.1095/biolreprod.109.082008

Awda, B. J., Mackenzie-Bell, M., & Buhr, M. M. (2009). Reactive Oxygen Species and Boar Sperm Function1. *Biology of Reproduction*, *81*(3), 553–561. https://doi.org/10.1095/biolreprod.109.076471

Baccetti, B., Burrini, A. G., Capitani, S., Collodel, G., Moretti, E., Piomboni, P., & Renieri, T. (1993). Notulae seminologicae. 2. The 'short tail' and 'stump' defect in human spermatozoa. *Andrologia*, 25(6), 331-335. https://doi.org/10.1111/j.1439-0272.1993.tb02736.x

Backert, L., & Kohlbacher, O. (2015). Immunoinformatics and epitope prediction in the age of genomic medicine. *Genome Medicine*, *7*(1), 119. https://doi.org/10.1186/s13073-015-0245-0

Bagrov, A. Y., Shapiro, J. I., & Fedorova, O. v. (2009). Endogenous cardiotonic steroids: Physiology, pharmacology, and novel therapeutic targets. *Pharmacological Reviews*. 61(1), 9-38. https://doi.org/10.1124/pr.108.000711

Bailey, J.L. (2010). Factors regulating sperm capacitation. *System Biology Reproduction Med* ,56(5):334-348. doi: 10.3109/19396368.2010.512377.

Baker, M. A., Hetherington, L., Reeves, G., Müller, J., & Aitken, R. J. (2008). The rat sperm proteome characterized via IPG strip prefractionation and LC-MS/MS identification. *Proteomics*, *8*(11), 2312–2321. https://doi.org/10.1002/pmic.200700876

Baker, M. A., Naumovski, N., Hetherington, L., Weinberg, A., Velkov, T., & Aitken, R. J. (2013). Head and flagella subcompartmental proteomic analysis of human spermatozoa. *Proteomics*, *13*(1), 61–74. https://doi.org/10.1002/pmic.201200350

Banerjee, S., & Mazumdar, S. (2012). Electrospray Ionization Mass Spectrometry: A Technique to Access the Information beyond the Molecular Weight of the Analyte. *International Journal of Analytical Chemistry*, *2012*, 1–40. https://doi.org/10.1155/2012/282574

Bantscheff, M., Schirle, M., Sweetman, G., Rick, J., & Kuster, B. (2007). Quantitative mass spectrometry in proteomics: a critical review. *Analytical and Bioanalytical Chemistry*, *389*(4), 1017–1031. https://doi.org/10.1007/s00216-007-1486-6

Barquero, V., Roldan, E. R. S., Soler, C., Vargas-Leitón, B., Sevilla, F., Camacho, M., & Valverde, A. (2021). Relationship between Fertility Traits and Kinematics in Clusters of Boar Ejaculates. *Biology*, *10*(7), 595. https://doi.org/10.3390/biology10070595

Battistone, M. A., da Ros, V. G., Salicioni, A. M., Navarrete, F. A., Krapf, D., Visconti, P. E., & Cuasnicu, P. S. (2013). Functional human sperm capacitation requires both bicarbonate-dependent PKA activation and down-regulation of Ser/Thr phosphatases by Src family kinases. *Molecular Human Reproduction*, *19*(9), 570–580. https://doi.org/10.1093/molehr/gat033

Beck, M., Schmidt, A., Malmstroem, J., Claassen, M., Ori, A., Szymborska, A., Herzog, F., Rinner, O., Ellenberg, J., & Aebersold, R. (2011). The quantitative proteome of a human cell line. *Molecular Systems Biology*, *7*(1), 549. https://doi.org/10.1038/msb.2011.82

Belleannee, C., Belghazi, M., Labas, V., Teixeira-Gomes, A.-P., Gatti, J. L., Dacheux, J.-L., & Dacheux, F. (2011). Purification and identification of sperm surface proteins and changes during epididymal maturation. *Proteomics*, *11*(10), 1952–1964. https://doi.org/10.1002/pmic.201000662

Bertaccini, E., & Trudell, J. R. (2002). Predicting the transmembrane secondary structure of ligand-gated ion channels. *Protein Engineering, Design and Selection*, *15*(6), 443–453. https://doi.org/10.1093/protein/15.6.443

Bjorndahl, L., & Kvist, U. (2010). Human sperm chromatin stabilization: a proposed model including zinc bridges. *Molecular Human Reproduction*, *16*(1), 23–29. https://doi.org/10.1093/molehr/gap099

Blanco, G., & Mercer, R. W. (1998). Isozymes of the Na-K-ATPase: heterogeneity in structure, diversity in function. *American Journal of Physiology-Renal Physiology*, *275*(5), F633–F650. https://doi.org/10.1152/ajprenal.1998.275.5.F633

Blom, N., Sicheritz-Pontén, T., Gupta, R., Gammeltoft, S., & Brunak, S. (2004). Prediction of post-translational glycosylation and phosphorylation of proteins from the amino acid sequence. *Proteomics*, *4*(6), 1633–1649. https://doi.org/10.1002/pmic.200300771

Boerke, A., van der Lit, J., Lolicato, F., Stout, T. A. E., Helms, J. B., & Gadella, B. M. (2014). Removal of GPI-anchored membrane proteins causes clustering of lipid microdomains in the apical head area of porcine sperm. *Theriogenology*, *81*(4), 613–624. https://doi.org/10.1016/j.theriogenology.2013.11.014

Boerke A, Tsai P.S, Garcia-Gil N, Brewis I.A, Gadella B.M. (2008). Capacitation-dependent reorganization of microdomains in the apical sperm head plasma membrane: functional relationship with zona binding and the zona-induced acrosome reaction. Theriogenology;70(8):1188-96. doi: 10.1016/j.theriogenology.2008.06.021.

Bondarenko, P. v., Chelius, D., & Shaler, T. A. (2002). Identification and Relative Quantitation of Protein Mixtures by Enzymatic Digestion Followed by Capillary Reversed-Phase Liquid Chromatography−Tandem Mass Spectrometry. *Analytical Chemistry*, *74*(18), 4741–4749. https://doi.org/10.1021/ac0256991

Brandt, C., McFie, P. J., Vu, H., Chumala, P., Katselis, G. S., & Stone, S. J. (2019). Identification of calnexin as a diacylglycerol acyltransferase-2 interacting protein. *PLoS ONE,* 14(1) https://doi.org/10.1371/journal.pone.0210396

Breitbart, H. (1997). The biochemistry of the acrosome reaction. *Molecular Human Reproduction*, *3*(3), 195–202. https://doi.org/10.1093/molehr/3.3.195

Breitbart, H., Cohen, G., & Rubinstein, S. (2005). Role of actin cytoskeleton in mammalian sperm capacitation and the acrosome reaction. *Reproduction*, *129*(3), 263–268. https://doi.org/10.1530/rep.1.00269

Broekhuijse, M. L. W. J., Šoštarić, E., Feitsma, H., & Gadella, B. M. (2012). Application of computer-assisted semen analysis to explain variations in pig fertility1. *Journal of Animal Science*, *90*(3), 779–789. https://doi.org/10.2527/jas.2011-4311

Browne, T., Concheiro-Guisan, M., & Prinz, M. (2019). Semi quantitative detection of signature peptides in body fluids by liquid chromatography tandem mass spectrometry (LC–MS/MS). *Forensic Science International: Genetics Supplement Series*, *7*(1), 208–210. https://doi.org/10.1016/j.fsigss.2019.09.080

Buhr, M. M., Curtis, E. F., Thompson, J. A., Wilton, J. W., & Johnson, W. H. (1993). Diet and breed influence the sperm membranes of beef bulls. *Theriogenology*, *39*(3), 581–592. https://doi.org/10.1016/0093-691X(93)90245-Z

Butler, M. L., Bormann, J. M., Weaber, R. L., Grieger, D. M., & Rolf, M. M. (2020). Selection for bull fertility: a review. *Translational Animal Science*, *4*(1), 423–441. https://doi.org/10.1093/tas/txz174

Byrne, K., Leahy, T., McCulloch, R., Colgrave, M. L., & Holland, M. K. (2012). Comprehensive mapping of the bull sperm surface proteome. *Proteomics*, *12*(23–24), 3559–3579. https://doi.org/10.1002/pmic.201200133

Caballero, J., Frenette, G., D'Amours, O., Belleannée, C., Lacroix-Pepin, N., Robert, C., & Sullivan, R. (2012). Bovine sperm raft membrane associated Glioma Pathogenesis-Related 1-like protein 1 (GliPr1L1) is modified during the epididymal transit and is potentially involved in sperm binding to the zona pellucida. *Journal of Cellular Physiology*, *227*(12), 3876–3886. https://doi.org/10.1002/jcp.24099

Cabelli, R. J., Dolan, K. M., Qian, L. P., & Oliver, D. B. (1991). Characterization of membrane-associated and soluble states of SecA protein from wild-type and SecA51(TS) mutant strains of Escherichia coli. *Journal of Biological Chemistry*, *266*(36), 24420–24427. https://doi.org/10.1016/S0021-9258(18)54245-9

Callaway, E. (2021). The mutation that helps Delta spread like wildfire. *Nature*, *596*(7873), 472–473. https://doi.org/10.1038/d41586-021-02275-2

Campbell, J. (2013). Progesterone significantly enhances the mobility of boar spermatozoa. *BioDiscovery*. 2013 (9), e8955. https://doi.org/10.7750/BioDiscovery.2013.9.5

Canfield, V. A., Loppin, B., Thisse, B., Thisse, C., Postlethwait, J. H., Mohideen, M. A. P. K., Rajarao, S. J. R., & Levenson, R. (2002). Na,K-ATPase alpha, and beta subunit genes exhibit unique expression patterns during zebrafish embryogenesis. *Mechanisms of Development*, *116*(1–2), 51–59. https://doi.org/10.1016/s0925-4773(02)00135-1

Canvin, A. T., & Buhr, M. M. (1989). Effect of temperature on the fluidity of boar sperm membranes. *Reproduction*, *85*(2), 533–540. https://doi.org/10.1530/jrf.0.0850533

Carlier, M. F., and Pantaloni, D. (1997). Control of actin dynamics in cell motility. *Journal of Molecular Biology*, 269, 459–467

Castillo, J., Amaral, A., Azpiazu, R., Vavouri, T., Estanyol, J. M., Ballesca, J. L., & Oliva, R. (2014). Genomic and proteomic dissection and characterization of the human sperm chromatin. *Molecular Human Reproduction*, *20*(11), 1041–1053. https://doi.org/10.1093/molehr/gau079

Cereijido, M., Contreras, R. G., & Shoshani, L. (2004). Cell Adhesion, Polarity, and Epithelia in the Dawn of Metazoans. *Physiological Reviews*, *84*(4), 1229–1262. https://doi.org/10.1152/physrev.00001.2004

Chang, M. C. (1951). Fertilizing Capacity of Spermatozoa deposited into the Fallopian Tubes. *Nature*, *168*(4277), 697–698. https://doi.org/10.1038/168697b0

Chelius, D., & Bondarenko, P. v. (2002). Quantitative Profiling of Proteins in Complex Mixtures Using Liquid Chromatography and Mass Spectrometry. *Journal of Proteome Research*, *1*(4), 317–323. https://doi.org/10.1021/pr025517j

Chemes, H. E. (2017). Sperm Ultrastructure in Fertile Men and Male Sterility. In *The Sperm Cell* (pp. 36–58). Cambridge University Press. https://doi.org/10.1017/9781316411124.005

Chen, D., Li, X. Y., Zhao, X., Qin, Y. S., Zhang, X. X., Li, J., Wang, J. M., & Wang, C. F. (2019). Proteomics and microstructure profiling of goat milk protein after homogenization. *Journal of Dairy Science*, *102*(5), 3839–3850. https://doi.org/10.3168/jds.2018-15363

Chen, H., Rossier, C., Morris, M. A., Scott, H. S., Gos, A., Bairoch, A., & Antonarakis, S. E. (1999). A testis-specific gene, TPTE, encodes a putative transmembrane tyrosine phosphatase and maps to the pericentromeric region of human chromosomes 21 and 13, and to

chromosomes 15, 22, and Y. *Human Genetics*, *105*(5). https://doi.org/10.1007/s004399900144

Chen, J., Wang, Y., Wei, B., Lai, Y., Yan, Q., Gui, Y., & Cai, Z. (2011). Functional Expression of Ropporin in Human Testis and Ejaculated Spermatozoa. *Journal of Andrology*, *32*(1), 26–32. https://doi.org/10.2164/jandrol.109.009662

Chen, X., Brown, T., & Tai, P. C. (1998). Identification and Characterization of Protease-Resistant SecA Fragments: SecA Has Two Membrane-Integral Forms. *Journal of Bacteriology*, *180*(3), 527–537. https://doi.org/10.1128/JB.180.3.527-537.1998

Chen, X., Wang, Y., Zhu, H., Hao, H., Zhao, X., Qin, T., & Wang, D. (2015). Comparative transcript profiling of gene expression of fresh and frozen-thawed bull sperm. *Theriogenology*, *83*(4), 504-511. https://doi.org/10.1016/j.theriogenology.2014.10.015

Chen, X., Xu, H., & Tai, P. C. (1996). A Significant Fraction of Functional SecA Is Permanently Embedded in the Membrane. *Journal of Biological Chemistry*, *271*(47), 29698–29706. https://doi.org/10.1074/jbc.271.47.29698

Chen, X., Zhu, H., Hu, C., Hao, H., Zhang, J., Li, K., Zhao, X., Qin, T., Zhao, K., Zhu, H., & Wang, D. (2014). Identification of differentially expressed proteins in fresh and frozen-thawed boar spermatozoa by iTRAQ-coupled 2D LC-MS/MS. *Reproduction*, *147*(3), 321-330. https://doi.org/10.1530/REP-13-0313

Cho, E. H., Huh, H. J., Jeong, I., Lee, N. Y., Koh, W., Park, H., & Ki, C. (2020). A nonsense variant in NME5 causes human primary ciliary dyskinesia with radial spoke defects. *Clinical Genetics*, *98*(1), 64–68. https://doi.org/10.1111/cge.13742

Choudhary, S., Singh, R., Meena, R. S., & Jethra, G. (2016). Secondary and tertiary structure prediction of fenugreek (Trigonella foenum-graecum) protein. *Legume Research - An International Journal*, *39*(1), 48-51. https://doi.org/10.18805/lr.v39i1.8863

Codina, M., Estanyol, J. M., Fidalgo, M. J., Ballescà, J. L., & Oliva, R. (2015). Advances in sperm proteomics: best-practise methodology and clinical potential. *Expert Review of Proteomics*, *12*(3), 255–277. https://doi.org/10.1586/14789450.2015.1040769

Coetzee, K. (1998). Predictive value of normal sperm morphology: a structured literature review. *Human Reproduction Update*, *4*(1), 73–82. https://doi.org/10.1093/humupd/4.1.73

Contreras, F.-X., Sánchez-Magraner, L., Alonso, A., & Goñi, F. M. (2010). Transbilayer (flip-flop) lipid motion and lipid scrambling in membranes. *FEBS Letters*, *584*(9), 1779–1786. https://doi.org/10.1016/j.febslet.2009.12.049

Cornwall, G. A. (2008). New insights into epididymal biology and function. *Human Reproduction Update*, *15*(2), 213–227. https://doi.org/10.1093/humupd/dmn055

Crambert, G., Hasler, U., Beggah, A. T., Yu, C., Modyanov, N. N., Horisberger, J.-D., Lelièvre, L., & Geering, K. (2000). Transport and Pharmacological Properties of Nine Different Human Na,K-ATPase Isozymes. *Journal of Biological Chemistry*, *275*(3), 1976–1986. https://doi.org/10.1074/jbc.275.3.1976

Creese, A. J., Shimwell, N. J., Larkins, K. P. B., Heath, J. K., & Cooper, H. J. (2013). Probing the complementarity of FAIMS and strong cation exchange chromatography in shotgun proteomics. *Journal of the American Society for Mass Spectrometry*, *24*(3), 431-443. https://doi.org/10.1007/s13361-012-0544-2

Cristea, I. M., Gaskell, S. J., & Whetton, A. D. (2004). Proteomics techniques and their application to hematology. *Blood*, *103*(10), 3624–3634. https://doi.org/10.1182/blood-2003-09-3295

Cristobal, A., Marino, F., Post, H., van den Toorn, H. W. P., Mohammed, S., & Heck, A. J. R. (2017). Toward an Optimized Workflow for Middle-Down Proteomics. *Analytical Chemistry*, *89*(6), 3318–3325. https://doi.org/10.1021/acs.analchem.6b03756

Cross, N. L. (2004). Reorganization of Lipid Rafts During Capacitation of Human Sperm1. *Biology of Reproduction*, *71*(4), 1367–1373. https://doi.org/10.1095/biolreprod.104.030502

Cui, X., & Xie, Z. (2017). Protein Interaction and Na/K-ATPase-Mediated Signal Transduction. *Molecules*, *22*(6), 990. https://doi.org/10.3390/molecules22060990

Cui, Z., Sharma, R., & Agarwal, A. (2016). Proteomic analysis of mature and immature ejaculated spermatozoa from fertile men. *Asian Journal of Andrology*, *18*(5), 735-746. https://doi.org/10.4103/1008-682X.164924

Dacheux, J.-L., & Dacheux, F. (2014). New insights into epididymal function in relation to sperm maturation. *Reproduction*, *147*(2), R27–R42. https://doi.org/10.1530/REP-13-0420

D'Amours, O., Calvo, É., Bourassa, S., Vincent, P., Blondin, P., & Sullivan, R. (2019). Proteomic markers of low and high fertility bovine spermatozoa separated by Percoll gradient. *Molecular Reproduction and Development*, *86*(8), 999–1012. https://doi.org/10.1002/mrd.23174

D'Amours, O., Frenette, G., Bourassa, S., Calvo, É., Blondin, P., & Sullivan, R. (2018). Proteomic Markers of Functional Sperm Population in Bovines: Comparison of Low- and High-Density Spermatozoa Following Cryopreservation. *Journal of Proteome Research*, *17*(1), 177–188. https://doi.org/10.1021/acs.jproteome.7b00493

D'Amours, O., Frenette, G., Fortier, M., Leclerc, P., & Sullivan, R. (2010). Proteomic comparison of detergent-extracted sperm proteins from bulls with different fertility indexes. *Reproduction*, *139*(3), 545–556. https://doi.org/10.1530/REP-09-0375

Daniel, L., Etkovitz, N., Weiss, S. R., Rubinstein, S., Ickowicz, D., & Breitbart, H. (2010). Regulation of the sperm EGF receptor by ouabain leads to initiation of the acrosome reaction. *Developmental Biology*, *344*(2), 650–657. https://doi.org/10.1016/j.ydbio.2010.05.490

de Godoy, L. M. F., Olsen, J. v., Cox, J., Nielsen, M. L., Hubner, N. C., Fröhlich, F., Walther, T. C., & Mann, M. (2008). Comprehensive mass-spectrometry-based proteome quantification of haploid versus diploid yeast. *Nature*, *455*(7217), 1251–1254. https://doi.org/10.1038/nature07341

de Juan-Sanz, J., Nunez, E., Villarejo-Lopez, L., Perez-Hernandez, D., Rodriguez-Fraticelli, A. E., Lopez-Corcuera, B., Vazquez, J., & Aragon, C. (2013). Na+/K+-ATPase Is a New Interacting Partner for the Neuronal Glycine Transporter GlyT2 That Downregulates Its Expression In Vitro and In Vivo. *Journal of Neuroscience*, *33*(35), 14269–14281. https://doi.org/10.1523/JNEUROSCI.1532-13.2013

de Lamirande, E. (1997). Capacitation as a regulatory event that primes spermatozoa for the acrosome reaction and fertilization. *Molecular Human Reproduction*, *3*(3), 175–194. https://doi.org/10.1093/molehr/3.3.175

de Lamirande, E., & O'Flaherty, C. (2012). Sperm Capacitation as an Oxidative Event. In *Studies on Men's Health and Fertility* (pp. 57–94). Humana Press. https://doi.org/10.1007/978-1-61779-776-7_4

de Lima Santos, H., & Ciancaglini, P. (2003). Kinetic characterization of Na,K-ATPase from rabbit outer renal medulla: Properties of the (αβ)2 dimer. *Comparative Biochemistry and*

Physiology - B Biochemistry and Molecular Biology, *135*(3), 539-549. https://doi.org/10.1016/S1096-4959(03)00139-8

de Mateo, S., Castillo, J., Estanyol, J. M., Ballescà, J. L., & Oliva, R. (2011). Proteomic characterization of the human sperm nucleus. *PROTEOMICS*, *11*(13), 2714–2726. https://doi.org/10.1002/pmic.201000799

de Oliveira, R. v, Dogan, S., Belser, L. E., Kaya, A., Topper, E., Moura, A., Thibaudeau, G., & Memili, E. (2013). Molecular morphology and function of bull spermatozoa linked to histones and associated with fertility. *Reproduction*, *146*(3), 263–272. https://doi.org/10.1530/REP-12-0399

Demarco, I. A., Espinosa, F., Edwards, J., Sosnik, J., de la Vega-Beltrán, J. L., Hockensmith, J. W., Kopf, G. S., Darszon, A., & Visconti, P. E. (2003). Involvement of a Na+/HCO3- cotransporter in mouse sperm capacitation. *Journal of Biological Chemistry*, *278*(9), 7001–7009. https://doi.org/10.1074/jbc.M206284200

Desfrere, L., Karlsson, M., Hiyoshi, H., Malmersjö, S., Nanou, E., Estrada, M., Miyakawa, A., Lagercrantz, H., el Manira, A., Lal, M., & Uhlén, P. (2009). Na,K-ATPase signal transduction triggers CREB activation and dendritic growth. *Proceedings of the National Academy of Sciences*, *106*(7), 2212–2217. https://doi.org/10.1073/pnas.0809253106

Didion, B. A. (2008). Computer-assisted semen analysis and its utility for profiling boar semen samples. *Theriogenology*, *70*(8), 1374–1376. https://doi.org/10.1016/j.theriogenology.2008.07.014

DiFranco, M., Hakimjavadi, H., Lingrel, J. B., & Heiny, J. A. (2015). Na,K-ATPase α2 activity in mammalian skeletal muscle T-tubules is acutely stimulated by extracellular K+. *Journal of General Physiology*, *146*(4), 281–294. https://doi.org/10.1085/jgp.201511407

Domon, B., & Aebersold, R. (2006). Mass Spectrometry and Protein Analysis. *Science*, *312*(5771), 212–217. https://doi.org/10.1126/science.1124619

Doormaal, B. J. van. (1993). Linear model evaluations of non-return rates for dairy and beef bulls in Canadian AI. *Canadian Journal of Animal Science*, *73*(4), 795–804. https://doi.org/10.4141/cjas93-082

Druart, X., Rickard, J. P., Mactier, S., Kohnke, P. L., Kershaw-Young, C. M., Bathgate, R., Gibb, Z., Crossett, B., Tsikis, G., Labas, V., Harichaux, G., Grupen, C. G., & de Graaf, S. P. (2013). Proteomic characterization and cross species comparison of mammalian seminal plasma. *Journal of Proteomics*, *91*, 13–22. https://doi.org/10.1016/j.jprot.2013.05.029

Dunn, M. J. (1991). New horizons in electrophoresis. Recent developments in gel electrophoresis of proteins. *Analytical Proceedings*, *28*(4), 123-124. https://doi.org/10.1039/ap9912800123

Dupree, E. J., Jayathirtha, M., Yorkey, H., Mihasan, M., Petre, B. A., & Darie, C. C. (2020). A Critical Review of Bottom-Up Proteomics: The Good, the Bad, and the Future of This Field. *Proteomes*, *8*(3), 1-26. https://doi.org/10.3390/proteomes8030014

Emily J.B. (2016). *The application of mass spectrometry-based techniques to full thickness skin tissue: method development and biochemical analysis in health and disease*. University College London Great Ormond Street Institute of Child Health.

Escobar, H., Reyes-Vargas, E., Jensen, P. E., Delgado, J. C., & Crockett, D. K. (2011). Utility of characteristic QTOF MS/MS fragmentation for MHC class I peptides. *Journal of Proteome Research*, *10*(5), 2494–2507. https://doi.org/10.1021/pr101272k

Farrell, P. B., Presicce, G. A., Brockett, C. C., & Foote, R. H. (1998). Quantification of bull sperm characteristics measured by computer-assisted sperm analysis (CASA) and the

relationship to fertility. *Theriogenology*, *49*(4), 871–879. https://doi.org/10.1016/S0093-691X(98)00036-3

Fenn, J. B., Mann, M., Meng, C. K., Wong, S. F., & Whitehouse, C. M. (1989). Electrospray Ionization for Mass Spectrometry of Large Biomolecules. *Science*, *246*(4926), 64–71. https://doi.org/10.1126/science.2675315

Fenyö, D., & Beavis, R. C. (2015). The GPMDB REST interface. *Bioinformatics*, *31*(12), 2056–2058. https://doi.org/10.1093/bioinformatics/btv107

Ferrer, M., Cornwall, G., & Oko, R. (2013). A Population of CRES Resides in the Outer Dense Fibers of Spermatozoa1. *Biology of Reproduction*, *88*(3). https://doi.org/10.1095/biolreprod.112.104745

Feugang, J. M., Rodriguez-Osorio, N., Kaya, A., Wang, H., Page, G., Ostermeier, G. C., Topper, E. K., & Memili, E. (2010). Transcriptome analysis of bull spermatozoa: Implications for male fertility. *Reproductive BioMedicine Online*, *21*(3), 312-324. https://doi.org/10.1016/j.rbmo.2010.06.022

Ficarro, S., Chertihin, O., Westbrook, V. A., White, F., Jayes, F., Kalab, P., Marto, J. A., Shabanowitz, J., Herr, J. C., Hunt, D. F., & Visconti, P. E. (2003). Phosphoproteome Analysis of Capacitated Human Sperm. *Journal of Biological Chemistry*, *278*(13), 11579–11589. https://doi.org/10.1074/jbc.M202325200

Fleri, W., Paul, S., Dhanda, S. K., Mahajan, S., Xu, X., Peters, B., & Sette, A. (2017). The immune epitope database and analysis resource in epitope discovery and synthetic vaccine design. In *Frontiers in Immunology*, 8, 278. https://doi.org/10.3389/fimmu.2017.00278

Flesch, F. M., & Gadella, B. M. (2000). Dynamics of the mammalian sperm plasma membrane in the process of fertilization. *Biochimica et Biophysica Acta (BBA) - Reviews on Biomembranes*, *1469*(3), 197–235. https://doi.org/10.1016/S0304-4157(00)00018-6

Florens, L., Carozza, M. J., Swanson, S. K., Fournier, M., Coleman, M. K., Workman, J. L., & Washburn, M. P. (2006). Analyzing chromatin remodeling complexes using shotgun proteomics and normalized spectral abundance factors. *Methods (San Diego, Calif.)*, *40*(4), 303–311. https://doi.org/10.1016/j.ymeth.2006.07.028

Florman, H. M., Arnoult, C., Kazam, I. G., Li, C., & O'Toole, C. M. B. (1998). A Perspective on the Control of Mammalian Fertilization by Egg-Activated Ion Channels in Sperm: A Tale of Two Channels1. *Biology of Reproduction*, *59*(1), 12–16. https://doi.org/10.1095/biolreprod59.1.12

Foote, R. H. (2003). Fertility estimation: a review of past experience and future prospects. *Animal Reproduction Science*, *75*(1–2), 119–139. https://doi.org/10.1016/S0378-4320(02)00233-6

Fraser, L. R. (1998). Interactions between a decapacitation factor and mouse spermatozoa appear to involve fucose residues and a GPI-anchored receptor. *Molecular Reproduction and Development*, 51(2),193-202. https://doi.org/10.1002/(SICI)1098-2795(199810)51:2<193::AID-MRD9>3.0.CO;2-L

Fraser, L. R., & Ahuja, K. K. (1988). Metabolic and surface events in fertilization. *Gamete Research*, *20*(4), 491–519. https://doi.org/10.1002/mrd.1120200409

Fraser, L. R., & Quinn, P. J. (1981). A glycolytic product is obligatory for initiation of the sperm acrosome reaction and whiplash motility required for fertilization in the mouse. *Reproduction*, *61*(1), 25–35. https://doi.org/10.1530/jrf.0.0610025

Fujita, A., Nakamura, K., Kato, T., Watanabe, N., Ishizaki, T., Kimura, K., Mizoguchi, A., & Narumiya, S. (2000). Ropporin, a sperm-specific binding protein of rhophilin, that is localized in the fibrous sheath of sperm flagella. *Journal of Cell Science*, *113*(1), 103–112. https://doi.org/10.1242/jcs.113.1.103

Gadella, B., & Leahy, T. (2015). New insights into the regulation of cholesterol efflux from the sperm membrane. *Asian Journal of Andrology*, *17*(4), 561-567. https://doi.org/10.4103/1008-682X.153309

Gadella, B. M., & Boerke, A. (2016). An update on post-ejaculatory remodeling of the sperm surface before mammalian fertilization. *Theriogenology*, *85*(1), 113–124. https://doi.org/10.1016/j.theriogenology.2015.07.018

Gadella, B. M., & Evans, J. P. (2011). *Membrane Fusions During Mammalian Fertilization, 711* (pp. 65–80). https://doi.org/10.1007/978-94-007-0763-4_5

Gadella, B. M., & Harrison, R. A. (2000). The capacitating agent bicarbonate induces protein kinase A-dependent changes in phospholipid transbilayer behavior in the sperm plasma membrane. *Development*, *127*(11), 2407–2420. https://doi.org/10.1242/dev.127.11.2407

Gadella, B. M., & Luna, C. (2014). Cell biology and functional dynamics of the mammalian sperm surface. *Theriogenology*, *81*(1), 74–84. https://doi.org/10.1016/j.theriogenology.2013.09.005

Gadella, B. M., Tsai, P., Boerke, A., & Brewis, I. A. (2008). Sperm head membrane reorganization during capacitation. *The International Journal of Developmental Biology*, *52*(5–6), 473–480. https://doi.org/10.1387/ijdb.082583bg

Garcia, A., Fry, N. A. S., Karimi, K., Liu, C., Apell, H.-J., Rasmussen, H. H., & Clarke, R. J. (2013). Extracellular Allosteric Na+ Binding to the Na+,K+-ATPase in Cardiac Myocytes. *Biophysical Journal*, *105*(12), 2695–2705. https://doi.org/10.1016/j.bpj.2013.11.004

García-Herrero, S., Garrido, N., Martínez-Conejero, J. A., Remohí, J., Pellicer, A., & Meseguer, M. (2010). Ontological evaluation of transcriptional differences between sperm of infertile males and fertile donors using microarray analysis. *Journal of Assisted Reproduction and Genetics*, *27*(2–3), 111-120. https://doi.org/10.1007/s10815-010-9388-5

Garg, A., Bhasin, M., & Raghava, G. P. S. (2005). Support Vector Machine-based Method for Subcellular Localization of Human Proteins Using Amino Acid Compositions, Their Order, and Similarity Search. *Journal of Biological Chemistry*, *280*(15), 14427–14432. https://doi.org/10.1074/jbc.M411789200

Garner, D. L., & Hafez, E. S. E. (1993). Spermatozoa and seminal plasma. In E.S.E Hafez (Ed.), *Reproduction in farm animals* (6th ed.). Lea & Febiger.

Garrett, L. J. A., Revell, S. G., & Leese, H. J. (2008). Adenosine Triphosphate Production by Bovine Spermatozoa and Its Relationship to Semen Fertilizing Ability. *Journal of Andrology*, *29*(4), 449–458. https://doi.org/10.2164/jandrol.107.003533

Garrido, N., Martínez-Conejero, J. A., Jauregui, J., Horcajadas, J. A., Simón, C., Remohí, J., & Meseguer, M. (2009). Microarray analysis in sperm from fertile and infertile men without basic sperm analysis abnormalities reveals a significantly different transcriptome. *Fertility and Sterility*, *91*(4), 1307-1310. https://doi.org/10.1016/j.fertnstert.2008.01.078

Gasteiger, E., Hoogland, C., Gattiker, A., Duvaud, S., Wilkins, M. R., Appel, R. D., & Bairoch, A. (2005). Protein Identification and Analysis Tools on the ExPASy Server. *The Proteomics*

Protocols Handbook (pp. 571–607). Humana Press. https://doi.org/10.1385/1-59259-890-0:571

Geering, K. (1991). The functional role of the beta-subunit in the maturation and intracellular transport of Na,K-ATPase. *FEBS Letters*, *285*(2), 189–193. https://doi.org/10.1016/0014-5793(91)80801-9

Geering, K. (2008). Functional roles of Na,K-ATPase subunits. *Current Opinion in Nephrology and Hypertension*, *17*(5), 526–532. https://doi.org/10.1097/MNH.0b013e3283036cbf

Geng, M., Ji, J., & Regnier, F. E. (2000). Signature-peptide approach to detecting proteins in complex mixtures. *Journal of Chromatography. A*, *870*(1–2), 295–313. https://doi.org/10.1016/s0021-9673(99)00951-6

Gilchrist, A., Au, C. E., Hiding, J., Bell, A. W., Fernandez-Rodriguez, J., Lesimple, S., Nagaya, H., Roy, L., Gosline, S. J. C., Hallett, M., Paiement, J., Kearney, R. E., Nilsson, T., & Bergeron, J. J. M. (2006). Quantitative Proteomics Analysis of the Secretory Pathway. *Cell*, *127*(6), 1265–1281. https://doi.org/10.1016/j.cell.2006.10.036

Girouard J, Frenette G, Sullivan R. (2011). Comparative proteome and lipid profiles of bovine epididymosomes collected in the intraluminal compartment of the caput and cauda epididymidis. International Journal of Adrology;34:e475–e486

Gliozzi, T. M., Turri, F., Manes, S., Cassinelli, C., & Pizzi, F. (2017). The combination of kinetic and flow cytometric semen parameters as a tool to predict fertility in cryopreserved bull semen. *Animal*, *11*(11), 1975–1982. https://doi.org/10.1017/S1751731117000684

Gòdia, M., Mayer, F. Q., Nafissi, J., Castelló, A., Rodríguez-Gil, J. E., Sánchez, A., & Clop, A. (2018). A technical assessment of the porcine ejaculated spermatozoa for a sperm-specific

RNA-seq analysis. *Systems Biology in Reproductive Medicine*, 64(4), 291-303. https://doi.org/10.1080/19396368.2018.1464610

Goettig, P. (2016). Effects of Glycosylation on the Enzymatic Activity and Mechanisms of Proteases. *International Journal of Molecular Sciences*, *17*(12), 1969. https://doi.org/10.3390/ijms17121969

Goldberg, E. (2021). The sperm-specific form of lactate dehydrogenase is required for fertility and is an attractive target for male contraception (a review). *Biology of Reproduction*, *104*(3), 521–526. https://doi.org/10.1093/biolre/ioaa217

Gracy, R. W. (1982). Glucosephosphate and triosephosphate isomerases: significance of isozyme structural differences in evolution, physiology, and aging. *Isozymes*, 6, 169-205.

Graham, J. K., & Mocé, E. (2005). Fertility evaluation of frozen/thawed semen. *Theriogenology*, *64*(3), 492–504. https://doi.org/10.1016/j.theriogenology.2005.05.006

Guerrero, C., Lecuona, E., Pesce, L., Ridge, K. M., & Sznajder, J. I. (2001b). Dopamine regulates Na-K-ATPase in alveolar epithelial cells via MAPK-ERK-dependent mechanisms. *American Journal of Physiology-Lung Cellular and Molecular Physiology*, *281*(1), L79–L85. https://doi.org/10.1152/ajplung.2001.281.1.L79

Gur, Y., & Breitbart, H. (2008). Protein synthesis in sperm: Dialog between mitochondria and cytoplasm. *Molecular and Cellular Endocrinology*, *282*(1–2), 45–55. https://doi.org/10.1016/j.mce.2007.11.015

Guzmán-Silva, A., Martínez-Morales, J. C., Medina, L. del C., Romero-Ávila, M. T., Villegas-Comonfort, S., Solís, K. H., & García-Sáinz, J. A. (2022). Mutation of putative phosphorylation sites in the free fatty acid receptor 1: Effects on signaling, receptor

phosphorylation, and internalization. *Molecular and Cellular Endocrinology*, *545*, 111573. https://doi.org/10.1016/j.mce.2022.111573

Hage, D. S., Anguizola, J. A., Bi, C., Li, R., Matsuda, R., Papastavros, E., Pfaunmiller, E., Vargas, J., & Zheng, X. (2012). Pharmaceutical and biomedical applications of affinity chromatography: Recent trends and developments. *Journal of Pharmaceutical and Biomedical Analysis*, *69*, 93–105. https://doi.org/10.1016/j.jpba.2012.01.004

Halquist, M. S., & Thomas Karnes, H. (2011). Quantitative liquid chromatography tandem mass spectrometry analysis of macromolecules using signature peptides in biological fluids. *Biomedical Chromatography*, *25*(1–2), 47–58. https://doi.org/10.1002/bmc.1545

Harper, C. v., Barratt, C. L. R., Publicover, S. J., & Kirkman-Brown, J. C. (2006). Kinetics of the Progesterone-Induced Acrosome Reaction and Its Relation to Intracellular Calcium Responses in Individual Human Spermatozoa1. *Biology of Reproduction*, *75*(6), 933–939. https://doi.org/10.1095/biolreprod.106.054627

Harrison, R. (1996). Capacitation mechanisms, and the role of capacitation as seen in eutherian mammals. *Reproduction, Fertility and Development*, *8*(4), 581-594. https://doi.org/10.1071/RD9960581

Harrison, R., & Gadella, B. M. (2005). Bicarbonate-induced membrane processing in sperm capacitation. Theriogenology, 63(2), 342–351. https://doi.org/10.1016/j.theriogenology.2004.09.016

Henry, M., Coleman, O., Prashant, Clynes, M., & Meleady, P. (2017). Phosphopeptide Enrichment and LC-MS/MS Analysis to Study the Phosphoproteome of Recombinant Chinese Hamster Ovary Cells. *Methods in Molecular Biology, 1603*, 195–208. https://doi.org/10.1007/978-1-4939-6972-2_13

Hickey, K. D., & Buhr, M. M. (2011). Lipid Bilayer Composition Affects Transmembrane Protein Orientation and Function. *Journal of Lipids*, *2011*, 1–9. https://doi.org/10.1155/2011/208457

Hickey, K. D., & Buhr, M. M. (2012). Characterization of Na+K+-ATPase in bovine sperm. *Theriogenology*, *77*(7), 1369–1380. https://doi.org/10.1016/j.theriogenology.2011.10.045

Hirsh, A. (2003). Male subfertility. *BMJ (Clinical Research Ed.)*, *327*(7416), 669–672. https://doi.org/10.1136/bmj.327.7416.669

Hoflack, G., Opsomer, G., Rijsselaere, T., van Soom, A., Maes, D., de Kruif, A., & Duchateau, L. (2007). Comparison of Computer-assisted Sperm Motility Analysis Parameters in Semen from Belgian Blue and Holstein Friesian Bulls. *Reproduction in Domestic Animals*, *42*(2), 153–161. https://doi.org/10.1111/j.1439-0531.2006.00745.x

Holt, W., & Palomo, M. (1996). Optimization of a continuous real-time computerized semen analysis system for ram sperm motility assessment, and evaluation of four methods of semen preparation. *Reproduction, Fertility and Development*, *8*(2), 219-230. https://doi.org/10.1071/RD9960219

Honda, A. (2002). Role of acrosomal matrix proteases in sperm-zona pellucida interactions. *Human Reproduction Update*, *8*(5), 405–412. https://doi.org/10.1093/humupd/8.5.405

Hwang K, Lamb D.J. (2013). The sperm penetration assay for the assessment of fertilization capacity. Methods of Molecular Biology. 927:103-11. doi: 10.1007/978-1-62703-038-0_10.

Ionescu, M. I. (2019). Adenylate Kinase: A Ubiquitous Enzyme Correlated with Medical Conditions. *The Protein Journal*, *38*(2), 120–133. https://doi.org/10.1007/s10930-019-09811-0

Issaq, H. J., & Veenstra, T. D. (2008). Two-dimensional polyacrylamide gel electrophoresis (2D-PAGE): advances and perspectives. *BioTechniques*, *44*(5), 697–700. https://doi.org/10.2144/000112823

Jagan Mohanarao, G., & Atreja, S. K. (2011). Identification of capacitation associated tyrosine phosphoproteins in buffalo (Bubalus bubalis) and cattle spermatozoa. *Animal Reproduction Science*, *123*(1–2), 40–47. https://doi.org/10.1016/j.anireprosci.2010.11.013

Jespersen, M. C., Peters, B., Nielsen, M., & Marcatili, P. (2017). BepiPred-2.0: improving sequence-based B-cell epitope prediction using conformational epitopes. *Nucleic Acids Research*, *45*(W1), W24–W29. https://doi.org/10.1093/nar/gkx346

Jha, K. N., & Shivaji, S. (2002). Identification of the major tyrosine phosphorylated protein of capacitated hamster spermatozoa as a homologue of mammalian sperm a kinase anchoring protein. *Molecular Reproduction and Development*, *61*(2), 258–270. https://doi.org/10.1002/mrd.1155

Ji, Y. (2015). *Mass spectrometry analysis of protein/peptide S-palmitoylation*. Boston University ProQuest Dissertations Publishing.

Jimenez, T., McDermott, J. P., Sanchez, G., & Blanco, G. (2011). Na,K-ATPase 4 isoform is essential for sperm fertility. *Proceedings of the National Academy of Sciences*, *108*(2), 644–649. https://doi.org/10.1073/pnas.1016902108

Jimenez, T., Sanchez, G., & Blanco, G. (2012). Activity of the Na,K-ATPase 4 Isoform Is Regulated During Sperm Capacitation to Support Sperm Motility. *Journal of Andrology*, *33*(5), 1047–1057. https://doi.org/10.2164/jandrol.111.015545

Jin, M., Fujiwara, E., Kakiuchi, Y., Okabe, M., Satouh, Y., Baba, S. A., Chiba, K., & Hirohashi, N. (2011). Most fertilizing mouse spermatozoa begin their acrosome reaction before contact

with the zona pellucida during in vitro fertilization. *Proceedings of the National Academy of Sciences*, *108*(12), 4892–4896. https://doi.org/10.1073/pnas.1018202108

Jivan, A., Earnest, S., Juang, Y.-C., & Cobb, M. H. (2009). Radial Spoke Protein 3 Is a Mammalian Protein Kinase A-anchoring Protein That Binds ERK1/2. *Journal of Biological Chemistry*, *284*(43), 29437–29445. https://doi.org/10.1074/jbc.M109.048181

Jodar, M., Selvaraju, S., Sendler, E., Diamond, M. P., & Krawetz, S. A. (2013). The presence, role, and clinical use of spermatozoal RNAs. *Human Reproduction Update*, *19*(6), 604-624. https://doi.org/10.1093/humupd/dmt031

Johnson, L. R., Foster, J. A., Haig-Ladewig, L., Vanscoy, H., Rubin, C. S., Moss, S. B., & Gerton, G. L. (1997). Assembly of AKAP82, a Protein Kinase A Anchor Protein, into the Fibrous Sheath of Mouse Sperm. *Developmental Biology*, *192*(2), 340–350. https://doi.org/10.1006/dbio.1997.8767

Jones, R., James, P. S., Howes, L., Bruckbauer, A., & Klenerman, D. (2007). Supramolecular organization of the sperm plasma membrane during maturation and capacitation. *Asian Journal of Andrology*, *9*(4), 438–444. https://doi.org/10.1111/j.1745-7262.2007.00282.x

Jorgensen, P. L., Håkansson, K. O., & Karlish, S. J. D. (2003). Structure and Mechanism of Na,K-ATPase: Functional Sites and Their Interactions. *Annual Review of Physiology*, *65*(1), 817–849. https://doi.org/10.1146/annurev.physiol.65.092101.142558

Juhaszova, M., & Blaustein, M. P. (1997). Na+ pump low and high ouabain affinity alpha subunit isoforms are differently distributed in cells. *Proceedings of the National Academy of Sciences*, *94*(5), 1800–1805. https://doi.org/10.1073/pnas.94.5.1800

Jung, M., Rüdiger, K., & Schulze, M. (2015). In Vitro Measures for Assessing Boar Semen Fertility. *Reproduction in Domestic Animals*, *50*, 20–24. https://doi.org/10.1111/rda.12533

Jungbauer, A., & Hahn, R. (2009). Ion-exchange chromatography. *Methods in Enzymology*, *463*, 349–371. https://doi.org/10.1016/S0076-6879(09)63022-6

Kadamur, G., & Ross, E. M. (2013). Mammalian phospholipase C. *Annual Review of Physiology*, 75(1), 127-154 . https://doi.org/10.1146/annurev-physiol-030212-183750

Kadivar, A., Shams Esfandabadi, N., Dehghani Nazhvani, E., Shirazi, A., & Ahmadi, E. (2020). Effects of cryopreservation on stallion sperm protamine messenger RNAs. *Reproduction in Domestic Animals*, *55*(3), 274-282. https://doi.org/10.1111/rda.13615

Kamacioglu, A., Tuncbag, N., & Ozlu, N. (2021). Structural analysis of mammalian protein phosphorylation at a proteome level. *Structure*, *29*(11), 1219-1229. https://doi.org/10.1016/j.str.2021.06.008

Kaplan, J. H. (2002a). Biochemistry of Na,K-ATPase. *Annual Review of Biochemistry*, *71*(1), 511–535. https://doi.org/10.1146/annurev.biochem.71.102201.141218

Kasimanickam, R. K., Kasimanickam, V. R., Arangasamy, A., & Kastelic, J. P. (2019). Sperm and seminal plasma proteomics of high- versus low-fertility Holstein bulls. *Theriogenology*, *126*, 41–48. https://doi.org/10.1016/j.theriogenology.2018.11.032

Kastelic, J. P. (2013). Male involvement in fertility and factors affecting semen quality in bulls. *Animal Frontiers*, *3*(4), 20–25. https://doi.org/10.2527/af.2013-0029

Katselis, G. S., Estrada, A., Gorecki, D. K. J., & Barl, B. (2007). Adjuvant activities of saponins from the root of Polygala senega L.This article is one of a selection of papers published in this special issue (part 2 of 2) on the Safety and Efficacy of Natural Health Products. *Canadian Journal of Physiology and Pharmacology*, *85*(11), 1184–1194. https://doi.org/10.1139/Y07-109

Kawano, N., Yoshida, K., Miyado, K., & Yoshida, M. (2011). Lipid Rafts: Keys to Sperm Maturation, Fertilization, and Early Embryogenesis. *Journal of Lipids*, *2011*, 1–10. https://doi.org/10.1155/2011/264706

Khalid, M., Suliman, R., Ahmed, R., Salim, H., & Clarke, R. J. (2014). The High and Low Affinity Binding Sites of Digitalis Glycosides to Na,K-ATPase. *Arabian Journal for Science and Engineering*. 39, 75–85. https://doi.org/10.1007/s13369-013-0828-2

Khalil, M. B., Chakrabandhu, K., Xu, H., Weerachatyanukul, W., Buhr, M., Berger, T., Carmona, E., Vuong, N., Kumarathasan, P., Wong, P. T. T., Carrier, D., & Tanphaichitr, N. (2006). Sperm capacitation induces an increase in lipid rafts having zona pellucida binding ability and containing sulfogalactosylglycerolipid. *Developmental Biology*, *290*(1), 220–235. https://doi.org/10.1016/j.ydbio.2005.11.030

Khan I.M., Cao Z, Liu H, Khan A, Rahman SU, Khan MZ, Sathanawongs A, Zhang Y. (2021) Impact of Cryopreservation on Spermatozoa Freeze-Thawed Traits and Relevance OMICS to Assess Sperm Cryo-Tolerance in Farm Animals. *Frontiers in Veterinary Science*. 8:609180. doi: 10.3389/fvets.2021.609180.

Kim, Y.-H., Haidl, G., Schaefer, M., Egner, U., Mandal, A., & Herr, J. C. (2007). Compartmentalization of a unique ADP/ATP carrier protein SFEC (Sperm Flagellar Energy Carrier, AAC4) with glycolytic enzymes in the fibrous sheath of the human sperm flagellar principal piece. *Developmental Biology*, *302*(2), 463–476. https://doi.org/10.1016/j.ydbio.2006.10.004

Kim G.Y. (2018). What should be done for men with sperm DNA fragmentation. Clinical and Experimental Reproductive Medicine.45(3):101-109. doi: 10.5653/cerm.2018.45.3.101.

Kinoshita, P. F., Orellana, A. M. M., Nakao, V. W., Souza Port's, N. M., Quintas, L. E. M., Kawamoto, E. M., & Scavone, C. (2022). The Janus face of ouabain in Na+/K+-ATPase and calcium signalling in neurons. *British Journal of Pharmacology*, *179*(8), 1512–1524. https://doi.org/10.1111/bph.15419

Kiser, J. Z., Post, M., Wang, B., & Miyagi, M. (2009). Streptomyces erythraeus trypsin for proteomics applications. *Journal of Proteome Research*, *8*(4), 1810–1817. https://doi.org/10.1021/pr8004919

Kliche, J., & Ivarsson, Y. (2022). Orchestrating serine/threonine phosphorylation and elucidating downstream effects by short linear motifs. *Biochemical Journal*, *479*(1), 1–22. https://doi.org/10.1042/BCJ20200714

Koehler, J. K. (1972). Human sperm head ultrastructure: A freeze-etching study. *Journal of Ultrastructure Research*, *39*(5–6), 520–539. https://doi.org/10.1016/S0022-5320(72)90118-9

Kota, V., Dhople, V. M., & Shivaji, S. (2009). Tyrosine phosphoproteome of hamster spermatozoa: Role of glycerol-3-phosphate dehydrogenase 2 in sperm capacitation. *Proteomics*, *9*(7), 1809–1826. https://doi.org/10.1002/pmic.200800519

Koziy, R. v., Bracamonte, J. L., Yoshimura, S., Chumala, P., Simko, E., & Katselis, G. S. (2022). Discovery proteomics for the detection of putative markers for eradication of infection in an experimental model of equine septic arthritis using LC-MS/MS. *Journal of Proteomics*, *261*, 104571. https://doi.org/10.1016/J.JPROT.2022.104571

Krishna, R. G., & Wold, F. (1993). Post-translational modification of proteins. *Advances in Enzymology and Related Areas of Molecular Biology*, *67*, 265–298. https://doi.org/10.1002/9780470123133.ch3

Kumaresan, A., Johannisson, A., Nordqvist, S., Kårehed, K., Åkerud, H., Lindgren, K. E., & Morrell, J. M. (2017). Relationship of DNA integrity to HRG C633T SNP and ART outcome in infertile couples. *Reproduction*, *153*(6), 865–876. https://doi.org/10.1530/REP-17-0058

Kutz, L. C., Cui, X., Xie, J. X., Mukherji, S. T., Terrell, K. C., Huang, M., Wang, X., Wang, J., Martin, A. J., Pessoa, M. T., Cai, L., Zhu, H., Heiny, J. A., Shapiro, J. I., Blanco, G., Xie, Z., & Pierre, S. v. (2021). The Na/K-ATPase α1/Src interaction regulates metabolic reserve and Western diet intolerance. *Acta Physiologica*, *232*(3). https://doi.org/10.1111/apha.13652

Kwon, W.-S., Rahman, M. S., Lee, J.-S., Kim, J., Yoon, S.-J., Park, Y.-J., You, Y.-A., Hwang, S., & Pang, M.-G. (2014). A comprehensive proteomic approach to identifying capacitation related proteins in boar spermatozoa. *BMC Genomics*, *15*(1), 897. https://doi.org/10.1186/1471-2164-15-897

Kwon, W.-S., Rahman, M. S., Lee, J.-S., You, Y.-A., & Pang, M.-G. (2015). Improving litter size by boar spermatozoa: application of combined H33258/CTC staining in field trial with artificial insemination. *Andrology*, *3*(3), 552–557. https://doi.org/10.1111/andr.12020

Lander, E. S., Linton, L. M., Birren, B., Nusbaum, C., Zody, M. C., Baldwin, J., Devon, K., Dewar, K., Doyle, M., FitzHugh, W., Funke, R., Gage, D., Harris, K., Heaford, A., Howland, J., Kann, L., Lehoczky, J., LeVine, R., McEwan, P., … Morgan, M. J. (2001). Initial sequencing and analysis of the human genome. *Nature*, *409*(6822), 860–921. https://doi.org/10.1038/35057062

Langley, S. R., & Mayr, M. (2015). Comparative analysis of statistical methods used for detecting differential expression in label-free mass spectrometry proteomics. *Journal of Proteomics*, *129*, 83–92. https://doi.org/10.1016/j.jprot.2015.07.012

Larsson, S., Jones, H. A., Göransson, O., Degerman, E., & Holm, C. (2016). Parathyroid hormone induces adipocyte lipolysis via PKA-mediated phosphorylation of hormone-sensitive lipase. *Cellular Signalling*, *28*(3), 204-213. https://doi.org/10.1016/j.cellsig.2015.12.012

Laughery, M., Todd, M., & Kaplan, J. H. (2004). Oligomerization of the Na,K-ATPase in Cell Membranes. *Journal of Biological Chemistry*, *279*(35), 36339–36348. https://doi.org/10.1074/jbc.M402778200

Leahy, T., & Gadella, B. M. (2015). New insights into the regulation of cholesterol efflux from the sperm membrane. *Asian Journal of Andrology*. 17(4), 561-567. https://doi.org/10.4103/1008-682X.153309

Lee, S., Hong, S. H., & Cho, C. (2020). Normal fertility in male mice lacking ADAM32 with testis-specific expression. *Reproductive Biology*, *20*(4), 589-594. https://doi.org/10.1016/j.repbio.2020.09.001

Lewis, S. E. M. (2007). Is sperm evaluation useful in predicting human fertility? *Reproduction*, *134*(1), 31–40. https://doi.org/10.1530/REP-07-0152

Li, Y.-F., He, W., Mandal, A., Kim, Y.-H., Digilio, L., Klotz, K., Flickinger, C. J., Herr, J. C., & Herr, J. C. (2011). CABYR binds to AKAP3 and Ropporin in the human sperm fibrous sheath. *Asian Journal of Andrology*, *13*(2), 266–274. https://doi.org/10.1038/aja.2010.149

Li, Z., Zhang, Z., Xie, J. X., Li, X., Tian, J., Cai, T., Cui, H., Ding, H., Shapiro, J. I., & Xie, Z. (2011). Na/K-ATPase mimetic pNaKtide peptide inhibits the growth of human cancer cells. *Journal of Biological Chemistry*, *286*(37), 32394-32403. https://doi.org/10.1074/jbc.M110.207597

Liang, M., Tian, J., Liu, L., Pierre, S., Liu, J., Shapiro, J., & Xie, Z. J. (2007). Identification of a pool of non-pumping Na/K-ATPase. *Journal of Biological Chemistry*, *282*(14), 10585-10593. https://doi.org/10.1074/jbc.M609181200

Lin, Y.-H., Ke, C.-C., Wang, Y.-Y., Chen, M.-F., Chen, T.-M., Ku, W.-C., Chiang, H.-S., & Yeh, C.-H. (2017). RAB10 Interacts with the Male Germ Cell-Specific GTPase-Activating Protein during Mammalian Spermiogenesis. *International Journal of Molecular Sciences*, *18*(1), 97. https://doi.org/10.3390/ijms18010097

Lin, Y.-N., Roy, A., Yan, W., Burns, K. H., & Matzuk, M. M. (2007). Loss of Zona Pellucida Binding Proteins in the Acrosomal Matrix Disrupts Acrosome Biogenesis and Sperm Morphogenesis. *Molecular and Cellular Biology*, *27*(19), 6794–6805. https://doi.org/10.1128/MCB.01029-07

Linck, R. W., Chemes, H., & Albertini, D. F. (2016). The axoneme: the propulsive engine of spermatozoa and cilia and associated ciliopathies leading to infertility. *Journal of Assisted Reproduction and Genetics*, *33*(2), 141–156. https://doi.org/10.1007/s10815-016-0652-1

Lingdong Quan, M. L. (2013). CID,ETD and HCD Fragmentation to Study Protein Post-Translational Modifications. *Modern Chemistry & Applications*, *01*(01). https://doi.org/10.4172/2329-6798.1000e102

Lingrel, J., Moseley, A., Dostanic, I., Cougnon, M., He, S., James, P., Woo, A., O'Connor, K., & Neumann, J. (2003). Functional Roles of the α Isoforms of the Na,K-ATPase. *Annals of the New York Academy of Sciences*, *986*(1), 354–359. https://doi.org/10.1111/j.1749-6632.2003.tb07214.x

Linnertz, H., Urbanova, P., Obsil, T., Herman, P., Amler, E., & Schoner, W. (1998). Molecular distance measurements reveal an (αβ)2 dimeric structure of Na+/K+-ATPase: High affinity

ATP binding site and K+-activated phosphatase reside on different α-subunits. *Journal of Biological Chemistry*, *273*(44), 28813-28821. https://doi.org/10.1074/jbc.273.44.28813

Listgarten, J., & Emili, A. (2005). Statistical and Computational Methods for Comparative Proteomic Profiling Using Liquid Chromatography-Tandem Mass Spectrometry. *Molecular & Cellular Proteomics*, *4*(4), 419–434. https://doi.org/10.1074/mcp.R500005-MCP200

Liu, H., Sadygov, R. G., & Yates, J. R. (2004). A Model for Random Sampling and Estimation of Relative Protein Abundance in Shotgun Proteomics. *Analytical Chemistry*, *76*(14), 4193–4201. https://doi.org/10.1021/ac0498563

Liu, J., Tian, J., Haas, M., Shapiro, J. I., Askari, A., & Xie, Z. (2000). Ouabain Interaction with Cardiac Na+/K+-ATPase Initiates Signal Cascades Independent of Changes in Intracellular Na+ and Ca2+ Concentrations. *Journal of Biological Chemistry*, *275*(36), 27838–27844. https://doi.org/10.1074/jbc.M002950200

Liu, J., & Xie, Z. (2010). The sodium pump and cardiotonic steroids-induced signal transduction protein kinases and calcium-signaling microdomain in regulation of transporter trafficking. *Biochimica et Biophysica Acta (BBA) - Molecular Basis of Disease*, *1802*(12), 1237–1245. https://doi.org/10.1016/j.bbadis.2010.01.013

Liu, L., & Askari, A. (2006). β-subunit of cardiac Na+-K+-ATPase dictates the concentration of the functional enzyme in caveolae. *American Journal of Physiology-Cell Physiology*, *291*(4), C569–C578. https://doi.org/10.1152/ajpcell.00002.2006

Liu, L., Ivanov, A. v., Gable, M. E., Jolivel, F., Morrill, G. A., & Askari, A. (2011). Comparative properties of caveolar and noncaveolar preparations of kidney Na +/K +-ATpase. *Biochemistry*, *50*(40), 8664–8673. https://doi.org/10.1021/bi2009008

Liu, X. X., Cai, L., & Liu, F. J. (2018). An in silico analysis of human sperm genes associated with asthenozoospermia and its implication in male infertility. *Medicine*, *97*(49), e13338. https://doi.org/10.1097/MD.0000000000013338

Liu, Y., Liu, J., Johnson, B. A., Xia, H., Ku, Z., Schindewolf, C., Widen, S. G., An, Z., Weaver, S. C., Menachery, V. D., Xie, X., & Shi, P.-Y. (2021). Delta spike P681R mutation enhances SARS-CoV-2 fitness over Alpha variant. *BioRxiv : The Preprint Server for Biology*. https://doi.org/10.1101/2021.08.12.456173

Lolkema, J. (1998). Hydropathy profile alignment: a tool to search for structural homologues of membrane proteins. *FEMS Microbiology Reviews*, *22*(4), 305–322. https://doi.org/10.1016/S0168-6445(98)00018-7

Loo, J. A., DeJohn, D. E., Du, P., Stevenson, T. I., & Ogorzalek Loo, R. R. (1999). Application of mass spectrometry for target identification and characterization. *Medicinal Research Reviews*, *19*(4), 307–319. https://doi.org/10.1002/(SICI)1098-1128(199907)19:4<307::AID-MED4>3.0.CO;2-2

Macías-García, B., González-Fernández, L., Loux, S. C., Rocha, A. M., Guimarães, T., Peña, F. J., Varner, D. D., & Hinrichs, K. (2015). Effect of calcium, bicarbonate, and albumin on capacitation-related events in equine sperm. *Reproduction*, *149*(1), 87–99. https://doi.org/10.1530/REP-14-0457

Madan, N., Xu, Y., Duan, Q., Banerjee, M., Larre, I., Pierre, S. v., & Xie, Z. (2017). Src-independent ERK signaling through the rat α3 isoform of Na/K-ATPase. *American Journal of Physiology-Cell Physiology*, *312*(3), C222–C232. https://doi.org/10.1152/ajpcell.00199.2016

Mahmoudi Gomari, M., Saraygord-Afshari, N., Farsimadan, M., Rostami, N., Aghamiri, S., & Farajollahi, M. M. (2020). Opportunities and challenges of the tag-assisted protein purification techniques: Applications in the pharmaceutical industry. *Biotechnology Advances*, *45*, 107653. https://doi.org/10.1016/j.biotechadv.2020.107653

Maiorino, M., Roveri, A., Benazzi, L., Bosello, V., Mauri, P., Toppo, S., Tosatto, S. C. E., & Ursini, F. (2005). Functional Interaction of Phospholipid Hydroperoxide Glutathione Peroxidase with Sperm Mitochondrion-associated Cysteine-rich Protein Discloses the Adjacent Cysteine Motif as a New Substrate of the Selenoperoxidase. *Journal of Biological Chemistry*, *280*(46), 38395–38402. https://doi.org/10.1074/jbc.M505983200

Manea, M., Mező, G., Hudecz, F., & Przybylski, M. (2007). Mass spectrometric identification of the trypsin cleavage pathway in lysyl-proline containing oligotuftsin peptides. *Journal of Peptide Science*, *13*(4), 227–236. https://doi.org/10.1002/psc.836

Maree, L., du Plessis, S. S., Menkveld, R., & van der Horst, G. (2010). Morphometric dimensions of the human sperm head depend on the staining method used. *Human Reproduction*, *25*(6), 1369–1382. https://doi.org/10.1093/humrep/deq075

Marouga, R., David, S., & Hawkins, E. (2005). The development of the DIGE system: 2D fluorescence difference gel analysis technology. *Analytical and Bioanalytical Chemistry*, *382*(3), 669–678. https://doi.org/10.1007/s00216-005-3126-3

Martínez P, & Morros, A. (1996). Membrane lipid dynamics during human sperm capacitation. *Frontiers in Bioscience*, *1*(4), A119. https://doi.org/10.2741/A119

Martínez-Heredia, J., Estanyol, J. M., Ballescà, J. L., & Oliva, R. (2006). Proteomic identification of human sperm proteins. *Proteomics*, *6*(15), 4356–4369. https://doi.org/10.1002/pmic.200600094

Martínez-López, P., Santi, C. M., Treviño, C. L., Ocampo-Gutiérrez, A. Y., Acevedo, J. J., Alisio, A., Salkoff, L. B., & Darszon, A. (2009). Mouse sperm K+ currents stimulated by pH and cAMP possibly coded by Slo3 channels. *Biochemical and Biophysical Research Communications*, *381*(2), 204–209. https://doi.org/10.1016/j.bbrc.2009.02.008

Martin-Hidalgo, D., Macias-Garcia, B., Garcia-Marin, L.J., Bragado, M.J., Gonzalez-Fernandez, L., (2020). Boar spermatozoa proteomic profile varies in sperm collected during the summer and winter. Animal Reproduction Science. 219, 106513.

McDermott J, Sánchez G, Nangia AK, Blanco G. (2015). Role of human Na,K-ATPase alpha 4 in sperm function, derived from studies in transgenic mice. Molecular Reproduction Development, 82(3):167-81. doi: 10.1002/mrd.22454. Epub 2015 Jan 14. PMID: 25640246; PMCID: PMC4376643.

McIlwain, S., Mathews, M., Bereman, M. S., Rubel, E. W., MacCoss, M. J., & Noble, W. S. (2012). Estimating relative abundances of proteins from shotgun proteomics data. *BMC Bioinformatics*, *13*(1), 308. https://doi.org/10.1186/1471-2105-13-308

Mi, Y., Shi, Z., & Li, J. (2015). Spata19 is critical for sperm mitochondrial function and male fertility. *Molecular Reproduction and Development*, *82*(11), 907–913. https://doi.org/10.1002/mrd.22536

Miki, K., & Eddy, E. M. (1999). Single Amino Acids Determine Specificity of Binding of Protein Kinase A Regulatory Subunits by Protein Kinase A Anchoring Proteins. *Journal of Biological Chemistry*, *274*(41), 29057–29062. https://doi.org/10.1074/jbc.274.41.29057

Miki, K., Willis, W. D., Brown, P. R., Goulding, E. H., Fulcher, K. D., & Eddy, E. M. (2002). Targeted Disruption of the Akap4 Gene Causes Defects in Sperm Flagellum and Motility. *Developmental Biology*, *248*(2), 331–342. https://doi.org/10.1006/dbio.2002.0728

Miller, D., & Charles Ostermeier, G. (2006b). Towards a better understanding of RNA carriage by ejaculate spermatozoa. *Human Reproduction Update*, *12*(6), 757–767. https://doi.org/10.1093/humupd/dml037

Miller, D., & Ostermeier, G. C. (2006a). Spermatozoal RNA: why is it there and what does it do? *Gynécologie Obstétrique & Fertilité*, *34*(9), 840–846. https://doi.org/10.1016/J.GYOBFE.2006.07.013

Mirzaei, H., & Regnier, F. (2006). Enrichment of carbonylated peptides using Girard P reagent and strong cation exchange chromatography. *Analytical Chemistry*, *78*(3), 770-778. https://doi.org/10.1021/ac0514220

Mohanta, T. K., Khan, A., Hashem, A., Abd_Allah, E. F., & Al-Harrasi, A. (2019). The molecular mass and isoelectric point of plant proteomes. *BMC Genomics*, *20*(1), 631. https://doi.org/10.1186/s12864-019-5983-8

Morotti, F., Lorenzetti, E., & Seneda, M. M. (2021). *Artificial Insemination Program in Cattle* (pp. 1–53). https://doi.org/10.1007/978-3-030-76529-3_1

Morrill, G. A., Kostellow, A. B., & Askari, A. (2008). Progesterone binding to the α1-subunit of the Na/K-ATPase on the cell surface: Insights from computational modeling. *Steroids*, *73*(1), 27–40. https://doi.org/10.1016/j.steroids.2007.08.012

Morrill, G. A., Kostellow, A. B., Liu, L., Gupta, R. K., & Askari, A. (2016). Evolution of the α-Subunit of Na/K-ATPase from Paramecium to Homo sapiens: Invariance of Transmembrane Helix Topology. *Journal of Molecular Evolution*, *82*(4–5), 183–198. https://doi.org/10.1007/s00239-016-9732-1

Morth, J. P., Pedersen, B. P., Toustrup-Jensen, M. S., Sørensen, T. L. M., Petersen, J., Andersen, J. P., Vilsen, B., & Nissen, P. (2007). Crystal structure of the sodium-potassium pump. *Nature*. 450 (7172), 1043-1049. https://doi.org/10.1038/nature06419

Mortimer D. (1994). *Practical Laboratory Andrology*. Oxford University Press.

Mortimer, D. (2018). The functional anatomy of the human spermatozoon: relating ultrastructure and function. *Molecular Human Reproduction*. 24(12), 567-592. https://doi.org/10.1093/molehr/gay040

Moss, S. B., Turner, R. M. O., Burkert, K. L., VanScoy Butt, H., & Gerton, G. L. (1999). Conservation and Function of a Bovine Sperm A-Kinase Anchor Protein Homologous to Mouse AKAP821. *Biology of Reproduction*, *61*(2), 335–342. https://doi.org/10.1095/biolreprod61.2.335

Mostek, A., Dietrich, M. A., Słowińska, M., & Ciereszko, A. (2017). Cryopreservation of bull semen is associated with carbonylation of sperm proteins. *Theriogenology*, *92*, 95–102. https://doi.org/10.1016/j.theriogenology.2017.01.011

Mostek, A., Janta, A., Majewska, A., & Ciereszko, A. (2021). Bull Sperm Capacitation Is Accompanied by Redox Modifications of Proteins. *International Journal of Molecular Sciences*, *22*(15), 7903. https://doi.org/10.3390/ijms22157903

Mountjoy, J. R., Xu, W., McLeod, D., Hyndman, D., & Oko, R. (2008). RAB2A: A Major Subacrosomal Protein of Bovine Spermatozoa Implicated in Acrosomal Biogenesis1. *Biology of Reproduction*, *79*(2), 223–232. https://doi.org/10.1095/biolreprod.107.065060

Muhammad Aslam, M. K., Kumaresan, A., Sharma, V. K., Tajmul, M., Chhillar, S., Chakravarty, A. K., Manimaran, A., Mohanty, T. K., Srinivasan, A., & Yadav, S. (2014). Identification of putative fertility markers in seminal plasma of crossbred bulls through

differential proteomics. *Theriogenology*, *82*(9), 1254-1262.e1. https://doi.org/10.1016/j.theriogenology.2014.08.007

Muhammad Aslam, M. K., Kumaresan, A., Yadav, S., Mohanty, T. K., & Datta, T. K. (2019). Comparative proteomic analysis of high- and low-fertile buffalo bull spermatozoa for identification of fertility-associated proteins. *Reproduction in Domestic Animals*. 54(5), 786-794. https://doi.org/10.1111/rda.13426

Muhammad Aslam, M. K., Sharma, V. K., Pandey, S., Kumaresan, A., Srinivasan, A., Datta, T. K., Mohanty, T. K., & Yadav, S. (2018). Identification of biomarker candidates for fertility in spermatozoa of crossbred bulls through comparative proteomics. *Theriogenology*, *119*, 43–51. https://doi.org/10.1016/j.theriogenology.2018.06.021

Muratori, M., Luconi, M., Marchiani, S., Forti, G., & Baldi, E. (2009). Molecular markers of human sperm functions. *International Journal of Andrology* 32(1), 25-45. https://doi.org/10.1111/j.1365-2605.2008.00875.x

Naaby-Hansen, S., & Herr, J. C. (2010). Heat shock proteins on the human sperm surface. *Journal of Reproductive Immunology*, *84*(1), 32–40. https://doi.org/10.1016/j.jri.2009.09.006

Nagaraj, N., Wisniewski, J. R., Geiger, T., Cox, J., Kircher, M., Kelso, J., Pääbo, S., & Mann, M. (2011). Deep proteome and transcriptome mapping of a human cancer cell line. *Molecular Systems Biology*, *7*(1), 548. https://doi.org/10.1038/msb.2011.81

Nair, M., Jagadeeshan, S., Katselis, G., Luan, X., Momeni, Z., Henao-Romero, N., Chumala, P., Tam, J. S., Yamamoto, Y., Ianowski, J. P., & Campanucci, V. A. (2021). Lipopolysaccharides induce a RAGE-mediated sensitization of sensory neurons and fluid hypersecretion in the upper airways. *Scientific Reports*. 11(1), 8336. https://doi.org/10.1038/s41598-021-86069-6

Narud, B., Khezri, A., Nordborg, A., Klinkenberg, G., Zeremichael, T. T., Stenseth, E.-B., Heringstad, B., Kommisrud, E., & Myromslien, F. D. (2022). Semen quality parameters including metabolites, sperm production traits and fertility in young Norwegian Red AI bulls. *Livestock Science*, *255*, 104803. https://doi.org/10.1016/j.livsci.2021.104803

Nassari, S., del Olmo, T., & Jean, S. (2020). Rabs in Signaling and Embryonic Development. *International Journal of Molecular Sciences*, *21*(3), 1064. https://doi.org/10.3390/ijms21031064

Navarrete, F. A., García-Vázquez, F. A., Alvau, A., Escoffier, J., Krapf, D., Sánchez-Cárdenas, C., Salicioni, A. M., Darszon, A., & Visconti, P. E. (2015). Biphasic Role of Calcium in Mouse Sperm Capacitation Signaling Pathways. *Journal of Cellular Physiology*, *230*(8), 1758–1769. https://doi.org/10.1002/jcp.24873

Naz, R. K., & Rajesh, P. B. (2004). Role of tyrosine phosphorylation in sperm capacitation/acrosome reaction. *Reproductive Biology and Endocrinology*, *2*(1), 75. https://doi.org/10.1186/1477-7827-2-75

Newton, L. D., Krishnakumar, S., Menon, A. G., Kastelic, J. P., Van Der Hoorn, F. A., & Thundathil, J. C. (2010). Na+/K+ATPase regulates sperm capacitation through a mechanism involving kinases and redistribution of its testis-specific isoform. *Molecular Reproduction and Development*, *77*(2), 136–148. https://doi.org/10.1002/mrd.21114

Nie, Y., Bai, F., Chaudhry, M. A., Pratt, R., Shapiro, J. I., & Liu, J. (2020). The Na/K-ATPase α1 and c-Src form signaling complex under native condition: A crosslinking approach. *Scientific Reports*, *10*(1), 6006. https://doi.org/10.1038/s41598-020-61920-4

Nixon, B., Bielanowicz, A., Anderson, A. L., Walsh, A., Hall, T., Mccloghry, A., & Aitken, R. J. (2010). Elucidation of the signaling pathways that underpin capacitation-associated surface

phosphotyrosine expression in mouse spermatozoa. *Journal of Cellular Physiology*, 224(1), 71-83. https://doi.org/10.1002/jcp.22090

Nixon, B., Mitchell, L. A., Anderson, A. L., Mclaughlin, E. A., O'bryan, M. K., & Aitken, R. J. (2011). Proteomic and functional analysis of human sperm detergent resistant membranes. *Journal of Cellular Physiology*, *226*(10), 2651–2665. https://doi.org/10.1002/jcp.22615

Noguchi, T., Fujinoki, M., Kitazawa, M., & Inaba, N. (2008). Regulation of hyperactivation of hamster spermatozoa by progesterone. *Reproductive Medicine and Biology*, *7*(2), 63–74. https://doi.org/10.1111/j.1447-0578.2008.00202.x

Norrander, J. M., DeCathelineau, A. M., Brown, J. A., Porter, M. E., & Linck, R. W. (2000). The rib43a protein is associated with forming the specialized protofilament ribbons of flagellar microtubules in Chlamydomonas. *Molecular Biology of the Cell*. 11(1), 201-215. https://doi.org/10.1091/mbc.11.1.201

Nourashrafeddin, S., Ebrahimzadeh-Vesal, R., Modarressi, M. H., Zekri, A., & Nouri, M. (2014). Identification of Spata-19 new variant with expression beyond meiotic phase of mouse testis development. *Reports of Biochemistry & Molecular Biology*, *2*(2), 89–93.

Nyblom, M., Poulsen, H., Gourdon, P., Reinhard, L., Andersson, M., Lindahl, E., Fedosova, N., & Nissen, P. (2013). Crystal structure of Na+, K+-ATPase in the Na +-bound State. *Science*, *342*(6154), 123–127. https://doi.org/10.1126/science.1243352

Obenauer, J. C. (2003). Scansite 2.0: proteome-wide prediction of cell signaling interactions using short sequence motifs. *Nucleic Acids Research*, *31*(13), 3635–3641. https://doi.org/10.1093/nar/gkg584

O'Flaherty, C., & Rico de Souza, A. (2011). Hydrogen Peroxide Modifies Human Sperm Peroxiredoxins in a Dose-Dependent Manner. *Biology of Reproduction*, *84*(2), 238–247. https://doi.org/10.1095/biolreprod.110.085712

Overview of Canada's agriculture and agri-food sector. (2021, November 5).

Özbek, M., Hitit, M., Kaya, A., Jousan, F. D., & Memili, E. (2021). Sperm Functional Genome Associated With Bull Fertility. *Frontiers in Veterinary Science*, *8*, 571. https://doi.org/10.3389/fvets.2021.610888

Pacheco, H. A., Battagin, M., Rossoni, A., Cecchinato, A., & Peñagaricano, F. (2021). Evaluation of bull fertility in Italian Brown Swiss dairy cattle using cow field data. *Journal of Dairy Science*, *104*(10), 10896–10904. https://doi.org/10.3168/jds.2021-20332

Parida, R., & Samanta, L. (2017). In silico analysis of candidate proteins sharing homology with Streptococcus agalactiae proteins and their role in male infertility. *Systems Biology in Reproductive Medicine*, *63*(1), 15–28. https://doi.org/10.1080/19396368.2016.1243741

Parisi, A. M., Thompson, S. K., Kaya, A., & Memili, E. (2014). Molecular, cellular, and physiological determinants of bull fertility. *Turkish Journal of Veterinary and Animal Sciences*, *38*, 637–642. https://doi.org/10.3906/vet-1404-76

Park, Y.-J., Kwon, W.-S., Oh, S.-A., & Pang, M.-G. (2012). Fertility-Related Proteomic Profiling Bull Spermatozoa Separated by Percoll. *Journal of Proteome Research*, *11*(8), 4162–4168. https://doi.org/10.1021/pr300248s

Parrish, J. J. (2014). Bovine in vitro fertilization: In vitro oocyte maturation and sperm capacitation with heparin. *Theriogenology* 81(1), 67-73. https://doi.org/10.1016/j.theriogenology.2013.08.005

Peacock TP, Sheppard CM, Brown JC, Goonawardane N, Zhou J, Whiteley M, de Silva TI, & Barclay WS. (2021). The SARS-CoV-2 variants associated with infections in India, B.1.617, show enhanced spike cleavage by furin. *BioRxiv : The Preprint Server for Biology*.

Peddinti, D., Nanduri, B., Kaya, A., Feugang, J. M., Burgess, S. C., & Memili, E. (2008). Comprehensive proteomic analysis of bovine spermatozoa of varying fertility rates and identification of biomarkers associated with fertility. *BMC Systems Biology*, *2*(1), 19. https://doi.org/10.1186/1752-0509-2-19

Peng, L., Li, P., Zhang, Q., Hong, L., Liu, L., Cui, X., & Cui, B. (2016). cAMP induction by ouabain promotes endothelin-1 secretion via MAPK/ERK signaling in beating rabbit atria. *The Korean Journal of Physiology & Pharmacology*, *20*(1), 9. https://doi.org/10.4196/kjpp.2016.20.1.9

Perez-Riverol, Y., Alpi, E., Wang, R., Hermjakob, H., & Vizcaíno, J. A. (2015). Making proteomics data accessible and reusable: Current state of proteomics databases and repositories. *Proteomics*, *15*(5–6), 930–950. https://doi.org/10.1002/pmic.201400302

Peterson, R. N., & Russell, L. D. (1985). The mammalian spermatozoon: A model for the study of regional specificity in plasma membrane organization and function. *Tissue and Cell*, *17*(6), 769–791. https://doi.org/10.1016/0040-8166(85)90035-7

Petit, F. M., Serres, C., Bourgeon, F., Pineau, C., & Auer, J. (2013). Identification of sperm head proteins involved in zona pellucida binding. *Human Reproduction*, *28*(4), 852–865. https://doi.org/10.1093/humrep/des452

Pierre, S. v., & Blanco, G. (2021). Na/K-ATPase Ion Transport and Receptor-Mediated Signaling Pathways. *The Journal of Membrane Biology*, *254*(5–6), 443–446. https://doi.org/10.1007/s00232-021-00207-9

Pierre, S. V., Sottejeau, Y., Gourbeau, J. M., Sánchez, G., Shidyak, A., & Blanco, G. (2008). Isoform specificity of Na-K-ATPase-mediated ouabain signaling. *American Journal of Physiology - Renal Physiology*, *294*(4), 859–866. https://doi.org/10.1152/ajprenal.00089.2007

Pini, T., Leahy, T., Soleilhavoup, C., Tsikis, G., Labas, V., Combes-Soia, L., Harichaux, G., Rickard, J. P., Druart, X., & de Graaf, S. P. (2016). Proteomic Investigation of Ram Spermatozoa and the Proteins Conferred by Seminal Plasma. *Journal of Proteome Research*, *15*(10), 3700–3711. https://doi.org/10.1021/acs.jproteome.6b00530

Pivovarov, A. S., Calahorro, F., & Walker, R. J. (2019). Na+/K+-pump and neurotransmitter membrane receptors. *Invertebrate Neuroscience*, *19*(1),1. https://doi.org/10.1007/s10158-018-0221-7

Podwojski, K., Eisenacher, M., Kohl, M., Turewicz, M., Meyer, H. E., Rahnenführer, J., & Stephan, C. (2010). Peek a peak: a glance at statistics for quantitative label-free proteomics. *Expert Review of Proteomics*, *7*(2), 249–261. https://doi.org/10.1586/epr.09.107

Primakoff, P., & Myles, D. G. (2002). Penetration, Adhesion, and Fusion in Mammalian Sperm-Egg Interaction. *Science*, *296*(5576), 2183–2185. https://doi.org/10.1126/science.1072029

Puglisi, R., Pozzi, A., Foglio, L., Spanò, M., Eleuteri, P., Grollino, M. G., Bongioni, G., & Galli, A. (2012). The usefulness of combining traditional sperm assessments with in vitro heterospermic insemination to identify bulls of low fertility as estimated in vivo. *Animal Reproduction Science*, *132*(1–2), 17–28. https://doi.org/10.1016/j.anireprosci.2012.04.006

Qian, C., Zhang Y., & Zhong J. (2021). Human cytomegalovirus ul138 protein: prediction of physicochemical properties, protein structure, and amino acid phosphorylation and mutation sites. *Southeast Asian Journal of Tropical Medicine and Public Health*, *52*(2), 222–229.

Quintas, L. E. M., Pierre, S. v., Liu, L., Bai, Y., Liu, X., & Xie, Z.-J. (2010). Alterations of Na+/K+-ATPase function in caveolin-1 knockout cardiac fibroblasts. *Journal of Molecular and Cellular Cardiology*, *49*(3), 525–531. https://doi.org/10.1016/j.yjmcc.2010.04.015

Radons, J. (2016). The human HSP70 family of chaperones: where do we stand? *Cell Stress and Chaperones*, *21*(3), 379–404. https://doi.org/10.1007/s12192-016-0676-6

Rahamim Ben-Navi, L., Almog, T., Yao, Z., Seger, R., & Naor, Z. (2016). A-Kinase Anchoring Protein 4 (AKAP4) is an ERK1/2 substrate and a switch molecule between cAMP/PKA and PKC/ERK1/2 in human spermatozoa. *Scientific Reports*, *6*(1), 37922. https://doi.org/10.1038/srep37922

Rahman, M. S., Kwon, W.-S., & Pang, M.-G. (2017). Prediction of male fertility using capacitation-associated proteins in spermatozoa. *Molecular Reproduction and Development*, *84*(9), 749–759. https://doi.org/10.1002/mrd.22810

Rahman, M. S., Lee, J. S., Kwon, W. S., & Pang, M. G. (2013). Sperm proteomics: Road to male fertility and contraception. *International Journal of Endocrinology,* 2013,1-13. https://doi.org/10.1155/2013/360986

Rajamanickam, G. D., Kastelic, J. P., & Thundathil, J. C. (2017a). Content of testis-specific isoform of Na/K-ATPase (ATP1A4) is increased during bovine sperm capacitation through translation in mitochondrial ribosomes. *Cell and Tissue Research*, *368*(1), 187–200. https://doi.org/10.1007/s00441-016-2514-7

Rajamanickam, G. D., Kastelic, J. P., & Thundathil, J. C. (2017b). Na/K-ATPase regulates bovine sperm capacitation through raft- and non-raft-mediated signaling mechanisms. *Molecular Reproduction and Development*, *84*(11), 1168–1182. https://doi.org/10.1002/mrd.22879

Rajamanickam, G. D., Kroetsch, T., Kastelic, J. P., & Thundathil, J. C. (2017c). Testis-specific isoform of Na/K-ATPase (ATP1A4) regulates sperm function and fertility in dairy bulls through potential mechanisms involving reactive oxygen species, calcium, and actin polymerization. *Andrology*, *5*(4), 814–823. https://doi.org/10.1111/andr.12377

Ramamurthy, V., & Oliver, D. (1997). Topology of the Integral Membrane Form of Escherichia coli SecA Protein Reveals Multiple Periplasmically Exposed Regions and Modulation by ATP Binding. *Journal of Biological Chemistry*, *272*(37), 23239–23246. https://doi.org/10.1074/jbc.272.37.23239

Ramesha, K. P., Mol, P., Kannegundla, U., Thota, L. N., Gopalakrishnan, L., Rana, E., Azharuddin, N., Mangalaparthi, K. K., Kumar, M., Dey, G., Patil, A., Saravanan, K., Behera, S. K., Jeyakumar, S., Kumaresan, A., Kataktalware, M. A., & Prasad, T. S. K. (2020b). Deep Proteome Profiling of Semen of Indian Indigenous Malnad Gidda (Bos indicus) Cattle. *Journal of Proteome Research*, *19*(8), 3364–3376. https://doi.org/10.1021/acs.jproteome.0c00237

Rana, A. P. S., Misra, S., Majumder, G. C., & Ghosh, A. (1993). Phospholipid asymmetry of goat sperm plasma membrane during epididymal maturation. *Biochimica et Biophysica Acta (BBA) - Lipids and Lipid Metabolism*, *1210*(1), 1–7. https://doi.org/10.1016/0005-2760(93)90041-7

Rashid, F., Baghla, R., Kale, P., Shah, M., Malakar, D., & Pillai, M. (2021). Absolute Quantification of Follicle Stimulating Hormone (FSH) Using Its Signature Peptides and Enzymatic Digestion in Human Serum by UPLC/LC–MS/MS. *Chromatographia*, *84*(8), 793–802. https://doi.org/10.1007/s10337-021-04057-4

Redgrove, K. A., Anderson, A. L., Dun, M. D., McLaughlin, E. A., O'Bryan, M. K., Aitken, R. J., & Nixon, B. (2011). Involvement of multimeric protein complexes in mediating the capacitation-dependent binding of human spermatozoa to homologous zonae pellucidae. *Developmental Biology*, *356*(2), 460–474. https://doi.org/10.1016/j.ydbio.2011.05.674

Reinhard, L., Tidow, H., Clausen, M. J., & Nissen, P. (2013b). Na+,K+-ATPase as a docking station: protein–protein complexes of the Na+,K+-ATPase. *Cellular and Molecular Life Sciences*, *70*(2), 205–222. https://doi.org/10.1007/s00018-012-1039-9

Revay, T., Quach, A. T., Maignel, L., Sullivan, B., & King, W. A. (2015). Copy number variations in high and low fertility breeding boars. *BMC Genomics*, *16*(1), 280. https://doi.org/10.1186/s12864-015-1473-9

Rijsselaere, T., van Soom, A., Hoflack, G., Maes, D., & de Kruif, A. (2004b). Automated sperm morphometry and morphology analysis of canine semen by the Hamilton-Thorne analyser. *Theriogenology*, *62*(7), 1292–1306. https://doi.org/10.1016/j.theriogenology.2004.01.005

Rogers, J. C., & Bomgarden, R. D. (2016). *Sample Preparation for Mass Spectrometry-Based Proteomics; from Proteomes to Peptides* (pp. 43–62). https://doi.org/10.1007/978-3-319-41448-5_3

Ruiz-Sánchez, A. L., O'Donoghue, R., Novak, S., Dyck, M. K., Cosgrove, J. R., Dixon, W. T., & Foxcroft, G. R. (2006). The predictive value of routine semen evaluation and IVF technology for determining relative boar fertility. *Theriogenology*, *66*(4), 736–748. https://doi.org/10.1016/j.theriogenology.2005.12.012

Saacke, R. G., & Almquist, J. O. (1964). Ultrastructure of bovine spermatozoa. I. The head of normal, ejaculated sperm. *American Journal of Anatomy*, *115*(1), 143–161. https://doi.org/10.1002/aja.1001150109

Saez, F., Ouvrier, A., & Drevet, J. R. (2011). Epididymis cholesterol homeostasis and sperm fertilizing ability. *Asian Journal of Andrology*, *13*(1), 11–17. https://doi.org/10.1038/aja.2010.64

Saidijam, M., Azizpour, S., & Patching, S. G. (2018). Comprehensive analysis of the numbers, lengths, and amino acid compositions of transmembrane helices in prokaryotic, eukaryotic, and viral integral membrane proteins of high-resolution structure. *Journal of Biomolecular Structure and Dynamics*, *36*(2), 443-464. https://doi.org/10.1080/07391102.2017.1285725

Sajeevadathan, M., Pettitt, M. J., & Buhr, M. (2019). Interaction of ouabain and progesterone on induction of bull sperm capacitation. *Theriogenology*, *126*, 191–198. https://doi.org/10.1016/j.theriogenology.2018.12.003

Sajeevadathan, M., Pettitt, M. J., & Buhr, M. M. (2021). Are isoforms of capacitating Na+K+-ATPase localized to sperm head rafts? *Molecular Reproduction and Development*, *88*(11), 731–743. https://doi.org/10.1002/mrd.23543

Salicioni, A. M., Platt, M. D., Wertheimer, E. v, Arcelay, E., Allaire, A., Sosnik, J., & Visconti, P. E. (2007). Signalling pathways involved in sperm capacitation. *Society of Reproduction and Fertility Supplement*, *65*, 245–259.

Sallam, S. (2017). *Mass Spectrometry Methods for the Analysis of Polymers and Bioconjugates*. The University of Akron.

Sanchez-Trincado, J. L., Gomez-Perosanz, M., & Reche, P. A. (2017). Fundamentals and Methods for T- and B-Cell Epitope Prediction. *Journal of Immunology Research*, *2017*, 1–14. https://doi.org/10.1155/2017/2680160

Sandtner, W., Egwolf, B., Khalili-Araghi, F., Sánchez-Rodríguez, J. E., Roux, B., Bezanilla, F., & Holmgren, M. (2011). Ouabain Binding Site in a Functioning Na+/K+ ATPase. *Journal of Biological Chemistry*, *286*(44), 38177–38183. https://doi.org/10.1074/jbc.M111.267682

Santos, H. L., Lamas, R. P., & Ciancaglini, P. (2002). Solubilization of Na,K-ATPase from rabbit kidney outer medulla using only C12E8. *Brazilian Journal of Medical and Biological Research*, *35*(3), 277-288. https://doi.org/10.1590/S0100-879X2002000300002

Sarvazyan, N. A., Ivanov, A., Modyanov, N. N., & Askari, A. (1997). Ligand-sensitive Interactions among the Transmembrane Helices of Na+/K+-ATPase. *Journal of Biological Chemistry*, *272*(12), 7855–7858. https://doi.org/10.1074/jbc.272.12.7855

Schrimpf, S. P., Weiss, M., Reiter, L., Ahrens, C. H., Jovanovic, M., Malmström, J., Brunner, E., Mohanty, S., Lercher, M. J., Hunziker, P. E., Aebersold, R., von Mering, C., & Hengartner, M. O. (2009). Comparative Functional Analysis of the Caenorhabditis elegans and Drosophila melanogaster Proteomes. *PLoS Biology*, *7*(3), e1000048. https://doi.org/10.1371/journal.pbio.1000048

Schwahn, A. B., Wong, J. W. H., & Downard, K. M. (2010). Typing of human and animal strains of influenza virus with conserved signature peptides of matrix M1 protein by high resolution mass spectrometry. *Journal of Virological Methods*, *165*(2), 178–185. https://doi.org/10.1016/j.jviromet.2010.01.015

Schwenk, J. M., Omenn, G. S., Sun, Z., Campbell, D. S., Baker, M. S., Overall, C. M., Aebersold, R., Moritz, R. L., & Deutsch, E. W. (2017). The Human Plasma Proteome Draft of 2017: Building on the Human Plasma PeptideAtlas from Mass Spectrometry and Complementary Assays. *Journal of Proteome Research*, *16*(12), 4299–4310. https://doi.org/10.1021/acs.jproteome.7b00467

Sebastian, W., Sukumaran, S., Zacharia, P. U., & Gopalakrishnan, A. (2018). Isolation and characterization of Aquaporin 1 (AQP1), sodium/potassium-transporting ATPase subunit alpha-1 (Na/K-ATPase α1), Heat Shock Protein 90 (HSP90), Heat Shock Cognate 71 (HSC71), Osmotic Stress Transcription Factor 1 (OSTF1) and Transcription Factor II B (TFIIB) genes from a euryhaline fish, Etroplus suratensis. *Molecular Biology Reports*, *45*(6), 2783–2789. https://doi.org/10.1007/s11033-018-4350-1

Senger P. L. (2012). *Pathways to pregnancy & parturition* (3rd edition). Redmond, OR : Current Conceptions.

Shannon, P., Markiel, A., Ozier, O., Baliga, N. S., Wang, J. T., Ramage, D., Amin, N., Schwikowski, B., & Ideker, T. (2003). Cytoscape: A Software Environment for Integrated Models of Biomolecular Interaction Networks. *Genome Research*, *13*(11), 2498–2504. https://doi.org/10.1101/gr.1239303

Shimada K, Uzawa K, Kato M, Endo Y, Shiiba M, Bukawa H, Yokoe H, Seki N, Tanzawa H. (2005). Aberrant expression of RAB1A in human tongue cancer. British Journal of Cancer, 92(10):1915-21. doi: 10.1038/sj.bjc.6602594. PMID: 15870709; PMCID: PMC2361773.

Shur, B. D. (2008). Reassessing the role of protein-carbohydrate complementarity during sperm-egg interactions in the mouse. *The International Journal of Developmental Biology*, *52*(5–6), 703–715. https://doi.org/10.1387/ijdb.082571bs

Signorelli, J., Diaz, E. S., & Morales, P. (2012). Kinases, phosphatases, and proteases during sperm capacitation. *Cell and Tissue Research*, *349*(3), 765–782. https://doi.org/10.1007/s00441-012-1370-3

Simons, K., & Sampaio, J. L. (2011). Membrane Organization and Lipid Rafts. *Cold Spring Harbor Perspectives in Biology*, *3*(10),1-17. https://doi.org/10.1101/cshperspect.a004697

Simons, K., & Toomre, D. (2000). Lipid rafts and signal transduction. *Nature Reviews Molecular Cell Biology*, *1*(1), 31–39. https://doi.org/10.1038/35036052

Singh, P., & Rizvi, S. I. (2015). Modulation Effects of Curcumin on Erythrocyte Ion-Transporter Activity. *International Journal of Cell Biology*, *2015*, 1–8. https://doi.org/10.1155/2015/630246

Singh, R., Sengar, G., Singh, U., Deb, R., Junghare, V., Hazra, S., Kumar, S., Tyagi, S., Das, A., Raja, T., & Kumar, A. (2018). Functional proteomic analysis of crossbred (Holstein Friesian × Sahiwal) bull spermatozoa. *Reproduction in Domestic Animals*, *53*(3), 588–608. https://doi.org/10.1111/rda.13146

Skroblin, P., Grossmann, S., Schäfer, G., Rosenthal, W., & Klussmann, E. (2010). *Mechanisms of Protein Kinase A Anchoring* (pp. 235–330). https://doi.org/10.1016/S1937-6448(10)83005-9

Somashekar, L., Selvaraju, S., Parthipan, S., Patil, S. K., Binsila, B. K., Venkataswamy, M. M., Karthik Bhat, S., & Ravindra, J. P. (2017). Comparative sperm protein profiling in bulls differing in fertility and identification of phosphatidylethanolamine-binding protein 4, a potential fertility marker. *Andrology*, *5*(5), 1032–1051. https://doi.org/10.1111/andr.12404

Song, J., & He, Q.-F. (2012). Bioinformatics analysis of the structure and linear B–cell epitopes of aquaporin–3 from Schistosoma japonicum. *Asian Pacific Journal of Tropical Medicine*, *5*(2), 107–109. https://doi.org/10.1016/S1995-7645(12)60005-4

Song, Y. F., Hogstrand, C., Wei, C. C., Wu, K., Pan, Y. X., & Luo, Z. (2017). Endoplasmic reticulum (ER) stress and cAMP/PKA pathway mediated Zn-induced hepatic lipolysis. *Environmental Pollution*, 228, 256-264. https://doi.org/10.1016/j.envpol.2017.05.046

Souza, A. P. B., Lopes, T. N., Silva, A. F. T., Santi, L., Beys-Da-Silva, W. O., Yates, J. R., & Bustamante-Filho, I. C. (2020). How does secondary hypogonadism affect the spermatozoa proteome? Lessons from a porcine animal model. *Reproduction, Fertility and Development*, *32*(13), 1125–1144. https://doi.org/10.1071/RD20017

Stackpole, C. W., & Devorkin, D. (1974). Membrane organization in mouse spermatozoa revealed by freeze-etching. *Journal of Ultrastructure Research*, *49*(2), 167–187. https://doi.org/10.1016/S0022-5320(74)80030-4

Steckler, D., Stout, T. A. E., Durandt, C., & Nöthling, J. O. (2015). Validation of merocyanine 540 staining as a technique for assessing capacitation-related membrane destabilization of fresh dog sperm. *Theriogenology*, *83*(9), 1451–1460. https://doi.org/10.1016/j.theriogenology.2015.01.019

Stenmark, H. (2009). Rab GTPases as coordinators of vesicle traffic. *Nature Reviews Molecular Cell Biology*, *10*(8), 513–525. https://doi.org/10.1038/nrm2728

Sudano, M. J., Crespilho, A. M., Fernandes, C. B., Junior, A. M., Papa, F. O., Rodrigues, J., Machado, R., & Landim-Alvarenga, F. D. C. (2011). Use of bayesian inference to correlate in vitro embryo production and in vivo fertility in Zebu Bulls. *Veterinary Medicine International*, *2011*, 1–6. https://doi.org/10.4061/2011/436381

Sutovsky, P. (2009). Sperm–egg adhesion and fusion in mammals. *Expert Reviews in Molecular Medicine*, *11*, e11. https://doi.org/10.1017/S1462399409001045

Sutovsky, P. (2018). Review: Sperm-oocyte interactions and their implications for bull fertility, with emphasis on the ubiquitin-proteasome system. *Animal*, *12* (1), s121–s132. https://doi.org/10.1017/S1751731118000253

Swegen, A., Curry, B. J., Gibb, Z., Lambourne, S. R., Smith, N. D., & Aitken, R. J. (2015). Investigation of the stallion sperm proteome by mass spectrometry. *Reproduction*, *149*(3), 235–244. https://doi.org/10.1530/REP-14-0500

Szklarczyk, D., Gable, A. L., Lyon, D., Junge, A., Wyder, S., Huerta-Cepas, J., Simonovic, M., Doncheva, N. T., Morris, J. H., Bork, P., Jensen, L. J., & Mering, C. von. (2019). STRING v11: protein–protein association networks with increased coverage, supporting functional discovery in genome-wide experimental datasets. *Nucleic Acids Research*, *47*(D1), D607–D613. https://doi.org/10.1093/nar/gky1131

Tahmasbpour, E., Balasubramanian, D., & Agarwal, A. (2014). A multi-faceted approach to understanding male infertility: gene mutations, molecular defects and assisted reproductive techniques (ART). *Journal of Assisted Reproduction and Genetics*, *31*(9), 1115–1137. https://doi.org/10.1007/s10815-014-0280-6

Talbot NC, Krasnec KV, Garrett WM, Shannon AE, Long JA. (2018). Finite cell lines of turkey sperm storage tubule cells: ultrastructure and protein analysis. Poultry Science, 97(10):3698-3708. doi: 10.3382/ps/pey208. PMID: 29860518; PMCID: PMC7107167.

Teves, M. E., & Roldan, E. R. S. (2022). Sperm bauplan and function and underlying processes of sperm formation and selection. *Physiological Reviews*, *102*(1), 7–60. https://doi.org/10.1152/physrev.00009.2020

Teves, M. E., Zhang, Z., Costanzo, R. M., Henderson, S. C., Corwin, F. D., Zweit, J., Sundaresan, G., Subler, M., Salloum, F. N., Rubin, B. K., & Strauss, J. F. (2013). Sperm-associated antigen-17 gene is essential for motile cilia function and neonatal survival. *American Journal of Respiratory Cell and Molecular Biology*, *48*(6), 765-772. https://doi.org/10.1165/rcmb.2012-0362OC

Thundathil, J. C., Anzar, M., & Buhr, M. M. (2006). Na+/K+ATPase as a signaling molecule during bovine sperm capacitation. *Biology of Reproduction*, *75*(3), 308–317. https://doi.org/10.1095/biolreprod.105.047852

Thundathil, J., Rajamanickam, G., Kastelic, J., & Newton, L. (2012). The Effects of Increased Testicular Temperature on Testis-Specific Isoform of Na+/K+-ATPase in Sperm and its Role in Spermatogenesis and Sperm Function. *Reproduction in Domestic Animals*, *47*, 170–177. https://doi.org/10.1111/j.1439-0531.2012.02072.x

Tian, J., Cai, T., Yuan, Z., Wang, H., Liu, L., Haas, M., Maksimova, E., Huang, X.-Y., & Xie, Z.-J. (2006). Binding of Src to Na+/K+-ATPase forms a functional signaling complex. *Molecular Biology of the Cell*, *17*(1), 317–326. https://doi.org/10.1091/mbc.e05-08-0735

Tian, J., & Xie, Z. (2008). The Na-K-ATPase and Calcium-Signaling Microdomains. *Physiology*, *23*(4), 205–211. https://doi.org/10.1152/physiol.00008.2008

Torra-Massana, M., Jodar, M., Barragán, M., Soler-Ventura, A., Delgado-Dueñas, D., Rodríguez, A., Oliva, R., & Vassena, R. (2021). Altered mitochondrial function in spermatozoa from patients with repetitive fertilization failure after ICSI revealed by proteomics. *Andrology*, *9*(4), 1192–1204. https://doi.org/10.1111/andr.12991

Tsiatsiani, L., & Heck, A. J. R. (2015). Proteomics beyond trypsin. *FEBS Journal*, *282*(14), 2612–2626. https://doi.org/10.1111/febs.13287

Tükenmez, H., Magnussen, H. M., Kovermann, M., Byström, A., & Wolf-Watz, M. (2016). Linkage between fitness of yeast cells and adenylate kinase catalysis. *PLoS ONE*, *11*(9), e0163115. https://doi.org/10.1371/journal.pone.0163115

Umesiobi, D. O. (2010). Boar Effects and Their Relations to Fertility and Litter Size in Sows. *South African Journal of Animal Science*, *40(5)*, 471–475.

Utt, M. D. (2016). Prediction of bull fertility. *Animal Reproduction Science*, *169*, 37–44. https://doi.org/10.1016/j.anireprosci.2015.12.011

Vagin, O., Dada, L. A., Tokhtaeva, E., & Sachs, G. (2012). The Na-K-ATPase α1β1 heterodimer as a cell adhesion molecule in epithelia. *American Journal of Physiology - Cell Physiology*, *302*(9), 1271–1281. https://doi.org/10.1152/ajpcell.00456.2011

Viana, A. G. A., Martins, A. M. A., Pontes, A. H., Fontes, W., Castro, M. S., Ricart, C. A. O., Sousa, M. v., Kaya, A., Topper, E., Memili, E., & Moura, A. A. (2018). Proteomic landscape of seminal plasma associated with dairy bull fertility. *Scientific Reports*, *8*(1), 16323. https://doi.org/10.1038/s41598-018-34152-w

Vignjevic D, Montagnac G. (2008). Reorganisation of the dendritic actin network during cancer cell migration and invasion. Seminars in Cancer Biology, 18(1):12-22. doi: 10.1016/j.semcancer.2007.08.001. Epub 2007 Sep 4. PMID: 17928234.

Vihinen, M. (2001). Bioinformatics in proteomics. *Biomolecular Engineering*, *18*(5), 241–248. https://doi.org/10.1016/S1389-0344(01)00099-5

Visconti, P. E. (2009). Understanding the molecular basis of sperm capacitation through kinase design. *Proceedings of the National Academy of Sciences*, *106*(3), 667–668. https://doi.org/10.1073/pnas.0811895106

Visconti, P. E., Galantino-Homer, H., Moore, G. D., Bailey, J. L., Ning, X., Fornes, M., & Kopf, G. S. (1998). The molecular basis of sperm capacitation. *Journal of Andrology*, *19*(2), 242–248.

Visconti, P. E., Westbrook, V. A., Chertihin, O., Demarco, I., Sleight, S., & Diekman, A. B. (2002). Novel signaling pathways involved in sperm acquisition of fertilizing capacity.

Journal of Reproductive Immunology, *53*(1–2), 133–150. https://doi.org/10.1016/S0165-0378(01)00103-6

Vlachakis D, Bencurova, E., Papageorgiou, L., Bhide, M., & Kossida, S. (2015). Protein phosphorylation prediction: limitations, merits, and pitfalls. *Journal of Molecular Biochemistry*, *4*(2), 145–155.

Voedisch, B., & Thie, H. (2010). Size Exclusion Chromatography. In *Antibody Engineering* (pp. 607–612). Springer Berlin Heidelberg. https://doi.org/10.1007/978-3-642-01144-3_38

Wagoner, K., Sanchez, G., Nguyen, A.-N., Enders, G. C., & Blanco, G. (2005). Different expression and activity of the a1 and a4 isoforms of the Na,K-ATPase during rat male germ cell ontogeny. *Reproduction*, *130(5)*, 627–641. https://doi.org/10.1530/rep.1.00806

Walton R. (2012). Important milestones in the AI industry. *In 24th Technical Conference on Artificial Insemination and Reproduction*.

Wang, C., & Swerdloff, R. S. (2014). Limitations of semen analysis as a test of male fertility and anticipated needs from newer tests. *Fertility and Sterility*, *102*(6), 1502–1507. https://doi.org/10.1016/j.fertnstert.2014.10.021

Wang, C., Xu, H., Lin, S., Deng, W., Zhou, J., Zhang, Y., Shi, Y., Peng, D., & Xue, Y. (2020b). GPS 5.0: An Update on the Prediction of Kinase-specific Phosphorylation Sites in Proteins. *Genomics, Proteomics & Bioinformatics*, *18*(1), 72–80. https://doi.org/10.1016/j.gpb.2020.01.001

Wang, D., Zeng, S., Xu, C., Qiu, W., Liang, Y., Joshi, T., & Xu, D. (2017). MusiteDeep: a deep-learning framework for general and kinase-specific phosphorylation site prediction. *Bioinformatics*, *33*(24), 3909–3916. https://doi.org/10.1093/bioinformatics/btx496

Wang, H., Haas, M., Liang, M., Cai, T., Tian, J., Li, S., & Xie, Z. (2004). Ouabain Assembles Signaling Cascades through the Caveolar Na+/K+-ATPase. *Journal of Biological Chemistry*, *279*(17), 17250–17259. https://doi.org/10.1074/jbc.M313239200

Wang, W., Chen, Y., Li, L., Zhou, L., Du, X., Liu, M., & Ge, M. (2022). Chemical composition of different size ultrafine particulate matter measured by nanoparticle chemical ionization mass spectrometer. *Journal of Environmental Sciences*, *114*, 434–443. https://doi.org/10.1016/j.jes.2021.09.036

Wang, X., Sun, Q., Ye, Z., Hua, Y., Shao, N., Du, Y., Zhang, Q., & Wan, C. (2016). Computational approach for predicting the conserved B-cell epitopes of hemagglutinin H7 subtype influenza virus. *Experimental and Therapeutic Medicine*, *12*(4), 2439–2446. https://doi.org/10.3892/etm.2016.3636

Washburn, M. P., Wolters, D., & Yates, J. R. (2001). Large-scale analysis of the yeast proteome by multidimensional protein identification technology. *Nature Biotechnology*, *19*(3), 242–247. https://doi.org/10.1038/85686

Watson, P. F. (2000). The causes of reduced fertility with cryopreserved semen. *Animal Reproduction Science*, *60–61*, 481–492. https://doi.org/10.1016/S0378-4320(00)00099-3

Weigand, K. M., Swarts, H. G. P., Fedosova, N. U., Russel, F. G. M., & Koenderink, J. B. (2012). Na,K-ATPase activity modulates Src activation: A role for ATP/ADP ratio. *Biochimica et Biophysica Acta (BBA) - Biomembranes*, *1818*(5), 1269–1273. https://doi.org/10.1016/j.bbamem.2012.01.015

Welch, E. J., Jones, B. W., & Scott, J. D. (2010). Networking with AKAPs: Context-dependent Regulation of Anchored Enzymes. *Molecular Interventions*, *10*(2), 86–97. https://doi.org/10.1124/mi.10.2.6

Whitfield, M., Thomas, L., Bequignon, E., Schmitt, A., Stouvenel, L., Montantin, G., Tissier, S., Duquesnoy, P., Copin, B., Chantot, S., Dastot, F., Faucon, C., Barbotin, A. L., Loyens, A., Siffroi, J. P., Papon, J. F., Escudier, E., Amselem, S., Mitchell, V., … Legendre, M. (2019). Mutations in DNAH17, Encoding a Sperm-Specific Axonemal Outer Dynein Arm Heavy Chain, Cause Isolated Male Infertility Due to Asthenozoospermia. *American Journal of Human Genetics*. 105(1), 198-212. https://doi.org/10.1016/j.ajhg.2019.04.015

Wilhelm, M., Schlegl, J., Hahne, H., Gholami, A. M., Lieberenz, M., Savitski, M. M., Ziegler, E., Butzmann, L., Gessulat, S., Marx, H., Mathieson, T., Lemeer, S., Schnatbaum, K., Reimer, U., Wenschuh, H., Mollenhauer, M., Slotta-Huspenina, J., Boese, J.-H., Bantscheff, M., … Kuster, B. (2014). Mass-spectrometry-based draft of the human proteome. *Nature*, *509*(7502), 582–587. https://doi.org/10.1038/nature13319

Wilkins, M. R., Gasteiger, E., Bairoch, A., Sanchez, J.-C., Williams, K. L., Appel, R. D., & Hochstrasser, D. F. (1999). Protein Identification and Analysis Tools in the ExPASy Server. In *2-D Proteome Analysis Protocols* (pp. 531–552). Humana Press. https://doi.org/10.1385/1-59259-584-7:531

Willems, J. L., Khamis, M. M., Mohammed Saeid, W., Purves, R. W., Katselis, G., Low, N. H., & El-Aneed, A. (2016). Analysis of a series of chlorogenic acid isomers using differential ion mobility and tandem mass spectrometry. *Analytica Chimica Acta*. 933, 164-174. https://doi.org/10.1016/j.aca.2016.05.041

Woo, A. L., James, P. F., & Lingrel, J. B. (2000). Sperm Motility Is Dependent on a Unique Isoform of the Na,K-ATPase. *Journal of Biological Chemistry*, *275*(27), 20693–20699. https://doi.org/10.1074/jbc.M002323200

World Health Organization. (2010). *WHO Laboratory Manual for the Examination and Processing of Human Semen*. pp 32-99.

Wright, P. C., Noirel, J., Ow, S.-Y., & Fazeli, A. (2012). A review of current proteomics technologies with a survey on their widespread use in reproductive biology investigations. *Theriogenology*, *77*(4), 738-765.e52. https://doi.org/10.1016/j.theriogenology.2011.11.012

Wu, H. J., Lü, Q., Quan, L. J., Chen, R., Chen, S. S., Li, H. O., & Qian, P. de. (2013). Modeling the structural topology and predicting the three-dimensional structure for transmembrane helixes of GPCR. *Jisuanji Xuebao/Chinese Journal of Computers*, *36*(10), 2168-2178. https://doi.org/10.3724/SP.J.1016.2013.02168

Xie, J., Ye, Q., Cui, X., Madan, N., Yi, Q., Pierre, S. v, & Xie, Z. (2015). Expression of rat Na-K-ATPase 2 enables ion pumping but not ouabain-induced signaling in 1-deficient porcine renal epithelial cells. *Am J Physiol Cell Physiol*, *309*, 373–382. https://doi.org/10.1152/ajpcell.00103.2015.-Na-K-AT

Xie, Q., Tian, Y., Hu, Z., Zhang, L., Tang, B., Wang, Y., Li, J., & Chen, G. (2021). Novel Translational and Phosphorylation Modification Regulation Mechanisms of Tomato (Solanum lycopersicum) Fruit Ripening Revealed by Integrative Proteomics and Phosphoproteomics. *International Journal of Molecular Sciences*, *22*(21), 11782. https://doi.org/10.3390/ijms222111782

Xie, Z. (2003). Molecular Mechanisms of Na/K-ATPase-Mediated Signal Transduction. *Annals of the New York Academy of Sciences*, *986*(1), 497–503. https://doi.org/10.1111/j.1749-6632.2003.tb07234.x

Xie, Z., & Askari, A. (2002). Na+/K+-ATPase as a signal transducer. *European Journal of Biochemistry*, *269*(10), 2434–2439. https://doi.org/10.1046/j.1432-1033.2002.02910.x

Xu, K., Yang, L., Zhang, L., & Qi, H. (2020). Lack of AKAP3 disrupts integrity of the subcellular structure and proteome of mouse sperm and causes male sterility. *Development (Cambridge)*, *147*(2), 181057. https://doi.org/10.1242/dev.181057

Xue, Y., Liu, Z., Cao, J., Ma, Q., Gao, X., Wang, Q., Jin, C., Zhou, Y., Wen, L., & Ren, J. (2011). GPS 2.1: enhanced prediction of kinase-specific phosphorylation sites with an algorithm of motif length selection. *Protein Engineering Design and Selection*, *24*(3), 255–260. https://doi.org/10.1093/protein/gzq094

Yanagimachi, R. (1994). Mammalian fertilization. In E. Knobil and J.D. Neill (Ed.), *In The Physiology of Reproduction* (2nd ed., pp. 189–317). Raven Press.

Yanagimachi, R. (1994b). Fertility of mammalian spermatozoa: its development and relativity. *Zygote*, *2*(4), 371–372. https://doi.org/10.1017/S0967199400002240

Yanagimachi, R., & Usui, N. (1974). Calcium dependence of the acrosome reaction and activation of guinea pig spermatozoa. *Experimental Cell Research*, *89*(1), 161–174. https://doi.org/10.1016/0014-4827(74)90199-2

Yates, J. R. (2011). A century of mass spectrometry: from atoms to proteomes. *Nature Methods*, *8*(8), 633–637. https://doi.org/10.1038/nmeth.1659

Yates, J. R., Ruse, C. I., & Nakorchevsky, A. (2009). Proteomics by Mass Spectrometry: Approaches, Advances, and Applications. *Annual Review of Biomedical Engineering*, *11*(1), 49–79. https://doi.org/10.1146/annurev-bioeng-061008-124934

Yu, J., Chen, B., Zheng, B., Qiao, C., Chen, X., Yan, Y., Luan, X., Xie, B., Liu, J., Shen, C., He, Z., Hu, X., Liu, M., Li, H., Shao, Q., & Fang, J. (2019). ATP synthase is required for male fertility and germ cell maturation in Drosophila testes. *Molecular Medicine Reports*.19(3), 1561-1570. https://doi.org/10.3892/mmr.2019.9834

Yu, Y., Xu, W., Yi, Y.-J., Sutovsky, P., & Oko, R. (2006). The extracellular protein coat of the inner acrosomal membrane is involved in zona pellucida binding and penetration during fertilization: Characterization of its most prominent polypeptide (IAM38). *Developmental Biology*, *290*(1), 32–43. https://doi.org/10.1016/j.ydbio.2005.11.003

Yuan, Z., Cai, T., Tian, J., Ivanov, A. V., Giovannucci, D. R., & Xie, Z. (2005). Na/K-ATPase tethers phospholipase C and IP3 receptor into a calcium-regulatory complex. *Molecular Biology of the Cell*. 16(9), 4034-4045. https://doi.org/10.1091/mbc.E05-04-0295

Zhang, J., Li, X., Yu, H., Larre, I., Dube, P. R., Kennedy, D. J., Tang, W. H. W., Westfall, K., Pierre, S. v, Xie, Z., & Chen, Y. (2020). Regulation of Na/K-ATPase expression by cholesterol: isoform specificity and the molecular mechanism. *American Journal of Physiology. Cell Physiology*, *319*(6), C1107–C1119. https://doi.org/10.1152/ajpcell.00083.2020

Zhang, L., Zhang, Z., Guo, H., & Wang, Y. (2008). Na+/K+-ATPase-mediated signal transduction and Na+/K+-ATPase regulation. *Fundamental & Clinical Pharmacology*, *22*(6), 615–621. https://doi.org/10.1111/j.1472-8206.2008.00620.x

Zhang, T., Wang, J., Niu, W., Wang, F., Liu, J., Xing, Y., Jia, P., Ren, X., Wang, J., Zang, W., & Chen, X. (2020a). Bioinformatic prediction of the structure and characteristics of human sperm acrosome membrane-associated protein 1 (hSAMP32) and evaluation of its antifertility function in vivo. *Reproduction, Fertility and Development*, *32*(16), 1282-1292. https://doi.org/10.1071/RD20198

Zhang, Y., Fonslow, B. R., Shan, B., Baek, M.-C., & Yates, J. R. (2013). Protein Analysis by Shotgun/Bottom-up Proteomics. *Chemical Reviews*, *113*(4), 2343–2394. https://doi.org/10.1021/cr3003533

Zhao, Q., Tao, C., Pan, J., Wei, Q., Zhu, Z., Wang, L., Liu, M., Huang, J., Yu, F., Chen, X., Zhang, L., & Li, J. (2021). Equine chorionic gonadotropin pretreatment 15 days before fixed-time artificial insemination improves the reproductive performance of replacement gilts. *Animal*, *15*(12), 100406. https://doi.org/10.1016/j.animal.2021.100406

Zhao, W., Li, Z., Ping, P., Wang, G., Yuan, X., & Sun, F. (2018). Outer dense fibers stabilize the axoneme to maintain sperm motility. *Journal of Cellular and Molecular Medicine*, *22*(3), 1755–1768. https://doi.org/10.1111/jcmm.13457

Zhao, Y., & Buhr, M. M. (1996). Localization of various ATPases in fresh and cryopreserved bovine spermatozoa. *Animal Reproduction Science*. *44*(3), 139–148. https://doi.org/10.1016/0378-4320(96)01547-3

Zhou, J., Chen, L., Li, J., Li, H., Hong, Z., Xie, M., Chen, S., & Yao, B. (2015). The Semen pH Affects Sperm Motility and Capacitation. *PLOS ONE*, *10*(7), e0132974. https://doi.org/10.1371/journal.pone.0132974

Zhou, J., Du, Y. R., Qin, W. H., Hu, Y. G., Huang, Y. N., Bao, L., Han, D., Mansouri, A., & Xu, G. L. (2009). RIM-BP3 is a manchette-associated protein essential for spermiogenesis. *Development*, *136*(3), 373-382. https://doi.org/10.1242/dev.030858

Zhu, J., & Lu, P. (2022). Computational design of transmembrane proteins. *Current Opinion in Structural Biology*, *74*, 102381. https://doi.org/10.1016/j.sbi.2022.102381

Zuccarello, D., Ferlin, A., Cazzadore, C., Pepe, A., Garolla, A., Moretti, A., Cordeschi, G., Francavilla, S., & Foresta, C. (2008). Mutations in dynein genes in patients affected by isolated non-syndromic asthenozoospermia. *Human Reproduction*. 23(8), 1957-1962. https://doi.org/10.1093/humrep/den193

Zuidema, D., Kerns, K., & Sutovsky, P. (2021). An Exploration of Current and Perspective Semen Analysis and Sperm Selection for Livestock Artificial Insemination. *Animals*, *11*(12), 3563. https://doi.org/10.3390/ani11123563

Zwald, N. R., Weigel, K. A., Chang, Y. M., Welper, R. D., & Clay, J. S. (2004). Genetic Selection for Health Traits Using Producer-Recorded Data. II. Genetic Correlations, Disease Probabilities, and Relationships with Existing Traits. *Journal of Dairy Science*, *87*(12), 4295–4302. https://doi.org/10.3168/jds.S0022-0302(04)73574-2